

T 304

**HYPERBRANCHED POLYURETHANE NANOCOMPOSITES  
AS SHAPE MEMORY MATERIALS**

*A thesis submitted in partial fulfillment of the requirements for the award of the  
degree of*

***Doctor of Philosophy***

**By**

**Hemjyoti Kalita**

*Registration No. TZ121489 of 2012*



**School of Sciences  
Department of Chemical Sciences  
Tezpur University  
Napaam, Tezpur - 784028  
Assam, India**

**December, 2013**

**DEDICATED TO MY  
PARENTS**

## **ABSTRACT**

---

Shape memory polymers (SMP) have generated immense interest in recent times because of their potential applications in different fields such as smart actuators, aerospace engineering, textile engineering and most importantly as intelligent biomedical devices. They have some advantages such as easier processing, lighter weight, lower cost, larger recoverable strain and lower toxicity as compared to other category of shape memory materials like shape memory alloys. Among different types of shape memory polymers, polyurethanes are the most versatile polymeric material due to their biocompatibility, wide range of tunable stiffness, large deformation, large recovery, good elastic property, water vapour permeability and multi responsive shape memory effect. Recently hyperbranched polymers have taken tremendous attentions in the development of advanced polymeric materials because of their unique characters. These polymers exhibited some special properties like low melt and solution viscosity, high solubility and chemical reactivity, enhanced compatibility, compact three dimensional non-entangled globular structures etc. Further the concept of partial entanglement in hyperbranched structure by incorporating long chain macroglycol offers better mechanical property. Thus it is worth thinking to utilize this concept to synthesize hyperbranched polyurethanes as shape memory polymers. Furthermore, realization of finite petroleum resources, growing environmental concerns and waste disposal problems encourage the utilization of bio resources like vegetable oils as raw materials for the preparation of polymeric materials. In addition to the above, the demands of the advanced applications required high performance polymeric materials. Recently polymer nanocomposites have taken commendable role in the domain of materials due to the significant improvement of many desired properties like mechanical strength, thermal, gas barrier, solvent resistance, flame retardant, shape memory and biodegradability of the neat polymers. Therefore vegetable oil based hyperbranched polyurethane nanocomposites with different nanomaterials may be utilized as advanced shape memory polymeric materials.

In this context, the thesis entitled, "Hyperbranched polyurethane nanocomposites as shape memory materials" is focused on the development of vegetable oil based hyperbranched polyurethanes and their nanocomposites with nanomaterials such as  $\text{Fe}_3\text{O}_4$ , MWCNT and  $\text{Fe}_3\text{O}_4$



decorated MWCNT. The introductory chapter of the thesis describes a brief review on shape memory polyurethane nanocomposites with special emphasis on vegetable oil based polyols for polyurethanes. The importance of such nanocomposites, history, general techniques for preparation, characterization, properties and applications have been described in this chapter. Second chapter consists of three subchapters. The first subchapter of this technical part deals with the synthesis, characterization and properties evaluation including shape memory behaviors of the hyperbranched polyurethanes with three different vegetable oils. The synthesized hyperbranched polyurethanes were characterized by the different characterization techniques such as FTIR, <sup>1</sup>HNMR, XRD, SEM etc. The performance characteristics such as tensile strength, flexibility, gloss, impact resistance and scratch hardness were determined. The *Mesua ferrea* L. seed oil based hyperbranched polyurethane showed the overall good performance as compared to the other and hence this was utilized for the further studies. The second subchapter describes the synthesis of hyperbranched polyurethanes with different amount of monoglyceride of *Mesua ferrea* L. seed oil. The synthesized hyperbranched polyurethanes were characterized and different properties were evaluated by the same way as stated above. However the third subchapter presented synthesis of the hyperbranched polyurethane with varying amount of multifunctional moiety, triethanolamine. The synthesized hyperbranched polyurethanes were characterized and different properties including shape memory behaviors were evaluated by the same way. All the above hyperbranched polyurethanes were prepared by the pre-polymerization technique. The third chapter deals with the study on modification of monoglyceride (10 wt%) of *Mesua ferrea* L. seed oil based hyperbranched polyurethane with the commercially available glycidyl ether of bisphenol-A based epoxy resin. The modified systems were characterized by the different characterization techniques such as FTIR, XRD, SEM etc. FTIR spectra were utilized to study the crosslinking reactions. The various performance characteristics like tensile strength, impact resistance, scratch hardness, thermal stability, chemical resistance in different media and shape memory behaviors showed improvements over the pristine hyperbranched polyurethane. The fourth chapter consists of two subchapters. The first subchapter describes the preparation of Fe<sub>3</sub>O<sub>4</sub> based hyperbranched polyurethane thermoplastic nanocomposites. The formation of the nanocomposites was characterized by FTIR, XRD, SEM and TEM analyses. The mechanical properties such as tensile strength, impact resistance, scratch hardness and

thermal properties were improved as compared to the pristine polyurethane. The nanocomposites showed the excellent shape recovery under the microwave actuation. The second subchapter deals with the thermosetting nanocomposites of the same. The prepared nanocomposites showed improved mechanical, thermal and microwave induced shape memory behaviors as compared to the pristine system. The study showed thermosetting nanocomposites exhibited the better performance as compared to the thermoplastic one. Fifth chapter describes the hyperbranched polyurethane/MWCNT thermoplastic (first subchapter) and thermosetting (second subchapter) nanocomposites. MWCNT were covalently modified with the triethanolamine. The modification of MWCNT was characterized by the FTIR and Raman spectroscopy. The formation of nanocomposites was characterized by the same way as stated above. The nanocomposites exhibited the significant improvement of the mechanical and thermal stability. The nanocomposites showed the faster shape recovery under the microwave actuation as compared to the pristine system. Moreover the thermosetting one exhibited enhanced performance as compared to the thermoplastic one. Similarly sixth chapter consists of two subchapters, where the first subchapter deals with preparation, characterization and properties evaluation including shape memory behaviors of the hyperbranched polyurethane/Fe<sub>3</sub>O<sub>4</sub> decorated MWCNT thermoplastic nanocomposites. Fe<sub>3</sub>O<sub>4</sub> nanoparticles were successfully decorated on the surface of MWCNT by the wet chemical technique. The decoration of Fe<sub>3</sub>O<sub>4</sub> on the surface of MWCNT was characterized by the FTIR, Raman and TEM analyses. The second subchapter concentrated on the same for the thermosetting nanocomposites. The nanocomposites showed enhanced mechanical, thermal stability and shape memory behaviors as compared to the pristine system. The shape recovery time found to be decreased in the nanocomposites under the microwave irradiation. However thermosetting one exhibited better mechanical, thermal and shape memory behaviors as compared to thermoplastic one.

## ***DECLARATION***

---

I do hereby declare that the thesis entitled "*Hyperbranched polyurethane nanocomposites as shape memory materials*", submitted to the Tezpur University in the Department of Chemical Sciences, is a record of original research work carried out by me. All sources of assistance have been assigned due acknowledgment. I also declare that neither this work as a whole nor a part of it has been submitted to any other University or Institute for any other degree, diploma or award.

Place: Tezpur University, Tezpur

Date: 19/12/2013

*Hemjyoti Kalita*  
(Hemjyoti Kalita)



**TEZPUR UNIVERSITY**

(A Central University established by an Act of Parliament)

Ph: 03712-267004

03712-267005

NAPAAM, TEZPUR-784028

Fax: 03712-267006

*DISTRICT: SONITPUR:: ASSAM:: INDIA*

03712-267005

E-mail: [nkarak@tezu.ernet.in](mailto:nkarak@tezu.ernet.in)

---

## **CERTIFICATE**

This is to certify that the thesis entitled "*Hyperbranched polyurethane nanocomposites as shape memory materials*" submitted to the Tezpur University in the Department of Chemical Sciences under the School of Sciences, in partial fulfilment for the award of the Degree of Doctor of Philosophy in Science, is a record of research work carried out by Hemjyoti Kalita under my supervision and guidance.

All helps received by him from various sources have been duly acknowledged. No part of this thesis has been reproduced elsewhere for award of any other degree.

Place: Tezpur University

Date: 19<sup>th</sup> December 2013

(Dr. Niranjan Karak)

Professor

Department of Chemical Sciences

School of Sciences



**TEZPUR UNIVERSITY**

(A Central University established by an Act of Parliament)

Ph: 03712-267004

03712-267005

NAPAAM, TEZPUR-784028

Fax: 03712-267006

*DISTRICT: SONITPUR:: ASSAM:: INDIA*

*03712-267005*

E-mail: [nkarak@tezu.ernet.in](mailto:nkarak@tezu.ernet.in)

---

## ***CERTIFICATE***

This is to certify that the thesis entitled “*Hyperbranched polyurethane nanocomposites as shape memory materials*” submitted to the Tezpur University in the Department of Chemical Sciences under the School of Sciences, in partial fulfilment for the award of the Degree of Doctor of Philosophy in Science, has been examined by us on ..... and found to be satisfactory.

We recommend the thesis for award of doctor of philosophy.

Principal Supervisor

Date:

External Examiner *Jose M. Ken*

Date: *June 2, 2014*

## ***PREFACE***

---

Shape memory polymers are an emerging class of smart materials and they are gaining enormous interest because of their potential application in different fields such as textile, automobile, aerospace and biomedical devices. Scientists and technologists are trying to develop new kind of shape memory materials and to tailor the shape memory behaviors of the existing shape memory polymers. Among the various shape memory polymers the vegetable oil based polyurethane represents one of the most fascinating materials because of its versatility and tunable structure-properties according to the desired need including shape memory behaviors for a variety of applications. The shape memory polymer nanocomposites have taken a prominent position in the current research and development owing to the significant improvement in the properties of the pristine polymer.

Thus the main objective of this thesis is to synthesize the hyperbranched polyurethane and its different nanocomposites as advanced shape memory materials. The thesis describes the synthesis, characterization, property evaluation of hyperbranched polyurethane, modified hyperbranched polyurethane and their nanocomposites to explore the potentiality of these materials as advanced shape memory materials. The properties of the pristine hyperbranched polyurethane and its modified systems were enhanced by the formation of nanocomposites with different types of nanomaterials such as  $\text{Fe}_3\text{O}_4$ , MWCNT and  $\text{Fe}_3\text{O}_4$  decorated MWCNT. The shape memory behaviors of the nanocomposites especially thermosetting nanocomposites were found to be enhanced as compared to the pristine one. A noncontact actuation using microwave energy was studied for all the prepared nanocomposites. Thus the prepared nanocomposites might be utilized as advanced shape memory materials in different field such as textile, automobile, aerospace and biomedical devices.

Place: Tezpur University

Date: 19/12/2013

*Hemjyoti Kalita*  
(Hemjyoti Kalita)

## **ACKNOWLEDGMENT**

---

*It is my greatest pleasure to express my gratitude to large numbers of people who have directly or indirectly influenced and encouraged me over the course of my studies and my life in general.*

*First of all, I would like to express my deep sense of gratitude and indebtedness to my research guide Dr. Niranjana Karak, Professor, Department of Chemical Sciences, Tezpur University for his invaluable guidance, support, advice and a wonderful accompany throughout my Ph.D. work. His dedication towards research and indomitable spirit would ever remain as a source of inspiration for me.*

*It is my pleasant duty to acknowledge with thanks the cooperation and support extended to me by the authority of Tezpur University and entire community of the Department of Chemical Sciences, for allowing me to use the administrative and technical facilities required for my research work.*

*I would also like to express my sincere gratitude and humble respect to my doctoral research committee members Dr. A.J. Thakur and Dr. M. Mandal, Associate Professor for their timely help and advices.*

*I am immensely grateful to the present (Prof. R.C. Deka) and former (Prof. N. Karak) HoDs and all the faculty members of Department of Chemical Sciences, Tezpur University for valuable suggestions and advices.*

*My heartfelt thanks go to my senior lab-mates Dr. Harekrishna Deka, Dr. Uday Konwar, Dr. Gautam Das, Dr. Buddbadev Roy and Dr. Rocktotpal Konwarh for their manifold help and active co-operation over all these years. I would also like to thank my junior group members Sujata Pramanik, Shaswat Barua, Beauty Das, Suman Thakur, Bibekananda De and Satyabrat Gogoi for their constant supports and helps during my Ph.D. work.*

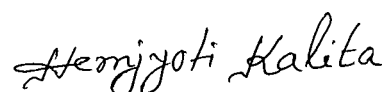
*I would like to offer my sincere thanks to Dr. Biren Gohain, Mr. Nipu Dutta, Mr. Raju K. Borah, Mr. Sankur Phukan, Mr. Biraj Borah, Mr. Arup Chakrabarty, Mr. Manaranjan Sarma, Mr. Ratan Baruah, Mr. Prakash Kurmi for instrumental and experimental helps. IIT Kharagpur,*

*NEHU Shillong and other institutions are highly acknowledged for their help in analyzing and testing works.*

*I would like to thank also the office staffs of Department of Chemical Sciences, Tezpur University, Ms Babita Das and Mr. Hemanta Gogoi for their kind help during my Ph.D. work.*

*I am also grateful to DST, New Delhi for financial support to me as JRF and SRF.*

*Finally, I owe heartfelt gratitude to my parents and all my family members for their blessings and support that constantly inspiring me to carry out my research work to completion. I am thankful to all my relatives and well-wisher for their encouragements. The endless love of them will always be in my heart that will inspire me in every step of my future life.*



(Hemjyoti Kalita)

Place: Tezpur University, Tezpur



# **CONTENTS**

---

<i>Content</i>	<i>Page No.</i>
Abstract	i
Declaration	iv
Certificate of supervisor	v
Certificate of examiners	vi
Preface	vii
Acknowledgement	viii
Contents	x
List of Abbreviations and Symbols	xix
List of Tables	xxi
List of Figures	xxiii
List of Schemes	xxviii

## ***Chapter 1***

### **General introduction**

1.1. Introduction	2
1.2. Background	5
1.3. Classification of SMP	6
1.4. Classification of polymer nanocomposites	8
1.5. Materials and methods	8
1.5.1. Materials	8
1.5.2. Nanomaterials	11
1.5.3. Method	14
1.5.3.1. Preparation of polyurethane	14
1.5.3.2. Preparation of polymer nanocomposite	14
1.6. Characterization	16
1.6.1. Nuclear magnetic resonance (NMR) spectroscopy	16

1.6.2. X-ray diffraction (XRD) study	17
1.6.3. Fourier transformed infrared spectroscopy (FTIR)	17
1.6.4. Scanning electron microscopy (SEM)	17
1.6.5. Transmission electron microscopy (TEM)	18
1.6.6. Thermo-gravimetric analysis (TGA)	18
1.6.7. Differential scanning calorimetry (DSC)	18
1.6.8. Raman spectroscopy	19
1.6.9. Vibrating sample magnetometric study	19
1.6.10. Biodegradation testing	19
1.6.11. Testing for shape memory behaviour	19
1.7. Property	21
1.7.1. Mechanical property	21
1.7.2. Thermal property	22
1.7.3. Magnetic property	22
1.7.4. Biodegradation behaviour	22
1.7.5. Shape memory property	23
1.8. Applications of shape memory polymers	24
1.9. Short review on shape memory polyurethane nanocomposites	27
1.10. Scopes and objectives of the present investigation	32
1.11. Plans of the present work	33
References	35

## ***Chapter 2***

### **Vegetable oil based hyperbranched polyurethanes**

2A. Effect of Different Vegetable Oils	46
2A.1. Introduction	46
2A.2. Experimental	47
2A.2.1. Materials	47
2A.2.2. Preparation of monoglyceride of the oil	48
2A.2.3. Synthesis of hyperbranched polyurethane	49

2A.2.4. Instrumentation	49
2A.2.5. Shape memory behavior testing	51
2A.3. Results and discussion	52
2A.3.1. Infrared spectroscopic study	52
2A.3.2. XRD study	52
2A.3.3. NMR study	52
2A.3.4. Thermal property	55
2A.3.5. Mechanical property	57
2A.3.6. Shape memory study	58
2A.4. Conclusion	59
2B. Effect of vegetable oil content	60
2B.1. Introduction	60
2B.2. Experimental	61
2B.2.1. Materials	61
2B.2.2. Synthesis of hyperbranched polyurethane	61
2B.2.3. Instrumentation	61
2B.3. Results and discussion	62
2B.3.1. Infrared spectroscopic study	62
2B.3.2. NMR study	63
2B.3.3. XRD study	64
2B.3.4. Morphological study	65
2B.3.5. Thermal property	65
2B.3.6. Mechanical property	67
2B.3.7. Chemical resistance	67
2B.3.8. Shape memory property	68
2B.4. Conclusion	69
2C. Effect of multifunctional component	70
2C.1. Introduction	70
2C.2. Experimental	71
2C.2.1. Materials	71

2C.2.2. Preparation of hyperbranched polyurethane	71
2C.2.3. Instrumentation	72
2C.3. Results and discussion	72
2C.3.1. Infrared spectroscopic study	72
2C.3.2. NMR study	73
2C.3.3. X-ray diffraction study	74
2C.3.4. Thermal property	75
2C.3.5. Mechanical property	77
2C.3.6. Shape memory property	78
2C.3.7. Chemical resistance	79
2C.4. Conclusion	80
References	81

## ***Chapter 3***

### **Modified hyperbranched polyurethane**

3.1. Introduction	86
3.2. Experimental	87
3.2.1. Materials	87
3.2.2. Preparation of hyperbranched polyurethane	87
3.2.3. Modification of hyperbranched polyurethane with epoxy resin	87
3.2.4. Broth culture technique for biodegradation	88
3.2.5. Instrumentation	88
3.3. Results and discussion	89
3.3.1. Curing study	89
3.3.2. Infrared spectroscopic study	91
3.3.3. X-ray diffraction study	91
3.3.4. Morphology study	93
3.3.5. Thermal property	94
3.3.6. Mechanical property	96
3.3.7. Chemical resistance	97

3.3.8. Biodegradation Study	97
3.3.9. Shape memory property	99
3.4. Conclusion	100
References	101

## **Chapter 4**

### **Hyperbranched polyurethane/Fe<sub>3</sub>O<sub>4</sub> nanocomposites**

4A. Hyperbranched thermoplastic polyurethane/Fe <sub>3</sub> O <sub>4</sub> nanocomposites	104
4A.1. Introduction	104
4A.2. Experimental	105
4A.2.1. Materials	105
4A.2.2. Preparation of Fe <sub>3</sub> O <sub>4</sub> nanoparticles	105
4A.2.3. Preparation of hyperbranched polyurethane/Fe <sub>3</sub> O <sub>4</sub> nanocomposite	105
4A.2.4. Instrumentation	106
4A.3. Results and discussion	106
4A.3.1. FTIR study	106
4A.3.2. X-ray diffraction study	107
4A.3.3. TEM study	107
4A.3.4. Thermal property	109
4A.3.5. Mechanical property	110
4A.3.6. Magnetic property	112
4A.3.7. Shape memory property	112
4A.4. Conclusion	115
4B. Hyperbranched polyurethane/Fe <sub>3</sub> O <sub>4</sub> thermosetting nanocomposites	116
4B.1. Introduction	116
4B.2. Experimental	117
4B.2.1. Materials	117
4B.2.2. Preparation of Fe <sub>3</sub> O <sub>4</sub> nanoparticles	117
4B.2.3. Preparation of hyperbranched polyurethane/Fe <sub>3</sub> O <sub>4</sub> thermosetting nanocomposite	117

4B.2.4. Instrumentation	118
4B.3. Results and discussion	118
4B.3.1. Curing study	118
4B.3.2. FTIR study	120
4B.3.3. X-ray diffraction study	120
4B.3.4. TEM study	122
4B.3.5. Thermal property	122
4B.3.6. Mechanical property	124
4B.3.7. Magnetic property	125
4B.3.8. Shape memory property	126
4B.4. Conclusion	128
References	129

## ***Chapter 5***

### **Hyperbranched polyurethane/MWCNT nanocomposites**

5A. Hyperbranched thermoplastic polyurethane/triethanolamine functionalized MWCNT nanocomposites	132
5A.1. Introduction	132
5A.2. Experimental	133
5A.2.1. Materials	133
5A.2.2. Modification of MWCNT	133
5A.2.3. Preparation of hyperbranched polyurethane/TEA-f-MWCNT nanocomposites	133
5A.2.4. Instrumentation	134
5A.3. Results and discussion	134
5A.3.1. FTIR study	134
5A.3.2. Raman spectroscopic study	136
5A.3.3. X-ray diffraction study	136
5A.3.4. Morphology study	137
5A.3.5. Thermal property	139

5A.3.6. Mechanical property	139
5A.3.7. Shape memory property	142
5A.4. Conclusion	144
5B. Hyperbranched thermosetting polyurethane/triethanolamine functionalized MWCNT nanocomposites	145
5B.1. Introduction	145
5B.2. Experimental	146
5B.2.1. Materials	146
5B.2.2. Modification of MWCNT	146
5B.2.3. Preparation of hyperbranched thermosetting polyurethane/TEA-f-MWCNT nanocomposites	146
5B.2.4. Instrumentation	146
5B.3. Results and discussion	147
5B.3.1. Curing study	147
5B.3.2. FTIR study	147
5B.3.3. XRD study	149
5B.3.4. Morphology study	150
5B.3.5. Thermal property	152
5B.3.6. Mechanical property	152
5B.3.7. Shape memory property	155
5B.4. Conclusion	156
References	157

## ***Chapter 6***

### **Fe<sub>3</sub>O<sub>4</sub> nanoparticles decorated MWCNT/hyperbranched polyurethane nanocomposites**

6A. Fe <sub>3</sub> O <sub>4</sub> nanoparticles decorated MWCNT/hyperbranched polyurethane thermoplastic nanocomposites	160
6A.1. Introduction	160
6A.2. Experimental	160

6A.2.1. Materials	160
6A.2.2. Preparation of Fe <sub>3</sub> O <sub>4</sub> decorated MWCNT (Fe <sub>3</sub> O <sub>4</sub> -MWCNT)	161
6A.2.3. Preparation of Fe <sub>3</sub> O <sub>4</sub> -MWCNT/hyperbranched polyurethane nanocomposites	161
6A.2.4. Instrumentation	162
6A.3. Results and discussion	162
6A.3.1. FTIR study	162
6A.3.2. Raman spectroscopic study	163
6A.3.3. X-ray diffraction study	165
6A.3.4. Morphology study	166
6A.3.5. Thermal property	168
6A.3.6. Mechanical property	169
6A.3.7. Shape memory property	170
6A.4. Conclusion	171
6B. Fe <sub>3</sub> O <sub>4</sub> nanoparticles decorated MWCNT/hyperbranched polyurethane thermosetting nanocomposites	172
6B.1. Introduction	172
6B.2. Experimental	172
6B.2.1. Materials	172
6B.2.2. Preparation of Fe <sub>3</sub> O <sub>4</sub> -MWCNT nanohybrid	173
6B.2.3. Preparation of thermosetting hyperbranched polyurethane/Fe <sub>3</sub> O <sub>4</sub> -MWCNT nanocomposites	173
6B.2.4. Instrumentation	173
6B.3. Results and discussion	174
6B.3.1. Curing study	174
6B.3.2. FTIR study	175
6B.3.3. X-ray diffraction study	175
6B.3.4. Magnetic property	175
6B.3.5. Morphology study	178
6B.3.6. Thermal property	178



6B.3.7. Mechanical property	180
6B.3.8. Shape memory property	183
6B.4. Conclusion	184
References	185

## ***Chapter 7***

### **Conclusions and future directions**

7.1. Summary and conclusions	189
7.2. Future directions	191
List of Publications	192
Conference/symposium	193

## ***LIST OF ABBREVIATIONS AND SYMBOLS***

---

b.p.	boiling point
cm <sup>3</sup>	cubic centimeter
cm	centimeter(s)
CNTs	carbon nanotubes
DSC	differential scanning calorimetry
°C	degree centigrade
FTIR	fourier transform infrared spectroscopy
F <sub>w</sub>	formula weight
g	gram(s)
kg	kilogram(s)
h	hour(s)
H <sub>c</sub>	coercivity
m	meter(s)
min	minute(s)
mL	milliliter
mm	millimeter
mol	mole
m.p.	melting point
MPa	megapascal
M <sub>n</sub>	number average molecular weight
M <sub>r</sub>	remanence magnetization
M <sub>w</sub>	weight average molecular weight
MWCNT	multi walled carbon nanotubes
NMR	nuclear magnetic resonance
nm	nano meter(s)
OD	optical density
ppm	parts per million
s	second(s)

SEM	scanning electron microscope
SWCNT	single walled carbon nanotube
TEM	transmission electron microscope
T <sub>g</sub>	glass transition temperature
TGA	thermogravimetric analysis
TMS	tetramethylsilane
UTM	universal testing machine
v	volume
wt	weight
XRD	X-ray diffraction
μm	micrometer
μL	microliter
%	percentage
θ	scattering angle

## ***LIST OF TABLES***

---

- Table 1.1: Comparison of the properties of SMP and SMA
- Table 1.2: Diisocyanates used for the synthesis of polyurethanes
- Table 1.3: Macroglycols used for the synthesis of polyurethanes
- Table 1.4: Chain extender used for the synthesis of polyurethanes
- Table 2A.1: Structure and composition of fatty acid of the vegetable oil
- Table 2A.2: Composition (mmol) of reactant
- Table 2A.3: Mechanical properties of the hyperbranched polyurethanes
- Table 2A.4: Shape memory behavior of hyperbranched polyurethanes
- Table 2B.1: Composition (mol) of reactant
- Table 2B.2: Mechanical properties of the hyperbranched polyurethanes
- Table 2B.3: Chemical resistance as changes of weight (g) of hyperbranched polyurethanes
- Table 2B.4: Shape memory properties of hyperbranched polyurethanes
- Table 2C.1: Composition (mmol) of reactant
- Table 2C.2: FTIR spectral data of the hyperbranched polyurethanes
- Table 2C.3: Thermal properties of hyperbranched polyurethanes
- Table 2C.4: Mechanical properties of the hyperbranched polyurethanes
- Table 2C.5: Shape memory properties of hyperbranched polyurethanes
- Table 2C.6: Chemical resistance as changes of weight (g) of hyperbranched polyurethanes
- Table 3.1: Composition and curing time of modified hyperbranched polyurethane at 120 °C
- Table 3.2: Mechanical properties of unmodified and modified hyperbranched polyurethanes
- Table 3.3: Chemical resistance as changes of weight (g) of unmodified and modified hyperbranched polyurethanes
- Table 3.4: Shape memory properties of hyperbranched polyurethane and modified hyperbranched polyurethane
- Table 4A.1: Mechanical properties of hyperbranched polyurethane and the nanocomposites
- Table 4A.2: Shape memory behaviors of hyperbranched polyurethane and the nanocomposites
- Table 4B.1: Composition and curing time of the nanocomposites at 120 °C
- Table 4B.2: Melting temperature and melting enthalpy of the thermosetting nanocomposites

Table 4B.3: Mechanical properties of hyperbranched polyurethane and the thermosetting nanocomposites

Table 4B.4: Shape memory behaviors of hyperbranched polyurethane and the nanocomposites

Table 5A.1: Mechanical properties of hyperbranched polyurethane and its nanocomposites

Table 5A.2: Shape memory behaviors of hyperbranched polyurethane and its nanocomposite at different microwave output powers\*

Table 5B.1: Composition and curing time of the nanocomposites at 120 °C

Table 5B.2: Mechanical properties of hyperbranched polyurethane and the nanocomposites

Table 6A.1: Mechanical properties of hyperbranched polyurethane and its nanocomposites

Table 6B.1: Compositions and curing time of the nanocomposites at 120 °C

Table 6B.2: Thermal behaviors of the hyperbranched polyurethane and its nanocomposites

Table 6B.3: Mechanical properties of hyperbranched polyurethane and its thermosetting nanocomposites

## ***LIST OF FIGURES***

---

- Fig. 1.1: Molecular mechanism of thermally induced SMP
- Fig. 1.2: (a) Single walled carbon nanotube (SWCNT) and (b) Multi-walled carbon nanotubes (MWCNT)
- Fig. 1.3: Schematic representation of the one shot method for the synthesis of polyurethane
- Fig. 1.4: Schematic representation of the pre-polymerization method for the synthesis of polyurethane
- Fig. 1.5: (a) The device first punctures the clot, (b) activate to a form of coil shape on the distal side of the clot and (c) pulled to remove both the device and clot simultaneously
- Fig. 1.6: A dialysis needle (a) is shown to produce jet impingent of flow (b), however, with the SMP adapter (c) the turbulence of the flow is decreased
- Fig. 1.7: The representative image of the vascular stents
- Fig. 1.8: The utilization of shape memory wire in orthodontic application
- Fig. 1.9: The use of shape memory polymer in surgical sutures
- Fig. 1.10: Fields of application for shape memory polyurethane nanocomposites
- Fig. 2A.1: FTIR spectra for (a) CHBPU10, (b) MHBPU10, (c) SHBPU10 and (d) HBPU
- Fig. 2A.2: X-ray diffractograms for (a) CHBPU10, (b) MHBPU10, (c) SHBPU10 and (d) HBPU
- Fig. 2A.3: <sup>1</sup>H-NMR spectra for (a) CHBPU10, (b) SHBPU10, (c) MHBPU10 and (d) HBPU
- Fig. 2A.4: TGA thermograms for (a) MHBPU10, (b) SHBPU10, (c) HBPU and (d) CHBPU10
- Fig. 2A.5: DSC curves for (a) CHBPU10, (b) MHBPU10, (c) SHBPU10 and (d) HBPU
- Fig. 2A.6: Shape memory behaviors of hyperbranched polyurethanes (a) original shape, (b) extended shape, (c) fixed shape and (d) recovered shape
- Fig. 2B.1: FTIR spectra for (a)HBPU, (b)MHBPU5, (c)MHBPU10 and (d)MHBPU15
- Fig. 2B.2: The <sup>1</sup>H NMR spectrum of hyperbranched polyurethane (MHBPU5)
- Fig. 2B.3: XRD diffractograms for (a)HBPU, (b)MHBPU5, (c)MHBPU10 and (d)MHBPU15
- Fig. 2B.4: SEM micrographs for (a)HBPU, (b)MHBPU5, (c)MHBPU10 and (d)MHBPU15
- Fig. 2B.5: Thermograms for (a)HBPU, (b)MHBPU5, (c)MHBPU10 and (d)MHBPU15
- Fig. 2B.6: Shape memory behaviors of hyperbranched polyurethanes (a) original shape, (b) stretched shape and (c) fixed shape
- Fig. 2C.1: FTIR spectra for (a)MHBPU0, (b)MHBPU10 and (c)MHBPUT5

Fig. 2C.2:  $^1\text{H}$  NMR spectrum of hyperbranched polyurethane (MHBPUT5)

Fig. 2C.3: X-ray diffractograms for (a)MHBPU0, (b)MHBPU10 and (c)MHBPUT5

Fig. 2C.4: Thermograms for (a) MHBPU0, (b)MHBPU10 and (c)MHBPUT5

Fig. 2C.5: DSC curves for (a) MHBPU0, (b)MHBPU10 and (c)MHBPUT5

Fig. 2C.6: Shape memory behaviors of hyperbranched polyurethanes (a) original shape, (b) extended shape, (c) fixed shape and (d) recovered shape

Fig. 3.1: FTIR spectra for (a) MHBPU10, (b) CEHPU30 before curing, (c) CEHPU10 after curing, (d) CEHPU20 after curing and (e) CEHPU30 after curing

Fig. 3.2: XRD diffracto-grams for (a) MHBPU10, (b) CEHPU10, (c) CEHPU20 and (d) CEHPU30

Fig. 3.3: SEM micrographs for (a) MHBPU10, (b) CEHPU10, (c) CEHPU20 and (d) CEHPU30

Fig. 3.4: TGA thermo-grams for (a) MHBPU10, (b) CEHPU10, (c) CEHPU20 and (d) CEHPU30

Fig. 3.5: DSC curves for (a) MHBPU10, (b) CEHPU10, (c) CEHPU20 and (d) CEHPU30

Fig. 3.6: Growth profiles of *P. aeruginosa* strain, MTCC 7814 for (a) MHBPU10, (b) CEHPU10, (c) CEHPU20 and (d) CEHPU30

Fig. 3.7: SEM micrographs for (a) MHBPU10, (b) CEHPU10, (c) CEHPU20 and (d) CEHPU30 after biodegradation

Fig. 3.8: Shape memory behaviors of hyperbranched polyurethane and it modified systems (a) original shape, (b) extended shape, (c) fixed shape and (d) recovered shape

Fig. 4A.1: FTIR spectra for (a)  $\text{Fe}_3\text{O}_4$ , (b) MHBPU10, (c) HPU2, (d) HPU5 and (e) HPU10

Fig. 4A.2: XRD diffractograms for (a)  $\text{Fe}_3\text{O}_4$ , (b) MHBPU10, (c) HPU2, (d) HPU5 and (e) HPU10

Fig. 4A.3: TEM image of HPU5

Fig. 4A.4: TGA thermograms for (a) MHBPU10, (b) HPU2, (c) HPU5 and (d) HPU10

Fig. 4A.5: DSC curves for (a) MHBPU10, (b) HPU2, (c) HPU5 and (d) HPU10

Fig. 4A.6: Magnetic hysteresis loops for (a)  $\text{Fe}_3\text{O}_4$  and (b) HPU2

Fig. 4A.6: Shape memory behaviors of hyperbranched polyurethane and the nanocomposites (a) original shape and (b) fixed shape

Fig. 4B.1: FTIR spectra of (a)  $\text{Fe}_3\text{O}_4$ , (b) MHBPU10, (c) EHPU2 before curing, (d) EHPU2, (e) EHPU5 and (f) EHPU10

Fig. 4B.2: XRD diffractograms of (a)  $\text{Fe}_3\text{O}_4$ , (b) MHBPU10, (c) EHPU2, (d) EHPU5 and (e) EHPU10

Fig. 4B.3: TEM image and distribution of nanoparticles for EHPU5

Fig. 4B.4: DSC curves of (a) MHBPU10, (b) EHPU2, (c) EHPU5 and (d) EHPU10

Fig. 4B.5: TGA thermograms of (a) MHBPU10, (b) EHPU2, (c) EHPU5 and (d) EHPU10

Fig. 4B.6: *Magnetic hysteresis loop for EHPU5*

Fig. 4B.7: Shape memory behaviors of the hyperbranched polyurethane and the thermoset nanocomposites (a) original shape and (b) fixed shape

Fig. 5A.1: FTIR spectra for (a) pristine MWCNT, (b) acid treated MWCNT and (c) TEA-f-MWCNT

Fig. 5A.2: FTIR spectra for (a) MHBPU10, (b) HPUCNT0.2, (c) HPUCNT1 and (d) HPUCNT2

Fig. 5A.3: Raman spectra for (a) pristine MWCNT, (b) a-MWCNT and (c) TEA-f-MWCNT

Fig. 5A.4: XRD diffractograms for (a) TEA-f-MWCNT, (b) MHBPU10, (c) HPUCNT0.2, (d) HPUCNT1 and (e) HPUCNT2

Fig. 5A.5: SEM micrographs for (a) MHBPU10, (b) HPUCNT0.2, (c) HPUCNT1 and (d) HPUCNT2

Fig. 5A.6: TEM image for HPUCNT1

Fig. 5A.7: TGA thermograms for (a) MHBPU10, (b) HPUCNT0.2, (c) HPUCNT1 and (d) HPUCNT2

Fig. 5A.8: DSC curves for (a) MHBPU10, (b) HPUCNT0.2, (c) HPUCNT1 and (d) HPUCNT2

Fig. 5A.9: Shape memory behaviors of hyperbranched polyurethane and its nanocomposites at microwave output power 455 W (a) original shape and (b) fixed shape

Fig. 5B.1: FTIR spectra for (a) MHBPU10, (b) BEHPUCNT1, (c) EHPUCNT0.2, (d) EHPUCNT1 and (e) EHPUCNT2

Fig. 5B.2: XRD diffractograms for (a) TEA-f-MWCNT, (b) MHBPU10, (c) EHPUCNT0.2, (d) EHPUCNT1 and (e) EHPUCNT2

Fig. 5B.3: SEM micrographs for (a) MHBPU10, (b) EHPUCNT0.2, (c) EHPUCNT1 and (d) EHPUCNT2



Fig. 5B.4: TEM image of EHPUCNT1

Fig. 5B.5: TGA thermographs for (a) MWCNT, (b) a-MWCNT and (c) TEA-f-MWCNT

Fig. 5B.6: TGA thermograms for (a) MHBPU10, (b) EHPUCNT0.2, (c) EHPUCNT1 and (d) EHPUCNT2

Fig. 5B.7: DSC curves for (a) MHBPU10, (b) EHPUCNT0.2, (c) EHPUCNT1 and (d) EHPUCNT2

Fig. 5B.8: Shape memory behaviors of hyperbranched polyurethane and its nanocomposites at microwave output power 455 W (a) original shape and (b) fixed shape

Fig. 6A.1: FTIR spectra for (a) pristine MWCNT, (b) a-MWCNT, (c) Fe<sub>3</sub>O<sub>4</sub> and (d) Fe<sub>3</sub>O<sub>4</sub>-MWCNT

Fig. 6A.2: FTIR spectra for (a) MHBPU10, (b) HPUFCNT0.2, (c) HPUFCNT1 and (d) HPUFCNT2

Fig. 6A.3: Raman spectra for (a) pristine MWCNT, (b) a-MWCNT and (c) Fe<sub>3</sub>O<sub>4</sub>-MWCNT

Fig. 6A.4: XRD diffractograms for (a) a-MWCNT, (b) Fe<sub>3</sub>O<sub>4</sub> and (c) Fe<sub>3</sub>O<sub>4</sub>-MWCNT

Fig. 6A.5: XRD diffractograms for (a) MHBPU10, (b) HPUFCNT0.2, (c) HPUFCNT1 and (d) HPUFCNT2

Fig. 6A.6: TEM image for (a) a-MWCNT, (b) and (c) Fe<sub>3</sub>O<sub>4</sub>-MWCNT and (d) HPUFCNT1

Fig. 6A.7: Dispersion stability in DMF for (a) pristine MWCNT, (b) Fe<sub>3</sub>O<sub>4</sub>-MWCNT and (c) response of Fe<sub>3</sub>O<sub>4</sub>-MWCNT to a magnet

Fig. 6A.8: TGA thermograms for (a) MHBPU10, (b) HPUFCNT0.2, (c) HPUFCNT1 and (d) HPUFCNT2

Fig. 6A.9: DSC curves for (a) MHBPU10, (b) HPUFCNT0.2, (c) HPUFCNT1 and (d) HPUFCNT2

Fig. 6A.10: Shape memory behaviors of hyperbranched polyurethane and the nanocomposites under microwave stimulus (a) original shape and (b) fixed shape

Fig. 6B.1: FTIR spectra for (a) MHBPU10, (b) EHPUFCNT0.2 (before curing), (c) EHPUFCNT0.2, (d) EHPUFCNT1 and (e) EHPUFCNT2

Fig. 6B.2: XRD diffractograms for (a) MHBPU10, (b) EHPUFCNT0.2, (c) EHPUFCNT1 and (d) EHPUFCNT2

Fig. 6B.3: Magnetic hysteresis loops for (a) Fe<sub>3</sub>O<sub>4</sub>-MWCNT and (b) EHPUFCNT0.2

Fig. 6B.4: TEM images for (a) a-MWCNT, (b) and (c) Fe<sub>3</sub>O<sub>4</sub>-MWCNT and (d) EHPUFCNT1

Fig. 6B.5: (I) TGA thermograms for (a) MHBPU10, (b) EHPUFCNT0.2, (c) EHPUFCNT1 and

(d) EHPUFCNT2, and (II) DTG curves for (a) MHBPU10, (b) EHPUFCNT0.2, (c)

EHPUFCNT1 and (d) EHPUFCNT2

Fig. 6B.6: DSC curves for (a) MHBPU10, (b) EHPUFCNT0.2, (c) EHPUFCNT1 and (d)

EHPUFCNT2

Fig. 6B.7: Shape memory behaviors of hyperbranched polyurethane and the thermosetting

nanocomposites under microwave stimulus (a) original shape and (b) fixed shape

## ***LIST OF SCHEMES***

---

Scheme 2A.1: Synthesis of hyperbranched polyurethane

Scheme 3.1: Proposed crosslinking reactions

Scheme 4B.1: Proposed crosslinking reactions

Scheme 5B.1: Proposed crosslinking reactions

Scheme 6B.1: Proposed crosslinking reactions

## ***Chapter 1***

### **General introduction**

#### ***Highlights***

This chapter provides the general introduction of the present investigation. It includes brief descriptions on biobased polyurethanes and nanocomposites, different characterization techniques such as FTIR, XRD, TGA, DSC, SEM, TEM etc. as well as various properties including shape memory behaviors for them. The importance of shape memory polyurethanes and the mechanism of shape memory behaviors are presented here. The chapter describes the importance of nanomaterials in the domain of polymer nanocomposites. The testing methods such as stretching and bending for shape memory behaviors of polymers are discussed here. This chapter provides various applications of shape memory polymers. The scopes, objectives and plans of the present investigation are also included here.

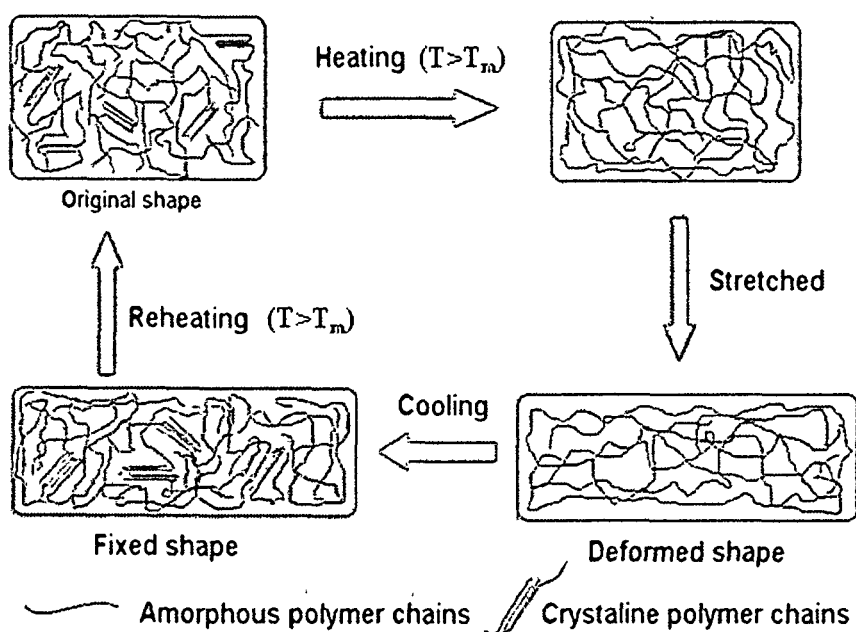
## 1.1. Introduction

Shape memory polymers (SMP) have generated immense interest in recent times because of their potential applications in different fields such as smart actuators, aerospace engineering, textile engineering and most importantly as intelligent biomedical devices.<sup>1-15</sup> Ni-Ti alloy (Nitinol) is the most widely used shape memory material because of its good shape memory performance, good processability, excellent mechanical properties, good biocompatibility etc. However the shape memory alloys (SMA) have some limitations such as low deformation rate, high stiffness, high cost, non biodegradability etc. SMP have some advantages such as easier processing, lighter weight, lower cost, larger recoverable strain and lower toxicity as compared to the SMA (Table 1.1). SMP are smart materials that can change their shapes when exposed to a suitable external stimulus such as heat, light, moisture, magnetic field or electric field etc.<sup>16-23</sup> The recovery of original shape from the deliberated fixed temporary shape is known as the shape memory effect. The shape memory behaviors i.e. the shape fixity and shape recovery of polymer network are the freezing and activation of the molecular chains below and above a transition temperature ( $T_{\text{trans}}$ ), respectively. The extent to which the switching segment is able to fix the temporary shape and to recover the original shape on exposure of stimulus is called the shape fixity and shape recovery, respectively. The shape recovery time is a shape memory property which refers to the time that SMP used to take recover the permanent shape from its fixed temporary shape. The transition temperature can be either a glass transition temperature ( $T_g$ ) or a melting temperature ( $T_m$ ).<sup>24-26</sup> For the amorphous polymers,  $T_g$  is considered as the transition temperature; whereas for crystalline polymers,  $T_m$  is considered as the transition temperature. On the other hand for the semi-crystalline polymers, either  $T_g$  or  $T_m$  can be used as the transition temperature. However,  $T_m$  is being considered as the preferred transition temperature because it is sharper than the  $T_g$ .<sup>27, 28</sup> The molecular mechanism of thermally induced SMP through which the shape memory effect observed is shown in Fig 1.1.

Now, most of the polymers showed the shape memory behaviors because polymer chains have the tendency to form network structures. However, due to the structural disadvantages (too low or too high  $T_{\text{trans}}$  or weak mechanical properties), limited numbers of SMP are used in practical applications. A few examples of thermosetting SMP are polyethylene,<sup>29</sup> polyisoprene,<sup>30</sup>

**Table 1.1:** Comparison of the properties of SMP and SMA

Physical properties	SMP	SMA
Density ( $\text{g/cm}^3$ )	0.9-1.1	6-8
Extent of deformation (%)	250-800	<8
Force required for deformation (MPa)	1-3	50-200
Recovery temperature ( $^{\circ}\text{C}$ )	25-90	-10-100
Recovery stress (MPa)	1-3	150-400
Processing conditions	<200 $^{\circ}\text{C}$ , low pressure	>1000 $^{\circ}\text{C}$ , high pressure

**Fig. 1.1:** Molecular mechanism of thermally induced SMP

polynorbornene,<sup>31</sup> styrene-butadiene copolymers,<sup>32</sup> polyurethane etc., whereas thermoplastics are polyurethane, block copolymers of polyethylene-nylon 6 and polyethylene-poly(vinyl acetate), copolymer based ionomers etc. Among different SMP, polyurethanes are the most versatile due to their biocompatibility, wide range tunable stiffness, large deformation, large recovery, good elastic property, water vapor permeability and multi responsive shape memory effect.<sup>33-38</sup> The segmented block polyurethanes are made up of alternating soft and hard segments. Owing to the polar character of urethane groups, the hard urethane domains are more hydrophilic in contrast to

the soft polyol domains that cause the micro-phase separation in the structure. The soft segment of the polyurethanes is usually moderately high-molecular weight long chain polyol which is flexible in nature. The hard segment is composed of diisocyanate with low-molecular weight diol or diamine chain extender and hence is rigid. The flexible soft segments are responsible for the reversible phase transformation that allows for the shape memory effect, while the hard segments are responsible for the memorizing of permanent shape. The shape memory properties as well as the performance of the polyurethanes can be tailored by the judicious variation of chemical constituents and the molar ratio of the hard and soft segments.<sup>39-43</sup>

Recently the hyperbranched polymers have taken tremendous attentions in the development of advanced polymeric materials because of their unique characters. The hyperbranched polymers are highly branched macromolecules with significantly less regular structural architecture and contain a number of surface defects and missing branches.<sup>44, 45</sup> Hyperbranched polymer was first coined by Kim and Webster in 1988 when the authors synthesized soluble hyperbranched polyphenylene.<sup>46, 47</sup> Hyperbranched polymers exhibited some special properties like low melt and solution viscosity, high solubility and chemical reactivity, enhanced compatibility, compact three dimensional non-entangled globular structures etc. Generally, two synthetic techniques are being used for the synthesis of such hyperbranched polymers. These are single-monomer methodology and double-monomer methodology. Among different approaches, step-growth polycondensation method of  $AB_n$  monomers is widely used to prepare a broad range of hyperbranched polymers. Again,  $A_2 + B_3$  approach is preferred to use largely now-a-days, because of its several advantages. These include easy availability of the reactants, tuning of property particularly mechanical property by using long segmented reactant etc. Thus the use of  $A_2 + B_3$  approach may offer a unique route and the resulted polymer exhibits the unique architectural features.

Furthermore, realization of finite petroleum resources, growing environmental concerns and waste disposal problems encourage utilization of bio resources like vegetable oils as raw materials for the preparation of polymeric materials.<sup>48, 49</sup> This is due to the fact that such oils have numerous advantages such as easy availability, relatively inexpensive, versatility in structure and property, inherent biodegradability and environmentally benign.<sup>50-53</sup> Again, hydroxylation of vegetable oils is one of the good approaches to obtain the required polyols to be

used as diol chain extenders in polyurethane syntheses. Properties of the vegetable oil based polyurethane depend on the characteristics like physical and chemical structures, which include the number of hydroxyl groups in the polyols, degree of unsaturation, length of the fatty acid chains and position of hydroxyl groups in the fatty acid chain. The vast forest resources and farm lands of India, particularly the North-Eastern region yields a large variety of oil bearing seeds. *Mesua ferrea* L. (Nahar) is such a plant, which has remarkable potential and its seeds surprisingly contain high amount (70%) of oil. This oil possesses mainly triglycerides of oleic (52.3%), linoleic (22.3%), palmitic (15.9%) and stearic (9.5%) acids.<sup>54, 55</sup>

The demands of the advanced applications required high performance polymeric materials. Recently polymer nanocomposites have taken commendable role in the domain of materials due to the significant improvement of many desired properties like mechanical strength, thermal, gas barrier, solvent resistance, flame retardant, shape memory and biodegradability of the neat polymers.<sup>56-62</sup> Polymer nanocomposites are the combination of two or more phases in which the domain of one phase must be in nano range (1-100 nm). This represents a better alternative to the conventional filled polymers or composites systems. The properties of nanocomposites depend on the various factors such as size and nature of the nanomaterial, aspect ratio, surface functionality, distribution of nanomaterial and interaction of nanomaterial in the polymer matrix.

Studies on vegetable oil based hyperbranched polyurethane nanocomposites with different nanomaterials, thus, will be a good proposition in recent times in the niche of advanced polymeric materials.

## **1.2. Background**

Polyurethanes are versatile polymeric materials with a wide range of physical and chemical properties. This polymer is first synthesized by Otto Bayer in the I.G. Farben laboratories way back in 1937.<sup>63</sup> In 1950's, polyurethane chemistry started to develop rapidly with toluene diisocyanate (TDI) and the first polyether polyol was reported from Dow Chemical. Again, the origin of shape memory effect can be traced back to 1932, though after the discovery of nickel-titanium alloy as shape memory material in 1963 led to real interest on the subject.<sup>64, 65</sup> The shape memory polyurethane was discovered by the Mitsubishi in 1988. A large number of



reports are available in the literature on the effect of different hard segments content on the mechanical, thermal and shape memory properties of polyurethane. Yang et al. studied the effect of different diisocyanates on the shape memory behaviors of polyurethanes.<sup>66</sup>

The term nanocomposite was first proposed by Theng in 1970.<sup>67</sup> Among different types of nanomaterials carbon nanotubes (CNT), which was discovered by Iijima in 1991,<sup>68</sup> opened the door to augment the performance and shape memory behaviors of polymer by incorporating small amount of it into the polymer matrix. Ajayan et al. reported the first polymer nanocomposites using CNT as a filler.<sup>69</sup> Koerner et al. reported that incorporation of 0.5–10 vol% of multiwall carbon nanotubes (MWCNT) into polyurethane matrix to fabricate thermoplastic polymer nanocomposites with high electrical conductivity (1–10 S/cm) and enhancement of mechanical properties including increased modulus and yield stress.<sup>70</sup> Deka et al. reported the enhancement of mechanical, thermal and shape memory behaviors of vegetable oil based polyurethane by incorporation of small amount of MWCNT into the hyperbranched matrix.<sup>71</sup> Lendlein et al. have great contribution to the SMP nanocomposites for the synthesis, functionalization and biological applications of polyurethanes.<sup>14, 72, 73</sup> Mather et al. have reported the modification of SMP (polyurethane, cross-linked polycyclooctene etc.) and their nanocomposites.<sup>74-77</sup> Tobushi et al. reported the structure property relationship of shape memory polymers.<sup>78-80</sup> Again by incorporation of suitable nanomaterials into the shape memory polymer, the actuation method can be tuned. Lee et al. studied the electro-active shape memory behavior of polyurethane-CNT hybrids.<sup>23</sup> Cai et al. reported the magnetic field responsive shape memory behaviors of Fe<sub>3</sub>O<sub>4</sub>/poly( $\epsilon$ -caprolactone)-polyurethane nanocomposites.<sup>81</sup> Leng et al. reported the infrared light-active shape memory behaviors of nanocarbon particles filled styrene based polymer nanocomposites.<sup>82</sup> Thus research on polyurethane nanocomposites including vegetable oil modified hyperbranched polyurethane with different nanomaterials based nanocomposites as contact and noncontact shape memory materials has strong background to be delved into.

### **1.3. Classification of SMP**

The classification of SMP is based on the nature of their molecular structures such as amorphous or crystalline and covalently cross-linked or physically cross-linked, as described below.<sup>6, 83</sup>

### 1.3.1. Covalently cross-linked glassy polymers

This type of SMP is covalently cross-linked glassy polymers below their  $T_g$  and rubbery elastic above  $T_g$ . It shows excellent shape fixity and shape recovery due to the nature of permanent cross-linking, that can be adjusted through the extent of cross-linking. However, since the primary shape is covalently fixed, once finally processed (casting or molding) these materials are difficult to reshape thereafter. Typical examples are thermosetting styrene-butadiene copolymer, polyethylene, thermosetting polyurethanes, co-polyester etc.<sup>6</sup>

### 1.3.2. Covalently cross-linked semi-crystalline elastomers

It is similar to the above type of SMP where the permanent shapes are established through the cross-linking. However the temporary shape can be controlled through deformation above  $T_m$  of the crystallization region and subsequent cooling below the crystallization temperature. This is because of the fact that both  $T_g$  and  $T_m$  can be used as a transition temperature for this type of SMP, though in most of the cases  $T_m$  is used, as stated earlier. The shape fixity of this type of SMP can be improved by choosing a relatively lower temperature compared to  $T_{trans}$  and that low temperature should be such so that it allows to a high degree of crystallization. The shape recovery speed is generally faster for this type of SMP as  $T_m$  is a first-order transition and a sharp transition. This class of materials includes bulk polymers, such as semi-crystalline polymers, liquid crystal elastomers and hydrogels with phase separated crystalline microdomains. Thermosetting semicrystalline polyisoprene, polycyclooctenes, polycaprolactone etc. are examples of this class.<sup>6</sup>

### 1.3.3. Physically cross-linked glassy polymers

In this SMP, the rigid amorphous domains serve as physical cross-links through the van der Waals forces, polar-polar interactions, hydrogen bonding etc. and afford the required elasticity for shape memory effect. These are mainly phase-separated block copolymers. When the temperature is higher than the  $T_g$  of these discrete physical domains, the material will be deformed easily that can be processed and reshaped. Another phase of lower  $T_g$  which softens to a rubbery state and fixes a secondary shape on cooling below  $T_g$ , present in the system. The

majority of SMP in this category are segmented shape memory thermoplastic amorphous polyurethanes.

#### 1.3.4. Physically cross-linked semi-crystalline block copolymers

In this SMP the soft domains are crystallized and  $T_m$  is used as the transition temperature for shape recovery. These polymers generally have hard and soft domain structures. The properties can be tailored by varying the hard to soft domain ratio. The secondary shapes are thus fixed by crystallization of the soft domains. The polyethylene oxide-co-polyethylene terephthalate, polystyrene-co-poly(butadiene) and the thermoplastic segmented shape memory semi-crystalline polyurethanes fall in this category.

### 1.4. Classification of polymer nanocomposites

Depending on the dimension of the nanomaterials, nanocomposites can be divided into three different categories. In the first category of polymer nanocomposites, all three dimensions of the nanomaterials are in the nano region. The spherical nanoparticles like zeolites, metal, metal oxides etc. containing polymer nanocomposites fall in this category.

In the second class of polymer nanocomposites, two dimensions of the nanomaterials are in the nano region, whereas the third dimension may be a few micrometers. Carbon nanotube, carbon nanofibre etc. nanomaterials based polymer nanocomposites are the examples of this class.

The polymer nanocomposites, where only one dimension of the nanomaterials is in the nano region, while other two dimensions are in micrometer size are categorized in third class of nanocomposites. Most of the cases the nanomaterials are in layer structure like silicate layers, clay etc. and such nanomaterials based polymer nanocomposites are included in this category.

### 1.5. Materials and methods

#### 1.5.1. Materials

*Polyurethane*

Polyurethanes are linear polymers that have a molecular backbone containing carbamate groups (-NHCOO-). These groups, called urethane, are produced through a rearrangement reaction between a diisocyanate and a polyol. The polyols used in preparation of polyurethanes are of two types, viz. macroglycol and chain extender. The brief descriptions of these components are presented below.

#### *Diisocyanate*

Isocyanates are highly reactive compounds and can readily react with the groups containing active hydrogen. These reactions are most important in the formation of polyurethanes. The properties of the polyurethane largely depend on the structure of isocyanate. The most commonly used diisocyanates in polyurethane synthesis are listed in Table 1.2. The most widely used diisocyanates for the preparation of polyurethanes are toluene diisocyanate (TDI) and 4,4'-diphenylmethane diisocyanate (MDI). In most of the cases TDI used is a mixture of the 2,4- and 2,6- isomers in 80:20 mol ratio. Similarly, MDI has three isomers namely 4,4-, 2,4-, and 2,2-diphenyl methane diisocyanates. However, 4,4-isomer is used in most of the commercial polyurethanes. Though aromatic diisocyanates are more reactive than aliphatic one but polyurethanes obtained from the aromatic diisocyanates have lower oxidation and weaker ultraviolet stabilization than the polymers with aliphatic diisocyanates. However, the aromatic diisocyanates based polyurethanes exhibited good shape memory behaviors.

#### *Macroglycol*

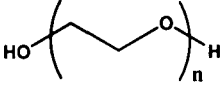
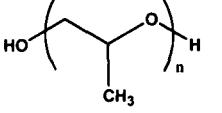
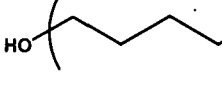
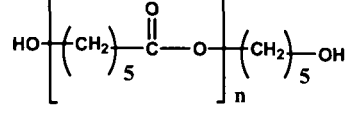
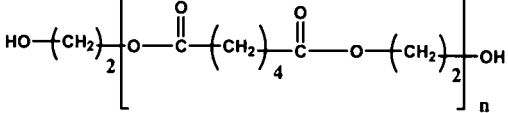
The diols/polyols with number average molecular weight 500 to 5000 g/mol are used as a macroglycol in the preparation of polyurethane. The polyols are generally categorized into two groups viz. polyether polyol and polyester polyol. The structure of the macroglycol is an important factor in governing the ultimate properties of the polyurethanes. Polyester polyols are widely used macroglycols as they exhibited excellent mechanical properties, thermal stability, outstanding tear strength and shape memory behaviors.

**Table 1.2:** Diisocyanates used for the synthesis of polyurethanes

Name of diisocyanate	Abbreviated name	Structure
2,4- and 2,6-Toluene diisocyanate	TDI	
4,4'-Methylenediphenyl diisocyanate	MDI	
1,5-Naphthalene diisocyanate	NDI	
1,6-Hexamethylene diisocyanate	HMDI	$\text{OCN}-(\text{CH}_2)_6-\text{NCO}$
1,4-Cyclohexyl diisocyanate	CHDI	
4,4'-Dicyclohexylmethane diisocyanate	DCHMDI	
Isophorone diisocyanate	IPDI	
Norbornane diisocyanate	NBDI	
<i>p</i> -Phenylene diisocyanate	PDI	

Among them, further the crystalline polycaprolactone (PCL) diol based polyurethane is the most convenient to use for the shape memory studies. The melting temperature can be used as the transition temperature. A few macroglycols used for the synthesis of polyurethanes are listed in Table 1.3.

**Table 1.3:** Macroglycols used for the synthesis of polyurethanes

Name of Polyol	Chemical structure
Polyethylene oxide (PEO)	
Polypropylene oxide (PPO)	
Polytetramethylene oxide (PTMO)	
Polycaprolactone (PCL)	
Polyethylene adipate (PEA)	

#### *Chain extender*

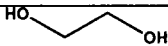
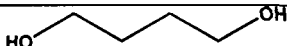
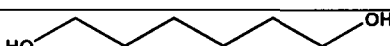
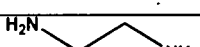
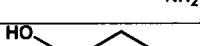
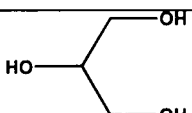
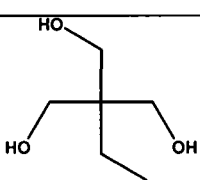
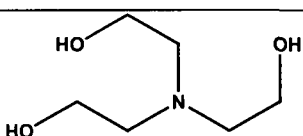
Chain extenders are low molecular weight (generally, below 400 g/mol) hydroxyl or amine compounds. The choices of chain extender and the diisocyanate determine the characteristics of the hard segment and the physical properties of the polyurethane. The most commonly used chain extenders are mentioned in Table 1.4.

#### 1.5.2. Nanomaterials

The nanomaterials with at least one of the dimensions in the region of 1-100 nm can be used as a nano-reinforcing agent in the polymer nanocomposites. The incorporation of nanomaterials in the polymer matrix significantly improves the mechanical, thermal, electrical and shape memory properties along with others. The properties of nanomaterials are remarkably

different from the bulk counterpart due to the confinement of electron wave function, their high surface area to volume ratio, and extremely high proportion of surface atom. They are of different types, though metals or their oxides and carbon nanotubes are only discussed here as these are widely used nanomaterials for tuning of shape memory property of polymers.

**Table 1.4:** Chain extender used for the synthesis of polyurethanes

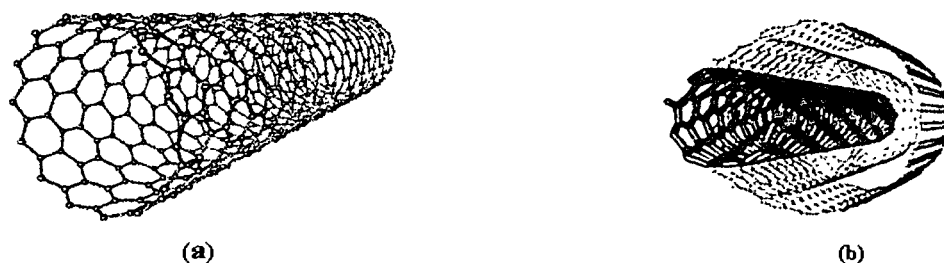
Name of chain extender	Chemical structure
Ethylene glycol	
1,4-Butanediol	
1,6-Hexanediol	
Ethylene diamine	
Ethanolamine	
Glycerol	
Trimethylol propane	
Triethanolamine	

#### *Metal/metal oxide nanoparticle*

Nanoparticles are the three dimensional nanomaterials with an average diameter smaller than 100 nm. These nanoparticles are synthesized by different methods such as co-precipitation, sol-gel, hydrothermal, microwave, sonochemical, template synthesis etc. The properties of the nanomaterials depend on the size, shape and distribution, which can be changed by changing the reaction parameters. Fe<sub>3</sub>O<sub>4</sub> nanoparticles are most widely studied metal oxide nanoparticles due to their easy synthesis, biocompatibility, magnetic property, microwave absorption characteristics etc. in shape memory polyurethane based nanocomposites.

### Carbon nanotube

Carbon nanotubes (CNT) are one dimensional tubular structure of graphitic sheet consisting of covalently bonded carbon atoms in hexagonal-type arrangement. CNT are generally classified into two classes: single wall carbon nanotube (SWCNT) and multi-walled carbon nanotubes (MWCNT) (Fig. 1.2 (a, b)). CNT are synthesized by the different techniques such as laser ablation technique, chemical vapor deposition, gas phase pyrolysis, arc discharge etc. CNT possess excellent elastic modulus ( $\sim 1$  TPa), strength ( $\sim 200$  GPa) electrical conductivity (1000 times of copper) and thermal conductivity ( $\sim 3000 \text{ Wm}^{-1}\text{K}^{-1}$ ).<sup>84, 85</sup> The dispersion of CNT in the polymer matrix is very difficult because of their strong van der Waals forces and numerous  $\pi$ - $\pi$  interactions between the tubes. Two different techniques are used for the modification of CNT viz. covalent and non-covalent techniques. Covalent modification based on the formation of covalent bond between the CNT and the attached functionality. On the other hand, non covalent modification is mainly the adsorption of functional molecules on the surface of the nanotube through various interactions such as van der Waals forces, hydrogen bonding, hydrophobic interaction, electrostatic forces and  $\pi$ - $\pi$  interactions.<sup>86, 87</sup> Again the decoration of CNT with the nanomaterials like ZnO, Cu, Fe,  $\text{Fe}_3\text{O}_4$  etc. increases the dispersion as well as modifies the intrinsic properties of the CNT. In the recent years, extensive studies have been made to decorate the CNT with magnetic nanomaterials due to their potential applications in magnetic recording media, electrical devices, color imaging, heterogeneous catalysis, magnetic force microscopy as nanoprobe, microwave absorption materials and smart materials.<sup>88-90</sup> Besides these, other nanomaterials like organically modified nanoclay, cellulose nanofibre, graphene etc. are also used to enhance the performance of the shape memory polymers. However these are not discussed here as these nanomaterials are not used in the present study.



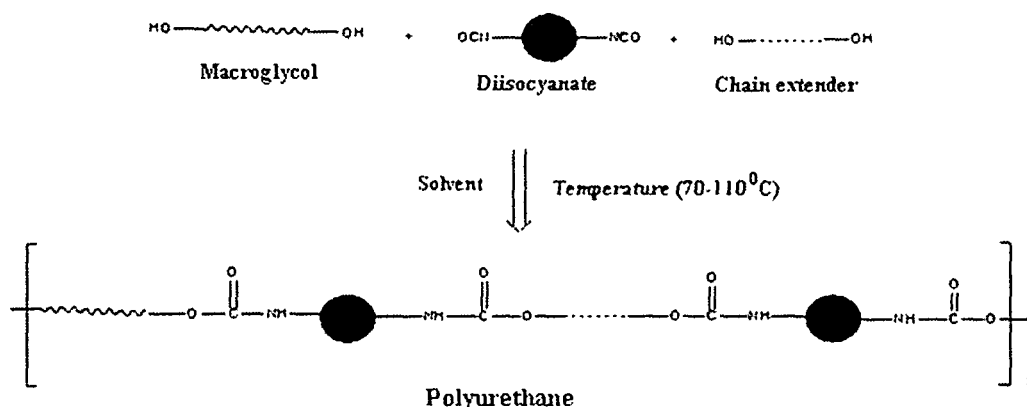
**Fig. 1.2:** (a) Single walled carbon nanotube (SWCNT) and (b) Multi-walled carbon nanotubes (MWCNT)



### 1.5.3. Method

#### 1.5.3.1. Preparation of polyurethane

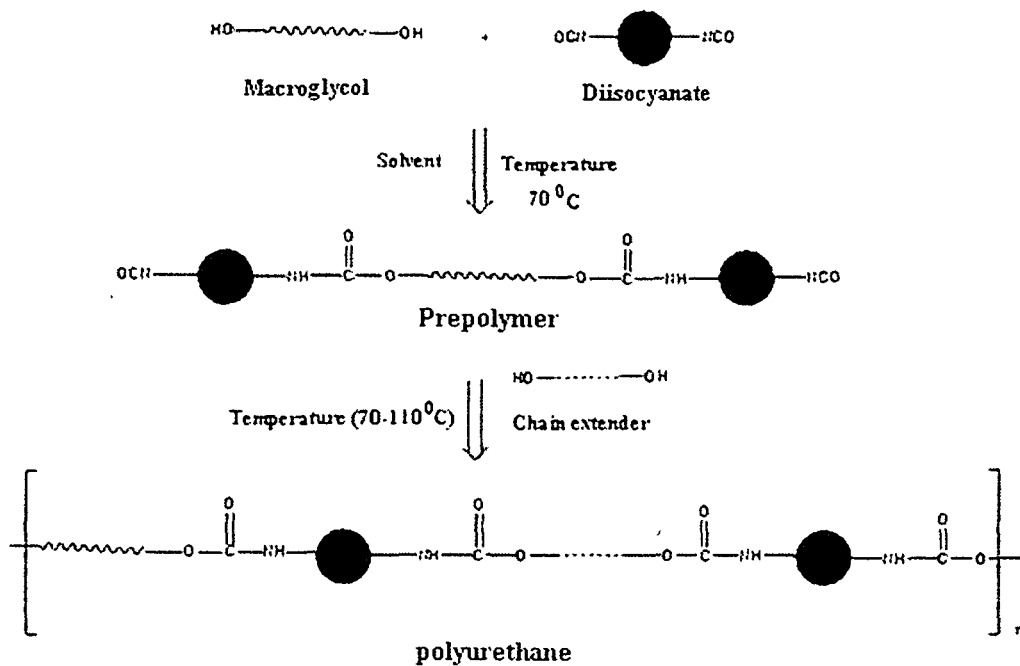
One-shot and pre-polymer methods are used for the preparation of polyurethanes (Fig. 1.3 and 1.4). In the one-shot method all the reactants namely macroglycol, diisocyanate and chain extender are added at once at the starting of the polymerization reaction. This process is easier, faster and more reproducible. A high order of crystallinity is obtained in this process. However controlling of reaction is difficult. In contrary, in the pre-polymerization method  $-NCO$  or  $-OH$  terminated pre-polymer is prepared by reacting a diisocyanate with a macroglycol in the first step. Then a chain extender is added to the pre-polymer in the second step and high molecular weight polyurethane is obtained. More regular chain sequences of polyurethane are obtained in the pre-polymerization technique. The solvents like xylene, dimethylformamide, dimethylacetamide etc. are generally used for the preparation of polyurethanes.



**Fig. 1.3:** Schematic representation of the one shot method for the synthesis of polyurethane

#### 1.5.3.2. Preparation of polymer nanocomposite

The polymer nanocomposites are generally prepared by three different methods as discussed below.



**Fig. 1.4:** Schematic representation of the pre-polymerization method for the synthesis of polyurethane

*Solution method*

In this method nanomaterials are swelled and dispersed by solvent in a polymer solution. The layers may be delaminated in a solvent or a solvent mixture due to the interactions of nanomaterials and the solvent molecules. Polymer chains are then adsorbed onto the delaminated individual layers or particles. However upon removal of the solvent, the layers or particles can reassemble to reform the stack with polymer chains sandwiched in between and forming a well-ordered intercalated nanocomposite. The formation of exfoliated nanocomposite is very rare by this technique. This technique is used in many cases in the laboratory for the preparation of nanocomposites but industry used only when water is used as the solvent. However this technique is not well accepted for the commercial production of nanocomposites due to the requirement of large volume of solvent and phase separation of the prepared product.<sup>91</sup>

*In situ polymerization*

In this method the nanomaterials are first dispersed in the liquid monomer or pre-polymer solution before polymerization. Polymerization can be initiated either by heat or radiation, or by the diffusion of a suitable initiator or catalyst inside the nanomaterials before the swelling step by the monomer. Polymerization produces long chain polymers within the nanomaterials. The homogeneous distribution of nanomaterials is obtained by using a high shear device because of the gradual increment of viscosity of the reaction mixture with progress of polymerization. Well-exfoliated nanocomposites can be prepared by this method and has been applied to a wide range of polymer systems. This technique is suitable to prepare clay/polymer and metal/polymer nanocomposites. This method is particularly useful for the thermosetting polymers.

#### *Melt-Mixing technique*

This method involves the mechanical mixing of a polymer with nanomaterials using extrusion and injection molding above the softening point or at processing temperature of the polymer. The intercalation or exfoliation of nanomaterials occurs during melting of polymer under shear conditions. The processing conditions play an important role on the structure evaluation of such polymer nanocomposites. Generally, temperature is kept well below the decomposition temperature of all the components of the nanocomposites. The absence of a solvent makes direct melt intercalation an environmentally sound and an economically favorable method for industries. Thus this technique has wide application for commercial production of polymer nanocomposites.

## **1.6. Characterization**

Polymers and their nanocomposites are characterized by different analytical and spectroscopic techniques as discussed below.

### 1.6.1. Nuclear magnetic resonance (NMR) spectroscopy

NMR is used to determine the structure of the polymers. Mainly proton ( $^1\text{H}$ ) and carbon ( $^{13}\text{C}$ ) NMR spectroscopic as NMR technique is utilized for this purpose. This technique is used to investigate the molecular weight, degree of branching, repeating units and distribution, tacticity as well as the presence of the non-reacted monomers.<sup>92</sup> This spectroscopic technique can

also be used to study the kinetic of the polymerization reaction, cross-linking reaction, composition of copolymer, degradation nature etc. NMR study of the polymer can be done in the solid state or in the swollen state. This technique can also be utilized to explain the effect on the nanomaterials with the polymer matrix.

#### 1.6.2. X-ray diffraction (XRD) study

XRD is used to study the degree of crystallinity, amorphousness, size of crystals and crystal structure of polymers. Polymer nanocomposites can be characterized by this technique. Two types of X-ray diffraction used for polymers. These are wide angle X-ray diffraction (WAXD) and small angle X-ray diffraction (SAXD). WAXD provides the information about the degree of crystallinity, orientation of crystalline region and nature of ordering structure.<sup>93</sup> On the other hand the SAXD is utilized to obtain information on the dimension of small crystalline regions as lamellae and the presence of voids and their shapes. The combined study of WAXD and SAXD present the quantitative characterization of nanostructure and crystalline structure of polymer nanocomposites.

#### 1.6.3. Fourier transformed infrared spectroscopy (FTIR)

FTIR spectroscopy is a commonly accepted method for characterizing the polymeric materials. This spectroscopy records the absorbance or transmittance intensity in percentage as a function of wavenumber ( $\text{cm}^{-1}$ ) or wavelength (nm) of the polymers under investigation. The rotational and vibration energies of any specific group or atom fall in the infrared region resulted the characteristic absorption band. So this spectroscopy is largely used to determine the functional groups present in the structure of the polymer. This technique is also used to identifying a polymer, monitoring the polymerization stage, and to characterize the structural changes under different conditions. The formation of nanocomposites can also be characterized by this technique.

#### 1.6.4. Scanning electron microscopy (SEM)

The scanning electron microscope is a type of electron microscope that creates images by the electrons emitted when the primary electrons coming from the source strike the surface and are

in-elastically scattered by atoms in the sample. The morphological study of the polymeric materials and nanocomposites is done by using the scanning electron microscopic technique. SEM is usually used to study topography such as three dimensional images of polymer blends, block and graft copolymers. Furthermore it can also be used to get information of crystallographic orientation and composition of polymeric materials by help of energy dispersive spectroscopic (EDS) attachment. The phase separated morphology of the SMP can be characterized by this technique in terms of domain sizes and number of phases.

#### 1.6.5. Transmission electron microscopy (TEM)

TEM is used to investigate the distribution of different phases, internal structure, defects structure etc. present in the nanocomposites. It can be used to get the information about crystallography and chemical composition of the materials. In TEM, the electron beam is allowed to penetrate to the very thin film and the transmitted electrons are directly used to produce the image of the specimen by the help of lenses. Varying the electron density in regions with different morphology leads to a contrasted image.

#### 1.6.6. Thermo-gravimetric analysis (TGA)

TGA is a very useful technique to determine the thermal stability of polymeric materials. The TGA thermogram is obtained by recording the change of weight of the polymer sample either with temperature or with time. The amount of moisture or any other volatiles, plasticizer, inorganic nanomaterials etc. present in the polymer can also be obtained from the TGA thermogram.

#### 1.6.7. Differential scanning calorimetry (DSC)

DSC is a very potential tool to evaluate the thermal properties of the polymeric materials. The glass transition temperature ( $T_g$ ), melting temperature ( $T_m$ ), crystallinity, kinetic of reaction, amount of endothermic or exothermic energy etc. can be studied by DSC.<sup>92, 94</sup> It can reveal the mobility of molecular chains by specific thermal energy variation.

#### 1.6.8. Raman spectroscopy

Raman spectroscopy relies on the inelastic scattering of monochromatic light usually from a laser in the visible, near infrared or near ultra-violet range with materials. Raman spectroscopy is highly sensitive to the material crystallinity, orientation and temperature. This is useful for analyzing molecules without a permanent dipole moment. This technique is mostly used for the study of carbon nanotube. It is used to determine the G band that represents the graphitic level of the tubes and the D band that indicates the presence of disorder.

#### 1.6.9. Vibrating sample magnetometric study

Vibrating sample magnetometer (VSM) is used to measure saturation magnetization, initial magnetization and Curie temperature of magnetic materials. VSM consists of an electromagnet assembly, a magnet power supply rack, a control electronics rack and a computer. It is based upon the Faraday's law according to which an electromagnetic frequency is induced in a conductor by a time varying magnetic flux.

#### 1.6.10. Biodegradation testing

The biodegradability of the polymers provides novel and additional properties which may also be beneficial for their uses. Different methods such as field test, simulation test, laboratory test etc. are used to study the biodegradation of the polymeric materials. Field tests such as burying plastic samples in soil, placing it in a river or full-scale composting performed represent ideal practical environmental conditions. However this method has some disadvantages. The environmental conditions such as temperature, humidity, or pH, cannot be efficiently controlled in nature. Simulation test has been developed to overcome the problems of field test. Here, the test for degradation is performed in a controlled laboratory reactor using a real environment (e.g. soil, compost or sea water). The most reproducible biodegradation tests are laboratory tests, where defined media with a mixed microbial population or individual microbial strains are used.

#### 1.6.11. Testing for shape memory behavior

Different testing methods are used to study the shape memory behaviors of SMP as discussed below.

### *Stretching technique*

In this technique the specimens are heated above the transition temperature ( $T_s$ ) and then they are stretched to twice of their original length ( $L_0$ ) and the stretched length is denoted as  $L_1$ . Immediately, the stretched samples are put into the low temperature (much below transition temperature) to fix the temporary shape for the specified period of time, and length is measured as  $L_2$  after releasing the stretch. The cooled samples are reheated at the same elevated temperature for the same period of time, and the length obtained is denoted as  $L_3$ . The percentage of shape recovery and percentage of shape fixity are calculated by using the following equations.

$$\text{Shape recovery (\%)} = [(L_1 - L_3)/L_0] \times 100 \text{ ----- (1.1)}$$

$$\text{Shape fixity (\%)} = [(L_2 - L_0)/L_0] \times 100 \text{ ----- (1.2)}$$

### *Bending technique*

In this technique the specimens are heated above the transition temperature ( $T_s$ ) for the specified period of time and then they are folded to a ring shape. Immediately, the folded samples are put into the fixing temperature (much below  $T_s$ ) for specified period of time to fix the temporary shape. Subsequently, they are reheated at the same elevated temperature for the same period of time for the shape recovery study. The shape recovery and shape fixity are two shape memory parameters calculated from the following equations:

$$\text{Shape recovery (\%)} = [(90 - \theta)/90] \times 100 \text{ ----- (1.3)}$$

$$\text{Shape fixity (\%)} = [\theta/90] \times 100 \text{ ----- (1.4)}$$

where  $\theta$  in degree denotes the angle between the tangential line at the midpoint of the sample and the line connecting the midpoint and the end of the curved sample.

### *Thermo-mechanical cyclic tensile technique*

In this technique the specimen is stretched to a maximum strain ( $\epsilon_m$ ) of 100% with a constant cross-head speed above transition temperature ( $T_s$ ). Immediately it is cooled to a low temperature (much below  $T_s$ ) to fix the deformed shape and the force of the specimen is released. Then the unloaded sample is reheated to study the shape recovery behavior. The shape recovery

ratio ( $R_r$ ) and shape fixity ratio ( $R_f$ ) are two shape memory parameters calculated from the following equations:

$$R_r = [\varepsilon_m - \varepsilon_p(N)] / \varepsilon_m \text{ ----- (1.5)}$$

$$R_f = \varepsilon_u(N) / \varepsilon_m \text{ ----- (1.6)}$$

Where  $\varepsilon_m$  denotes the maximum strain in the tensile test,  $\varepsilon_p(N)$  is the residual strain after shape recovery in the  $N^{\text{th}}$  cycle and  $\varepsilon_u(N)$  is the residual strain at stress free state of  $N^{\text{th}}$  cycle.

## 1.7. Property

The desired properties like mechanical, thermal, biodegradability, shape memory etc. at required values of polymers and their nanocomposites are useful for SMP and hence discussed below.

### 1.7.1. Mechanical property

Mechanical properties of polymers and the nanocomposites are very important for applications as SMP. The mechanical properties include tensile strength, elongation at break, scratch hardness, impact resistance, fracture toughness etc. Very low loading of suitable nanomaterials drastically improved the mechanical properties of many polymers in their nanocomposites.<sup>95, 96</sup> The extent of improvement depends on the functionalization, dispersion, size and shape, orientation, aspect ratio etc. of the nanomaterials. However the high level of loading of the nanomaterial deteriorated the mechanical properties of the nanocomposite. This is due to the agglomeration of the nanomaterials in the nanocomposite. Tensile strength of the nanocomposites increased due to the efficient load transfer from the matrix to the nanomaterial. However the elongation at break is generally decreased in the nanocomposites. This is due to the restricted movement of the polymer chains on the surface of the nanomaterials. Scratch hardness of the nanocomposites increases with the increase of toughness and rigidity of the material. Impact strength of the material may be defined from the angle of toughness of the films that is the ability to absorb the applied external energy as well as the transfer of energy to its adjacent molecular chains. Impact resistance of the nanocomposites also increases with the increase of toughness of the nanocomposites. The fracture toughness of the nanocomposites measures the



ability of the material containing a crack to resist the fracture. It depends on the strength and flexibility of the material.

#### 1.7.2. Thermal property

Thermal properties of nanocomposites are very important for their service life. Various thermal techniques such as TGA, DSC, DTA etc. are available for this purpose. Thermal stability of the nanocomposites is determined by using TGA. The thermal stability of the nanocomposites generally increases due to the restriction of thermal motion of the macromolecular chains on incorporation of nanomaterial in the polymer matrix. Also nanomaterials act as physical barrier, so the volatile products formed during the thermal decomposition process have to overcome longer zigzag path to escape the matrix. Moreover the nanomaterials may act as a superior insulator and assist the formation of char after the thermal decomposition. DSC is used to investigate the thermal transition behavior such as glass transition temperature and melting temperature. The glass transition temperature may be shifted to higher region due to the increased toughness and rigidity of the nanocomposites as compared to the pristine polymers.

#### 1.7.3. Magnetic property

Recently magnetic nanomaterials taking tremendous attention in the polymer domain due to their potential applications in magnetic recording media, electrical devices, color imaging, heterogeneous catalysis, magnetic force microscopy as nanoprobe, microwave absorption materials and smart materials. Most of the shape memory materials are actuated by the direct heating, which have the adverse effect in the biomedical applications. Magnetic nanoparticles based nanocomposites have added advantages in this respect as shape memory materials. This type of shape memory materials can be actuated by the non-contact mode using the alternating magnetic field.

#### 1.7.4. Biodegradation behavior

Biodegradable polymers have attracted great attention for the protection of natural wealthy environment. Again biodegradable shape memory polymers have potential application in biomedical field. The interesting and exciting aspect of polymer nanocomposites is their

significant improvement of biodegradability. The improved biodegradability may be due to the catalytic role of the nanomaterials in the biodegradation mechanism. The biodegradation process involves mainly in the four steps viz. water absorption, ester cleavage and formation of oligomeric fragments, solubilization of oligomer fragments and finally utilization of soluble oligomers by the bacteria. Thus any factor which increases the hydrolysis tendency of the polymer influences the biodegradation process.

#### 1.7.5. Shape memory property

The following properties of SMP are very important and hence mentioned here.

##### *Shape fixity*

Shape fixity is proposed to depict the extent of a temporary shape being fixed in one cycle of shape memory test. It is similar to strain fixity and shape retention. Shape fixity ( $R_f$ ) is equal to the amplitude ratio of the fixed deformation to the total deformation of the sample. The shape fixity is thus equal to the percentage of the ratio of fixed deformation to total deformation.

##### *Shape recovery*

Shape recovery ( $R_r$ ) define how well an original shape can be memorized by SMP. The shape recovery of SMP is therefore percentage of the ratio of the deformation recovered by specimen in a complete cycle of test to the deformation taken place to the specimen in the first cycle.

##### *Recovery rate*

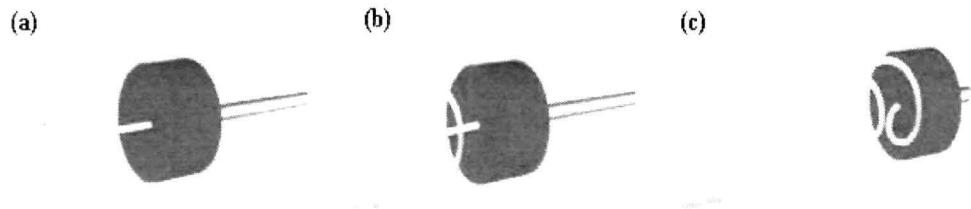
This parameter describes the speed i.e. the rate of recovery from a fixed temporary shape to its original shape during the recovery process of SMP under the application of appropriate stimulus. It can also be said as speed of recovery process or shape recovery speed.

## 1.8. Applications of shape memory polymers

SMP have different applications such as sensors and actuators, aerospace engineering, textile engineering, deployable structure, packaging, self-peeling reversible adhesive and biomedical field. SMP have wide applications in biology and medicine, especially for biomedical devices, which might open new medical procedure of minimally invasive surgery. The bulky SMP device can be inserted into the body in a small fixed shape by a small laparoscopic and the permanent shape can be recovered under the application of suitable stimulus. Again the biodegradable SMP can be used as short term implant as they are degraded to non toxic substances in the body environment. The different biomedical fields of applications are given below.

### *Clot removal device*

SMP can be utilized for the treatment of ischemic stroke. The Maitland research group has developed SMP devices for the clot removal.<sup>97, 5</sup> These devices were designed to be delivered through a catheter and punctured the clot in a narrow form, and then actuated by the radiation into a clot-grabbing form for clot extraction (Fig. 1.5).

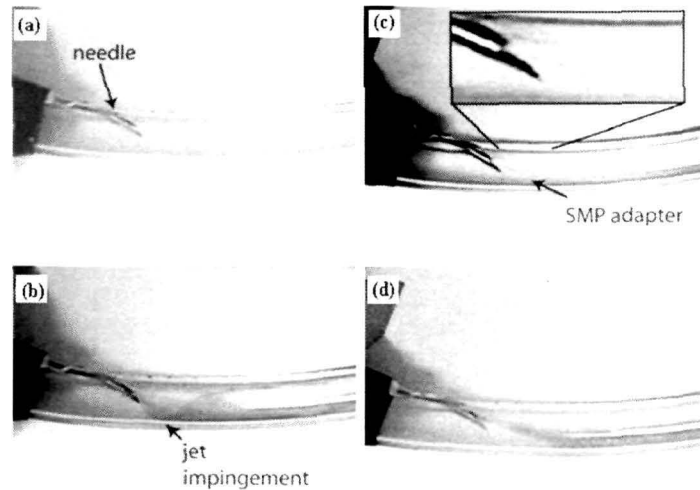


**Fig. 1.5:** (a) The device first punctures the clot, (b) activate to a form of coil shape on the distal side of the clot and (c) pulled to remove both the device and clot simultaneously (*Reproduced from Small, W., et al. Laser-activated shape memory polymer intravascular thrombectomy device, Opt. Expr. 13 (20), 8204-8213, 2005*)

### *Dialysis needle*

SMP adapter for a kidney dialysis needle has been developed to decrease the hemodynamic stresses during dialysis.<sup>98</sup> A SMP adapter has been proposed to pass through the dialysis needle in a compact form, thermally expanded upon heating to body temperature, and be

retracted when the procedure is completed (Fig. 1.6). Flow visualization experiments exhibited that the wall shear stresses were decreased by the adapter's elimination of jet impingement.



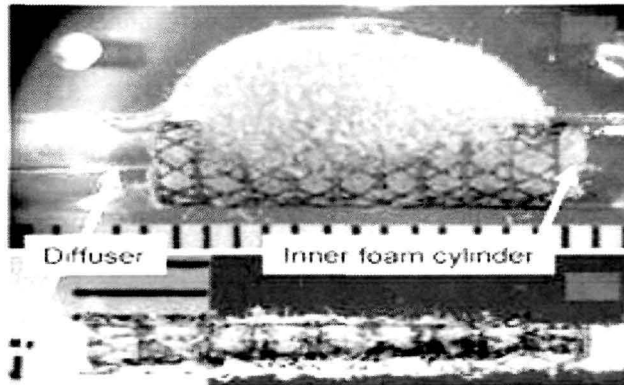
**Fig. 1.6:** A dialysis needle (a) is shown to produce jet impingement of flow (b), however, with the SMP adapter (c) the turbulence of the flow is decreased (d) (*Reproduced from ref. 98*)

#### *Vascular stent*

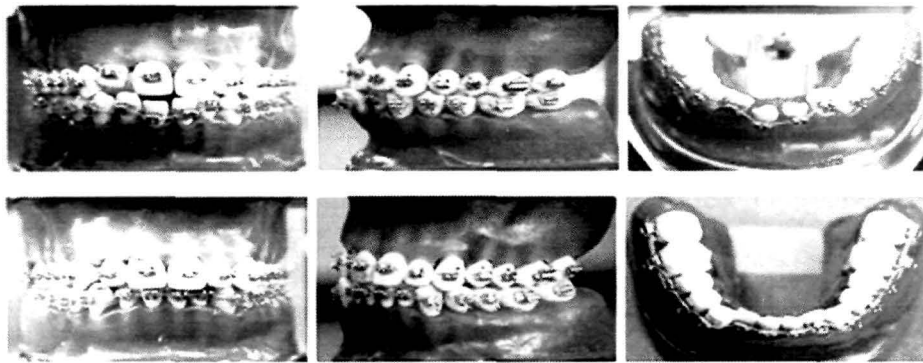
SMP can be utilized as stent applications because of their less thrombogenesis and initial hyperplasia, biodegradability and high elongation. Vascular stents are tiny tubular scaffolds used to retain the patency of an artery. They are extensively used in conjunction with transluminal angioplasty in the treatment of arterial stenosis to avoid acute vessel closure (Fig. 1.7).<sup>15</sup>

#### *Orthodontic wire*

Orthodontics is an area in which polymeric materials are required for both their esthetic appeal and shape-memory effect (Fig. 1.8). Nakasima et al. proposed the concept of using a thermoresponsive SMP arch wire in orthodontic braces for aligning teeth and noting that the recovery force was sufficient for moving teeth and that the SMP was more aesthetically appealing than a metallic archwire.<sup>99</sup> Jung and Cho reported the use of shape-memory polyurethanes for archwires.<sup>100</sup>



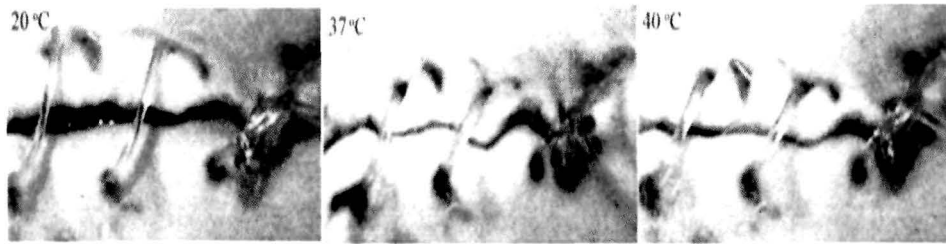
**Fig. 1.7:** The representative image of the vascular stents (*Reproduced from Small, W., et al. Shape memory polymer stent with expandable foam: a new concept for endovascular embolization of fusiform aneurysms, IEEE Trans. Biomed. Eng. 54 (6), 1157-1160, 2007*)



**Fig. 1.8:** The utilization of shape memory wire in orthodontic application (*Reproduced from ref. 100*)

#### *Suture*

SMP can be used as surgical suture, which will play a significant role in endoscopic surgery.<sup>14</sup> Generally the sutures are to be stitched very carefully. They may damage the cells of the skin if the threads are stitched very tightly; on the other hand, if the threads are too loose, it will not do the function properly. SMP if used, the threads can be stitched loosely and when the threads come into contact with the body temperature, it tightened as required (Fig. 1.9).



**Fig. 1.9:** The use of shape memory polymer in surgical sutures (*Reproduced from ref. 14*)

## **1.9. Short review on shape memory polyurethane nanocomposites**

### *Introduction*

Nowadays shape memory polyurethane nanocomposites are widely used to fulfill the demand of advanced applications such as aerospace engineering, automotive engineering, self deployable structure etc. The segmented polyurethanes usually show the shape memory behaviors. The hard and soft segments are responsible for the shape memory effect of the polyurethanes. The shape memory behavior of polyurethanes can be tuned by changing the nature and composition of reactants as well as the ratio of hard to soft segment. The observed shape recovery and shape fixity of such polyurethanes are not sufficient to meet the demands for some advanced applications. From the literature it has been seen that on incorporation of nanomaterials the shape memory behaviors of the polyurethanes increased. It is reported that due to the presence of nanomaterials the stored strain energy in the system increased and thereby increased the shape recovery and shape fixity.<sup>71, 101</sup> Moreover the shape recovery speed and reproducibility of the nanocomposites increased. Different nanomaterials such as nanoclay, metal oxides, carbon nanotubes, carbon nanofiber etc. can be used for the preparation of polyurethane nanocomposites. The performance including the shape memory behaviors of the nanocomposites depend on the size and shape, aspect ratio, surface modification etc. of the nanomaterials. Furthermore, the non contact actuation of shape memory polymer is more important in some specific applications. Incorporation of suitable nanomaterials in the shape memory polymer helps to actuate them by the magnetic field, electric field, radiation etc. in non contact mode.<sup>22, 23</sup> The research in this area is gaining importance in the recent times.

### *Background*

Meng et al. studied MWCNT based polyurethane nanocomposites that exhibited enhanced recovery ratio and recovery force.<sup>102</sup> According to the report MWCNT helped to store the internal elastic energy during stretching and fixing. Cao et al. reported that the shape recovery force of shape memory polyurethane can be increased significantly with the addition of small amount of reactive nanoclay particles.<sup>103</sup> Jang et al. reported that 2 wt% surface modified silica nanoparticles/polyurethane nanocomposites showed over 99% shape fixity.<sup>104</sup> Jana et al. reported the enhancement of mechanical and shape memory properties of polyurethane nanocomposites reinforced with poly( $\epsilon$ -caprolactone)-grafted carbon nanotubes.<sup>105</sup> Luo et al. reported the path dependent and multi-shape recovery of polyurethane/cellulose whisker nanocomposites.<sup>106</sup> Haghayegh et al. studied shape memory, thermal and mechanical properties of polyurethane/clay nanocomposites.<sup>107</sup> From the study it was found that on incorporation of nanoclay shape recovery behavior found to enhance. Recently authors studied the shape memory behaviors of polyurethane nanocomposites by employing non contact actuation strategy. Razzaq et al. studied the shape recovery behavior of magnetite filled polyurethane nanocomposites.<sup>108</sup> Sahoo et al. reported that carbon nanotubes based polyurethane nanocomposites exhibited the good shape recovery (90-95%) under the actuation of electric field.<sup>109</sup> Yoo et al. reported the carbon nanotube based polyurethane nanocomposites as electro-active shape memory materials.<sup>110</sup> The prepared materials exhibited the enhanced mechanical and shape memory behaviors. Cai et al. reported the synthesis and properties of magnetic responsive shape memory  $\text{Fe}_3\text{O}_4$ /poly( $\epsilon$ -caprolactone)-polyurethane nanocomposites.<sup>111</sup>

### *Preparation*

The polyurethane nanocomposites are also prepared by utilizing the similar technique as discussed in subsection 1.5.3.2. These nanocomposites can be prepared by in situ or ex situ polymerization technique. The nanocomposites prepared by the in situ polymerization technique generally provide high tensile strength, high thermal stability etc. This is due to the well dispersion of nanomaterials in the polymer matrix. Meng et al. prepared the shape memory polyurethane by the pre-polymerization technique taking polycaprolacton diol (PCL) for soft segment, and diphenylmethane-4,4-diisocyanate (MDI) and molecular chain extender 1,4-

butanediol for hard segment.<sup>102</sup> Jang et al. prepared the polyurethane tacking the poly(tetramethylene glycol), isophorone diisocyanate, butyl amine and glycidol by the pre-polymerization technique.<sup>104</sup> Deka et al. prepared the shape memory polyurethane using the PCL for soft segment, and toluene diisocyanate, bio-based chain extender monoglyceride of the *Mesua ferrea* L. seed oil and multifunctional moiety glycerol for hard segment by the pre-polymerization technique.<sup>71</sup> The nanocomposites of the same were prepared by the in-situ polymerization method using the acid treated MWCNT. Choi et al. reported the preparation of graphene based shape memory polyurethane nanocomposites.<sup>112</sup> In this preparation the dispersed graphene was first reacted with PCL and then reacted with the required amount of MDI and finally reacted with the chain extender butanediol under proper conditions. Chung et al. reported the preparation of nanocomposites of covalently bonded surface modified montmorillonite nanomaterials with the polyurethane by the melt-mixing method.<sup>113</sup> Lee et al. reported the preparation of polyurethane from PCL, MDI and 1,4-butanediol by two step polymerization method and then polyurethane/SWCNT is prepared by the solution polymerization technique.<sup>114</sup> Cai et al. prepared the Fe<sub>3</sub>O<sub>4</sub> based polyurethane nanocomposites by the in situ polymerization technique at molar ratio of polycaprolacton diol: diphenylmethane-4,4-diisocyanate:1,4-butanediol=1:4:3 with different loading of Fe<sub>3</sub>O<sub>4</sub>.<sup>111</sup>

### *Characterization*

The shape memory polyurethane nanocomposites are characterized by the different techniques as discussed in section 1.6. The presence of different types of interaction between polyurethane and the nanomaterial of the nanocomposites can be characterized by the FTIR study. The shifting and broadening of the peaks implies the interaction of nanomaterials with the polymer matrix. The transmission electron microscopic study also confirmed the formation of nanocomposites. The homogeneous distribution of nanomaterials in the polymer matrix confirmed the presence of interactions with the polymer matrix. The thermal behaviors of the polyurethane nanocomposites are characterized by the TGA and DSC analyses. The thermal stability is determined by using the TGA analysis. The thermal transition behaviors are characterized by the DSC study. The T<sub>g</sub> and T<sub>m</sub> are very important parameters for the shape memory polyurethane nanocomposites because they can act as switching temperatures. The



Shape memory properties of the nanocomposites are evaluated by using the bending or stretching technique as discussed in subsection 1.6.11. Rana et al. characterized the prepared polyurethane-carbon nanotube nanocomposites by XRD, SEM, TEM, TGA and DSC studies. The shape memory behavior was studied as thermo-responsive shape memory materials using the bending test. Jang et al. characterized the surface modified silica particles based shape memory polyurethane by FTIR and TEM studies. The shape memory behaviors were studied by the thermo-mechanical cyclic test.<sup>104</sup> Cai et al. characterized the polyurethane-carbon nanotube hybrid by the XRD, TGA and DSC. The shape recovery was studied (at 30 V and 0.1 A) as electro-active noncontact actuation method.<sup>111</sup> Yoo et al. characterized the polyurethane-carbon nanotube nanocomposites by using DSC, SEM and AFM. The authors also studied the shape recovery using electric field of 50 V.<sup>110</sup>

### *Property*

The properties required to study for polyurethane nanocomposites are same as discussed for pristine polyurethanes. However, the polyurethane nanocomposites showed better performance compared to their pristine analogs. The properties of the polyurethanes were described in section 1.7.

The tensile strength of the polyurethane nanocomposites is found to be greater than the polyurethane matrix due to the homogeneous distribution of the nanomaterials in matrix. The elongation at break is generally decreased, though it may remain constant or even increased in the nanocomposites. The decrease in elongation is mainly due to the molecular restriction of polymer chains by the rigid nanomaterials. Deka et al. reported the enhancement of tensile strength of hyperbranched polyurethane/clay nanocomposites.<sup>115</sup> Zhou et al. reported that the tensile strength of MWCNT/polyurethane nanocomposites increases with increase of content of surface modified MWCNT.<sup>116</sup> The polyurethane nanocomposites exhibited better impact and scratch resistance as compared to the pristine polyurethane. This is due to good toughness and high elasticity of the polyurethane nanocomposites. The nanocomposites possess enhanced chemical resistance as compared to the neat polymers.

The polyurethane nanocomposites exhibited good thermal stability. The thermal stability of the system increased due to the increased compactness of the system as well as the presence of

highly thermo-stable nanomaterials. The  $T_g$  and  $T_m$  are the two important thermal transition parameters for polyurethane nanocomposites and are found to be altered from the pristine system. The changes of these parameters resulted changes in performance of the nanocomposites. Xu et al. reported the enhancement of thermal stability and the melting enthalpy ( $\Delta H$ ) of shape memory polyurethane/silica nanocomposites.<sup>117</sup> Suen et al. reported that  $T_m$  and  $T_g$  of soft segment increased with the increase of ZnC in the polyurethane.<sup>118</sup>

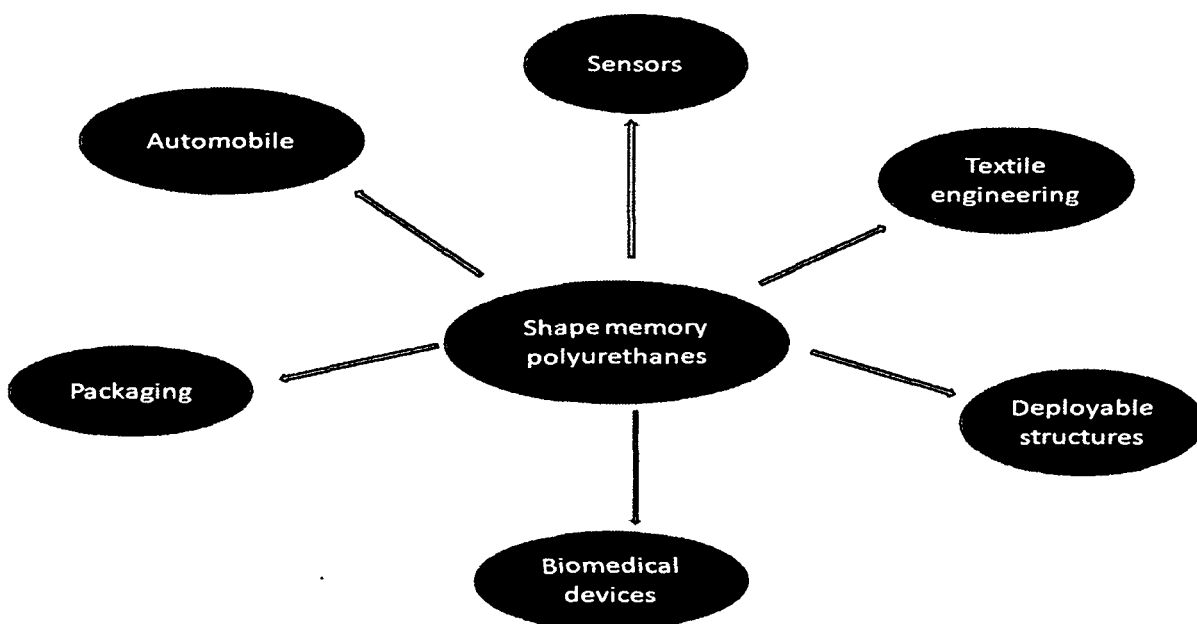
The polyurethane nanocomposites showed enhanced shape recovery and shape fixity as compared to the pristine one. The shape recovery speed is also increased in the nanocomposites. This is due to various interactions in the system and thereby stored more strain energy in the system. Cai et al. reported that the shape recovery time decreased with the increase of the content of  $Fe_3O_4$  nanoparticles in the polyurethane nanocomposites under the actuation of magnetic field.<sup>111</sup> Cho et al. reported the electro-active shape memory behaviors of MWCNT based polyurethane nanocomposites.<sup>119</sup>

### *Application*

Shape memory polyurethane nanocomposites have potential applications in the different fields especially in the biomedical domain. It can be utilized in packaging, aerospace, automotive, sensors and actuators, robotics, textile etc. The polyurethane nanocomposites have potential application in the biomedical field such as minimally invasive surgery, drug delivery systems, tissue engineering etc. Ahmad et al. reported that polyurethane based shape memory polymer actuators have possible application in medical pressure bandages where gradient pressure is required between the ankle and the knee for treatment of leg ulcer.<sup>120</sup> Ahn et al. reported the shape memory polyurethane membrane where the pore size can be tuned by repeating heating and cooling.<sup>121</sup> Paik et al. reported the application of conducting shape memory polyurethane as actuators.<sup>122</sup> Jung et al. reported a polyurethane of 4,4'-methylene bis(phenylisocyanate), poly( $\epsilon$ -caprolactone)diol (PCL) and 1,4-butanediol for the orthodontic application.<sup>100</sup> Baer et al. studied that shape memory polyurethane may be suitable for the application in stents or clot extractors.<sup>123</sup> A few applications of shape memory polyurethanes are shown in Fig. 1.10

### 1.10. Scopes and objectives of the present investigation

From the above discussion, thus, it has been found that shape memory behaviors of different polyurethanes and their nanocomposites have been studied. However the shape memory behaviors of  $\text{Fe}_3\text{O}_4$ , functionalized MWCNT and  $\text{Fe}_3\text{O}_4$  decorated MWCNT based vegetable oil modified hyperbranched polyurethane nanocomposites are rare to find out in the literature, though they have strong potential for the same.



**Fig. 1.10:** Fields of application for shape memory polyurethane nanocomposites

Further, microwave actuated shape memory studies of such nanocomposites have not been explored till date, though microwave energy has largely used recently in different chemical transformations and also it could be used as a noncontact stimulant for the shape memory study. Thus the main objective of the present investigation is to develop a vegetable oil modified hyperbranched polyurethane nanocomposite as a shape memory material with tuning performance. This main objective is associated with the following sub-objectives.

1. To synthesize vegetable oil based hyperbranched polyurethanes with different compositions and to characterize them by different spectroscopic and analytical techniques.

2. To modify the above hyperbranched polyurethanes for improvement of their properties and to characterize the modified polymers by different spectroscopic and analytical techniques.
3. To prepare nanocomposites of the modified hyperbranched polyurethane with the  $\text{Fe}_3\text{O}_4$  nanoparticles and to characterize them.
4. To prepare nanocomposites of the modified hyperbranched polyurethane with the functionalized MWCNT and to characterize them.
5. To prepare nanocomposites of the modified hyperbranched polyurethane with the magnetic nanoparticles ( $\text{Fe}_3\text{O}_4$ ) decorated MWCNT and to characterize them.
6. To study the various properties such as physical, thermal, mechanical, shape memory etc. of the synthesized hyperbranched polyurethanes, modified hyperbranched polyurethanes and their nanocomposites.
7. To optimize the performance characteristics of the nanocomposites for their shape memory applications.

### 1.11. Plans of the present work

To fulfill the above objectives the following plans of work are demonstrated.

1. Vegetable oil based hyperbranched polyurethanes with different compositions will be synthesized by  $\text{A}_2 + \text{B}_3$  approach using high the dilution and slow addition technique.
2. The synthesized polyurethanes will be modified with the epoxy resin.
3. The synthesized and the modified hyperbranched polyurethanes will be characterized by different spectroscopic techniques such as FTIR, XRD, NMR etc.
4. The nanocomposites of the synthesized hyperbranched polyurethanes and the modified hyperbranched polyurethanes with  $\text{Fe}_3\text{O}_4$  and functionalized MWCNT will be prepared by *in-situ* polymerization technique as reported in the literature.
5. The magnetic nanoparticles ( $\text{Fe}_3\text{O}_4$ ) decorated MWCNT/hyperbranched polyurethane nanocomposites will also be prepared by *in-situ* polymerization technique.
6. The prepared nanocomposites will be characterized using FTIR, XRD, TEM, SEM etc. to determine the presence of various interactions and the morphology of the nanocomposites.
7. The performance characteristics of the characterized nanocomposites will be investigated by determination of physical properties, tensile strength, elongation at break, scratch hardness,

impact resistance, thermal properties like glass transition temperature, thermo-stability etc., chemical resistance characteristics in different chemical media and shape memory properties.

8. Shape memory properties will be studied by stretching and bending techniques.
9. A comparative study on the performance characteristics will be conducted to find out the best nanocomposite among the above.

## References

1. Kunzelman, J., et al. Shape memory polymers with built-in threshold temperature sensors, *J. Mater. Chem.* **18** (10), 1082-1086, 2008.
2. Sokolowski, W., et al. Medical applications of shape memory polymers, *Biomed. Mater.* **2** (1), 23-27, 2007.
3. Lu, H., & Gou, J. Fabrication and electro-active responsive behavior of shape-memory nanocomposite incorporated with self-assembled multiwalled carbon nanotube nanopaper, *Polym. Adv. Technol.* **23** (2), 1529-1535, 2012.
4. Xue, L., et al. Synthesis and characterization of three-arm poly( $\epsilon$ -caprolactone)-based poly(ester-urethanes) with shape-memory effect at body temperature, *Macromolecules* **42** (4), 964-972, 2009.
5. Metzger, M., et al. Mechanical properties of mechanical actuator for treating ischemic stroke *Biomed. Microdevices* **4** (2), 89-96, 2002.
6. Liu, C., et al. Review of progress in shape-memory polymers, *J. Mater. Chem.* **17** (16), 1543-1558, 2007.
7. Dietsch, B., & Tong, T. A review: features and benefits of shape memory polymers (SMPs), *J. Adv. Mater.* **39** (2), 3-12, 2007.
8. Gunes, I.S., & Jana, S.C. Shape memory polymers and their nanocomposites: a review of science and technology of new multifunctional materials, *J. Nanosci. Nanotechnol.* **8** (4), 1616-1637, 2008.
9. Mano, J.F. Stimuli-responsive polymeric systems for biomedical applications, *Adv. Eng. Mater.* **10** (6), 515-527, 2008.
10. Ratna, D., & Karger-Kocsis, J. Recent advances in shape memory polymers and composites: a review, *J. Mater. Sci.* **43** (1), 254-269, 2008.
11. Schmaljohann, D. Thermo and pH-responsive polymers in drug delivery, *Adv. Drug Deliver. Rev.* **58** (15), 1655-1670, 2006.
12. Sharp, A.A., et al. Toward a self-deploying shape memory polymer neuronal electrode, *J. Neural. Eng.* **3** (4), 23-30, 2006.
13. Chen, M.C., et al. Rapidly self-expandable polymeric stents with a shape-memory property, *Biomacromolecules* **8** (9), 2774-2780, 2007.

14. Lendlein, A., & Langer, R. Biodegradable, elastic shape-memory polymers for potential biomedical applications, *Science* **296** (5573), 1673-1676, 2002.
15. Small, W., et al. Biomedical applications of thermally activated shape memory polymers, *J. Mater. Chem.* **20** (17), 3356-3366, 2010.
16. Luo, X., & Mather, P.T. Preparation and characterization of shape memory elastomeric composites, *Macromolecules* **42** (19), 7251-7253, 2009.
17. Lu, X.L., et al. Shape memory effects of poly (L-lactide) and its copolymer with poly ( $\epsilon$ -caprolactone), *Polym. Bull.* **58** (2), 381-391, 2007.
18. Kang, S.M., et al. Carbon nanotube reinforced shape memory polyurethane foam, *Polym. Bull.* **70** (3), 885-893, 2013.
19. Wu, L., et al. Synthesis, properties, and light-induced shape memory effect of multiblock polyesterurethanes containing biodegradable segments and pendant cinnamamide groups, *Biomacromolecules* **12** (1), 235-241, 2011.
20. Lee, K.M., et al. Light-activated shape memory of glassy, azobenzene liquid crystalline polymer networks, *Soft Matter* **7** (9), 4318-4324, 2011.
21. Chen, S., et al. Novel moisture-sensitive shape memory polyurethanes containing pyridine moieties, *Polymer* **50** (19), 4424-4428, 2009.
22. Schmidt, A.M., et al. Electromagnetic activation of shape memory polymer networks containing magnetic nanoparticles, *Macromol. Rapid. Commun.* **27** (14), 1168-1172, 2006.
23. Lee, H.F., & Yu, H.H. Study of electroactive shape memory polyurethane-carbon nanotube hybrids, *Soft Matter* **7** (8), 3801-3807, 2011.
24. Sun, L., et al. Optimization of the shape memory effect in shape memory polymers, *J. Polym. Sci. Part A: Polym. Chem.* **49** (16), 3574-3581, 2011.
25. Knight, P.T., et al. PLGA-POSS end-linked networks tailored degradation and shape memory behavior, *Macromolecules* **42** (17), 6596-6605, 2009.
26. Weng, S., et al. Shape memory properties of polycaprolactone-based polyurethanes prepared by reactive extrusion, *J. Appl. Polym. Sci.* **127** (1), 748-759, 2012.
27. Zhang, J., et al. Unique multifunctional thermally-induced shape memory poly(p-dioxanone)-poly(tetramethylene oxide)glycol multiblock copolymers based on the synergistic effect of two segments, *J. Phys. Chem. C* **116** (9), 5835-5845, 2012.

28. Xue, L., et al. Synthesis and characterization of three-arm poly( $\epsilon$ -caprolactone)-based poly(ester-urethanes) with shape-memory effect at body temperature, *Macromolecules* **42** (4), 964-972, 2009.
29. Li, F., et al. Shape memory effect of polyethylene/nylon 6 graft copolymers, *Polymer* **39** (26), 6929-6934, 1998.
30. Liu, C., et al. Chemically cross-linked polycyclooctene: synthesis, characterization, and shape memory behavior, *Macromolecules* **35** (27), 9868-9874, 2002.
31. Jeon, H.G., et al. Shape memory and nanostructure in poly (norbornyl-POSS) copolymers, *Polym. Int.* **49** (5), 453-457, 2000.
32. Sakurai, K., et al. Shape-memorizable styrene-butadiene block copolymer. I. thermal and mechanical behaviors and structural change with deformation, *J. Macromol. Sci., Phys. B* **36** (6), 703-716, 1997.
33. Oprea, S. Novel quinoline-based polyurethane elastomers. the effect of the hard segment structure in properties enhancement, *J. Polym. Res.* **19** (1), 9767-9776, 2012.
34. Oertel, G. *Polyurethane Handbook 2*, Hanser, New York, 1993.
35. Chen, J.H., et al. Studies on segmented polyetherurethane for biomedical application: effects of composition and hard-segment content on biocompatibility, *J. Biomed. Mater. Res.* **41** (4), 633-648, 1998.
36. Gunatillake, P.A., et al. Poly(dimethylsiloxane)/poly(hexamethylene oxide) mixed macrodiol based polyurethane elastomers. I. synthesis and properties, *J. Appl. Polym. Sci.* **76** (14), 2026-2040, 2000.
37. Kaushik, A., & Singh, P. Kinetics of reaction of castor oil trimethylol propane polyol and 4,4' diphenyl methane diisocyanate, *Int. J. Polym. Mater.* **57** (8), 815-831, 2008.
38. Shen, Y., et al. Synthesis and mechanical properties of membranes prepared from hydroxyl-terminated polyurethane alcohol dispersion modified by epoxy resin, *Polym. Plast. Technol. Eng.* **51** (1), 1077-1082, 2012.
39. Bhowmick, A.K., & Stephens, H.L. *Handbook of Elastomers*, Marcel Dekker, New York, 1998.
40. Wirpsza, Z. *Polyurethanes, Chemistry, Technology and Applications*, Ellis Horwood Ltd., New York, 1993.



41. Camberlin, Y., et al. Model hard segments from diphenyl methane diisocyanate and different chain extenders, and corresponding linear block polyurethanes, *J. Polym. Sci. Polym. Chem. Ed.* **20** (6), 1445-1456, 1982.
42. Martin, D.J., et al. Effect of soft-segment CH<sub>2</sub>/O ratio on morphology and properties of a series of polyurethane elastomers, *J. Appl. Polym. Sci.* **60** (4), 557-571, 1996.
43. Linliu, K., et al. A small-angle X-ray scattering study of microphase separation transition of polyurethanes: effect of hard segments, *J. Polym. Res.* **2** (1), 63-70, 1995.
44. Karak, N., & Maiti, S. *Dendrimer and Hyperbranched Polymer Synthesis to Applications*, MD publication Pvt. Ltd., New Delhi, 2008.
45. Gao, C., & Yan, D. Hyperbranched polymers: from synthesis to applications, *Prog. Polym. Sci.* **29** (3), 183-275, 2004.
46. Kim, Y.H., & Webster, O.W. Hyperbranched polyphenylenes, *Macromolecules* **25** (21), 5561-5572, 1992.
47. Kim, Y.H., & Webster, O.W. Water soluble hyperbranched polyphenylene: a unimolecular micelle, *J. Am. Chem. Soc.* **112** (11), 4592-4593, 1990.
48. Miyagawa, H., et al. Fracture toughness and impact strength of anhydride-cured bio-based epoxy, *Polym. Eng. Sci.* **45** (4), 487-495, 2005.
49. Williams, C.K., & Hillmyer, M.A. Polymers from renewable resources: a perspective for a special issue of polymer reviews, *Polym. Rev.* **48** (1), 1-10, 2008.
50. Deka, H., & Karak, N. Shape-memory property and characterization of epoxy resin-modified *Mesua ferrea* L. seed oil-based hyperbranched polyurethane, *J. Appl. Polym. Sci.* **116** (1), 106-115, 2010.
51. Riaz, U., & Ashraf, S.M. Plant oil renewable-resource-based biodegradable blends as green alternatives in biopackaging, *Int. J. Polym. Mater.* **61** (3), 229-239, 2012.
52. Xia, Y., & Larock, R.C. Vegetable oil-based polymeric materials: synthesis, properties, and applications, *Green Chem.* **12** (11), 1893-1909, 2010.
53. Tellez, G.L., et al. Synthesis and thermal cross-linking study of partially-aminated epoxidized linseed oil, *Des. Monomers Polym.* **11** (5), 435-445, 2008.
54. Erhan, S.Z., & Bagby, M.O. Vegetable-oil-based printing ink formulation and degradation, *Ind. Crops Prod.* **3** (4), 237-246, 1995.

55. Dutta, N., et al. Synthesis and characterization of polyester resins based on nahar seed oil, *Prog. Org. Coat.* **49** (2), 146-152, 2004.
56. Pan, M., et al. Morphology and properties of PVC/clay nanocomposites via in situ emulsion polymerization, *J. Appl. Polym. Sci.* **94** (1), 277-286, 2004.
57. Zhu, J., et al. Fire properties of polystyrene-clay nanocomposites, *Chem. Mater.* **13** (10), 3774-3780, 2001.
58. Fornes, T.D., et al. Effect of organoclay structure on nylon 6 nanocomposite morphology and properties, *Polymer* **43** (22), 5915-5933, 2002.
59. Yano, K., et al. Synthesis and properties of polyimide-clay hybrid films, *J. Polym. Sci. Part A: Polym. Chem.* **35** (11), 2289-2294, 1997.
60. Ray, S.S., & Okamoto, M. Polymer/layered silicate nanocomposites: a review from preparation to processing, *Prog. Polym. Sci.* **28** (11), 1539-1641, 2003.
61. Keledi, G., et al. Polymer nanocomposites: structure, interaction, and functionality, *Nanoscale* **4** (6), 1919-1938, 2012.
62. Yoon, J.T., et al. Effects of grafted chain length on mechanical and electrical properties of nanocomposites containing polylactide-grafted carbon nanotubes, *Compos. Sci. Technol.* **70** (5), 776-782, 2010.
63. Bayer, O. *A process for the production of polyurethanes and polyureas*, **German patent DRP 728981**, November 13, 1937.
64. Buehler, W.J., et al. Effect of low-temperature phase changes on the mechanical properties of alloys near composition TiNi, *J. Appl. Phys.* **34** (5), 1475-1477, 1963.
65. Sun, L., et al. Stimulus-responsive shape memory materials: a review, *Mater. Des.* **33**, 577-640, 2012.
66. Yang, J.H., et al. Comparison of thermal/mechanical properties and shape memory effect of polyurethane block-copolymers with planar or bent shape of hard segment, *Polymer* **44** (11), 3251-3258, 2003.
67. Theng, B.K.G. *Formation and Properties of Clay-Polymer Complexes*, Oxford, UK, 1970.
68. Iijima, S. Helical microtubules of graphitic carbon, *Nature* **354**, 56-58, 1991.
69. Ajayan, P.M., et al. Aligned carbon nanotube arrays formed by cutting a polymer resin-nanotube composite, *Science* **265** (5176), 1212-1214, 1994.

70. Koerner, H., et al. Deformation–morphology correlations in electrically conductive carbon nanotube-thermoplastic polyurethane nanocomposites, *Polymer* **46** (12), 4405-4420, 2005.
71. Deka, H., et al. Biocompatible hyperbranched polyurethane/multi-walled carbon nanotube composites as shape memory materials, *Carbon* **48** (7), 2013-2022, 2010.
72. Weigel, T., et al. Investigation of parameters to achieve temperatures required to initiate the shape-memory effect of magnetic nanocomposites by inductive heating, *Smart Mater. Struct.* **18** (2), 025011-025020, 2009.
73. Kumar, U.N., et al. Non-contact actuation of triple-shape effect in multiphase polymer network nanocomposites in alternating magnetic field, *J. Mater. Chem.* **20** (17), 3404-3415, 2010.
74. Jeon, H.G., et al. Shape memory and nanostructure in poly(norbornyl-POSS) copolymers, *Polym. Int.* **49** (5), 453-457, 2000.
75. Liu, C., et al. Chemically cross-linked polycyclooctene: synthesis, characterization, and shape memory behavior, *Macromolecules*, **35** (27), 9868-9874, 2002.
76. Rousseau, I.A., & Mather, P.T. Shape memory effect exhibited by smectic-C liquid crystalline elastomers, *J. Am. Chem. Soc.* **125** (50), 15300-15301, 2003.
77. Chung, T., et al. Two-way reversible shape memory in a semicrystalline network, *Macromolecules* **41** (1), 184-192, 2008.
78. Tobushi, H., et al. Thermomechanical properties in a thin film of shape memory polymer of polyurethane series, *Smart Mater. Struct.* **5** (4), 483-491, 1996.
79. Tobushi, H., et al. Thermomechanical constitutive model of shape memory polymer, *Mech. Mater.* **33** (10), 545-554, 2001.
80. Tobushi, H., et al. The influence of shape-holding conditions on shape recovery of polyurethane-shape memory polymer foams, *Smart Mater. Struct.* **13** (4), 881-887, 2004.
81. Cai, Y., et al. Synthesis and properties of magnetic sensitive shape memory Fe<sub>3</sub>O<sub>4</sub>/poly( $\epsilon$ -caprolactone)-polyurethane nanocomposites, *J. Appl. Polym. Sci.* **127** (1), 49-56, 2013.
82. Leng, J., et al. Infrared light-active shape memory polymer filled with nanocarbon particles, *J. Appl. Polym. Sci.* **114** (4), 2455-2460, 2009.

83. Weiss, R.A., et al. New design of shape memory polymers: mixtures of an elastomeric ionomer and low molar mass fatty acids and their salts, *Macromolecules* **41** (9), 2978-2980, 2008.
84. Wang, M., et al. Enhancement of the mechanical properties of poly(styrene-co-acrylonitrile) with poly(methyl methacrylate)-grafted multiwalled carbon nanotubes, *Polymer* **46** (26), 11510-11516, 2005.
85. Xie, X.L., et al. Dispersion and alignment of carbon nanotubes in polymer matrix: a review, *Mat. Sci. Eng. R* **49** (4), 89-112, 2005.
86. Wang, M., et al. Enhancement of the mechanical properties of poly(styrene-co-acrylonitrile) with poly(methyl methacrylate)-grafted multiwalled carbon nanotubes, *Polymer* **46** (25), 11510-11516, 2005.
87. Petrov, P.D., et al. Dispersion of multi-walled carbon nanotubes with pyrene-functionalized polymeric micelles in aqueous media, *Polymer* **53** (24), 5502-5506, 2012.
88. Zhou, H., et al. Decoration of Fe<sub>3</sub>O<sub>4</sub> nanoparticles on the surface of poly(acrylic acid) functionalized multi-walled carbon nanotubes by covalent bonding, *J. Polym. Sci. Part A: Polym. Chem.* **48** (21), 4697-4703, 2010.
89. Kong, L., et al. Facile synthesis of multifunctional multiwalled carbon nanotubes/Fe<sub>3</sub>O<sub>4</sub> nanoparticles/polyaniline composite nanotubes, *J. Solid State Chem.* **181** (3), 628-636, 2008.
90. Wang, X., et al. Fabrication and characterization of magnetic Fe<sub>3</sub>O<sub>4</sub>-CNT composites, *J. Phys. Chem. Solids* **71** (4), 673-676, 2010.
91. Ray, S.S., & Bousima, M. Biodegradable polymers and their layered silicate nanocomposites: In greening the 21st century materials world, *Prog. Mater. Sci.* **50** (8), 962-1079, 2005.
92. Karak, N. *Fundamentals of Polymers*, PHI learning private limited, New Delhi, 2009.
93. Kasai, N., & Kakudo, M. *X-ray Diffraction by Macromolecules*, Kodansha, Tokyo, 2005.
94. Hu, J. *Shape Memory Polymers and Textiles*, CRC press, New York, 2007.
95. Paul, D.R., & Robeson, L.M. Polymer nanotechnology: nanocomposites, *Polymer* **49** (15), 3187-3204, 2008.
96. Hussain, F., et al. Review article: polymer-matrix nanocomposites, processing, manufacturing, and application: an overview, *J. Compos. Mater.* **40** (17), 1511-1575, 2006.

97. Maitland, D.J., et al. Photothermal properties of shape memory polymer micro-actuators for treating stroke, *Lasers Surg. Med.* **30** (1), 1-11, 2002.
98. Ortega, J.M., et al. A shape memory polymer dialysis needle adapter for the reduction of hemodynamic stress within arteriovenous grafts, *IEEE Trans Biomed. Eng.* **54** (9), 1722-1724, 2007.
99. Nakasima, A., et al. Potential application of shape memory plastic as elastic material in clinical orthodontics, *Eur. J. Orthod.* **13** (3), 179-186, 1991.
100. Jung, Y.C., & Cho, J.W. Application of shape memory polyurethane in orthodontic, *J. Mater. Sci. Mater. Med.* **21** (10), 1881-1888, 2008.
101. Gunes, I.S., et al. Evaluation of nanoparticulate fillers for development of shape memory polyurethane nanocomposites, *Polymer* **49** (9), 2223-2234, 2008.
102. Meng, Q., et al. Shape-memory polyurethane/multiwalled carbon nanotube fibers, *J. Appl. Polym. Sci.* **106** (2), 837-848, 2007.
103. Cao, F., & Jana, S.C. Nanoclay-tethered shape memory polyurethane nanocomposites, *Polymer* **48** (13), 3790-3800, 2007.
104. Jang, M.K., et al. Shape memory polyurethanes cross-linked by surface modified silica particles, *J. Mater. Chem.* **19** (8), 1166-1172, 2009.
105. Jana, R.N., et al. Synthesis and properties of shape memory polyurethane nanocomposites reinforced with poly( $\epsilon$ -caprolactone)-grafted carbon nanotubes, *Fiber Polym.* **9** (3), 247-254, 2008.
106. Luo, H., et al. Path-dependent and selective multi-shape recovery of a polyurethane/cellulose-whisker nanocomposite, *Mater. Lett.* **89**, 172-175, 2012.
107. Haghayegh, M., & Sadeghi, G.M.M. Synthesis of shape memory polyurethane/clay nanocomposites and analysis of shape memory, thermal, and mechanical properties, *Polym. Compos.* **33** (6), 843-849, 2012.
108. Razzaq, M.Y., et al. Thermal, electrical and magnetic studies of magnetite filled polyurethane shape memory polymers, *Mater. Sci. Eng. A* **444** (1-2), 227-235, 2007.
109. Sahoo, N.G., et al. Influence of carbon nanotubes and polypyrrole on the thermal, mechanical and electroactive shape-memory properties of polyurethane nanocomposites, *Compos. Sci. Technol.* **67** (9), 1920-1929, 2007.

110. Yoo, H.J., et al. Polyurethane-carbon nanotube nanocomposites prepared by in-situ polymerization with electroactive shape memory, *J. Macromol. Sci., Phys. B* **45** (4), 441-451, 2006.
111. Cai, Y., et al. Synthesis and properties of magnetic sensitive shape memory Fe<sub>3</sub>O<sub>4</sub>/poly( $\epsilon$ -caprolactone)-polyurethane nanocomposites, *J. Appl. Polym. Sci.* **127** (1), 49-56, 2013.
112. Choi, J.T., et al. Shape memory polyurethane nanocomposites with functionalized graphene, *Smart Mater. Struct.* **21** (7), 075017-075026, 2012.
113. Chung, Y.C., et al. Covalent bonding of surface-modified montmorillonite nanoparticle with polyurethane and its impact on shape memory effect and mechanical properties, *J. Thermoplast. Compos. Mater.* **24** (4), 477-497, 2011.
114. Lee H.F., & Yu, H.H. Study of electroactive shape memory polyurethane-carbon nanotube hybrids, *Soft Matter* **7** (8), 3801-3807, 2011.
115. Deka, H., & Karak, N. Bio-based hyperbranched polyurethane/clay nanocomposites: adhesive, mechanical, and thermal properties, *Polym. Adv. Technol.* **22** (6), 973-980, 2011.
116. Zhou, L., et al. Synthesis and characterization of multiwalled carbon nanotube/polyurethane composites via surface modification multiwalled carbon nanotubes using silane coupling agent, *Polym. Compos.* **33** (11), 1866-1873, 2012.
117. Xu, L., et al. Investigation on structures and properties of shape memory polyurethane/silica nanocomposites, *Chin. J. Chem.* **29** (4), 703-710, 2011.
118. Suen, M.C., & Chen, C.C. Thermal and structural characterization of quasi-nanometer zirconium carbon/polyurethane composites prepared under roller pressure, *J. Appl. Polym. Sci.* **100** (1), 191-197, 2006.
119. Cho, J.W., et al. Electroactive shape-memory polyurethane composites incorporating carbon nanotubes, *Macromol. Rapid Commun.* **26** (5), 412-416, 2005.
120. Ahmad, M., et al. Feasibility study of polyurethane shape-memory polymer actuators for pressure bandage application, *Sci. Technol. Adv. Mater.* **13** (1), 015006-015013, 2012.
121. Ahn, J.S., et al. In situ temperature tunable pores of shape memory polyurethane membranes, *Smart Mater. Struct.* **20** (10), 105024-105033. 2011.
122. Paik, H., et al. Development and application of conducting shape memory polyurethane actuators, *Smart Mater. Struct.* **15** (5), 1476-1482, 2006.

## **Chapter 2**

# **Vegetable oil based hyperbranched polyurethanes**

### **Highlights**

This chapter consists of three subchapters, where the first subchapter describes the utilization of different vegetable oils for the synthesis of hyperbranched polyurethane. Hyperbranched polyurethanes were synthesized from poly( $\epsilon$ -caprolactone)diol as a macroglycol, 1,4-butanediol as a chain extender, monoglyceride of different vegetable oils (*Mesua ferrea*, castor and sunflower, separately) as a bio-based chain extender, triethanolamine as a multifunctional moiety and toluene diisocyanate by pre-polymerization technique using of A<sub>2</sub> + B<sub>3</sub> approach. The effect of composition and structure of the fatty acids of the above three vegetable oils on the performance of the synthesized hyperbranched polyurethanes was described in this subchapter. In the second subchapter hyperbranched polyurethanes were synthesized using different amount of monoglyceride of *Mesua ferrea* L. seed oil by utilizing the same preparative method. The hyperbranched polyurethanes were also synthesized by using different amount of multifunctional moiety, triethanolamine; which is described in the third subchapter. The structures of the synthesized hyperbranched polyurethanes were characterized by Fourier transform infrared spectroscopy, nuclear magnetic resonance spectroscopy and X-ray diffraction studies. The thermal stability; mechanical properties such as tensile strength, elongation at break, impact resistance and scratch resistance; and chemical resistance were studied for all the above hyperbranched polyurethanes. The shape memory behavior for individual hyperbranched polyurethane was also studied. From this chapter it is clear that the hyperbranched polyurethane with 10 wt% monoglyceride of *Mesua ferrea* L. seed oil with 2.5 wt% triethanolamine is the best polymer for further study as a shape memory material.

---

*Parts of this work are published in*

1. Kalita, H., & Karak, N., *J. Appl. Polym. Sci.* **131** (1), 39579-39587, 2014.
2. Kalita, H., & Karak, N., *Iran. Polym. J.* **21** (4), 263-271, 2012.
3. Kalita, H., & Karak, N., *Polym. Eng. Sci.* **52** (11), 2454-2461, 2012.

## 2A. Effect of different vegetable oils

### 2A.1. Introduction

Polyurethane is found to be a versatile polymeric material, as discussed in Chapter 1. The realization of finite petroleum resources, growing environmental concerns and waste disposal problems encourage the utilization of bio-resources like vegetable oils as raw materials for the preparation of polyurethanes.<sup>1-4</sup> This is due to the fact that such oils have numerous advantages such as easy availability, relatively inexpensive, versatility in structure and property, inherent biodegradability and environmentally benign.<sup>5</sup> Again, hydroxylation of vegetable oils is one of the good approaches to obtain the required polyol to be used in polyurethane synthesis. In the present investigation different vegetable oils were modified through transesterification to obtain the desired diols. Properties of the vegetable oil based polyurethane depend on the characteristics i.e. physical and chemical structures, which include the number of hydroxyl groups in the polyols, degree of unsaturation, length of the fatty acid chains and position of hydroxyl groups in the fatty acid chain.<sup>6,7</sup> Thus in this study, monoglycerides of three vegetable oils with different structures and compositions were utilized to obtain shape memory polyurethanes with unique structural architecture.

Among different polymeric architectures, hyperbranched polyurethanes are winning great attention to the material scientists and technologists due to their highly functionalized non-entangled structure and easy synthesis.<sup>8</sup> They offer many advantages like lower melt and solution viscosity, higher solubility and higher reactivity than their linear analogs as discussed in Chapter 1. However, in general they suffer from brittleness character. This problem is addressed in this report by incorporating long chain containing flexible macroglycol, poly( $\epsilon$ -caprolactone)diol as well as by the presence of long flexible hydrocarbon chain of the vegetable oils. Therefore, hyperbranched polyurethanes with different vegetable oils and a flexible macroglycol were synthesized as shape memory polymers.

Nature shows examples of stimuli-responsive phenomenon like leaves of *Mimosa pudica* fold inward rapidly when touched, sunflower bend towards the sun, chameleons change color according to the environmental situation.<sup>9</sup> Thus to mimic nature, enormous efforts are being made to design stimuli-responsive polymers particularly segmented polyurethanes, which have the potential applications in fields of sensors, micro-actuators, intelligent biomedical devices,



implant materials, self deployable structures, smart textiles, sporting goods and so on.<sup>10-15</sup> Shape memory polyurethanes are not only the stimuli-responsive smart polymeric materials, which can respond to a particular external stimuli such as temperature, light, solvent, magnetic field and electric field by changing their shape but also possess desired other performance.<sup>16, 17, 11</sup> The net-points that are chemically or physically cross-linked network structures of segmented polyurethanes determine the permanent shape of the polymer network whereas switching segment acts as a mobile phase.<sup>18-22</sup> Shapes are driven by the specific transition temperature ( $T_{trans}$ ) which is either near to the glass transition temperature ( $T_g$ ) or close to melting temperature ( $T_m$ ). Thus the synthesis of elastic polyurethanes with different structures and properties is an apt choice in recent time.

In the present study hyperbranched polyurethanes with long segment, therefore, were synthesized using monoglyceride of different vegetable oils (*Mesua ferrea*, castor and sunflower) to investigate the effect of structure and composition of vegetable oils on various properties including shape memory behavior of them. Polyurethane without vegetable oil was synthesized for comparison purpose.

## 2A.2. Experimental

### 2A.2.1. Materials

*Mesua ferrea* L. seeds were collected from Darang, Assam, India and the oil was isolated by solvent soaking method. It was purified by alkali refining technique using 0.01% aqueous NaOH solution and washed with distilled water. Finally the washed oil was dried under vacuum. Sunflower and castor oil were purchased from Sigma, Germany and Aldrich Chemical, Australia, respectively and used after drying in a vacuum oven at 60 °C for 12 h. The composition and structure of the fatty acids of the oils are given in Table 2A.1.

Glycerol was obtained from Merck, India. Its density is 1.26 g/mL, maximum 0.005% sulphated ash and minimum assay 99%. It was used after drying under vacuum at 60 °C for 12 h.

Calcium oxide was purchased from S.D. Fine Chemical Ltd., Mumbai. The minimum assay is 95%. It was used as received.

Poly( $\epsilon$ -caprolactone) diol (PCL) was obtained from Solvay Co., UK. PCL has the density 1.071 g/c.c., hydroxyl number 37 mg KOH/g and number average molecular weight ( $M_n$ ) 3000 g/mol. It was used after drying under vacuum at 60 °C for 12 h.

Toluene diisocyanate (TDI) a mixture of 80% 2,4 and 20% 2,6 isomers was purchased from Sigma-Aldrich, Germany. It has formula weight ( $F_w$ ) 174.16 g/mol, density 1.214 g/c.c., melting point (m.p.) 21.8 °C and boiling point (b.p.) 251 °C. It was used as received.



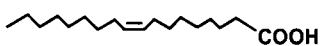

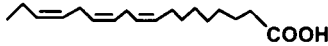

1,4-butanediol was obtained from Merck, Germany. Its density is 1.02 g/mL and minimum assay 99%. It was used after drying under vacuum at 60 °C for 12 h.

Triethanolamine was obtained from Merck, India. Its density is 1.12 g/mL and minimum assay is 99%. It was used after drying under vacuum at 60 °C for 12 h.

Xylene was purchased from Merck, India. It was vacuum distilled and kept in 4A type molecular sieves before use.

Methanol was obtained from Merck, India. It has  $F_w$  58.0 g/mol, density 0.971 g/c.c. and b.p. 56-57 °C. It is used after distillation.

**Table 2A.1:** Structure and composition of fatty acid of the vegetable oil

Fatty acid	Structure	<i>Mesua ferrea</i> L. seed oil	Sunflower oil	Castor oil
Palmitic acid (%)		15.9	5.2	0.5
Stearic acid (%)		9.5	2.7	0.5
Oleic acid (%)		52.3	37.2	2
Linoleic acid (%)		22.3	53.8	1
Linolenic acid (%)		-	1.0	0.5
Ricinoleic acid (%)		-	-	95

#### 2A.2.2. Preparation of monoglyceride of the oil

The monoglyceride (MG) of the oils was prepared by glycerolysis process as reported earlier.<sup>23</sup> Briefly, a 250 mL three-neck round bottom flask equipped with a nitrogen inlet tube, a thermometer and a mechanical stirrer was used for the preparation of monoglyceride of the vegetable oil. The required amount of oil (0.023 mol) and glycerol (0.046 mol) were taken in the above flask with constant stirring. An amount of 0.05% (with respect to the oil) of CaO was

added into the reaction mixture and then the temperature was gradually increased up to the 220 °C and stirred for 2 h. The formation of the monoglyceride was confirmed by its solubility in methanol (MG: methanol=1:3 vol/vol) at room temperature.

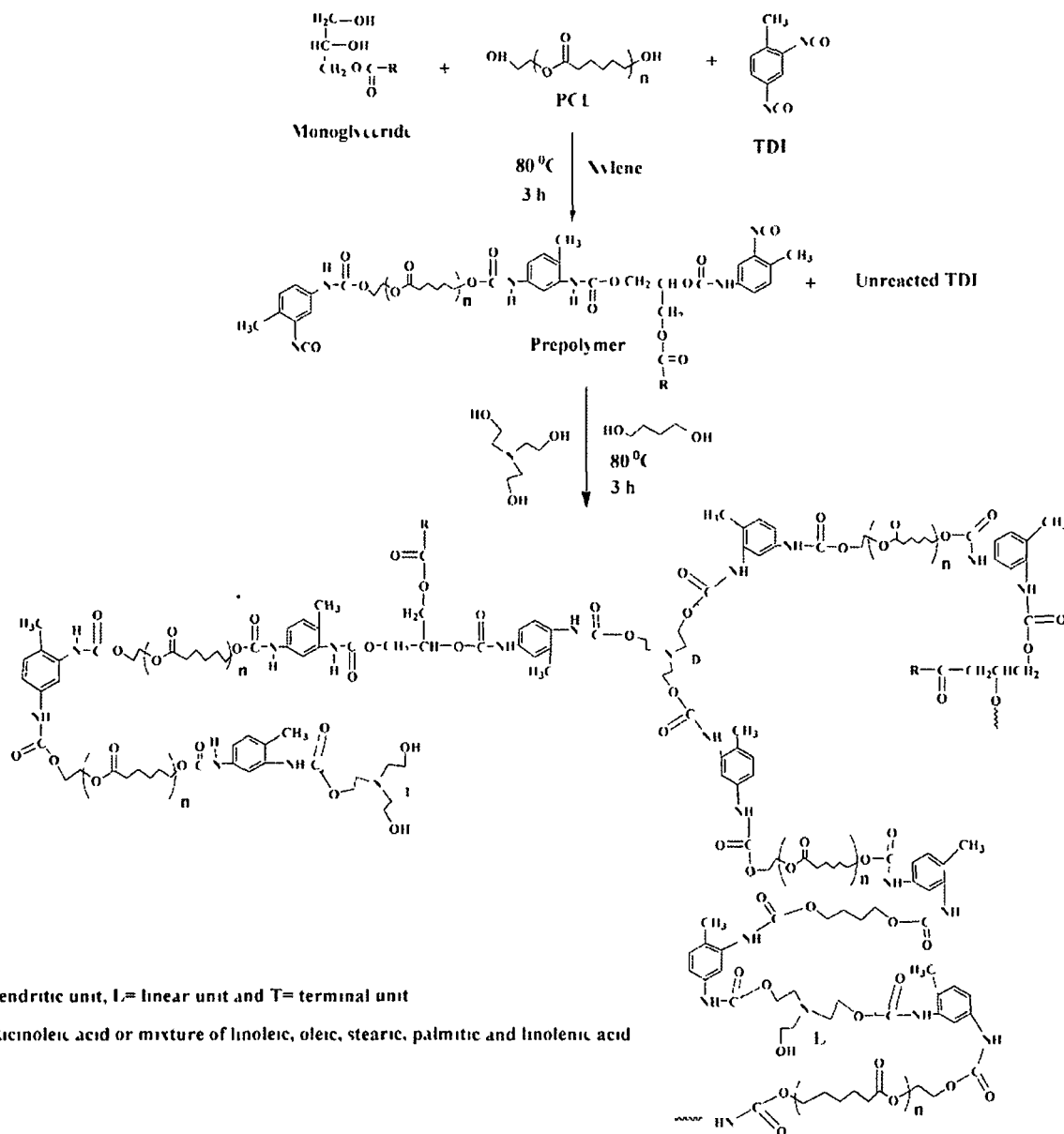
#### 2A.2.3. Synthesis of hyperbranched polyurethane

Hyperbranched polyurethanes were synthesized by a two step one pot  $A_2 + B_3$  approach (Scheme 2A.1). A 250 mL three-neck round bottom flask equipped with a mechanical stirrer, nitrogen inlet tube, and a thermometer was taken on an oil bath for this polymerization reaction. The MG of *Mesua ferrea* L. seed oil (3 mmol) and PCL (2 mmol) were taken in the above reaction flask with 30 mL of xylene at constant stirring. TDI (10 mmol) was slowly injected into the above reaction mixture by the help of a glass syringe at room temperature. The reaction mixture was allowed to react for 3 h at  $(80 \pm 5)$  °C to obtain the pre-polymer. The reaction mixture was then allowed to cool to room temperature followed by drop by drop addition of 1, 4-butanediol (2.75 mmol) and triethanolamine (1.5 mmol) into the pre-polymer solution (NCO/OH ratio 1.0). The temperature of the reaction mixture was again raised to  $(80 \pm 5)$  °C and stirred continuously for another ~3 h. After completion of the reaction, a part of the viscous product was precipitated in water and then dried in a vacuum oven at 60 °C for 24 h for the NMR analysis. The remaining part was solution cast on different substrates for other testing. The same procedure was followed for the synthesis of other vegetable oil based polyurethanes (monoglyceride of the vegetable oil content was 10 wt% in all the cases) and without oil based (instead of oil, 1, 4-butanediol is used) polyurethane. The synthesized hyperbranched polyurethanes were coded as CHBPU10, MHBPU10, SHBPU10 and HBPU for castor, *Mesua ferrea*, sunflower and without oil based polyurethanes respectively. The compositions of these polyurethanes are given in Table 2A.2.

#### 2A.2.4. Instrumentation

The infrared spectra of the hyperbranched polyurethanes were recorded by impact 410, Nicolet (Madison, USA) Fourier transform infrared (FTIR) spectrophotometer using KBr pellets. Nuclear magnetic resonance ( $^1\text{H-NMR}$ ) spectrum of the polymers was recorded by a 400 MHz NMR spectrometer (JEOL, Japan) using  $d_6$ -DMSO as the solvent and TMS as an internal

standard The X-ray diffraction study was carried out at room temperature (ca 25 °C) by a Rigaku X-ray diffractometer (Miniflex, UK) over a range of  $2\theta=10-70^\circ$  The thermal analysis was done by a Simadzu, Japan thermal analyzer, TG50, with a nitrogen flow rate of 30 mL/min at a heating rate of 10 °C/min The differential scanning calorimetry (DSC) study was done by DSC 60, Simadzu, Japan at a 3 °C/min heating rate under the nitrogen flow rate of 30 mL/min from -30 to 150 °C.



**Scheme 2A.1:** Synthesis of hyperbranched polyurethane

**Table 2A.2:** Composition (mmol) of reactant

Reactant	CHBPU10	MHBPU10	SHBPU10	HBPU
Poly( $\epsilon$ -caprolactone)diol	2	2	2	2
Monoglyceride	2.8	3	2.9	-
Toluene diisocyanate	10	10	10	10
1, 4-butanediol	2.95	2.75	2.85	5.75
Triethanolamine	1.5	1.5	1.5	1.5
NCO/OH	1	1	1	1

The mechanical properties such as tensile strength and elongation at break were measured with the help of an Universal Testing Machine (UTM), Zwick Z010, Germany with a  $10 \times 10^3$  N load cell and crosshead speed of 0.05 m/min using sample of dimension: 0.1 m  $\times$  0.01 m  $\times$  0.00035 m. Scratch resistance of the dry films was measured by using a scratch hardness tester, model number 705 (Sheen instrument Ltd., UK) with stylus accessory and a travel speed of 0.03-0.04 m/s. The impact resistance was measured by an impact tester (S.C. Dey & Co., India, 1.0 m is the maximum height) using the standard ASTM D 1037 falling weight method. A weight of 0.85 kg was allowed to fall on the mild steel plate coated film from minimum to maximum height up to which the film was not damaged. The maximum height was taken as the impact resistance.

#### 2A.2.5. Shape memory behavior testing

The shape memory properties of the hyperbranched polyurethanes were determined through a series of thermo-cyclic tensile experiments. At first, films were cut into rectangular strips with the dimension of 0.04 m  $\times$  0.005 m  $\times$  0.0006 m and heated at 60 °C ( $T_m + 20$  °C) for 5 min. Then they were stretched to twice of their original length ( $L_0$ ) using a stretching rate of 0.02 m/min and stretched length is denoted as  $L_1$ . Immediately, the stretched samples were freezed at 0 to 5 °C ( $T_m - 40$  °C) for 5 min to fix the temporary shape and the length was measured as  $L_2$  after removal of the load. Subsequently, the samples were reheated at the same temperature (60 °C) for the same period of time for the shape recovery and the length obtained is denoted as  $L_3$ . The same procedure was followed for the repeated cycles of test. The shape

recovery and shape fixity are two shape memory parameters calculated from the following equations:

$$\text{Shape recovery (\%)} = [(L_1 - L_3) / L_0] \times 100 \text{ ----- (2A.1)}$$

$$\text{Shape fixity (\%)} = [(L_2 - L_0) / L_0] \times 100 \text{ ----- (2A.2)}$$

## 2A.3. Results and discussion

### 2A.3.1. Infrared spectroscopic study

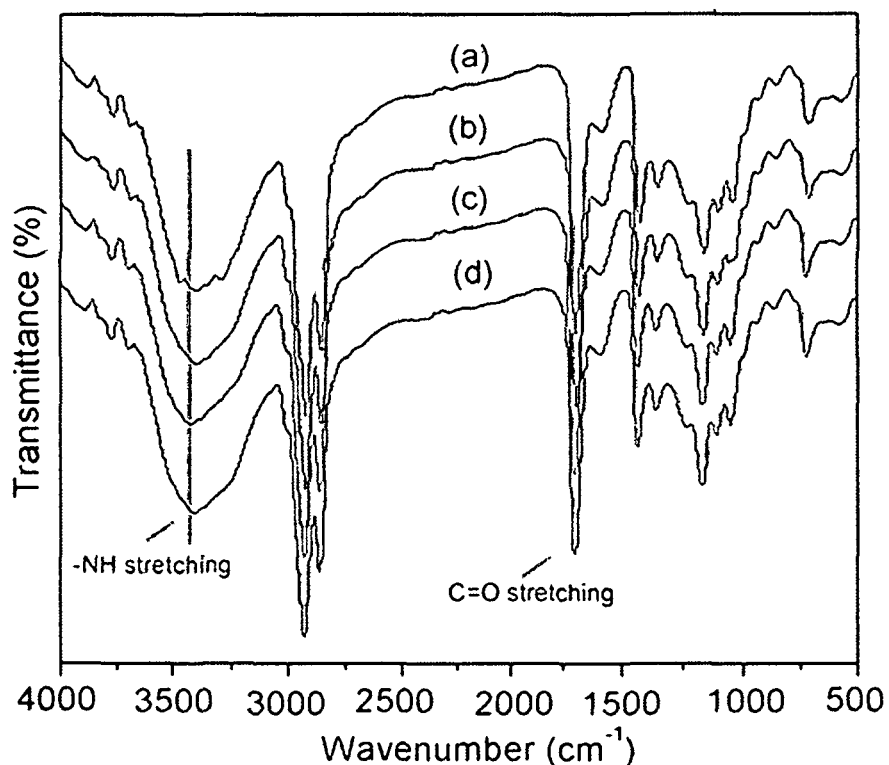
FTIR spectra of all the synthesized hyperbranched polyurethanes are shown in Fig. 2A.1. The bands appeared at 3406-3430  $\text{cm}^{-1}$  for the hydrogen bonded -NH stretching vibration, 1720-1725  $\text{cm}^{-1}$  for -C=O stretching vibration and 1061  $\text{cm}^{-1}$  for the C-O-C stretching vibration are the three characteristic bands of urethane group. Polyurethane contains proton donor group (-NH) and proton acceptor group (>C=O). The -NH groups of the urethane linkages in polyurethane is hydrogen bonded with -C=O of the urethane linkages and ether oxygen of the soft segments. Therefore, the -NH stretching frequency was shifted to lower frequency.<sup>24, 25</sup> The band assigned at 2926  $\text{cm}^{-1}$  for the -CH stretching of -CH<sub>2</sub> and -CH<sub>3</sub>. The bands at 870  $\text{cm}^{-1}$  and 730  $\text{cm}^{-1}$  are due to the substituted aromatic ring of TDI. All the above bands confirmed the formation of urethane group in the synthesized hyperbranched polyurethanes.

### 2A.3.2. XRD study

Fig. 2A.2 shows X-ray diffractograms of all the hyperbranched polyurethanes. XRD analysis confirmed the presence of crystallinity of the thermoplastic hyperbranched polyurethanes. Two strong diffraction peaks at  $2\theta=21.6^\circ$  and  $2\theta=23.7^\circ$  are due to the (100) and (200) planes of PCL crystals. *Mesua ferrea* L. seed oil based polyurethane showed the highest crystallinity as compared to the other two vegetable oils based polyurethanes.

### 2A.3.3. NMR study

The structure of the hyperbranched polyurethanes was studied by the <sup>1</sup>H-NMR spectral analyses. <sup>1</sup>H-NMR spectra of all the hyperbranched polyurethanes are shown in Fig. 2A.3.



**Fig. 2A.1:** FTIR spectra for (a) CHBPU10, (b) MHBPU10, (c) SHBPU10 and (d) HBPU

The peaks at  $\delta=0.80-0.87$  ppm,  $\delta=1.19-1.27$  ppm and  $\delta=1.47-1.51$  ppm are due to the terminal methyl group, all internal  $-\text{CH}_2-$  groups and the protons for  $-\text{CH}_2-$  groups attached next to the terminal methyl group of the fatty acid chain of the monoglyceride of the oil, respectively.<sup>26, 23</sup> The protons of allylic  $-\text{CH}_2-$ ,  $-\text{CH}_2-$  adjacent to  $-\text{O}-$  of urethane group and  $-\text{CH}_3$  of TDI showed peaks at  $\delta=2.19-2.26$  ppm,  $\delta=2.23-2.27$  ppm and  $\delta=2.40-2.68$  ppm, respectively. The  $-\text{CH}_2-$  protons of triethanolamine moiety attached to the urethane linkages and  $-\text{CH}_2-$  protons attached to  $-\text{OH}$  groups were found at  $\delta=3.1-3.3$  ppm and  $\delta=3.96-4.03$  ppm, respectively. The integration ratio of these two peaks indicates the extent of substitution of the  $-\text{OH}$  of the branch generating moiety, triethanolamine. The observed ratio was found to be 2.50 for the CHBPU10,

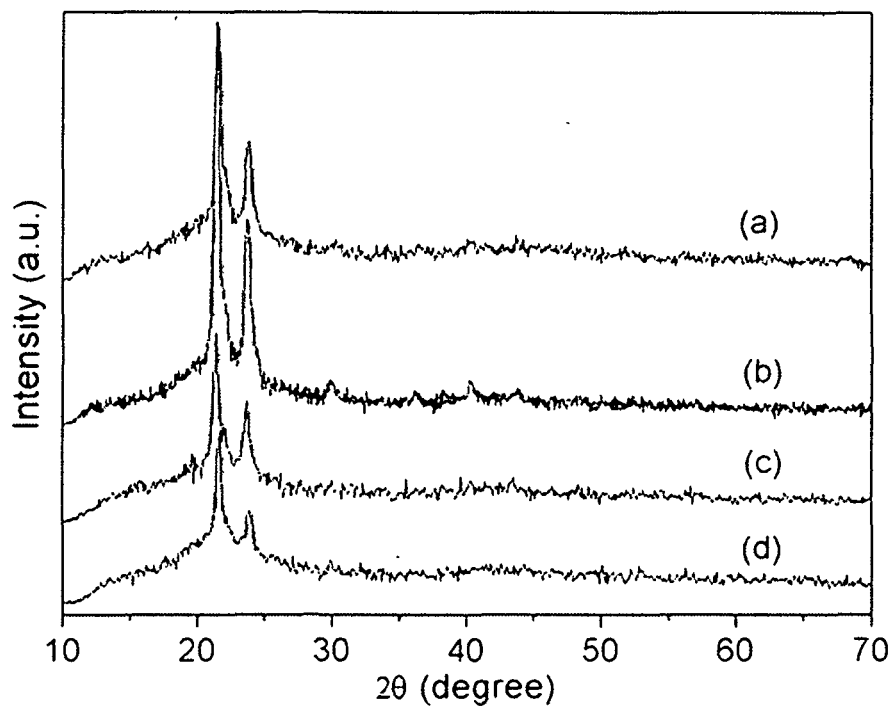


Fig. 2A.2: X-ray diffractograms for (a) CHBPU10, (b) MHBPU10, (c) SHBPU10 and (d) HBPU

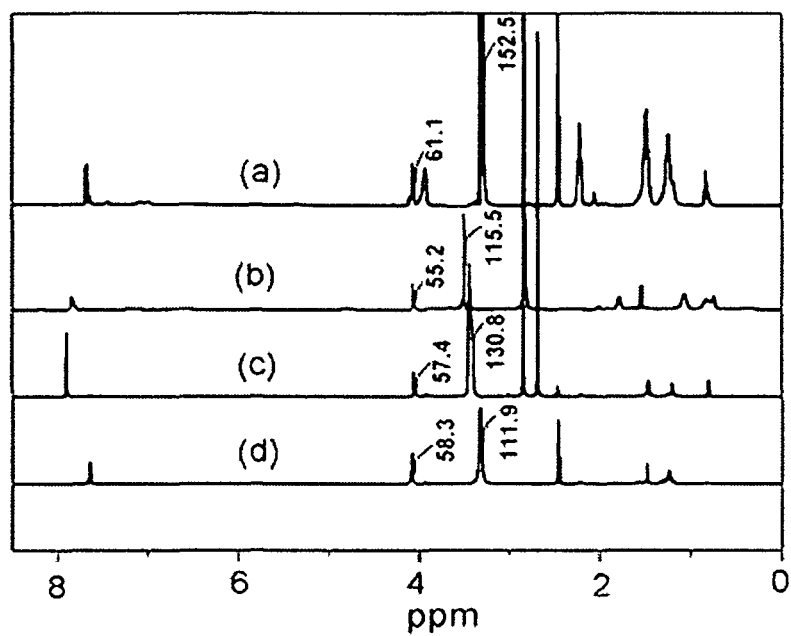


Fig. 2A. 3:  $^1\text{H}$ -NMR spectra for (a) CHBPU10, (b) SHBPU10, (c) MHBPU10 and (d) HBPU



which indicated that out of three –OH groups, 2.50 groups were substituted i.e. the degree of branching is about 0.83. Similarly, the degree of branching was found to be 0.76, 0.70 and 0.64 for MHBPU10, SHBPU10 and HBPU, respectively. The chemical shifts of protons of aromatic moiety were observed at around  $\delta=7.7-8.00$  ppm. However, there was another peak for castor oil based hyperbranched polyurethane at  $\delta=3.8$  ppm for the –CH– proton attached to the –OH of the ricinoleic moiety. All the above spectral analyses confirmed the formation of hyperbranched polyurethane.

#### 2A.3.4. Thermal property

The thermal stability of all the hyperbranched polyurethanes is shown in Fig. 2A.4. The thermal stability of the polyurethane depends on the structures of the hard segment and soft segment, degree of the urethane linkage, hard to soft segments ratio, extent of physical cross-linking, molecular weight and its distribution. From the result it is seen that the synthesized polyurethane exhibited two steps degradation pattern. The first step is due to the degradation of the aliphatic chains as well as the breakage of urethane linkages, whereas the second step is due to the degradation of the aromatic moieties. From the thermograms, it can be seen that the castor oil based polyurethane showed the lowest thermal stability. The hydroxyl functionality of the castor oil is higher than the other oils and therefore the degree of urethane linkage is more. It is reported that higher the degree of urethane linkage, lower is the thermal degradation.<sup>27</sup> *Mesua ferrea* L. seed oil based polyurethane showed the highest thermal stability as compared to the other two vegetable oil based polyurethanes. This is due to higher crystallinity as supported by the XRD study. DSC curves of all the hyperbranched polyurethanes are shown in Fig. 2A.5. From the figure it is observed that the castor oil based hyperbranched polyurethane showed the highest melting temperature ( $T_m$ ). In the castor oil based polyurethane the degree of urethane linkages is more and hence the secondary interactions such as H-bonding and polar-polar interactions are also more. The crystallinity of these hyperbranched polyurethanes is coming from the crystalline nature of the PCL moiety.

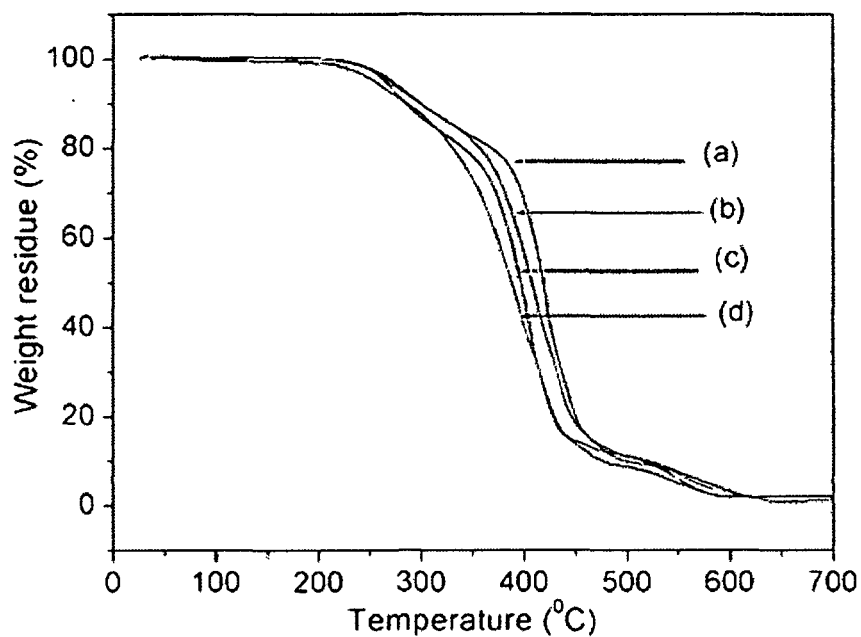


Fig. 2A.4: TGA thermograms for (a) MHBPU10, (b) SHBPU10, (c) HBPU and (d) CHBPU10

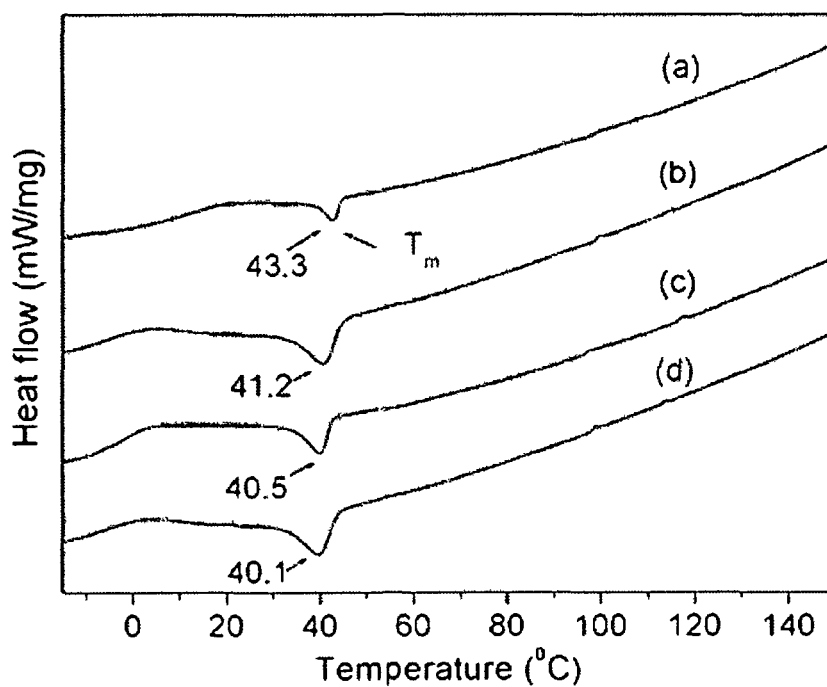


Fig. 2A.5: DSC curves for (a) CHBPU10, (b) MHBPU10, (c) SHBPU10 and (d) HBPU

### 2A.3.5. Mechanical property

The mechanical properties of all the hyperbranched polyurethanes are shown in Table 2A.3. The performance of polyurethane depends on the degree of the urethane groups, virtual or physical cross-linking density and the various interactions such as H- bonding, polar-polar etc. interactions.<sup>26</sup> All the polyurethanes showed overall good tensile strength. However, the castor oil based polyurethane showed the highest tensile strength. This may be due to the unusual characterization of the castor oil, which typically comprises of 95% ricinoleic acid and the average hydroxyl value 2.7. Therefore, the degree of the urethane linkages and physical cross-linking are higher in castor oil based polyurethane than the others. However, the elongation at break is lower than the other vegetable oil based polyurethanes due to rigidity of the structure that is generated though various secondary interactions in the polymer chains. All the synthesized polyurethanes exhibited overall good scratch hardness. However, the castor oil based polyurethane exhibited the highest scratch hardness due to increased overall toughness of the material. All the synthesized vegetable oil based polyurethanes showed the excellent impact resistance. Impact resistance of the material may be explained from the angle of toughness of the films that is the ability to absorb the applied external energy as well as the transfer of energy to its adjacent molecular networks. All the samples exhibited good flexibility as observed by the bending test, as the films could be bent onto a rod of 0.001 m diameter without any fracture on the bent films. This is due to the high flexibility of the soft segments and the presence of long chain fatty acid moiety in the structure of the polyurethanes.<sup>23</sup> The results revealed that the castor oil based polyurethane exhibited the superior mechanical property to those of the other vegetable oil based polyurethanes.

**Table 2A.3:** Mechanical properties of the hyperbranched polyurethanes

Property	CHBPU10	MHBPU10	SHBPU10	HBPU
Tensile strength (MPa)	7.5 ± 0.2	6.2 ± 0.2	5 ± 0.4	7.4 ± 0.3
Elongation at break (%)	607 ± 3.2	614 ± 3.4	620 ± 3.1	595 ± 3.3
Scratch hardness (kg)	6 ± 0.2	5.4 ± 0.1	5 ± 0.1	5 ± 0.2
Impact resistance (m)	0.9 ± 0.05	0.9 ± 0.05	0.9 ± 0.05	0.9 ± 0.05
Bending (m)	<0.001	<0.001	<0.001	<0.001
Gloss (60°)	88 ± 3	86 ± 2	85 ± 3	85 ± 3

### 2A.3.6. Shape memory property

Shape memory behaviors of different hyperbranched polyurethanes are shown in Fig. 2A.6. All vegetable oil based polyurethanes exhibited good shape fixity, indicating that the micro-Brownian movements of molecular chains in physical network of soft segment are frozen at fixing temperature and thereby stored the applied load as strain energy. The vegetable oil based polyurethanes showed higher shape fixity as comparable to the oil free polyurethane. This may be due to the presence of long chain fatty acid moieties in the structure that enhanced the secondary interactions during the vitrification. All the vegetable oil based polyurethanes showed the good shape recovery though the castor oil based one showed the best shape recovery (Table 2A.4). This can be attributed to the presence of more physical cross-linking due to higher urethane linkages that cause storing of more deformed energy in the system. The sample immediately releases the deformed stored energy and returned to the original shape on reheating.

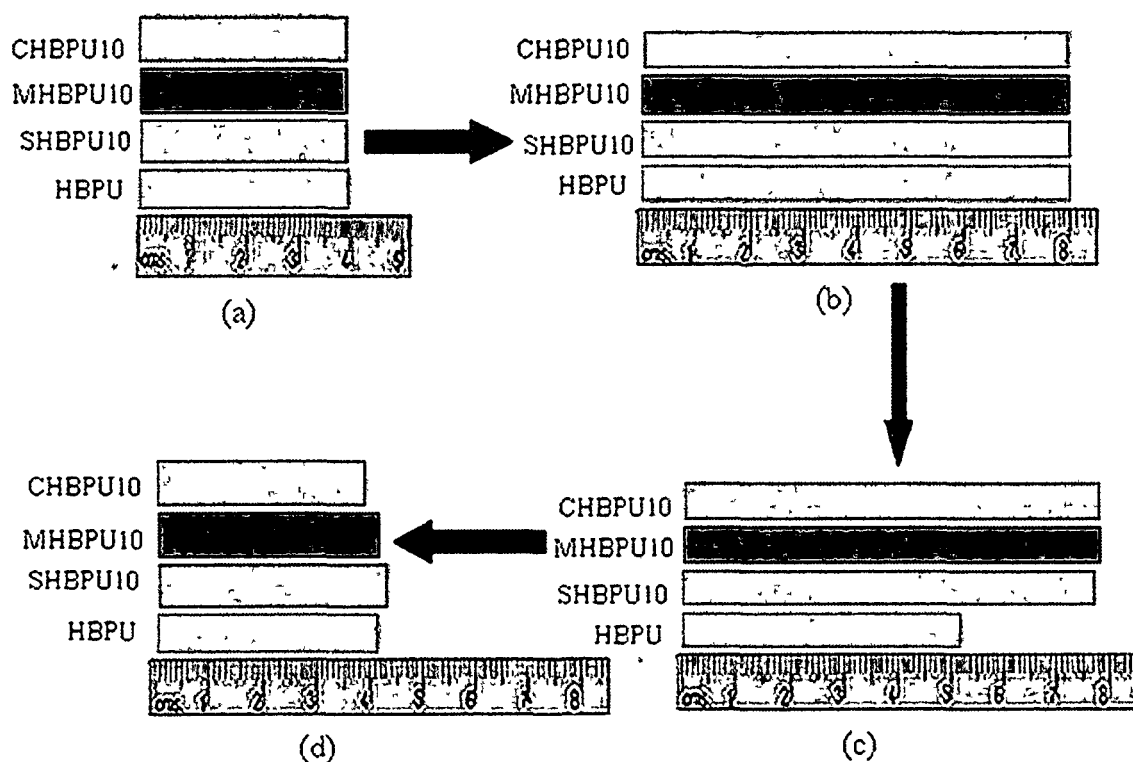


Fig. 2A.6: Shape memory behaviors of hyperbranched polyurethanes (a) original shape, (b) extended shape, (c) fixed shape and (d) recovered shape

The *Mesua ferrea* L. seed oil based hyperbranched polyurethane also exhibited good shape recovery. This may be due to the presence of various secondary interactions as well as high crystalline region of this hyperbranched polyurethane. No significant change of shape fixity and shape recovery was obtained for all the hyperbranched polyurethanes for five cycles of test.

**Table 2A.4:** Shape memory behavior of hyperbranched polyurethanes

Sample code	Shape fixity (%)	Shape recovery (%)
CHBPU10	96.6 ± 0.1	98.5 ± 0.2
MHBPU10	98 ± 0.2	96 ± 0.1
SHBPU10	96.5 ± 0.3	94.8 ± 0.2
HBPU	32.5 ± 0.3	96.5 ± 0.1

#### 2A.4. Conclusion

In this study different vegetable oil based polyurethanes were synthesized successfully. All the synthesized polyurethanes showed overall good performance. However, the castor oil based hyperbranched polyurethane exhibited the highest tensile strength, whereas *Mesua ferrea* L. seed oil based polyurethane showed the highest thermal stability among all the studied hyperbranched polyurethanes. The castor oil based polyurethane showed the highest shape recovery, though all the polyurethanes showed good shape fixity except the free oil based one. Thus the characteristics of the oils have the strong influence on the performance including shape memory effect of hyperbranched polyurethanes. The synthesized vegetable oil based hyperbranched polyurethanes might be utilized in different potential fields such as surgical sutures, catheters, drug delivery, micro-actuators and sensors and so on. Further, it can be concluded that based on overall desired performance including thermostability, melting temperature (near to body temperature), shape memory property, availability and cost, the *Mesua ferrea* L. seed oil based hyperbranched polyurethane is the best polymer as shape memory material for future study.

## 2B. Effect of vegetable oil content

### 2B.1. Introduction

As it has been seen that vegetable oil based polyurethane, a useful polymeric material, has diversified applications in different fields such as coating, adhesive, leather, composite, elastomer, biomedical etc.<sup>28, 29</sup> So more details study on the amount of vegetable oil is necessary to be performed. This is due to the fact that the incompatibility of the hard and soft segments and subsequent phase segregation into separate domain can enhance desirable properties of polyurethane.<sup>30</sup> The properties of the polyurethane can be observed by the judicious variation of chemical constituents as well as composition of soft and hard segments. A large number of reports are in the literature on the effects of the structure of the hard and soft segments on the physical, thermal and chemical properties of these polymers.<sup>31, 32</sup> The importance of vegetable oils has already discussed in the above subchapter 2A. Karak et al. studied various properties of the synthesized castor oil based hyperbranched polyurethanes.<sup>33</sup> Cao et al. reported the structure and mechanical properties of hyperbranched polyurethane using hyperbranched polyester as a precursor.<sup>34</sup> The effect of vegetable oil content also has important role in the structure-property relationship of the polyurethanes. Again, the advantages of the hyperbranched structure are elaborated in subchapter 2A, so vegetable oil based hyperbranched polyurethane with varying amount of oil was presented in this chapter. As the *Mesua ferrea* L. seed oil based hyperbranched polyurethane exhibited overall suitability as shape memory polymer, so this oil is used in the present investigation.

In order to study the effect of amount of bio-based component on the performance and shape memory behavior of segmented polyurethane, three different weight percentages of monoglyceride of *Mesua ferrea* L. seed oil (5%, 10%, and 15% by wt/wt) were used to synthesize the hyperbranched polyurethanes along with the other components as used in subchapter 2A, in the present investigation. Hyperbranched polyurethanes without any vegetable oil were also synthesized for comparison purpose. In this chapter, therefore, the synthesis, characterization and properties of bio-based hyperbranched polyurethanes with different amount of vegetable oil was used to study the effect of oil content on the performance including shape memory behaviors.

## 2B.2. Experimental

### 2B.2.1. Materials

*Mesua ferrea* L. seed oil is used to synthesize the hyperbranched polyurethanes in the present study. The same technique was used for the isolation and purification of oil as described in subchapter 2A, section 2A.2.1. The monoglyceride of the *Mesua ferrea* L. seed oil was prepared by the glycerolysis process as described in subchapter 2A, section 2A.2.2. The chemicals such as TDI, PCL, 1, 4-butanediol and triethanolamine used are same as described in subchapter 2A, section 2A.2.1.

### 2B.2.2. Synthesis of hyperbranched polyurethane

The same synthetic procedure was used as described in subchapter 2A, section 2A.2.3 for the synthesis of different amount of monoglyceride of the *Mesua ferrea* L. seed oil based hyperbranched polyurethanes. The compositions of the reactants are given in Table 2B.1. The synthesized polyurethanes were coded as HBPU, MHBPU5, MHBPU10, MHBPU15 for 0%, 5%, 10%, and 15% of monoglyceride of the *Mesua ferrea* L. seed oil by wt/wt, respectively.

### 2B.2.3. Instrumentation

The FTIR, XRD, SEM, TGA and DSC analyses of the synthesized hyperbranched polyurethanes were carried out by using the same instruments and same procedures as described in subchapter 2A, section 2A.2.4.

The mechanical properties such as tensile strength, elongation at break, scratch resistance and impact resistance were performed by the same way as described in subchapter 2A, section 2A.2.4. The chemical resistance test was performed using the standard ASTM D 543-67 method by taking the weighted amount of dry film in different chemical media of 250 mL beakers containing 150 mL of the individual chemical medium for the specified period of time. The chemical resistance was determined by measuring the weight change for the individual film after the completion of test period.

The shape memory behaviors of the hyperbranched polyurethanes were studied by the same method as described in subchapter 2A, section 2A.2.5.

**Table 2B.1:** Composition (mmol) of reactant

Reactant*	mmol of the reactant				Functionality of reactant
	HBPU	MHBPU5	MHBPU10	MHBPU15	
Poly( $\epsilon$ -caprolactone)diol	2	2	2	2.4	2
Monoglyceride	0	1.35	3	4.4	2
1, 4-butanediol	5.75	4.4	2.75	1.05	2
Triethanolamine	1.5	1.5	1.5	1.7	3
Total equivalents of -OH = mol $\times$ functionality of -OH	20	20	20	20.8	-
Toluene diisocyanate	10	10	10	10.4	2
Total equivalents of -NCO = mol $\times$ functionality of -NCO	20	20	20	20.8	-
-OH:-NCO equivalent ratio	1	1	1	1	-

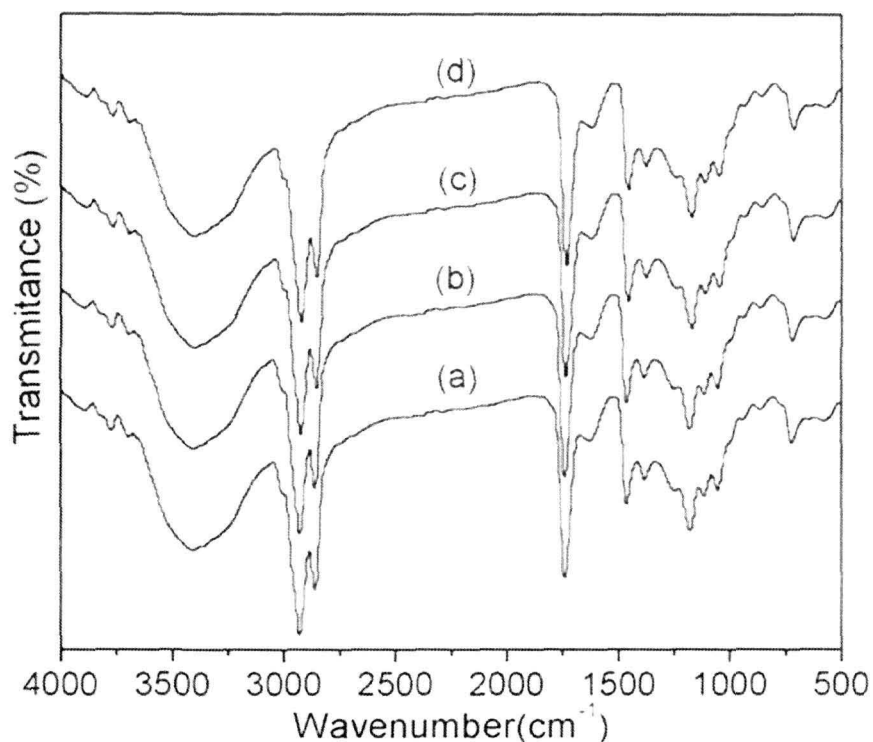
\* Hard segment content = 32-35% and multifunctional moiety = 2.5% (wt/wt)

## 2B.3. Results and discussion

### 2B.3.1. Infrared spectroscopic study

The FTIR spectra have been studied to monitor the conformation, extend of hydrogen bonding along with the confirmation of polyurethane formation. The FTIR spectra of all the hyperbranched polyurethanes are shown in Fig. 2B.1. The disappearance of band 2250-2270  $\text{cm}^{-1}$  indicates that there is no free -NCO group present in the hyperbranched polymer structure. The band corresponds to the free -NH group diminished and the band assigned for the hydrogen bonded -NH group appeared.<sup>35, 36</sup> This indicates that the majority of -NH groups of urethane linkages (-NH-COO-) participated in hydrogen bonding as already stated in the above subchapter.



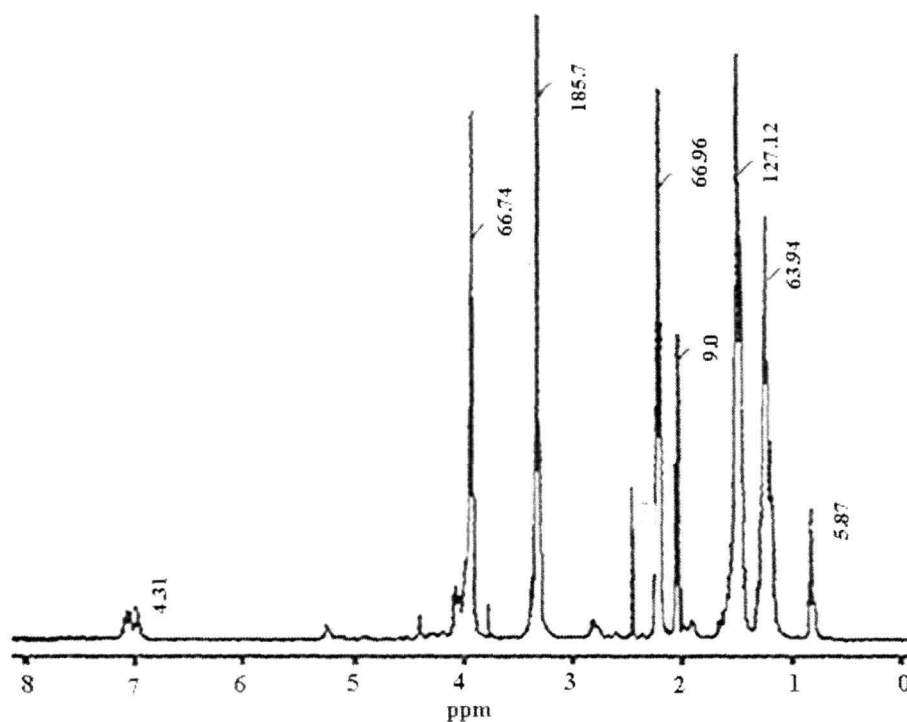


**Fig. 2B.1:** FTIR spectra for (a) HBPU, (b) MHBPU5, (c) MHBPU10 and (d) MHBPU15

### 2B.3.2. NMR study

The  $^1\text{H-NMR}$  spectrum of hyperbranched polyurethane (MHBPU5) is shown in Fig. 2B.2. The peaks at  $\delta=0.83$  ppm,  $\delta=1.25$  ppm and  $\delta=1.5$  ppm are due to the protons of terminal methyl group, all internal  $-\text{CH}_2-$  groups and the protons for  $-\text{CH}_2-$  groups attached next to the terminal methyl group of the fatty acid chain of the monoglyceride of the oil, respectively.<sup>37</sup> The protons of allylic  $-\text{CH}_2-$ ,  $-\text{CH}_2-$  adjacent to  $-\text{O}-$  of urethane group and  $-\text{CH}_3$  of TDI showed peaks at  $\delta=2.03$  ppm,  $\delta=2.23$  ppm and  $\delta=2.35$  ppm respectively.<sup>38</sup> The  $-\text{CH}_2-$  protons of triethanolamine moiety attached to the urethane linkages and  $-\text{CH}_2-$  protons adjacent to  $-\text{OH}$  groups were found at  $\delta=3.21$  ppm and  $\delta=3.92$  ppm, respectively. The integration ratio of these two peaks was 2.78. Thus the degree of branching is about 0.93. Thus the synthesized polyurethane is a highly branched polymer. The peak at  $\delta=5.30$  ppm may be due to the protons of the unsaturated carbons of the fatty acid segment. The protons of aromatic moiety were

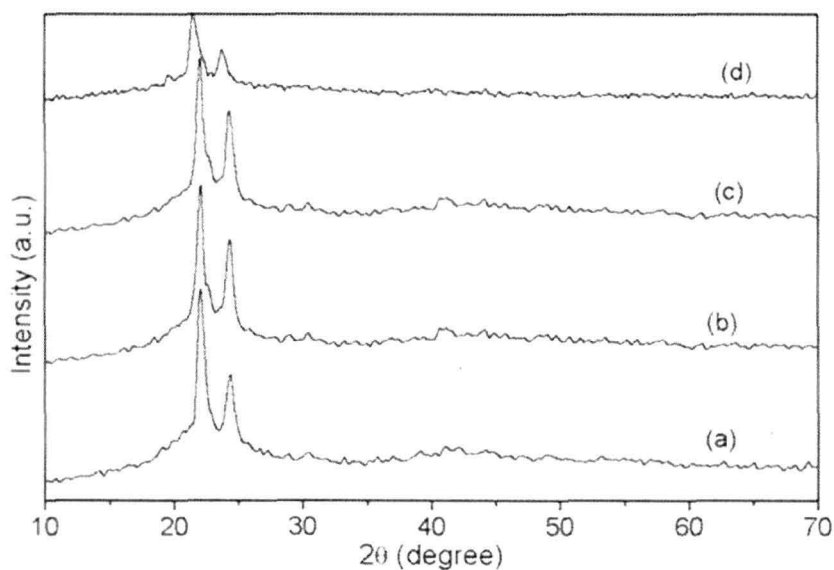
observed at around  $\delta=7.00$  ppm. The above spectral analyses established the formation of vegetable oil based hyperbranched polyurethane (MHBPU5).



**Fig. 2B.2:** The <sup>1</sup>H-NMR spectrum of hyperbranched polyurethane (MHBPU5)

### 2B.3.3. XRD study

Fig. 2B.3 shows X-ray diffractograms of hyperbranched polyurethanes. The two diffraction peaks at  $2\theta=21.9^\circ$  and  $2\theta=23.8^\circ$  are due to the (100) and (200) planes of PCL crystals. The position of the peaks remained same for all the hyperbranched polyurethanes which indicated that there is no effect of the amount of monoglyceride on the nature of crystallinity, though slight variation was observed at higher dose of monoglyceride.



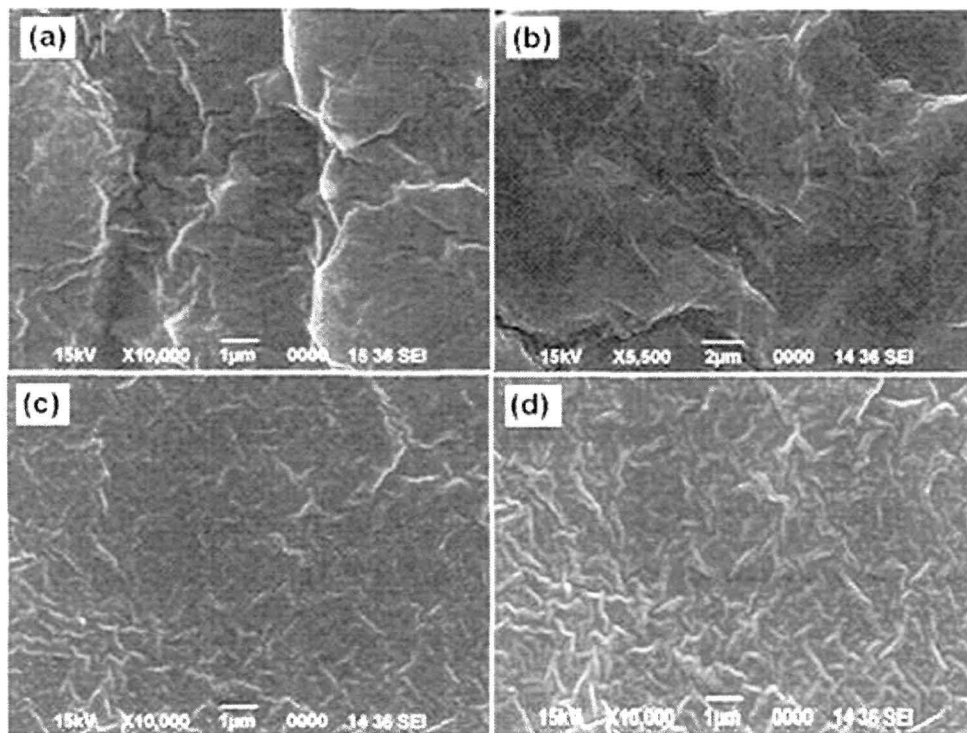
**Fig. 2B.3:** XRD diffractograms for (a) HBPU, (b) MHBPU5, (c) MHBPU10 and (d) MHBPU15

#### 2B.3.4. Morphological study

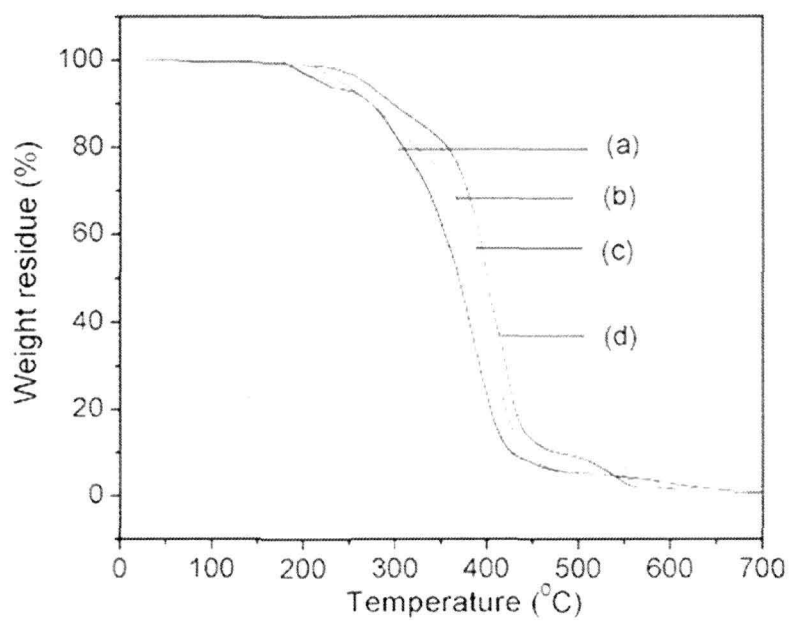
The morphological study of the hyperbranched polyurethanes was carried out with the help of scanning electron microscope. Fig. 2B.4. shows the SEM micrographs of hyperbranched polyurethanes. The SEM micrographs indicate uniform phase distribution of the polymers at different amount of monoglyceride of the *Mesua ferrea* L. seed oil.

#### 2B.3.5. Thermal property

Thermal stability of the hyperbranched polyurethanes are shown in Fig. 2B.5. The thermal stability of the hyperbranched polyurethanes was found to be significantly improved with the increase of amount of monoglyceride of *Mesua ferrea* L. seed oil. This may be due to the increase of mesuaferrol, tocopherol and other aromatic moieties in the structure with the increase of the monoglyceride of *Mesua ferrea* L. seed oil.<sup>39</sup>



**Fig. 2B.4:** SEM micrographs for (a) HBPU, (b) MHBPU5, (c) MHBPU10 and (d) MHBPU15



**Fig. 2B.5:** Thermograms for (a) HBPU, (b) MHBPU5, (c) MHBPU10 and (d) MHBPU15

### 2B.3.6. Mechanical property

From Table 2B.2, it is observed that the hyperbranched polyurethanes possess good mechanical properties viz. tensile strength, scratch hardness and impact resistance along with desirable elongation at break. This is due to the presence of intermolecular attractions between -NH and -CO through H-bonding, polar-polar interaction etc.<sup>26</sup> However, the tensile strength decreased from 7.4 MPa to 5.5 MPa with the increase in amount of bio-based component. This can be attributed to the decrease of degree of secondary interactions like H-bonding,  $\pi$ - $\pi$  interaction between aromatic moieties etc. in the structure due to the increase in amount of long chain hydrocarbon moiety. All the hyperbranched polyurethanes exhibited good scratch hardness and impact strength. The bending test results indicated that all the hyperbranched polyurethanes have sufficient flexibility. This is due to the high flexibility of the soft segments as already discussed in subchapter 2A, section 2A.3.5.<sup>23</sup>

**Table 2B.2:** Mechanical properties of the hyperbranched polyurethanes

Property	HBPU	MHBPU5	MHBPU10	MHBPU15
Tensile strength (MPa)	7.4 ± 1.2	7.1 ± 1.4	6.2 ± 1.1	5.5 ± 1.1
Elongation at break (%)	596 ± 3.5	745 ± 3.2	615 ± 2.7	598 ± 2.6
Scratch hardness (kg)	3 ± 0.1	3 ± 0.1	3.3 ± 0.1	3.4 ± 0.2
Impact resistance* (m)	0.9 ± 0.05	0.9 ± 0.05	0.9 ± 0.05	0.9 ± 0.05
Bending (m)	<0.001	<0.001	<0.001	<0.001

\*1 m is the limit of the instrument

### 2B.3.7. Chemical resistance

Chemical resistance tests of the hyperbranched polyurethanes were studied under various chemical environments (Table 2B.3) such as 3% NaOH, 10% EtOH, 5% HCl, 10% NaCl and distilled water for 30 days and the changes of weights were determined after the tests. All the films showed good chemical resistance in almost all the chemical environments, except in NaOH solution. This is due to the presence of alkali hydrolyzable ester groups of PCL and monoglyceride segments. Good chemical resistance of all the films is due to the presence of secondary interactions such as polar-polar and H-bonding, virtual cross-linking, presence of aromatic moiety etc.

**Table 2B.3:** Chemical resistance as changes of weight (g) of hyperbranched polyurethanes

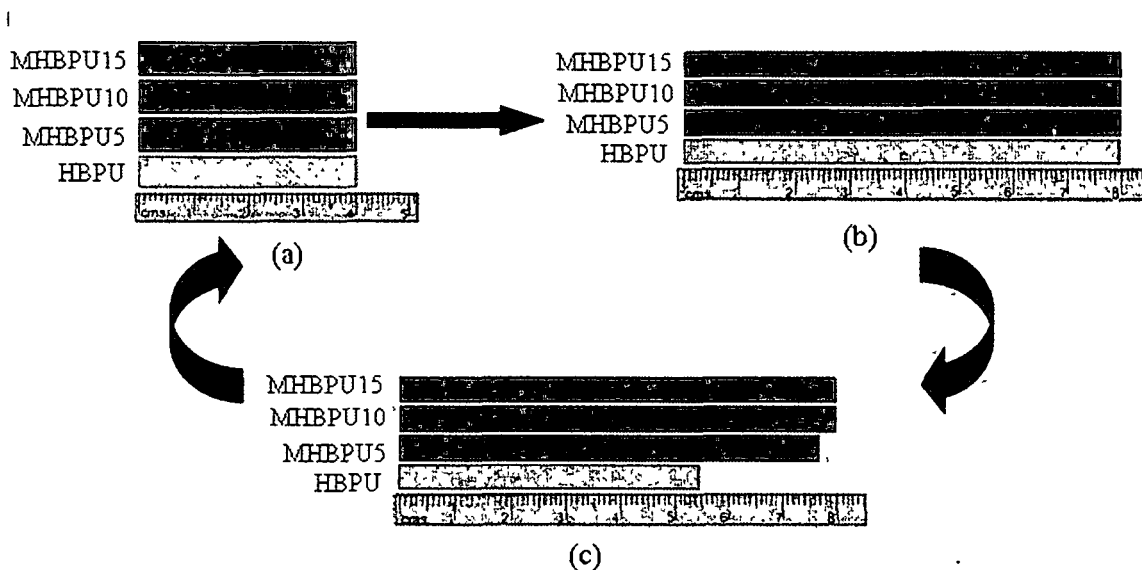
Chemical medium	HBPU	MHBPU5	MHBPU10	MHBPU15
3% NaOH	-0.048	-0.071	-0.078	-0.089
10% EtOH	+0.001	+0.002	+0.004	+0.006
5% HCL	-0.001	-0.003	-0.006	-0.003
10% NaCl	+0.003	+0.004	+0.004	+0.002
Distilled Water	+0.011	+0.015	+0.019	+0.018

#### 2B.3.8. Shape memory property

The shape memory behaviors of the polyurethanes are shown in Fig. 2B.6. The shape recovery was measured after the samples were fixed for 5 min at (-3 to 0) °C, below the transition temperature of PCL crystals. All the prepared hyperbranched polyurethanes exhibited good shape recovery, (95-96.2)% (Table 2B.4). Good shape recovery of the hyperbranched polyurethanes may be attributed to the increased stored energy of system due to uniform distribution of hard segments including triethanolamine moiety in the structure.<sup>40, 41</sup> The bio-based hyperbranched polyurethanes exhibited excellent shape fixity (95-99)%. However, the prepared polyurethane without monoglyceride of *Mesua ferrea* L. seed oil showed shape fixity of 32.5% only. The shape fixity of the polyurethane increases with the increase of monoglyceride content, which may be due to the increase of physical cross-linking in the system during cooling process.

**Table 2B.4:** Shape memory properties of hyperbranched polyurethanes

Property	HBPU	MHBPU5	MHBPU10	MHBPU15
Shape recovery (%)	95 ± 1.2	96 ± 0.7	96 ± 0.8	96.2 ± 0.8
Shape fixity (%)	32.5 ± 1.0	95 ± 1.4	98 ± 1.1	99 ± 0.8



**Fig. 2B.6:** Shape memory behaviors of hyperbranched polyurethanes (a) original shape, (b) stretched shape and (c) fixed shape

## 2B.4. Conclusion

The study revealed that the hyperbranched polyurethane containing different amounts of monoglyceride of *Mesua ferrea* L. seed oil can be synthesized successfully. The prepared hyperbranched polyurethanes showed good mechanical and thermal property. The thermal stability found to be increased with increase of the content of monoglyceride of *Mesua ferrea* L. seed oil. The hyperbranched polyurethanes exhibited good shape recovery. The shape fixity of the hyperbranched polyurethanes was found to be enhanced with increase of the amount of monoglyceride of *Mesua ferrea* L. seed oil. Thus the bio-based hyperbranched polyurethanes indicate the prospect of utilization as thermoresponsive smart materials for different potential applications. The study also indicated that the hyperbranched polyurethane with 10 wt% of monoglyceride along with other components exhibited the optimum performance.

## 2C. Effect of multifunctional component

### 2C.1. Introduction

The effects of composition and structure of fatty acids of vegetable oil, and the content of vegetable oil on the performance including shape memory behavior of oil-based hyperbranched polyurethanes are discussed in the earlier two subchapters. It has also been noticed that hyperbranched polymers have added advantages over their linear analogs. Thus deliberate and controlled branches in the structure of the polymer have prominent influence on the ultimate properties of the polymer. The physical properties and the final applications of the hyperbranched polymer depend on the chemical composition, polydispersity index, molecular weight and the degree of branching. Degree of branching, one of the most important parameters of hyperbranched polymers, which strongly influences the unique characters such as low solution and melt viscosity, high solubility, high reactivity, good compatibility with other components etc. of such polymers.<sup>42</sup> Thus controlling of degree of branching is paramount important for vegetable oil based polyurethanes too. Most of the hyperbranched polymers exhibited relatively high polydispersity indices, though that can be controlled by taking the suitable multifunctional moiety and proper choice of reaction conditions.<sup>43, 44</sup> Furthermore controlling the degree of branching of the hyperbranched polymers can control the properties of such vegetable oil based hyperbranched polyurethanes. The degree of branching can be varied by utilizing the different branch generating moieties with varying multiplicity. Deka et al. reported the synthesis of hyperbranched polyurethane using glycerol as a multifunctional moiety.<sup>26</sup> The properties of the hyperbranched polyurethane found to be significantly improved as compared to the linear analog. Jena et al. reported the synthesis of hyperbranched poly(urethane urea) by utilizing the different multifunctional moieties such as pentaerythritol, glycerol and trimethylolpropane, and studied their different properties.<sup>45</sup> Moreover the amount of multifunctional moiety has also the prominent role to control the properties of hyperbranched polyurethanes. As the amount of multifunctional moiety has strong effect on the structure property relationship of the hyperbranched polymers, so this effect is studied in this subchapter.

Authors, therefore, wish to present here the synthesis of *Mesua ferrea* L. seed oil based hyperbranched polyurethanes to investigate the effect of amount of multifunctional moiety,



triethanolamine (0%, 2.5% and 5% wt/wt) on various properties including shape memory behavior of hyperbranched polyurethane.

## 2C.2. Experimental

### 2C.2.1. Materials

*Mesua ferrea* L. seed oil is used in the present investigation. The same technique was utilized for the isolation and purification of this oil as stated in subchapter 2A, section 2A.2.1. The monoglyceride of the *Mesua ferrea* L. seed oil was prepared by the same process as described in subchapter 2A, section 2A.2.2. The chemicals used for the synthesis of hyperbranched polyurethane such as TDI, PCL, 1, 4-butanediol and triethanolamine are same as described in subchapter 2A, section 2A.2.1.

### 2C.2.2. Preparation of hyperbranched polyurethane

The same synthetic method is followed as stated earlier. The hyperbranched polyurethanes of *Mesua ferrea* L. seed oil were synthesized by taking different amount of multifunctional moiety, triethanolamine and other components like TDI, 1, 4-butanediol and PCL were same as used in subchapter 2A, section 2A.2.3. The synthesized hyperbranched polyurethanes were coded as MHBPU0, MHBPU10 and MHBPUT5 for 0%, 2.5% and 5% wt/wt of triethanolamine, respectively. The compositions of the components are given in Table 2C.1.

**Table 2C.1:** Composition (mmol) of reactant

Reactant	MHBPU0	MHBPU10	MHBPUT5
Poly( $\epsilon$ -caprolactone)diol	2	2	2.2
Monoglyceride	3	3	3
Toluene diisocyanate	11	10	11.4
1, 4-butanediol	6	2.75	1.4
Triethanolamine	0	1.5	3.2
NCO/OH	1	1	1

### 2C.2.3. Instrumentation

The FTIR, XRD, SEM, TGA and DSC analyses were done by using the same instruments as described in subchapter 2A, section 2A.2.4.

The mechanical properties such as tensile strength, elongation at break, scratch resistance and impact resistance were performed by the same method as described in subchapter 2A, section 2A.2.4.

The shape memory behaviors of the synthesized hyperbranched polyurethanes were measured by the same method as described in subchapter 2A, section 2A.2.5.

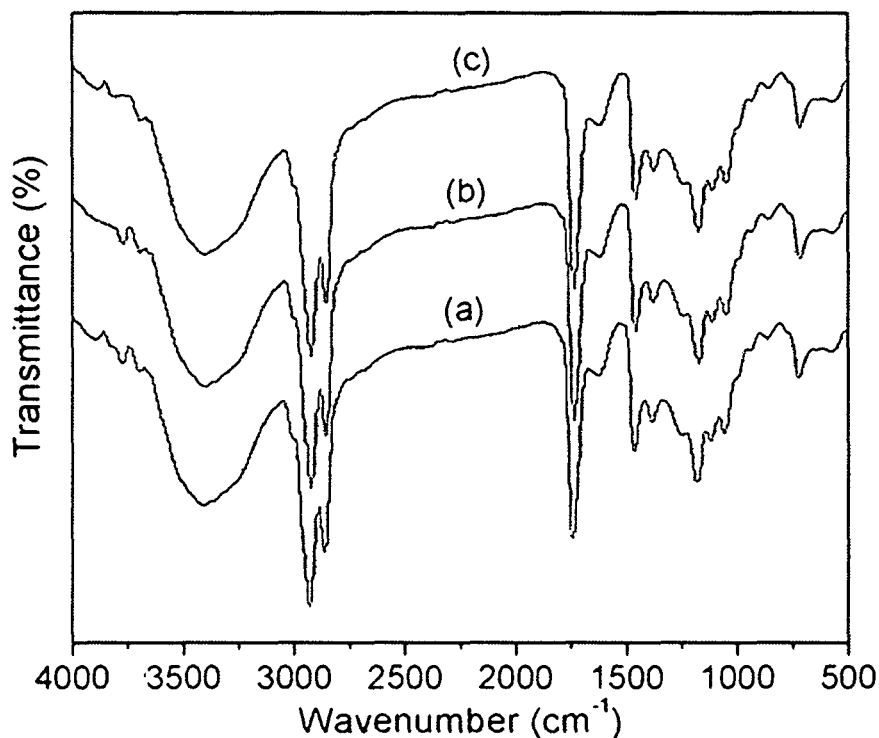
## 2C.3. Results and discussion

### 2C.3.1. Infrared spectroscopic study

The FTIR spectra of all the hyperbranched polyurethanes are shown in Fig. 2C.1. The band corresponds to the free -NH group diminished and the band assigned for the hydrogen bonded -NH group appeared is same as discussed in subchapter 2A, section 2A.3.1.<sup>46</sup> This indicates that the majority of -NH groups of urethane linkages (-NH-COO-) participated in the various interactions as stated in subchapter 2A, section 2A.3.1. The band at 1724 cm<sup>-1</sup> is attributed to the absorption of carbonyl of urethane linkages. All the characteristic bands of vegetable oil based hyperbranched polyurethane are given in Table 2C.2.

**Table 2C.2:** FTIR spectral data of the hyperbranched polyurethanes

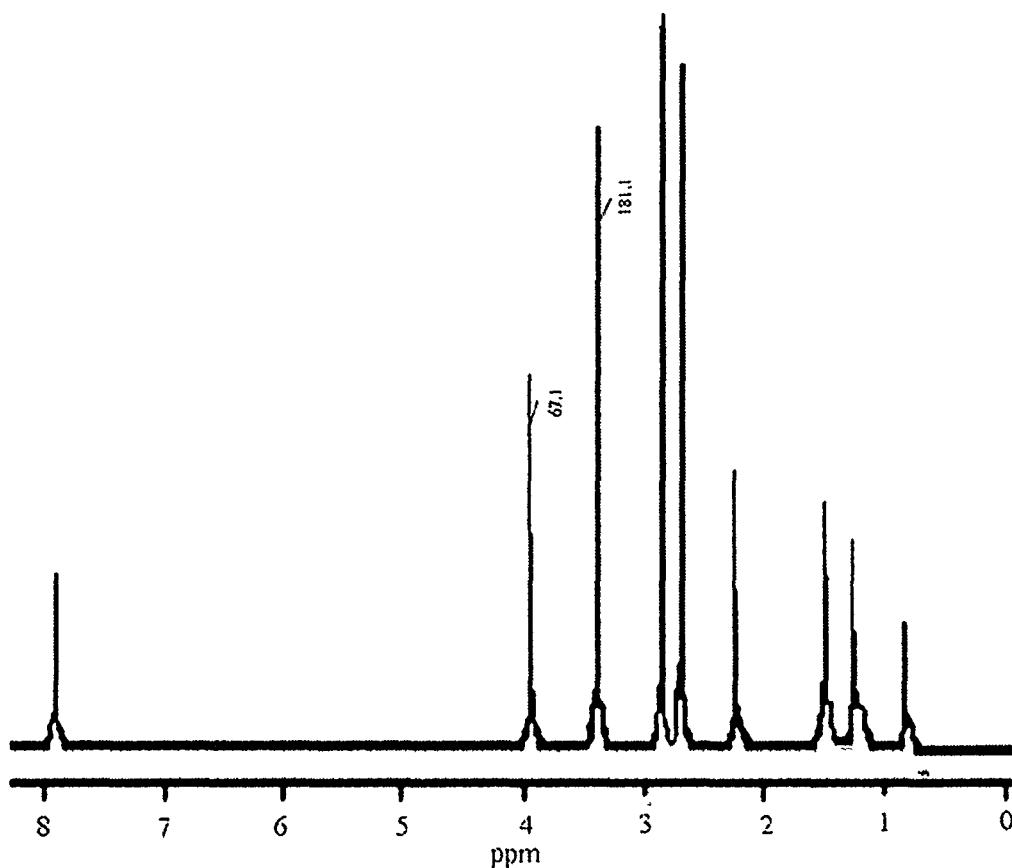
Band position (cm <sup>-1</sup> )	Functional groups
3406-3430	-NH stretching vibrations
2850-2950	-CH <sub>2</sub> symmetric and anti-symmetric stretching vibrations
1630-1740	Amide I, >C=O stretching vibrations
1450-1465	-CH <sub>2</sub> scissoring, -CH <sub>3</sub> deformation and -CH <sub>2</sub> bending vibration
1045-1060	-O-C=O stretching vibration of urethane/ester group



**Fig. 2C.1:** FTIR spectra for (a) MHBPU0, (b) MHBPU10 and (c) MHBPUT5

### 2C.3.2. NMR study

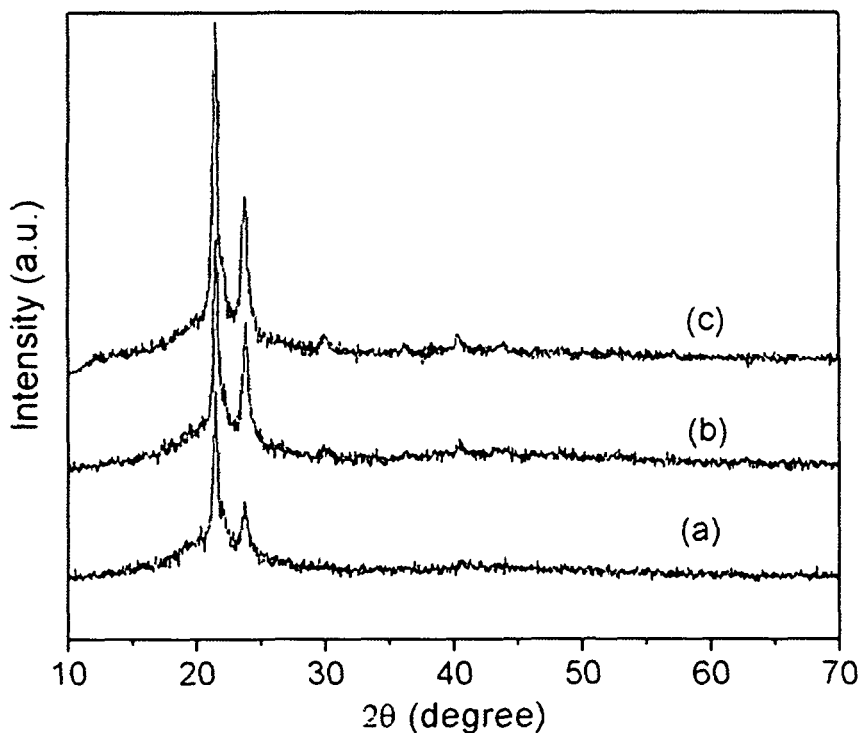
$^1\text{H-NMR}$  spectrum of hyperbranched polyurethane (MHBPUT5) is shown in Fig. 2C.2. The peaks at  $\delta=0.80$  ppm,  $\delta=1.19$  ppm and  $\delta=1.47$  ppm are due to the terminal methyl group, all terminal  $-\text{CH}_2-$  groups and the protons for  $-\text{CH}_2-$  groups attached next to the terminal methyl group of the fatty acid chain of the monoglyceride of the oil, respectively, as already discussed in the above subchapter.<sup>37, 38</sup> The protons of allylic  $-\text{CH}_2-$ ,  $-\text{CH}_2-$  adjacent to  $-\text{O}-$  of urethane group and  $-\text{CH}_3$  of TDI showed peaks at  $\delta=2.19$  ppm,  $\delta=2.23$  ppm and  $\delta=2.68$  ppm, respectively. The  $-\text{CH}_2-$  protons of triethanolamine moiety attached to the urethane linkages and  $-\text{CH}_2-$  protons attached to  $-\text{OH}$  groups were found at  $\delta=2.8$  ppm and  $\delta=3.92$  ppm, respectively. The integration ratio of the above two peaks is 2.70. Thus the degree of branching is about 0.9. Thus the synthesized polyurethane is a highly branched polymer. The protons of aromatic moiety were observed at around  $\delta=8.00$  ppm.



**Fig. 2C.2:** <sup>1</sup>H-NMR spectrum of hyperbranched polyurethane (MHBPUT5)

### 2C.3.3. X-ray diffraction study

Fig. 2C.3 shows X-ray diffractograms of hyperbranched polyurethanes. The peaks at  $2\theta=21.9^\circ$  and  $2\theta=23.8^\circ$  are due to the (100) and (200) planes of PCL crystals. The peak intensity increases with the increase of multifunctional moiety, triethanolamine content. This may be due to the increased secondary interaction in the polymer as indicated by the FTIR study. Due to the increased secondary interaction, the hard segments were forced to stay close to the cross-linking points and the relative order of hard segment alignment increased the intensity of the peak.



**Fig. 2C.3:** X-ray diffractograms for (a) MHBPU0, (b) MHBPU10 and (c) MHBPUT5

#### 2C.3.4. Thermal property

Generally the thermo-stability of polyurethanes depends on the number of aromatic moieties and urethane linkages, as they can withstand a considerable amount of heat.<sup>33</sup> Furthermore, the presence of secondary interactions such as H-bonding and polar-polar interactions augment the thermo-stability of the polyurethane. Thermal degradation of the polyurethane usually starts with the dissociation of the urethane bond followed by evaporation of carbon dioxide and isocyanate.<sup>7</sup> The thermal stability of the polyurethanes were found to be significantly improved from 225 °C to 260 °C with the increase of multifunctional moiety content (Fig. 2C.4) and causes the increased secondary interactions such as H-bonding, polar-polar interaction etc. in the polymer. The alignment of the hard segment and rigidity of the structure may be a consequence of the increased secondary interactions in the polymer. Fig. 2C.5 shows the DSC curves of hyperbranched polyurethanes. The glass transition temperature and

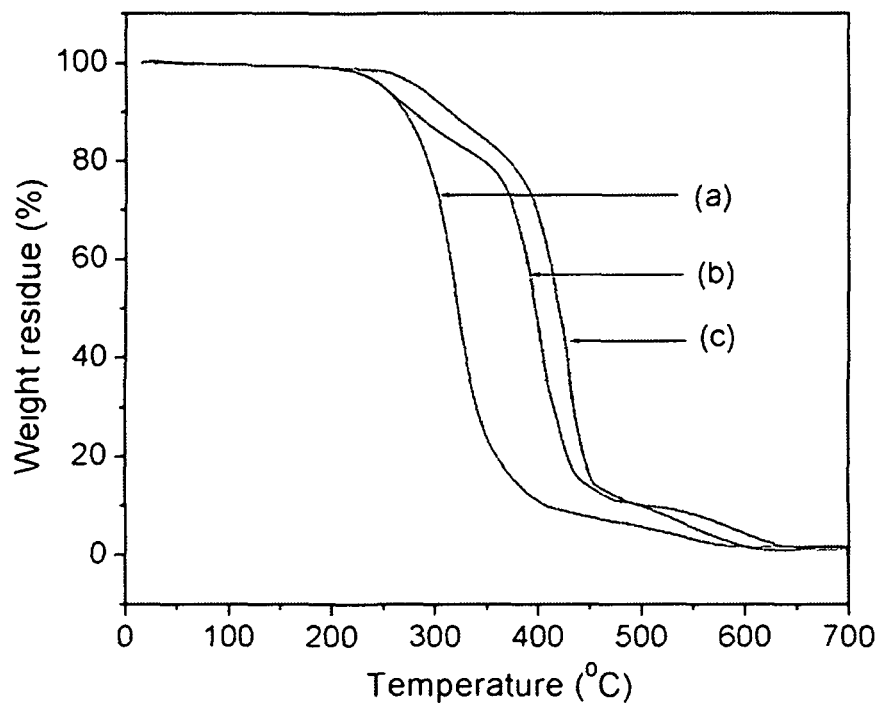


Fig. 2C.4: Thermograms for (a) MHBPU0, (b) MHBPU10 and (c) MHBPUT5

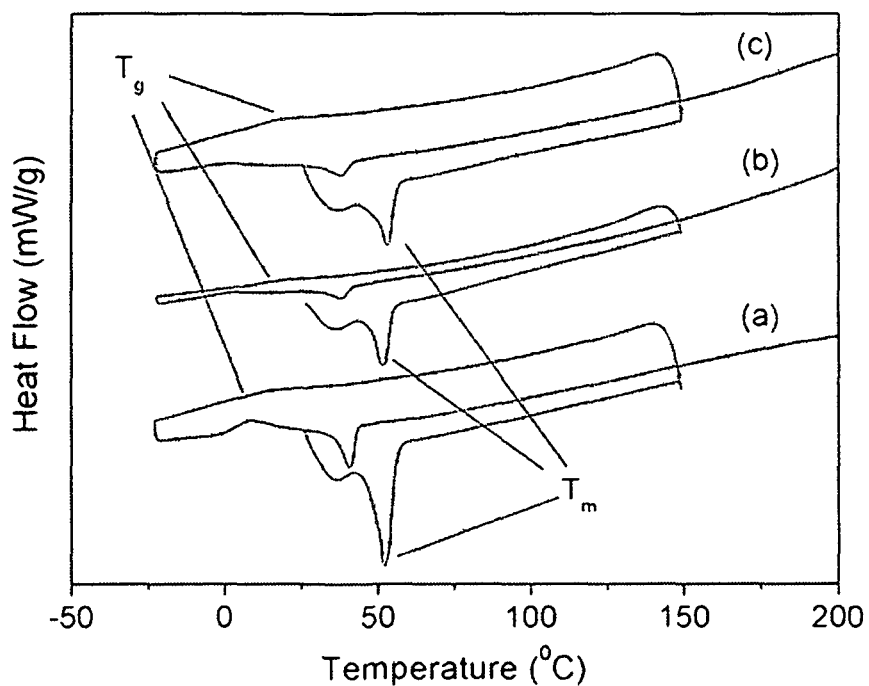


Fig. 2C.5: DSC curves for (a) MHBPU0, (b) MHBPU10 and (c) MHBPUT5

the melting temperature of hyperbranched polyurethanes increased with the increase of multifunctional moiety content (Table 2C.3). This may be due to the formation of compact structure that is formed through different types of secondary interactions as stated earlier.

**Table 2C.3:** Thermal properties of hyperbranched polyurethanes

Code	Glass transition temperature ( $T_g$ °C)	Melting temperature ( $T_m$ °C)
MHBPU0	5.1	50
MHBPU10	5.8	51.5
MHBPUT5	7	53.5

#### 2C.3.5. Mechanical property

The mechanical properties of hyperbranched polyurethanes are given in Table 2C.4. The tensile strength of the prepared polyurethane increases with increase of the amount of multifunctional moiety, triethanolamine which causes the increase of secondary interaction such as H-bonding, polar-polar interaction etc. in the structure. All the polymers showed good scratch hardness and the values increased with the increase of multifunctional moiety content in the structure due to the increase of overall toughness of the polymer. The hyperbranched polyurethane exhibited good impact resistance. The bending test results indicated that all the hyperbranched polyurethanes possess excellent flexibility. The cause of excellent flexibility is already stated in the above subchapter.<sup>23</sup> All the prepared polyurethanes also showed good adhesive strength for the plywood substrates. However, the adhesive strength decreases with the increase of multifunctional moiety content. This may be due to the increase of secondary interaction and which causes the decrease of reactive functional moiety. The gloss found to be increased with the increase of amount of multifunctional moiety. This is due to the increased dimension stability of the systems.

**Table 2C.4:** Mechanical properties of the hyperbranched polyurethanes

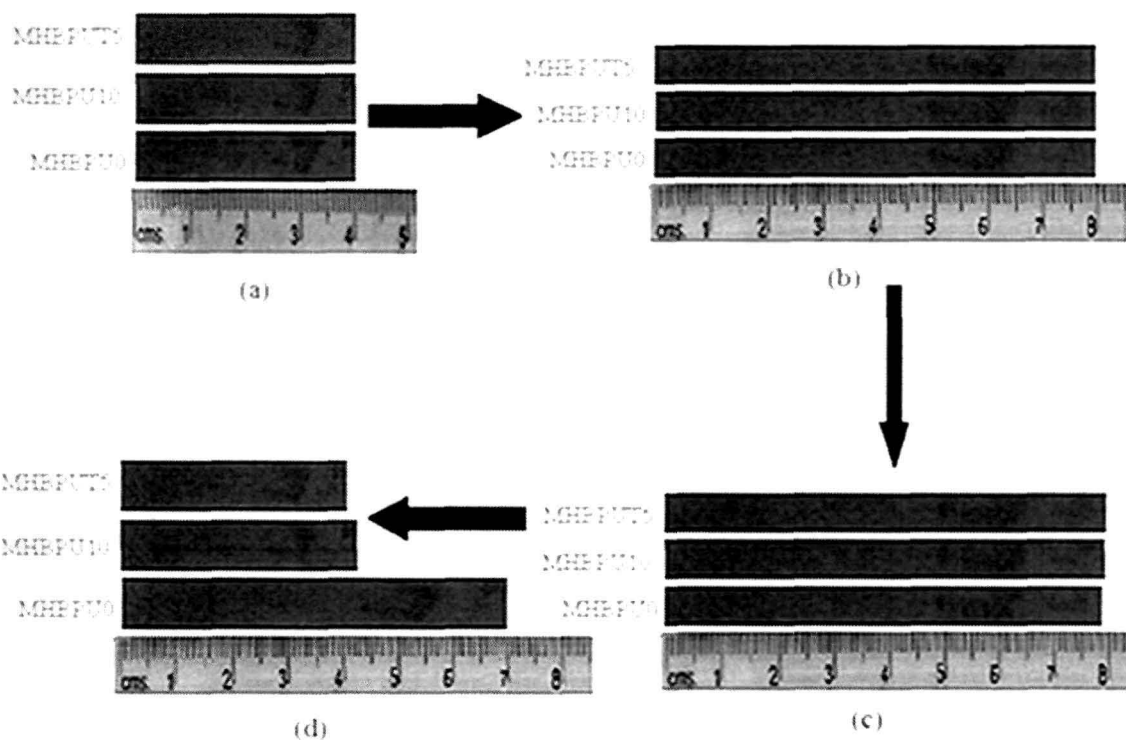
Property	MHBPU0	MHBPU10	MHBPUT5
Tensile strength (MPa)	4 ± 0.2	6.2 ± 0.4	8 ± 0.2
Elongation at break (%)	605 ± 3.4	615 ± 3.1	814 ± 3.2
Scratch hardness (kg)	2 ± 0.1	3 ± 0.1	6 ± 0.2
Impact resistance* (m)	0.8 ± 0.05	0.95 ± 0.05	0.95 ± 0.05
Bending (m)	<0.001	<0.001	<0.001
Adhesive strength (MPa)	309 ± 1.1	210 ± 1.3	200 ± 1.3
Gloss (60°)	80 ± 2	85 ± 3	85 ± 3

\*1.0 m is the limit of the instrument

#### 2C.3.6. Shape memory property

The shape memory behaviors of the polyurethanes are shown in Fig. 2C.6. The samples were stretched above the melting temperature of the hyperbranched polyurethane to facilitate the elongation as flexibility is high at that temperature. The temperature was fixed at 0 to 5 °C to freeze the molecular motion of amorphous as well as crystalline zone of the polymer chain, which prevents the molecular chains from immediate reforming the coil structure and from spontaneous recovery of the permanent shape, hence deformed shape is fixed. The shape recovery of the prepared polyurethanes increased with the increase in content of multifunctional moiety (Table 2C.5). This excellent shape recovery of the synthesized hyperbranched polyurethanes can be attributed to the increased stored energy in the system due to the homogeneous distribution of hard segments and multifunctional moiety, triethanolamine in the hyperbranched structure and the increased secondary interactions in the hyperbranched polyurethanes.<sup>40, 41</sup> All the prepared polyurethanes also exhibited excellent shape fixity. When the polymers are heated at ambient temperature and stretched, the polymer segments are elongated which led to change of orientation of the polymer chains and dislocation of net points. The excellent shape fixity is due to the increased physical or virtual cross-links among the new orientational polymer segments upon cooling.





**Fig. 2C.6:** Shape memory behaviors of hyperbranched polyurethanes (a) original shape, (b) extended shape, (c) fixed shape and (d) recovered shape

**Table 2C.5:** Shape memory properties of hyperbranched polyurethanes

Property	MHBPU0	MHBPU10	MHBPUT5
Shape recovery (%)	21 ± 0.01	96 ± 0.02	97 ± 0.02
Shape fixity (%)	96 ± 0.01	98 ± 0.01	96.5 ± 0.01

### 2C.3.7. Chemical resistance

Chemical resistance tests were studied under different chemical medium (Table 2C.6) such as 3% NaOH, 10% EtOH, 5% HCl, 10% NaCl and distilled water for 15 days and the changes of weight were determined after the tests. The samples exhibited good chemical resistance in almost all the chemical media. However, in the NaOH solution the samples showed the erosion on the surface. This can be attributed to the presence of alkali hydrolyzable ester

groups of PCL and monoglyceride segments. Good chemical resistance of the films is due to the presence of secondary interactions as stated in subchapter 2B, section 2B.3.7.

**Table 2C.6:** Chemical resistance as changes of weight (g) of hyperbranched polyurethanes

Chemical medium	MHBPU0	MHBPU10	MHBPUT5
3% NaOH	-0.045	-0.052	-0.054
10% EtOH	+0.007	+0.005	+0.012
5% HCL	-0.002	-0.005	-0.005
10% NaCl	+0.004	+0.004	+0.008
Distilled water	+0.011	+0.012	+0.012

#### 2C.4. Conclusion

In this study, *Mesua ferrea* L. seed oil based hyperbranched shape memory polyurethanes with different amount of multifunctional moiety, triethanolamine were successfully synthesized. The synthesized polyurethanes showed good tensile strength, elongation at break and thermal property. The tensile strength and elongation at break were found to be increased with the increase of the amount of triethanolamine. The thermal stability significantly increased with the increase of content of multifunctional moiety. Introduction of multifunctional moiety in the polyurethane improved the shape memory behavior. From the study it could be concluded that the synthesized hyperbranched polyurethanes might be utilized as thermo-responsive shape memory materials.

## References

1. Xia, Y., & Larock, R.C. Vegetable oil-based polymeric materials: synthesis, properties, and applications, *Green Chem.* **12** (11), 1893–1909, 2010.
2. Sharma, V., & Kundu, P.P. Condensation polymers from natural oils, *Prog. Polym. Sci.* **33** (12), 1199–1215, 2008.
3. Meier, M.A.R., et al. Plant oil renewable resources as green alternatives in polymer science, *Chem. Soc. Rev.* **36** (11), 1788–1802, 2007.
4. Tan, S.G., & Chow, W.S. Biobased epoxidized vegetable oils and its greener epoxy blends: a review, *Polym. Plast. Techn. Eng.* **49** (15), 1581–1590, 2010.
5. Sharma, V., & Kundu, P.P. Addition polymers from natural oils-a review, *Prog. Polym. Sci.* **31** (11), 983–1008, 2006.
6. Zlatanic, A., et al. Effect of structure on properties of polyols and polyurethanes based on different vegetable oils, *J. Polym. Sci. Part B: Polym. Phys.* **42** (5), 809–819, 2004.
7. Javni, I., et al. Thermal stability of polyurethanes based on vegetable oils, *J. Appl. Polym. Sci.* **77** (8), 1723–1734, 2000.
8. Karak, N., & Maiti, S. *Dendrimers and Hyperbranched Polymers-Synthesis to Applications*, MD publication Pvt. Ltd., New Delhi, 2008.
9. Hu, J., et al. A review of stimuli-responsive polymers for smart textile applications, *Smart Mater. Struct.* **21** (5), 053001-053024, 2012.
10. Dong, J., & Weiss, R. Shape memory behavior of zinc oleate-filled elastomeric ionomers, *Macromolecules* **44** (22), 8871–8879, 2011.
11. Small, W., et al. Biomedical applications of thermally activated shape memory polymers, *J. Mater. Chem.* **20** (17), 3356–3366, 2010.
12. Yu, K., et al. Mechanisms of multi-shape memory effects and associated energy release in shape memory polymers, *Soft Matter* **8** (20), 5687–5695, 2012.
13. Liu, C., et al. Review of progress in shape-memory polymers, *J. Mater. Chem.* **17** (16), 1543–1558, 2007.
14. Farzaneh, S., et al. Shape memory effect and properties memory effect of polyurethane, *J. Appl. Polym. Sci.* **128** (5), 3240–3249, 2012.

15. Choi, N.Y., & Lendlein, A. Degradable shape-memory polymer networks from oligo[(L-lactide)-ran-glycolide]dimethacrylates, *Soft Matter* **3** (7), 901–909, 2007.
16. Lendlein, A., et al. Controlling the switching temperature of biodegradable, amorphous, shape-memory poly(rac-lactide)urethane networks by incorporation of different co-monomers, *Biomacromolecules* **10** (4), 975-982, 2009.
17. Jang, M.K., et al. Shape memory polyurethanes cross-linked by surface modified silica particles, *J. Mater. Chem.* **19** (8), 1166–1172, 2009.
18. Min, C., et al. Effect of comonomer on thermal/mechanical and shape memory property of L-lactide-based shape-memory copolymers, *Polym. Adv. Technol.* **18** (4), 299-305, 2007.
19. Garle, A., et al. Thermoresponsive semicrystalline poly( $\epsilon$ -caprolactone) networks: exploiting cross-linking with cinnamoyl moieties to design polymers with tunable shape memory, *Appl. Mater. Interfaces* **4** (2), 645-657, 2012.
20. Zini, E., & Scandola, M. Shape memory behavior of novel (L-lactide–glycolide–trimethylene carbonate) terpolymers, *Biomacromolecules* **8** (11), 3661-3667, 2007.
21. Zhang, J., et al. Unique multifunctional thermally-induced shape memory poly(p-dioxanone)–poly(tetramethylene oxide)glycol multiblock copolymers based on the synergistic effect of two segments, *J. Phys. Chem. C* **116** (9), 5835–5845, 2012.
22. Xue, L., et al. Synthesis and characterization of three-arm poly( $\epsilon$ -caprolactone)-based poly(ester–urethanes) with shape-memory effect at body temperature, *Macromolecules* **42** (4), 964-972, 2009.
23. Dutta, S., & Karak, N. Effect of the NCO/OH ratio on the properties of *Mesua Ferrea* L. seed oil-modified polyurethane resins, *Polym. Int.* **55** (1), 49-56, 2006.
24. Jung, H.C., et al. Properties of crosslinked polyurethanes synthesized from 4,4'-diphenylmethane diisocyanate and polyester polyol, *J. Appl. Polym. Sci.* **78** (3), 624–630, 2000.
25. Huang, J., & Zhang, L. Effects of NCO/OH molar ratio on structure and properties of graft-interpenetrating polymer networks from polyurethane and nitrolignin, *Polymer* **43** (8), 2287-2294, 2002.
26. Deka, H., & Karak, N. Bio-based hyperbranched polyurethanes for surface coating application, *Prog. Org. Coat.* **66** (3), 192-198, 2009.

27. Chattopadhyay, D.K., & Webster, D.C. Thermal stability and flame retardancy of polyurethanes, *Prog. Polym. Sci.* **34** (10), 1068–1133, 2009.
28. Lamba, N.M.K., et al. *Polyurethanes in Biomedical Applications*, CRC Press, Boca Raton, 1998.
29. Baer, G., et al. Shape-memory behavior of thermally stimulated polyurethane for medical applications, *J. Appl. Polym. Sci.* **103** (6), 3882-3892, 2007.
30. Huang, S.L., & Lai, J.Y. Structure-tensile properties of polyurethanes, *Eur. Polym. J.* **42** (10), 1563-1567, 1997.
31. Yilgor, E., & Yilgor, I. Hydrogen bonding: a critical parameter in designing silicone copolymers, *Polymer* **42** (19), 7953-7959, 2001.
32. Aneja, A., & Wilkes, G.L. A systematic series of 'model' PTMO based segmented polyurethanes reinvestigated using atomic force microscopy, *Polymer* **44** (23), 7221-7228, 2003.
33. Karak, N., et al. Synthesis and characterization of castor-oil-modified hyperbranched polyurethanes, *J. Appl. Polym. Sci.* **112** (2), 736-743, 2009.
34. Cao, Q., & Liu, P. Structure and mechanical properties of shape memory polyurethane based on hyperbranched polyesters, *Polym. Bull.* **57** (6), 889–899, 2006.
35. Kumari, S., et al. Synthesis and characterization of hyperbranched polyesters and polyurethane coatings, *J. Appl. Polym. Sci. Part A: Polym. Chem.* **45** (13), 2673-2688, 2007.
36. Rubner, M.F. Synthesis and characterization of polyurethane-diacetylene segmented copolymers, *Macromolecules* **19** (8), 2114-2128, 1986.
37. Rana, S., et al. Enhanced dispersion of carbon nanotubes in hyperbranched polyurethane and properties of nanocomposites, *Nanotechnology* **19** (49), 495707-495715, 2008.
38. Mahapatra, S.S., & Karak, N. Synthesis and characterization of polyesteramide resins from Nahar seed oil for surface coating applications, *Prog. Org. Coat.* **51** (2), 103-108, 2004.
39. Chahar, M.K., et al. *Mesua ferrea* L.: a review of the medical evidence for its phytochemistry and pharmacological actions, *Afr. J. Pharm. Pharmacol.* **7** (6), 211-219, 2013.
40. Meng, Q., et al. The shape memory properties of biodegradable chitosan/poly(L-lactide) composites, *J. Polym. Environ.* **17** (3), 212-224, 2009.

41. Chun, B.C., et al. Blocking of soft segments with different chain lengths and its impact on the shape memory property of polyurethane copolymer, *J. Appl. Polym. Sci.* **103** (3), 1435-1441, 2007.
42. Gao, C., & Yan, D. Hyperbranched polymers: from synthesis to applications, *Prog. Polym. Sci.* **29** (3), 183–275, 2004.
43. Sunder, A., et al. Controlled synthesis of hyperbranched polyglycerols by ring-opening multibranching polymerization, *Macromolecules* **32** (13), 4240-4246, 1999.
44. Bharathi, P., & Moore, J.S. Controlled synthesis of hyperbranched polymers by slow monomer addition to a core, *Macromolecules* **33** (9), 3212-3218, 2000.
45. Jena, K.K., et al. Synthesis and characterization of hyperbranched polyurethane–urea coatings, *Eur. Polym. J.* **43** (5), 1825–1837, 2007.
46. Oprea, S. Novel quinoline-based polyurethane elastomers. the effect of the hard segment structure in properties enhancement, *J. Polym. Res.* **19** (1), 9767-9776, 2011.

## ***Chapter 3***

### **Modified hyperbranched polyurethane**

#### ***Highlights***

The modification of existing polymers with other polymers significantly improved their properties including the shape memory behaviors. In this chapter hyperbranched polyurethane was modified with the commercially available glycidyl ether epoxy of bisphenol-A in the presence of cycloaliphatic amine. The modified polyurethanes were characterized by Fourier transform infrared spectroscopy and X-ray diffraction studies. The mechanical, thermal and the shape memory properties of the modified hyperbranched polyurethanes were evaluated. The modified system showed significant improvements of mechanical, thermal and shape memory behaviors over the pristine one. The biodegradation of unmodified and modified hyperbranched polyurethanes were performed using the broth culture technique. All the samples showed overall good biodegradability. Thus the modified hyperbranched polyurethane has the potential to be used as a superior shape memory material over the pristine one.

---

*Parts of this work are published in*

1. Kalita, H., & Karak, N., *Des. Monomers Polym.* **16** (5), 447-455, 2012.

### 3.1. Introduction

From the earlier chapters, it is clearly observed that the structures of the hard and soft segments have strong effect on the physical, thermal and chemical properties including shape memory behaviors of hyperbranched polyurethanes in the line of other polyurethanes.<sup>1-3</sup> The importance of vegetable oils and biodegradability of polyurethanes are already discussed in Chapter 1. The vegetable oil based polymeric materials exhibit better flexibility and biodegradability as compared to their synthetic analogs. However, the existing properties of polyurethanes cannot be fully addressed the needs of many advanced applications because of their poor mechanical properties and chemical resistance. As modification of polymers by physical means like blending, incorporation of other additives etc. or chemical ways such as creating chemical cross-linked three dimensional networks, grafting or functionalization with other active agents can improve the desired properties. So chemical modification of the synthesized *Mesua ferrea* L. seed oil based hyperbranched polyurethane to improve the performance of it, is a good proposition. Epoxy resins are low molecular weight, oligomeric or polymeric compounds consisting of more than one epoxy group per molecule. It has some good properties such as good mechanical, thermal, dielectric behavior, low shrinkage during curing, low creep, good adhesive strength, excellent corrosion and weather resistance, good chemical resistance, dimensional stability, wide range of cure schedules, good compatibility with polyurethane and their easy processibilities.<sup>4-8</sup> Polyurethane, because of the presence of reactive urethane linkage, can be cross linked with epoxy resin through physical as well as chemical interactions and hence it can be used to modify polyurethane to obtain the desired properties including good shape memory behaviors.<sup>9, 10</sup> Again the fracture toughness of the polyurethane can be improved without significant reduction of mechanical and thermal properties of it by crosslinked with the epoxy resin. The increase of crosslinked net points through this modification may also strongly influence the shape memory behaviors of such hyperbranched polyurethanes. In addition to the above, the unique hyperbranched architecture as well as long chain fatty acid moiety of the vegetable oil of hyperbranched polyurethane may lead to some unusual and useful properties of the resultant modified system. Thus it is expected that the modification of *Mesua ferrea* L. seed oil based hyperbranched polyurethane by epoxy resin would fulfill the desired demand of some advanced applications. In this chapter, therefore, the modification,



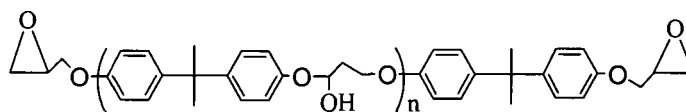
characterization and properties evaluation of commercially available glycidyl ether epoxy of bisphenol-A modified vegetable oil based hyperbranched polyurethane were presented.

## 3.2. Experimental

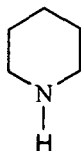
### 3.2.1. Materials

The monoglyceride of the *Mesua ferrea* L. seed oil, TDI, PCL, 1,4-butanediol and triethanolamine were used for the preparation of hyperbranched polyurethane as same as described in Chapter 2, section 2A.2.1. The same hyperbranched polyurethane with 10 wt% monoglyceride of the oil (MHBPU10) was used as mentioned in Chapter 2, as the base polyurethane.

The epoxy resin, a glycidyl bisphenol-A based epoxy (product of epichlorohydrin and bisphenol-A, Fig. 3.1) with viscosity 450-650 mPas, epoxy equivalent of 182-192 g/equivalent, epoxy content 5.2-5.5 equivalent/kg, density 1.15 g/c.c. and a hardener, cycloaliphatic amine (Fig. 3.2) with viscosity 250-380 cPs and specific gravity 1.03 were purchased from Ciba Geigy, India.



**Fig. 3.1:** Structure of glycidyl bisphenol-A based epoxy resin



**Fig.3.2:** Structure of cycloaliphatic amine

### 3.2.2. Preparation of hyperbranched polyurethane

Hyperbranched polyurethane was prepared by the same approach as described in Chapter 2, section 2A.2.3. The polymer was obtained as a solution of 30-35% solid content (w/v) in xylene. The yield obtained after the isolation from solution by precipitation in a non-solvent followed by vacuum drying in an oven at 40 °C for 2 days, was 98%.

### 3.2.3. Modification of hyperbranched polyurethane with epoxy resin

The hyperbranched polyurethane of 30-35% solid content in xylene directly obtained from the polymerization reaction was mixed with epoxy resin (100% solid content) and cycloaliphatic amine (50% by weight with respect to the epoxy resin) in the desired proportion as given in Table 3.1. The mixing was carried out under constant and vigorous stirring at room temperature for about half an hour for proper homogenization of the components. The modified hyperbranched polyurethane films were obtained by casting the homogenous mixture of the solution in glass plates followed by vacuum degassing and cured at specified time and temperature for further testing and analysis. The modified hyperbranched polyurethanes were coded as CEHPU10, CEHPU20 and CEHPU30 for 10%, 20% and 30% of epoxy content, respectively.

#### 3.2.4. Broth culture technique for biodegradation

Mineral salt medium with the following composition was prepared for biodegradation study. 2.0 g  $\text{Na}_2\text{HPO}_4$ , 2.0 g  $(\text{NH}_4)_2\text{SO}_4$ , 70 mg  $\text{ZnSO}_4 \cdot 7\text{H}_2\text{O}$ , 4.75 g  $\text{KH}_2\text{PO}_4$ , 1.2 g  $\text{MgSO}_4 \cdot 7\text{H}_2\text{O}$ , 0.5 mg  $\text{CaCl}_2 \cdot 2\text{H}_2\text{O}$ , 10 mg  $\text{H}_3\text{BO}_3 \cdot 5\text{H}_2\text{O}$ , 100 mg  $\text{MnSO}_4 \cdot 5\text{H}_2\text{O}$ , 100 mg  $\text{CuSO}_4 \cdot 7\text{H}_2\text{O}$ , 1 mg  $\text{FeSO}_4 \cdot 7\text{H}_2\text{O}$  and 10 mg  $\text{MoO}_3$  were dissolved in 1.0 L of demineralized water. An amount of 10 mL of this liquid culture medium was poured into 50 mL conical flask and sterilized using autoclave at 121 °C and 15 lb pressure for 15 min. The autoclaved media were then allowed to cool room temperature and the polymer films were immersed to the media under sterile condition inside a laminar air hood. Media containing no polymer film was also cultured as negative control. *P. aeruginosa* strain MTCC 7814 bacteria was selected for this study. The bacterial strain was cultured in the above prepared mineral media for 48 h at 37 °C. The 100  $\mu\text{L}$  of cultured medium containing  $10^8 \text{ mL}^{-1}$  microbes (as calculated from McFarland turbidity method) was inoculated to the conical flask containing 10 mL media. The flask was then incubated under sterile condition at 37 °C for the biodegradation study.

#### 3.2.5. Instrumentation

The modified systems were characterized by the same techniques such as FTIR, XRD and SEM as described in Chapter 2, section 2A.2.4.

The mechanical properties such as tensile strength, elongation at break, scratch resistance and impact resistance were measured by the same way as described in Chapter 2, section 2A.2.4. The thermal stability and chemical resistance were studied by the same way as described in Chapter 2, section 2A.2.4. The chemical resistance test was performed by the same way as described in subchapter 2B, section 2B.2.3. The swelling test was carried out by immersing weighted amount ( $W_d$ ) of cured film in DMF. The samples were removed from the solvent after attaining equilibrium state and the weight of the swollen film ( $W_s$ ) was measured. The swelling value was calculated by using the following formula:

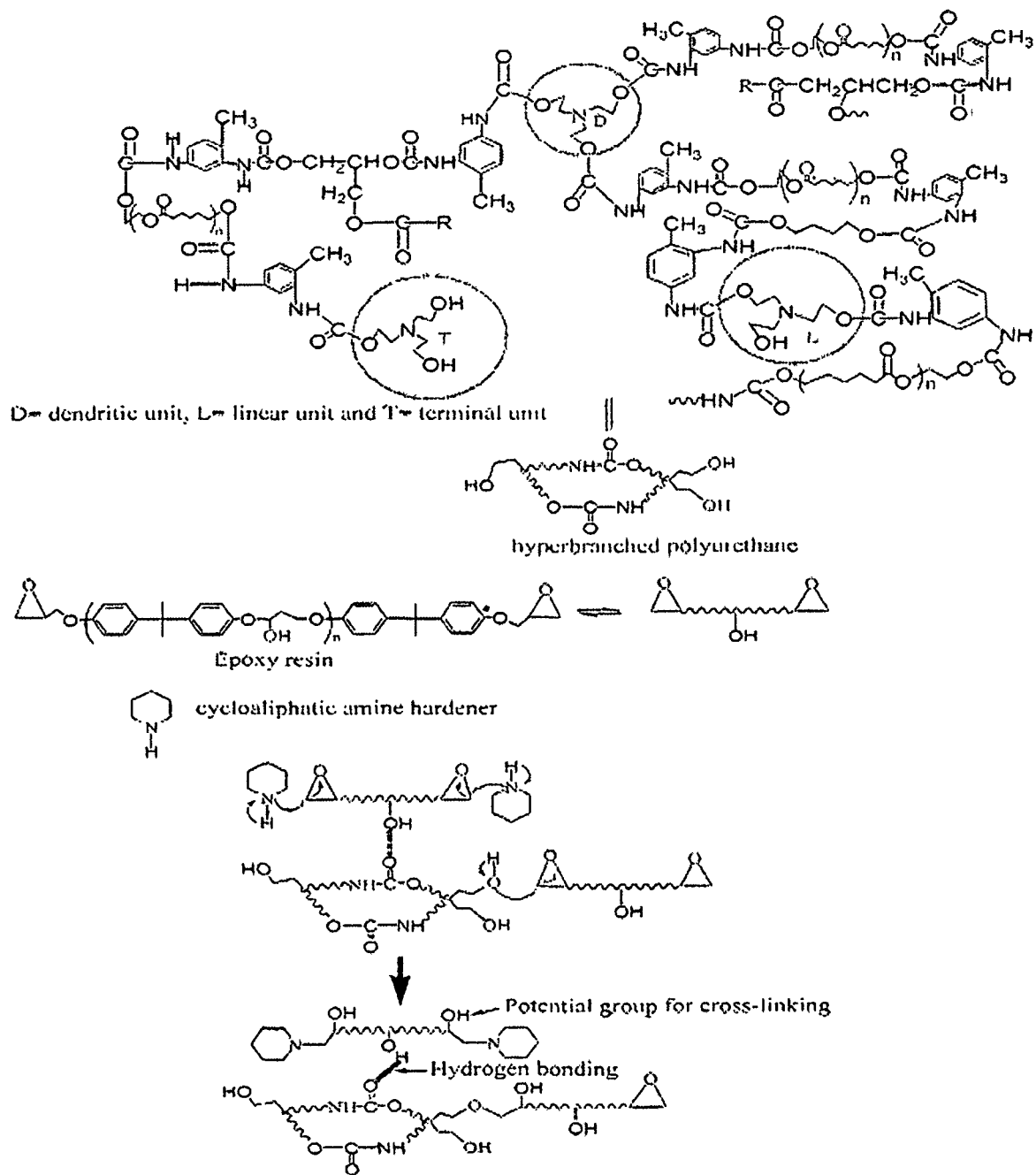
$$\text{Swelling (\%)} = (W_s - W_d)/W_d \times 100 \text{ ----- (3.1)}$$

The shape memory behaviors were carried out by the same process as described in subchapter 2A, section 2A.2.5.

### 3.3. Results and discussion

#### 3.3.1. Curing study

From the curing study it was found that the touch free time (minimum time required by the system to resist impression on touching its surface by thumb) and drying time (determined by indenting the cured film by an indenter) decreased with the increase of amount of epoxy resin and cycloaliphatic amine hardener at 120 °C as shown in Table 3.1. This may be due to the increased cross-linking reaction between the epoxy/hydroxyl groups of the epoxy resin with hydroxyl/urethane groups of hyperbranched polyurethane in the presence of amine hardener.<sup>11</sup> This can be easily understood from the proposed mechanism of cross-linking (Scheme 3.1). Due to the increase of the amount of epoxy and hardener, the number of strained oxirane and reactive amino groups increases, so the degree of intercross-linking network formation also increased. Thereby a three dimensional network structure was formed. Furthermore, there is a possibility of the formation of intermolecular H-bonding between  $-C=O$  of the urethane linkage and the  $-OH$  of the epoxy resin present in the system. The formation of network structure in the modified polyurethanes is confirmed by the decrease in intensity of hydroxyl band and carbonyl band. The disappearance of epoxy band at  $916 \text{ cm}^{-1}$  is also confirmed the formation of network structure.



Scheme 3.1: Proposed crosslinking reactions

**Table 3.1:** Composition and curing time of modified hyperbranched polyurethane at 120 °C

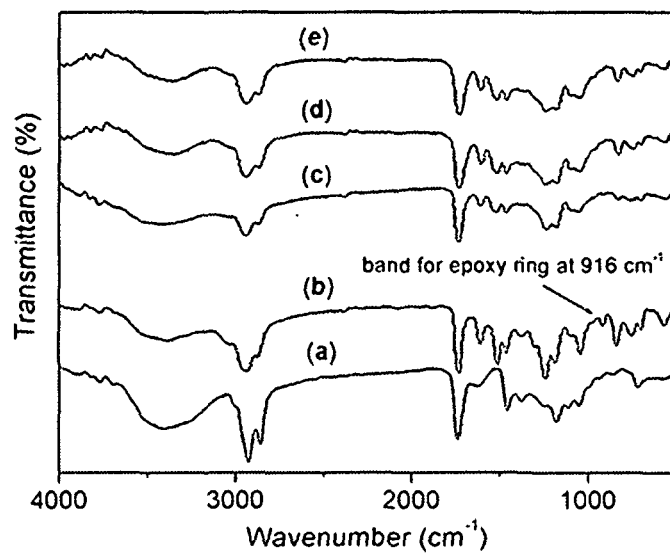
Code	MHBPU10 (wt%)	Epoxy (wt%)	Cycloaliphatic amine (wt%)	Touch free time (min)	Drying time (min)
MHBPU10	100	0	0	-	-
CEHPU10	100	10	5	40	55
CEHPU20	100	20	10	35	46
CEHPU30	100	30	15	30	40

### 3.3.2. Infrared spectroscopic study

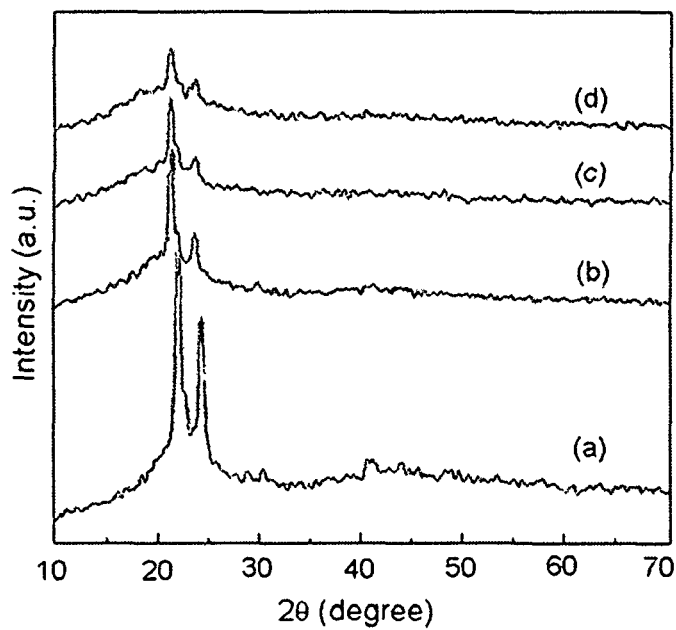
The FTIR spectra of pristine hyperbranched polyurethane and modified hyperbranched polyurethanes are shown in Fig. 3.1. The characteristic bands of urethane group appeared at 3406-3430  $\text{cm}^{-1}$  (N-H stretching) and 1729  $\text{cm}^{-1}$  (-C=O stretching of urethane linkage).<sup>2, 12</sup> There are two bands at 1627  $\text{cm}^{-1}$  for amide I of urethane, 1470  $\text{cm}^{-1}$  for amide II of urethane. The bands at 870 and 730  $\text{cm}^{-1}$  are due to the substituted aromatic ring of TDI. The characteristic band of epoxy group was appeared at 916  $\text{cm}^{-1}$  for the epoxy modified hyperbranched polyurethane before curing, whereas the same was absent after curing that confirmed the participation of epoxy groups in various reactions as stated above.

### 3.3.3. X-ray diffraction study

X-ray diffractograms of unmodified and modified hyperbranched polyurethanes are shown in Fig. 3.2. The presence of crystallinity in the thermoplastic hyperbranched polyurethane and modified thermosetting polyurethanes is confirmed by the XRD analysis. Two strong diffraction peaks at  $2\theta=21.9^\circ$  and  $2\theta=23.8^\circ$  are due to the (100) and (200) planes of PCL crystals. The position of the peaks remained same after the modification of hyperbranched polyurethane, though the intensity gradually decreases with the increase of epoxy content. This may be due to the increase of molecular restriction through cross-linking and also decrease in percentage of PCL in the matrix.



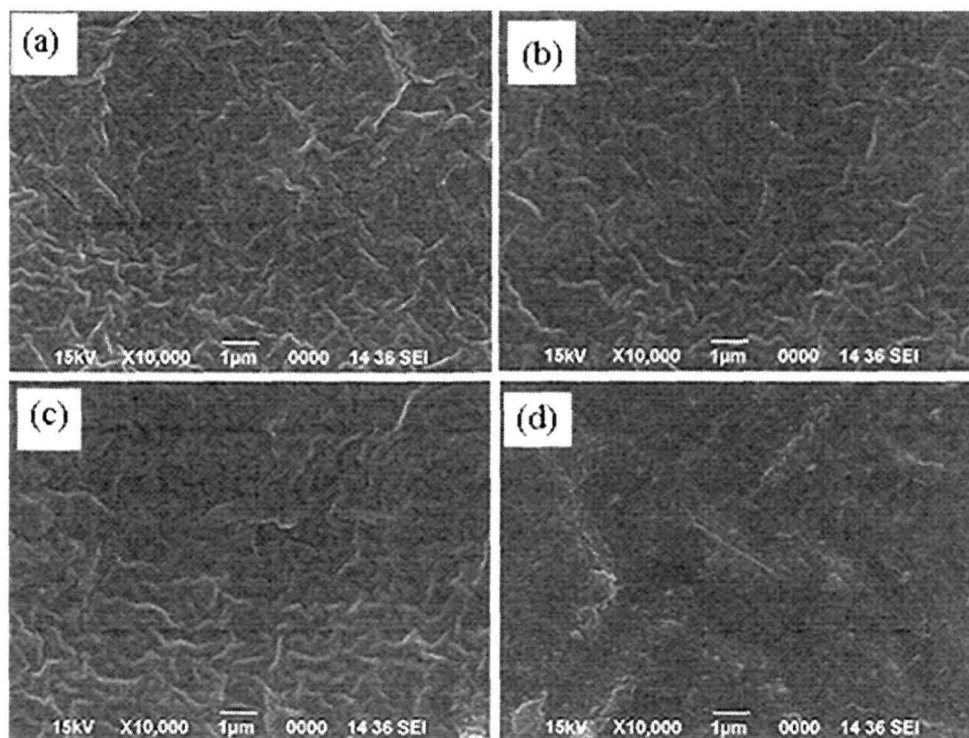
**Fig. 3.1:** FTIR spectra for (a) MHBPU10, (b) CEHPU30 before curing, (c) CEHPU10 after curing, (d) CEHPU20 after curing and (e) CEHPU30 after curing



**Fig. 3.2:** XRD diffractograms for (a) MHBPU10, (b) CEHPU10, (c) CEHPU20 and (d) CEHPU30

### 3.3.4. Morphology study

The morphological study of the hyperbranched polyurethane and the modified systems was carried out with the help of scanning electron microscope (SEM). SEM micrographs of hyperbranched polyurethane and all the modified polyurethanes are shown in Fig. 3.3. The SEM micrographs indicate the uniform phase distribution of all the components of modified polyurethanes and also they confirmed the formation of homogeneous intercross-linked network of the epoxy with polyurethane as no extra phase was observed. The compatibility of the systems is attributed due to the hyperbranched structure of the polyurethane as well as polar-polar interactions.<sup>12, 13</sup> Furthermore, there is a possibility of H-bonding between the urethane linkages and the -OH groups of epoxy resin present in the system. Thus, cycloaliphatic amine hardener acts as cross-linking and compatibilizing agent for this modified system.



**Fig. 3.3:** SEM micrographs for (a) MHBPU10, (b) CEHPU10, (c) CEHPU20 and (d) CEHPU30

### 3.3.5. Thermal property

The thermograms of the modified hyperbranched polyurethanes and unmodified hyperbranched polyurethane are shown in Fig. 3.4. The mechanism of thermal decomposition of polyurethane involves three steps. The urethane linkage degradation starts from 180-230 °C, which is called as the temperature of onset degradation. The degradation of aromatic moiety occurs at about 340-380 °C. The final stage at about 400-600 °C may be attributed to thermal degradation of isocyanurate rings and carbodiimide linkages, which leads to the evaporation of CO<sub>2</sub> and the formation of char.<sup>14</sup> The thermal stability of the modified system depends on the amount of thermo-stable moiety, cross-linking density and free volume present in the systems. One of the most effective ways to augment the thermal stability of polyurethane is introduction of aromatic ring in the hard or soft segments of the polyurethane, because an aromatic ring has a high stabilizing effect against thermal degradation.<sup>15</sup> On the other hand thermal stability depends on the molecular rigidity because chemical reaction and degradation depends on macromolecular chain excitation and motion gained from the thermal energy during exposure to a heat. It was seen that the thermal stability of the modified systems increased with the increase of epoxy content. The incorporation of epoxy resin in the polar polyurethane matrix increases the cross-linking density as well as the aromatic ring concentration. Thus, the molecular mobility of the chain is restricted and thereby making the material rigid. As a result, the bond breaking inside the bulk polymeric matrix requires high thermal energy and makes inert from the oxidative environment. Thus, the thermal stability enhances for the modified polyurethanes. The DSC curves of unmodified and modified hyperbranched polyurethanes are shown in Fig. 3.5. The experimental results indicate that the glass transition temperature ( $T_g$ ) increased with the increase of epoxy content. This is due to the increased rigidity of the structure that is formed through different types of interactions as stated earlier.



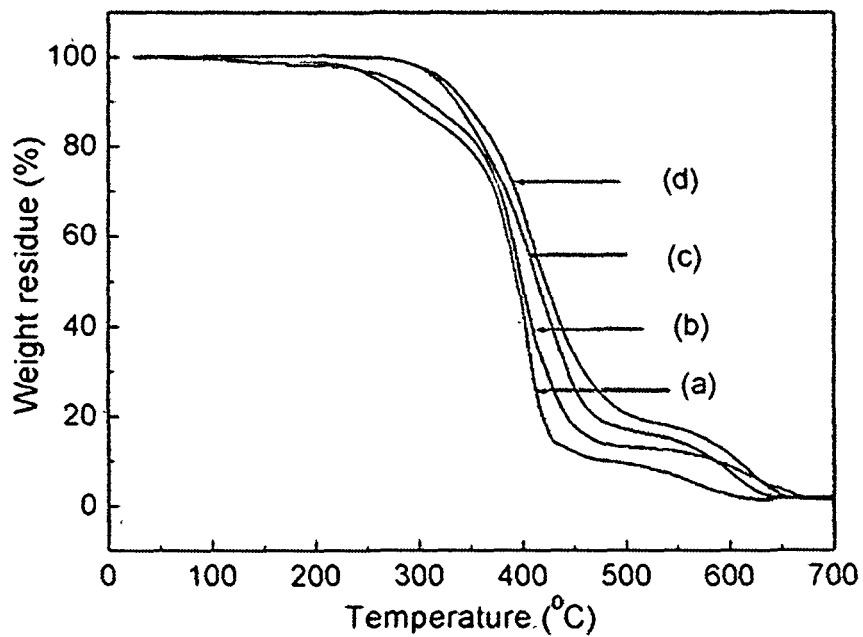


Fig. 3.4: TGA thermo-grams for (a) MHBPU10, (b) CEHPU10, (c) CEHPU20 and (d) CEHPU30

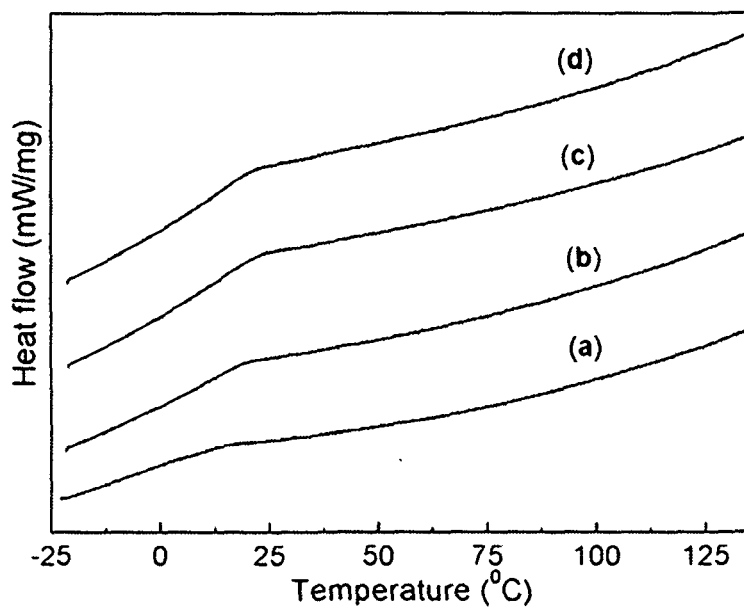


Fig. 3.5: DSC curves for (a) MHBPU10, (b) CEHPU10, (c) CEHPU20 and (d) CEHPU30

### 3.3.6. Mechanical property

From Table 3.2 it is found that the tensile strength of the modified hyperbranched polyurethanes increases with the increase of epoxy content. The enhancement can be attributed to the increase in overall cross-linking density and compatibility of the aromatic moieties present in the system through polar-polar interaction and uniform distribution of epoxy in the polyurethane matrix.<sup>16</sup> The increase in cross-linking density is supported by swelling test in DMF. Due to the increase cross-linking density makes the material stiffer and causes higher ultimate strength. However, the elongation at break decreased with the increase of the epoxy content. This is due to the decrease in chain mobility and increase in rigidity of the structure. The scratch hardness of the modified polyurethanes also increased with the increase of epoxy content that causes the increase in rigidity of the structure. The bending test results showed that all the samples possess sufficient flexibility. This can be attributed to the flexibility nature of the soft segment, PCL and the presence of long chain fatty acid moiety in the structure of the polyurethane. All the modified polyurethanes showed excellent impact resistance. Impact strength of the material may be explained from the angle of toughness of the films that is the ability to absorb the applied external energy as well as the transfer of energy to its adjacent molecular chains. The gloss is an optical property of materials and depends on the smoothness of the surface. The gloss property measured at an angle of 60° and it was seen that all the films exhibited good gloss.

**Table 3.2:** Mechanical properties of unmodified and modified hyperbranched polyurethanes

Property	MHBPU10	CEHPU10	CEHPU20	CEHPU30
Tensile strength (MPa)	6.2 ± 0.2	11.4 ± 0.2	14.5 ± 0.2	16 ± 0.2
Elongation at break (%)	607 ± 3.1	270 ± 1.4	250 ± 1.4	244 ± 1.1
Scratch hardness (kg)	3 ± 0.1	6 ± 0.1	7.5 ± 0.1	10 ± 0.15
Impact resistance* (m)	0.95 ± 0.05	0.95 ± 0.05	0.95 ± 0.05	0.95 ± 0.02
Bending (m)	<0.002	<0.002	<0.002	<0.002
Swelling (%)	-	25 ± 1.2	20 ± 1.2	16 ± 1.1
Gloss (60°)	85 ± 2	89 ± 3	94 ± 3	94 ± 3

\*1.0 m is the limit of the instrument

### 3.3.7. Chemical resistance

Chemical resistance tests of all the modified and unmodified hyperbranched polyurethanes were studied using different chemical environments (Table 3.3) such as 3% NaOH, 10% EtOH, 5% HCl, 10% NaCl and distilled water for 15 days. The samples showed good chemical resistance in all the chemical environments, except aqueous NaOH solution. This is due to the presence of alkali hydrolysable ester groups of PCL and monoglyceride segments. Good chemical resistance of the films may be due to the presence of secondary interactions such as polar-polar and H-bonding, increased cross-linking density, compact structure and presence of aromatic moiety etc.

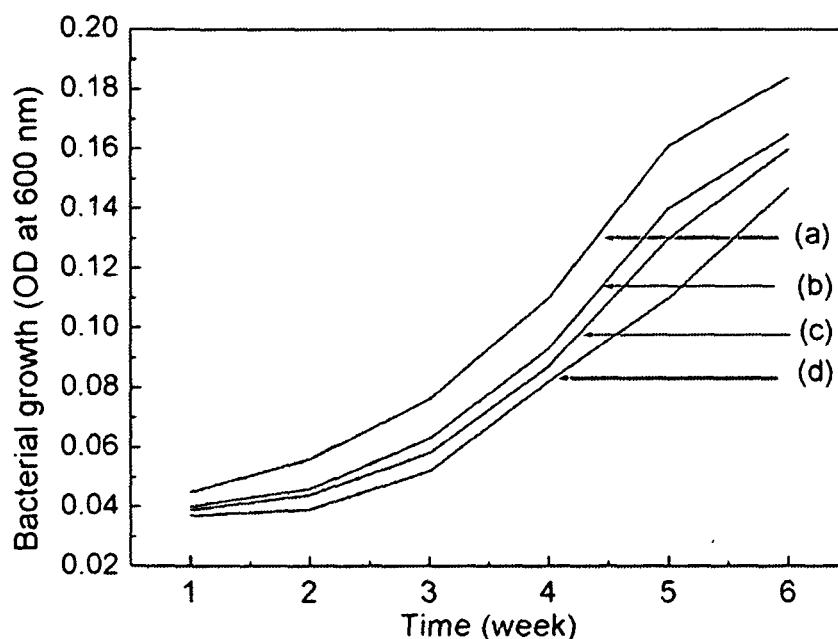
**Table 3.3:** Chemical resistance as changes of weight (g) of unmodified and modified hyperbranched polyurethanes

Chemical medium	MHBPU10	CEHPU10	CEHPU20	CEHPU30
3% NaOH	-0.085	-0.059	-0.054	-0.052
10% EtOH	+0.017	-0.015	-0.012	-0.011
5% HCL	-0.012	-0.005	-0.005	-0.002
10% NaCl	+0.004	-0.004	-0.008	-0.003
Distilled water	+0.011	+0.003	+0.001	0.000

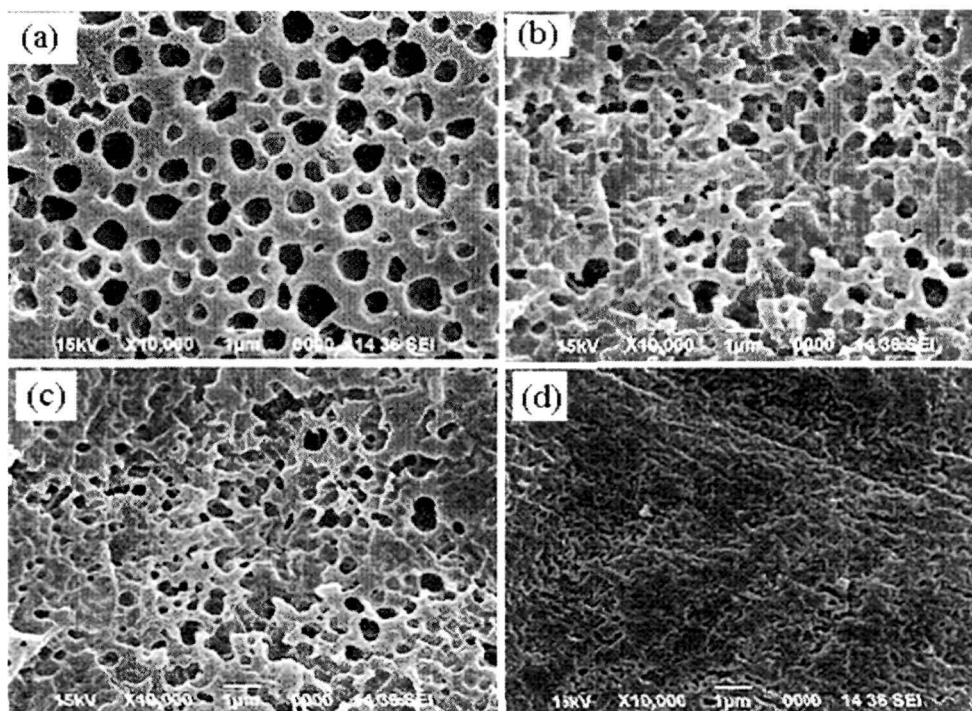
### 3.3.8. Biodegradation Study

The biodegradation of the unmodified hyperbranched polyurethane and modified hyperbranched polyurethanes were tested and confirmed by direct exposure to bacterial strain by broth culture technique. In the present investigation, *P. aeruginosa* of strain number MTCC 7814 was used for the biodegradation study. The growth of the bacterial strain as obtained from McFarland Turbidity method is shown in Fig. 3.6. The bacterial population was found to be less in the modified hyperbranched polyurethanes as compared to the unmodified polyurethane. This is due to the presence of cross-linking, synthetic bisphenol-A based epoxy moiety etc. in the modified system. Therefore, it is very difficult to assess the modified system by the microorganisms. However, the bacterial growth decreased with the increase of the content of epoxy in the modified systems. This is due to the increased cross-linking density that makes the structure more compact and rigid. On keeping the samples in broth culture media for 45 days,

they were found to be degraded. The scanning electron micrographs of the unmodified hyperbranched polyurethane and the modified hyperbranched polyurethanes after the bacterial exposure are shown in Fig. 3.7. Both the unmodified hyperbranched polyurethane and modified hyperbranched polyurethanes showed the surface erosion after the biodegradation study. Biodegradation of the polyurethane depends on the process conditions, chemical structure and compositions, morphology, crystallinity, hard and soft segment ratio etc.<sup>17</sup> Microorganisms utilized polyurethane as carbon and/or nitrogen source. Generally, microbial degradation takes place in two steps. The high molecular weight polymer is initially hydrolyzed to form low molecular weight oligomeric products with weak mechanical property, which makes it more accessible for the microbial assimilation of oligomeric products to produce CO<sub>2</sub>, H<sub>2</sub>O, humus etc.<sup>18</sup> The presence of amorphous long chain fatty acid moieties and PCL in the bio-based hyperbranched polyurethane promotes microbial attack.



**Fig. 3.6:** Growth profiles of *P. aeruginosa* strain, MTCC 7814 for (a) MHBPU10, (b) CEHPU10, (c) CEHPU20 and (d) CEHPU30



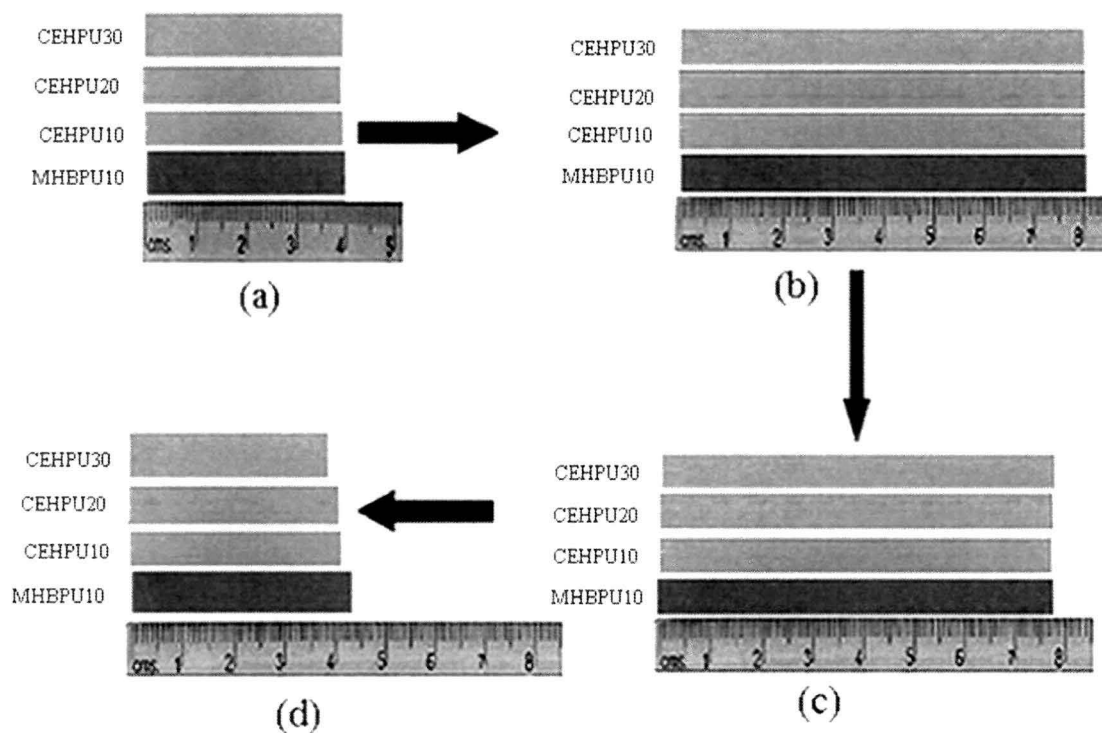
**Fig. 3.7:** SEM micrographs for (a) MHBPU10, (b) CEHPU10, (c) CEHPU20 and (d) CEHPU30 after biodegradation

### 3.3.9. Shape memory property

The shape memory behaviors of the hyperbranched polyurethane and the modified systems are shown in Fig. 3.8. The unmodified hyperbranched polyurethane and the modified polyurethanes showed good shape fixity. The shape recovery behavior found to be enhanced in the modified systems (Table 3.4). This can be attributed to the increased stored energy in the system due to the increased net point in the systems.<sup>19, 20</sup> The net points are increased in the modified systems due to the increased interactions as stated earlier. The modified systems exhibited good reproducibility of the shape memory behaviors over the repeated cycles of test.

**Table 3.4:** Shape memory properties of hyperbranched polyurethane and modified hyperbranched polyurethanes

Property	MHBPU10	CEHPU10	CEHPU20	CEHPU30
Shape recovery (%)	96 ± 0.05	96.5 ± 0.02	97.5 ± 0.02	98.5 ± 0.02
Shape fixity (%)	98 ± 0.01	98 ± 0.01	98 ± 0.01	98 ± 0.01



**Fig. 3.8:** Shape memory behaviors of hyperbranched polyurethane and its modified systems (a) original shape, (b) extended shape, (c) fixed shape and (d) recovered shape

### 3.4. Conclusion

From the study it can be concluded that bisphenol-A based diglycidyl ether epoxy along with cycloaliphatic amine successfully modified the hyperbranched polyurethane with good performance. The properties like tensile strength, scratch hardness, gloss and thermal stability significantly increased with the increase of epoxy content. The uniform and homogeneous mixing of the components in all the modified systems results such performance. The modified hyperbranched polyurethanes also showed the significant biodegradation as indicated by the broth culture technique. The modified systems showed the enhanced shape recovery with the increase of epoxy content. Thus the epoxy modified hyperbranched polyurethanes can be used as an advanced thin film thermosetting and shape memory material.

## References

1. Camberlin, Y., et al. Model hard segments from diphenyl methane diisocyanate and different chain extenders, and corresponding linear block polyurethanes, *J. Polym. Sci. Polym. Chem. Ed.* **20** (6), 1445-1456, 1982.
2. Martin, D.J., et al. Effect of soft-segment CH<sub>2</sub>/O ratio on morphology and properties of a series of polyurethane elastomers, *J. Appl. Polym. Sci.* **60** (4), 557-571, 1996.
3. Linliu, K., et al. A small angle scattering study of microphase separation transition of polyurethane: effect of hard segments, *J. Polym. Res.* **2** (1), 63-70, 1995.
4. Bucknull, C.B. *Toughened Plastics*, Applied Science Publishers Ltd., London, 1977.
5. Unnikrishnan, K.P., & Thachil, E.T. Toughening of epoxy resins, *Des. Monomers Polym.* **9** (2), 129-152, 2006.
6. Rajasekaran R., & Alagar, M. Mechanical properties of bismaleimides modified polysulfone epoxy matrices, *Int. J. Polym. Mater.* **56** (9), 911-927, 2007.
7. Issam, A.M., et al. Physical and mechanical properties of different ratios of palm oil-based alkyd/epoxy resins, *Polym. Plast. Techn. Eng.* **50** (12), 1256-1261, 2011.
8. Lin, Y., et al. Synthesis and properties of a novel flame-retardant epoxy resin containing biphenyl/phenyl phosphonic moieties, *Polym. Plast. Techn. Eng.* **51** (9), 896-903, 2012.
9. Hsieh, K.H., & Han, J.L. Graft interpenetrating polymer networks of polyurethane and epoxy. II. toughening mechanism, *J. Polym. Sci. Part B: Polym. Phys.* **28** (6), 783-794, 1990.
10. Hsieh, K.H., et al. Graft interpenetrating polymer networks of urethane-modified bismaleimide and epoxy (1): mechanical behavior and morphology, *Polymer* **42** (6), 2491-2500, 2001.
11. Hepburn, C. *Polyurethane Elastomers*, Elsevier Applied Science, London and New York, 1992.
12. Zhang, Y. Morphology, mechanical properties, and thermal stability of polyurethane-epoxide resin interpenetrating polymer network rigid foams, *J. Appl. Polym. Sci.* **75** (3), 406-416, 2000.
13. Brydson, J.A. *Plastics Materials*, Butterworths Heinemann, London, 1982.
14. Semsarzadeh, M. A., & Navarchian, A. H. Effects of NCO/OH ratio and catalyst concentration on structure, thermal stability, and crosslink density of poly(urethane-isocyanurate), *J. Appl. Polym. Sci.* **90** (4), 963-972, 2003.

15. Chattopadhyay, D.K., & Webster, D.C. Thermal stability and flame retardancy of polyurethanes, *Prog. Polym. Sci.* **34** (10), 1068-1133, 2009.
16. Deka, H., & Karak, N. Shape-memory property and characterization of epoxy resin-modified *Mesua ferrea* L. seed oil-based hyperbranched polyurethane, *J. Appl. Polym. Sci.* **116** (1), 106-115, 2010.
17. Urgun-Demirtas, M., et al. Laboratory investigation of biodegradability of a polyurethane foam under anaerobic conditions, *Polym. Degrad. Stabil.* **92** (8), 1599-1610, 2007.
18. Seo, J.S., et al. Bacterial degradation of aromatic compounds, *Int. J. Environ. Res.* **6** (1), 278-309, 2009.
19. Hu, J., et al. Crosslinked polyurethanes with shape memory properties, *Polym. Int.* **54** (5), 854-859, 2005.
20. Lee, B.S., et al. Structure and thermomechanical properties of polyurethane block copolymers with shape memory effect, *Macromolecules* **34** (18), 6431-6437, 2001.



## **Chapter 4**

# **Hyperbranched polyurethane/Fe<sub>3</sub>O<sub>4</sub> nanocomposites**

### ***Highlights***

This chapter consists of two subchapters, one on thermoplastic and other on thermosetting hyperbranched polyurethane/Fe<sub>3</sub>O<sub>4</sub> nanocomposites. The first subchapter describes the preparation, characterization and properties evaluation of hyperbranched polyurethane/Fe<sub>3</sub>O<sub>4</sub> thermoplastic nanocomposites. The prepared nanocomposites were characterized by Fourier transform infrared spectroscopy and X-ray diffraction studies. The mechanical, thermal and shape memory behaviors were studied for the prepared nanocomposites. The shape memory behaviors were studied by using microwave energy as the stimulus. While in the second subchapter epoxy modified thermosetting hyperbranched polyurethane/Fe<sub>3</sub>O<sub>4</sub> nanocomposites were demonstrated. The thermoset nanocomposites were characterized similarly by using Fourier transform infrared spectroscopy and X-ray diffraction studies. The performance of the nanocomposites was also studied exactly on the same ways. The study showed that the thermosetting nanocomposites are better compared to their thermoplastic analogs with respect to their overall performance including shape memory behaviors.

---

*Parts of this work are published in*

1. Kalita, H., & Karak, N., *Polym. Adv. Technol.* **24** (9), 819-823, 2013.
2. Kalita, H., & Karak, N., *Polym. Bull.* **70** (11), 2953-2965, 2013.

## **4A. Hyperbranched thermoplastic polyurethane/Fe<sub>3</sub>O<sub>4</sub> nanocomposites**

### **4A.1. Introduction**

The importance of shape memory polymers (SMP) and their nanocomposites are already discussed in Chapter 1. The shape memory polyurethanes (as discussed in Chapter 2) have some disadvantages such as low mechanical properties, low recovery, low cycle life that make the barrier for the advanced applications. In Chapter 3, it has been found that the modification with epoxy and hardener can improve the performance including shape recovery of hyperbranched polyurethanes. However, the pristine hyperbranched polyurethanes or their epoxy modified thermosets cannot be addressed the demands of many advanced applications. Now recently, it is clearly understood that the fabrication of suitable polymer nanocomposites has significant importance to overcome these problems. Fe<sub>3</sub>O<sub>4</sub> nanoparticles were chosen here as nanomaterials due to their easy synthesis, low toxicity and good microwave absorption characteristic.<sup>1-5</sup> Again, the shape memory behaviors were studied by the direct heating, in most of the cases.<sup>6-8</sup> On the other hand, transition temperature ( $T_{trans}$ ) of many of such SMP is far from the normal human body's temperature and causes adverse impact in the clinical applications. Recently, thus research is focused on induced heating actuation of SMP by indirect ways. Cai et al. studied the magnetic field responsive shape memory behaviors of Fe<sub>3</sub>O<sub>4</sub>/poly( $\epsilon$ -caprolactone)-polyurethane nanocomposites.<sup>9</sup> Xiao et al. reported the electro-active shape memory properties of poly( $\epsilon$ -caprolactone)/functionalized MWCNT nanocomposite.<sup>10</sup> Microwave energy is used in the present study to investigate the shape memory behaviors of the nanocomposites. Microwave is an electromagnetic wave in the range of 300 MHz to 300 GHz. The corresponding wavelengths are 1 m to 1 mm. It can be used as stimulus in a non-contact way to actuate the SMP. The absorbed microwave energy is transferred to heat energy through the molecular friction and collisions and the shape memory effect is observed once the induced heat is close to the  $T_{trans}$ . Thus in this chapter thermoplastic hyperbranched polyurethane/Fe<sub>3</sub>O<sub>4</sub> nanocomposites were prepared to investigate the effect of Fe<sub>3</sub>O<sub>4</sub> nanoparticles on the performance including shape memory behaviors of the nanocomposites.

## 4A.2. Experimental

### 4A.2.1. Materials

The monoglyceride of the *Mesua ferrea* L. seed oil, TDI, PCL, 1,4-butanediol and triethanolamine used for the preparation of hyperbranched polyurethane were same as described in Chapter 2, section 2A.2.1.

Iron (III) chloride hexahydrate was purchased from Merck, India. The minimum assay is 96.0%. The impurity present is 1.0% iron (II) chloride. It was used as received.

Iron (II) chloride tetrahydrate was purchased from Merck, Germany. The minimum assay is 99.0%. The other impurities are 0.01% sulphate, 0.0005% arsenic, 0.002% copper, 0.2% iron (III) salt, 0.001% lead and 0.003% zinc. It was used as received.

Polyethylene glycol (PEG) was obtained from Merck, India. The number average molecular weight ( $M_n$ ) is 4000 g/mol. It was used as received.

Ammonia solution was purchased from Qualigens Fine Chemicals Ltd., India. The concentration and specific gravity are 30% and 0.89, respectively.

### 4A.2.2. Preparation of Fe<sub>3</sub>O<sub>4</sub> nanoparticles

Fe<sub>3</sub>O<sub>4</sub> nanoparticles were prepared by the co-precipitation method. Required amount of FeCl<sub>3</sub>.6H<sub>2</sub>O (2.0 g), FeCl<sub>2</sub>.4H<sub>2</sub>O (1.225 g) and PEG (1.5 g) were dissolved in deionized water (50 mL) under the nitrogen atmosphere with vigorous stirring at room temperature. An aqueous solution of ammonia (30%) was then added slowly into the mixture until it turns black. The black solution was then stirred continuously for 30 min. The resultant magnetic nanoparticles were separated by magnetic decantation and rinsed with deionized water followed by acetone until the supernatant become neutral. Finally, the washed Fe<sub>3</sub>O<sub>4</sub> nanoparticles were dispersed and stored in DMF.

### 4A.2.3. Preparation of hyperbranched polyurethane/Fe<sub>3</sub>O<sub>4</sub> nanocomposite

Hyperbranched polyurethane was prepared by the pre-polymerization technique by the same method as described in Chapter 2, section 2A.2.3. For the preparation of nanocomposite, required amount of dispersed Fe<sub>3</sub>O<sub>4</sub> was injected into the polymerization reaction before 1 h of completion and the reaction was continued. After completion of reaction the solution was cast on

the inert substrates followed by vacuum degassing and drying at 60 °C for 24 h for the different testing and analyses. The nanocomposites were denoted as MHBPU10, HPU2, HPU5 and HPU10 corresponding to the Fe<sub>3</sub>O<sub>4</sub> content of 0, 2, 5 and 10 wt%, respectively.

#### 4A.2.4. Instrumentation

The hyperbranched polyurethane and its nanocomposites were characterized by the same techniques such as FTIR, XRD and SEM as described in Chapter 2, section 2A.2.4. The distribution of Fe<sub>3</sub>O<sub>4</sub> in the nanocomposite was studied by using transmission electron microscope (TEM) JEM 2100, JEOL, Japan at operating voltage of 200 kV. Lakeshore vibrating sample magnetometer (VSM; Model 7410) within the range of +20000 to -20000 Oe at room temperature was used to study the magnetic behavior of Fe<sub>3</sub>O<sub>4</sub> and nanocomposite.

The mechanical properties such as tensile strength, elongation at break, scratch resistance and impact resistance were measured by the same way as described in Chapter 2, section 2A.2.4. The thermal stability was studied by the same way as described in Chapter 2, section 2A.2.4.

In order to observe the shape memory effect strip like samples (0.04 m × 0.002 m × 0.0007 m) were heated at 60 °C (T<sub>m</sub> + 20 °C) for 5 min and then folded to a ring shape. Immediately, the folded samples were put into the fixing temperature at 0 to 5 °C (T<sub>m</sub> - 40 °C) for 5 min to fix the temporary shape. Subsequently, the samples were exposed to the microwave irradiation (Scientific microwave system, catalyst systems, 2450 MHz, output power: 140-700 W, India) for the shape recovery study at microwave output power 350 W. The shape recovery and shape fixity are two shape memory parameters calculated from the following equations:

$$\text{Shape recovery (\%)} = [(90-\theta)/90] \times 100 \text{ ----- (4A.1)}$$

$$\text{Shape fixity (\%)} = [\theta/90] \times 100 \text{ ----- (4A.2)}$$

where  $\theta$  in degree denotes the angle between the tangential line at the midpoint of the sample and the line connecting the midpoint and the end of the curved sample.

### 4A.3. Results and discussion

#### 4A.3.1. FTIR study

FTIR spectra of Fe<sub>3</sub>O<sub>4</sub>, hyperbranched polyurethane and the nanocomposites are shown in Fig. 4A.1. The characteristic absorption band of Fe<sub>3</sub>O<sub>4</sub> at 580 cm<sup>-1</sup> corresponding to Fe-O

stretching vibration.<sup>11</sup> The band at  $3429\text{ cm}^{-1}$  is assigned to the stretching vibration of Fe-OH groups absorbed on the surface of  $\text{Fe}_3\text{O}_4$  nanoparticles. The characteristic bands of urethane group appeared at  $3406\text{-}3430\text{ cm}^{-1}$  (N-H stretching) and  $1728\text{ cm}^{-1}$  (-C=O stretching of urethane linkage) as already discussed in the earlier chapter. The disappearance of band at  $2250\text{-}2270\text{ cm}^{-1}$  indicates that there was no free -NCO group present in the hyperbranched polyurethane structure. The band at  $3406\text{-}3430\text{ cm}^{-1}$  (N-H stretching) of nanocomposites was found to be broadened after the nanocomposite formation as compared to the pristine polyurethane. This confirmed the presence of strong interaction of  $\text{Fe}_3\text{O}_4$  nanoparticles with the polymer matrix. Further, the characteristic band corresponding to Fe-O of  $\text{Fe}_3\text{O}_4$  nanoparticles was also broadened after the formation of nanocomposite. This indicates that polymer chains are bound to the surface of the nanoparticles. The above results showed overall strong interactions between the nanoparticles and the polymer matrix.

#### 4A.3.2. X-ray diffraction study

The X-ray diffractograms of  $\text{Fe}_3\text{O}_4$ , hyperbranched polyurethane and the nanocomposites are shown in Fig. 4A.2. The peaks appear at  $2\theta=30.35^\circ$ ,  $35.51^\circ$ ,  $56.71^\circ$  and  $62.73^\circ$  corresponding to (220), (311), (511) and (440) planes of  $\text{Fe}_3\text{O}_4$ , respectively.<sup>11</sup> The two peaks at  $2\theta=21.90^\circ$  and  $2\theta=23.80^\circ$  are due to the (100) and (200) planes of PCL crystals of the hyperbranched polyurethane. The intensity of these peaks decreases after the formation of nanocomposite. This may be due to the increased molecular restriction through the different interfacial interactions.

#### 4A.3.3. TEM study

The size and distribution of  $\text{Fe}_3\text{O}_4$  nanoparticles in the polymer matrix was studied by the TEM analysis (Fig. 4A.3). The TEM micrograph indicates the homogeneous distribution of  $\text{Fe}_3\text{O}_4$  nanoparticles with an average diameter of 13 nm in the polyurethane matrix. This can be attributed to the good interfacial interaction between the nanoparticles and the polymer matrix.

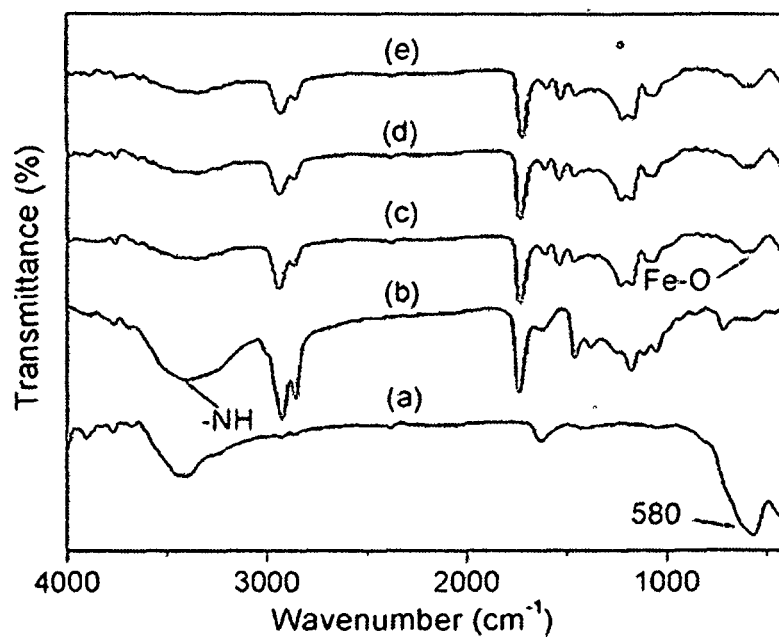


Fig. 4A.1: FTIR spectra for (a)  $\text{Fe}_3\text{O}_4$ , (b) MHBPU10, (c) HPU2, (d) HPU5 and (e) HPU10

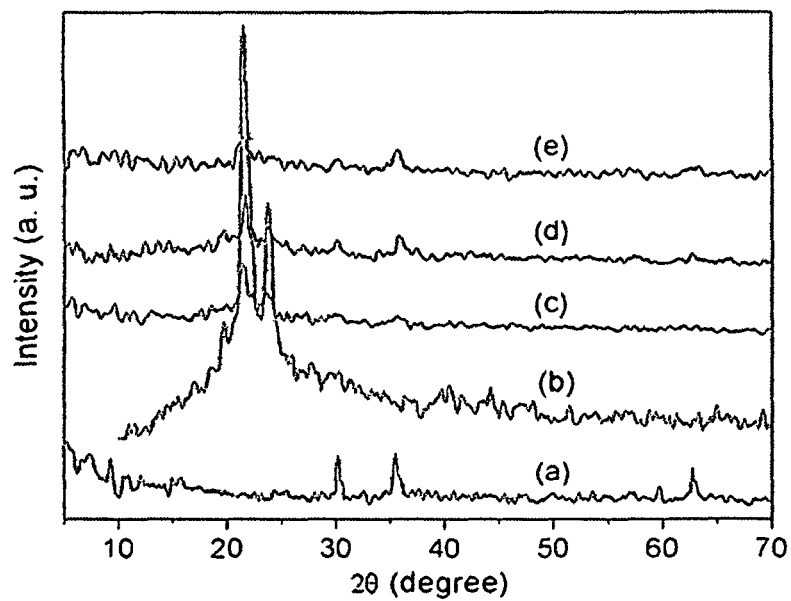
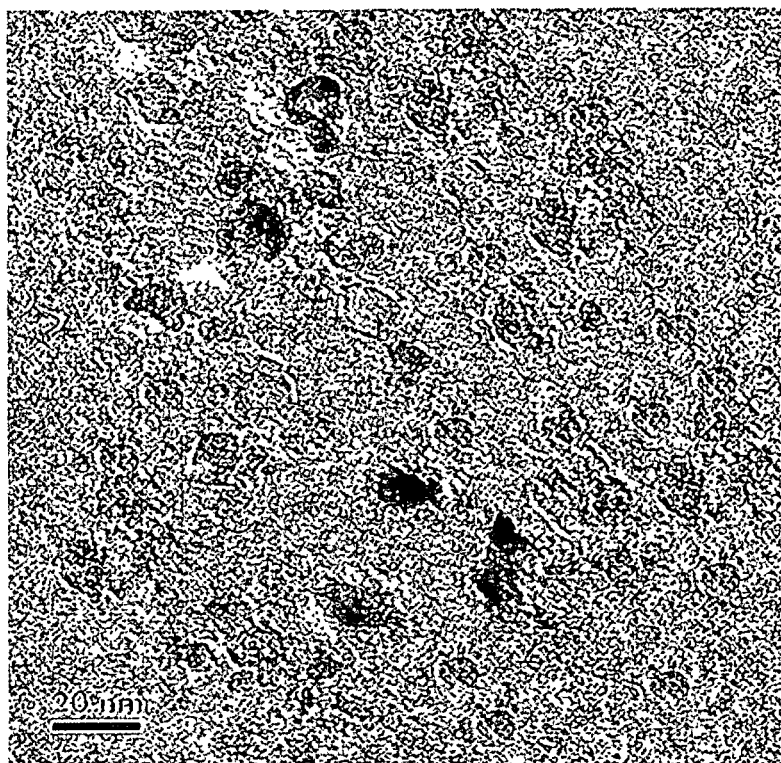


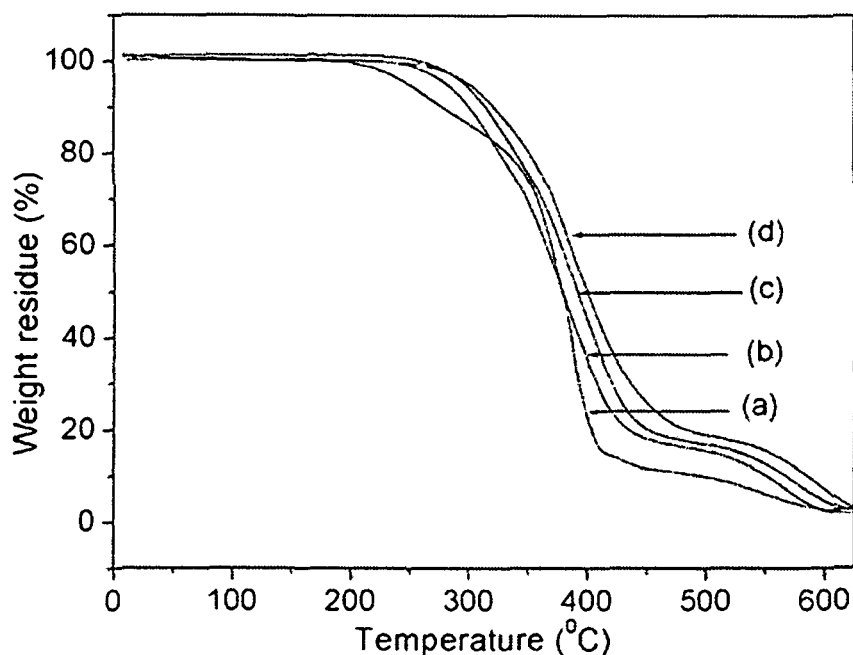
Fig. 4A.2: XRD diffractograms for (a)  $\text{Fe}_3\text{O}_4$ , (b) MHBPU10, (c) HPU2, (d) HPU5 and (e) HPU10



**Fig. 4A.3:** TEM image of HPU5

#### 4A.3.4. Thermal property

The thermal stability of the nanocomposites was studied by TGA and the thermograms are shown in Fig. 4A.4. Inorganic compounds are more thermo-stable as compared to the organic polymers. Thermal stability of the nanocomposites depends on the size, shape, nature, loading of nanoparticles, dispersion and degree of interfacial interaction between the nanoparticles and the polymer matrix.<sup>12</sup> Incorporation of  $\text{Fe}_3\text{O}_4$  nanoparticles into the hyperbranched polyurethane matrix increases its thermal stability (240 to 270 °C). This is due to the uniform distribution, compatibility and strong interfacial interactions of  $\text{Fe}_3\text{O}_4$  nanoparticles with the polymer matrix. Due to the various interfacial interactions such as physical cross-linking, polar-polar interactions and H-bonding, the polymer chains were immobilized on the surface of the nanoparticles. Thus the segmental motion of the polymer chains in the nanocomposites was restricted and thereby making the material more rigid. Hence the bond breaking requires high thermal energy.



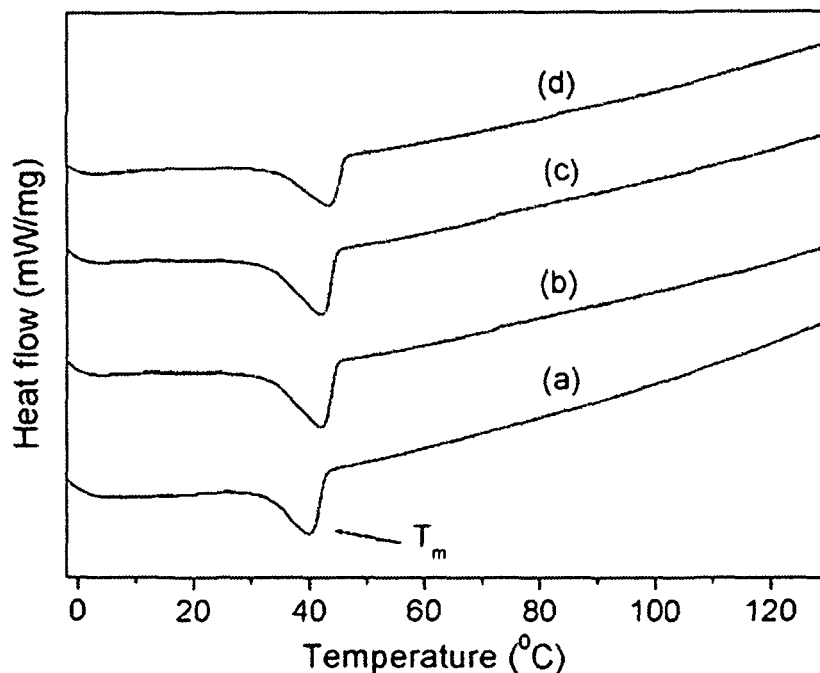
**Fig. 4A.4:** TGA thermograms for (a) MHBPU10, (b) HPU2, (c) HPU5 and (d) HPU10

Furthermore volatile products formed during the thermal degradation process have to follow a longer path to escape from the matrix. The DSC thermograms for all the samples were found to almost similar, but the melting temperature ( $T_m$ ) was enhanced from 40.2 to 42.1 °C with the increase of  $Fe_3O_4$  nanoparticles content in the nanocomposites (Fig. 4A.5). This may be due to the formation of rigid and compact structure in the nanocomposites arises from the various interactions between the nanoparticles and the polymer matrix as stated earlier.

#### 4A.3.5. Mechanical property

From Table 4A.1, it is found that nanocomposites possess good mechanical properties viz. tensile strength, impact resistance and scratch resistance along with adequate elongation at break. The mechanical property of the nanocomposite depends on the several factors such as distribution, dimension, aspect ratio of nanomaterials as well as degree of interfacial interactions between the matrix and the nanomaterials. The tensile strength increases with the increase of





**Fig. 4A.5:** DSC curves for (a) MHBPU10, (b) HPU2, (c) HPU5 and (d) HPU10

$\text{Fe}_3\text{O}_4$  nanoparticles content in the nanocomposites. This is due to the well distribution and enhanced interfacial interactions of  $\text{Fe}_3\text{O}_4$  nanoparticles with the polymer matrix. The interfacial interactions increased the load transfer capability of the polymer matrix to the nanoparticles. However, the elongation at break decreases with the increase of  $\text{Fe}_3\text{O}_4$  nanoparticles content in the nanocomposites. This is due to the increased molecular restrictions of the polymer chains in the nanocomposites.<sup>13</sup> The scratch resistance of the nanocomposites increases with the increase of content of  $\text{Fe}_3\text{O}_4$  nanoparticles. This can be attributed to the overall increase in toughness of the nanocomposites. The bending test results indicated that all the samples have sufficient flexibility as the films could be bent onto a rod of 0.001m diameter without any crack generation. This is mainly due to the high flexibility of the soft segment and the presence of long chain fatty acid moiety in the structure of hyperbranched polyurethane. Moreover all the films showed the excellent impact resistance.

**Table 4A.1:** Mechanical properties of hyperbranched polyurethane and the nanocomposites

Property	MHBPU10	HPU2	HPU5	HPU10
Tensile strength (MPa)	6.2 ± 0.4	9.2 ± 0.2	12.3 ± 0.2	15 ± 0.2
Elongation at break (%)	607 ± 3.1	492 ± 1.4	441 ± 1.4	403 ± 1.1
Scratch resistance (kg)	3 ± 0.1	5 ± 0.1	5.6 ± 0.1	6 ± 0.15
Impact resistance* (m)	0.95 ± 0.05	0.95 ± 0.05	0.95 ± 0.05	0.95 ± 0.02
Bending (m)	<0.001	<0.001	<0.001	<0.001

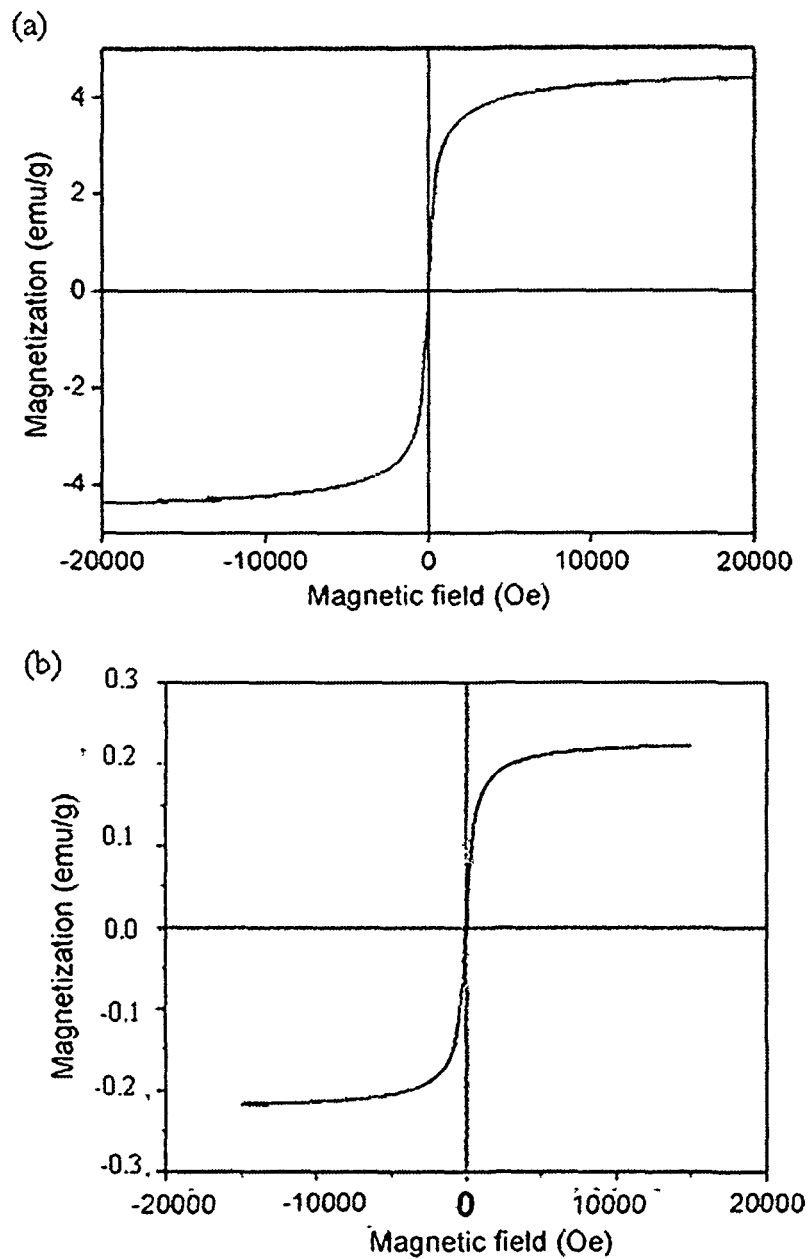
\* 1.0 m is the limit of the instrument

#### 4A.3.6. Magnetic property

The magnetic hysteresis loops of Fe<sub>3</sub>O<sub>4</sub> and nanocomposite (HPU2) at room temperature are shown in Fig. 4A.6. From the figure it is confirmed that the prepared Fe<sub>3</sub>O<sub>4</sub> showed the super-paramagnetic behavior as their low coercivity ( $H_c$ ) and remanence ( $M_r$ ) on the magnetization loop. The saturation magnetization of the nanocomposite was much lower than that of the pure Fe<sub>3</sub>O<sub>4</sub> nanoparticles. This can be attributed to the low content (2 wt%), smaller size as well as surface coating of Fe<sub>3</sub>O<sub>4</sub> by the polymer chains in the nanocomposite.

#### 4A.3.7. Shape memory property

The shape memory behaviors of the hyperbranched polyurethane and the nanocomposites are shown in Fig. 4A.7. All the samples exhibited almost full shape fixity behavior (Table 4A.2). This is due to the frozen of micro-Brownian movements of molecular chains during the vitrification. The shape recovery behavior was observed under the microwave irradiation. All the nanocomposites also exhibited almost full shape recovery. This is due to the fact that on microwave irradiation to the samples the dipole moment moves to align to the external field. But the electric field component of the wave oscillates and hence the dipole field attempts to follow these oscillations. These molecular friction and collisions resulted the required heat generation. Again, the polymer chains are activated when the heat is close to the transition temperature ( $T_{trans}$ ) and thereby releasing the stored strain energy to recover the original shape. No significant



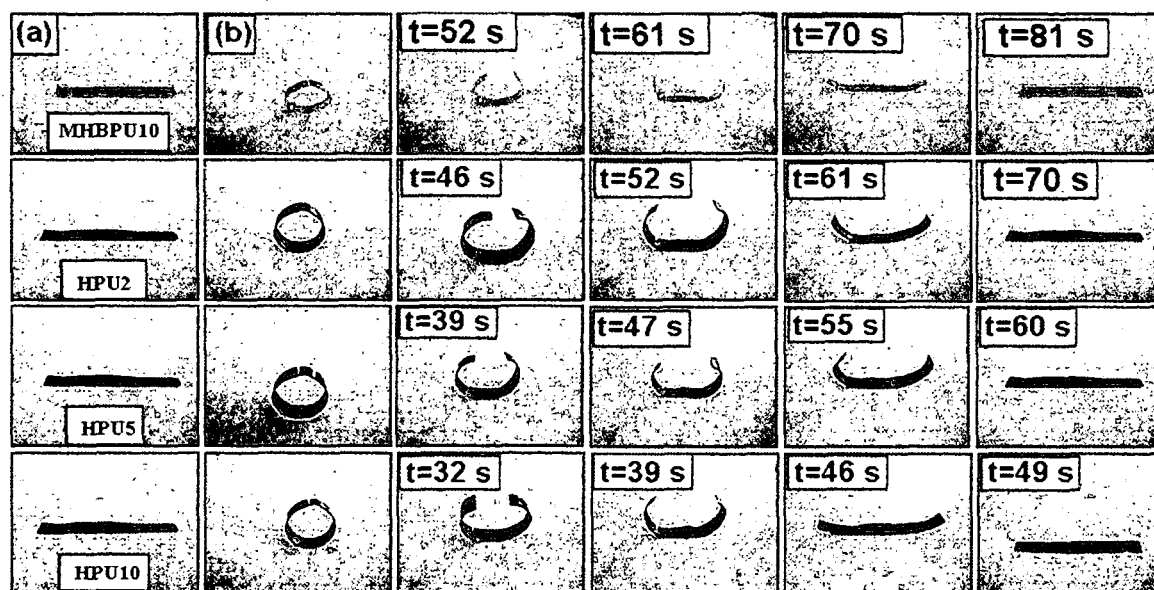
**Fig. 4A.6:** Magnetic hysteresis loops for (a)  $\text{Fe}_3\text{O}_4$  and (b) HPU2

change of shape recovery of the nanocomposites was observed over the five cycles of test. The shape recovery time was decreased (81-49 s) with the increase of  $\text{Fe}_3\text{O}_4$  nanoparticles content in the nanocomposites (Table 4A.2). This can be attributed to the increased store energy with the

loss of elastic entropy as a result of homogeneous distribution of the Fe<sub>3</sub>O<sub>4</sub> nanoparticles and increased physical cross-linking in the polymer matrix. Furthermore, the increased shape recovery speed may be due to the enhanced microwave absorption characteristic of the nanocomposites with the increase of Fe<sub>3</sub>O<sub>4</sub> nanoparticles content.<sup>4, 5</sup> From the above result it is seen that the prepared nanocomposites showed the excellent shape recovery and shape fixity behaviors. Thus these materials might be used as advanced shape memory materials in various potential fields.

**Table 4A.2:** Shape memory behaviors of hyperbranched polyurethane and the nanocomposites

Code	Shape fixity (%)	Shape recovery (%)	Shape recovery time (s)
MHBPU10	98.7 ± 0.5	98.5 ± 0.6	81 ± 4
HPU2	99.3 ± 0.2	99.2 ± 0.1	70 ± 2
HPU5	99.3 ± 0.2	99.2 ± 0.1	60 ± 2
HPU10	99.3 ± 0.2	99.2 ± 0.1	49 ± 2



**Fig. 4A.7:** Shape memory behaviors of hyperbranched polyurethane and the nanocomposites (a) original shape and (b) fixed shape

#### **4A.4. Conclusion**

In this study, we have successfully prepared *Mesua ferrea* L. seed oil based hyperbranched polyurethane/Fe<sub>3</sub>O<sub>4</sub> nanocomposites. The prepared nanocomposites showed improved mechanical and thermal properties. The hyperbranched polyurethane and the nanocomposites exhibited almost full shape fixity and almost full shape recovery under the application of microwave stimulus. The shape recovery speed increases with the increase of Fe<sub>3</sub>O<sub>4</sub> nanoparticles content in the nanocomposites. Thus the hyperbranched polyurethane/Fe<sub>3</sub>O<sub>4</sub> nanocomposites might be utilized as advanced shape memory materials in the different fields especially in the biomedical domain like smart surgical sutures, catheters, stents, drug delivery materials etc.

## **4B. Hyperbranched polyurethane/Fe<sub>3</sub>O<sub>4</sub> thermosetting nanocomposites**

### **4B.1. Introduction**

The effects of the chemical modification using glycidyl ether epoxy of bisphenol-A on the performance including shape memory behavior of the hyperbranched polyurethane thermosets is discussed in the third chapter of this thesis. From this study it is clear that the properties of such polyurethane can be improved by chemical cross-linking. However, as already mentioned in the above subchapter that this modification is unable to address many advanced applications, so more improvement is demanded. The above subchapter also showed that the formation nanocomposites with Fe<sub>3</sub>O<sub>4</sub> nanoparticles also enhance the performance including shape memory property of such polyurethane. It is an apt proposition to investigate the effect of such nanomaterial on different properties of above thermosetting polyurethane. This is due to the fact that the epoxy ring is reactive towards polyurethane linkages leading to cross-link through a rearrangement polymerization of reaction as well as the hydroxyl groups present in the surface of Fe<sub>3</sub>O<sub>4</sub> nanoparticles would interact both the epoxy and hyperbranched polyurethane.<sup>14</sup> This process is expected to help in overall crosslinking reactions of the system and hence cycloaliphatic amine which is used as a hardener in Chapter 3 along with epoxy for obtaining hyperbranched polyurethane thermoset is not necessary. Thus in the present study the vegetable oil based hyperbranched polyurethane thermosetting nanocomposites were prepared without any additional external hardener. It is also assumed that the presence of various physico-chemical interactions significantly improved the performance of nanocomposite.<sup>15, 16</sup> Further, the shape memory properties of the polymers also depend on the degree of net point in the system. Large numbers of reports are available to improve the shape memory behaviors of the polymers by incorporation of suitable nanomaterials and/or crosslinking with the other compatible materials.<sup>17-19</sup> Again, the importance of noncontact actuation of shape memory polymers is already discussed in subchapter 4A, section 4A.1. Although there are many reports on noncontact actuation of shape memory polyurethanes using magnetic field, electric field, IR radiation etc., here the microwave energy was used to investigate the shape memory behaviors of the thermosets polyurethane nanocomposites as described in subchapter 4A, section 4A.1. In this

subchapter, therefore, hyperbranched polyurethane/Fe<sub>3</sub>O<sub>4</sub> thermosetting nanocomposites were prepared to investigate the performance including shape memory behaviors.

## **4B.2. Experimental**

### **4B.2.1. Materials**

The monoglyceride of the *Mesua ferrea* L. seed oil, TDI, PCL, 1,4-butanediol and triethanolamine used for the preparation of hyperbranched polyurethane were same as described in Chapter 2, section 2A.2.1.

The epoxy resin, a glycidyl bisphenol-A based epoxy used was same as described in Chapter 3, section 3.2.1. Iron (III) chloride hexahydrate (Merck, India), iron (II) chloride tetrahydrate (Merck, Germany), polyethylene glycol (PEG, Merck, India,  $M_n = 4000$  g/mol) and ammonia solution (Qualigens Fine Chemicals Ltd., India) used were same as described in subchapter 4A, section 4A.2.1.

### **4B.2.2. Preparation of Fe<sub>3</sub>O<sub>4</sub> nanoparticles**

Fe<sub>3</sub>O<sub>4</sub> nanoparticles were prepared by the co-precipitation method and taking required amount of FeCl<sub>3</sub>.6H<sub>2</sub>O (2.0 g), FeCl<sub>2</sub>.4H<sub>2</sub>O (1.225 g) and PEG (1.5 g) by using the same procedure as described in subchapter 4A, section 4A.2.2.

### **4B.2.3. Preparation of hyperbranched polyurethane/Fe<sub>3</sub>O<sub>4</sub> thermosetting nanocomposite**

Hyperbranched polyurethane nanocomposites were prepared by the same technique as described in subchapter 4A, section 4A.2.3. To prepare the thermosetting polymer the above nanocomposite solution was mixed with 10 wt% of glycidyl bisphenol-A based epoxy resin (100% solid content) by vigorous mechanical stirring followed by 20 min ultra-sonication. The polymer solution was cast on the inert substrates followed by vacuum degassing to remove the air bubbles and curing was done at 120 °C. The cured films were denoted as EHPU2, EHPU5 and EHPU10 corresponding to the Fe<sub>3</sub>O<sub>4</sub> content of 2, 5 and 10 wt%, respectively.

#### 4B.2.4. Instrumentation

The hyperbranched polyurethane and its thermosetting nanocomposites were characterized by the same techniques such as FTIR, XRD and SEM as described in Chapter 2, section 2A.2.4.

The mechanical properties such as tensile strength, elongation at break, scratch resistance and impact resistance were measured by the same way as described in Chapter 2, section 2A.2.4. The thermal stability was studied by the same method as described in Chapter 2, section 2A.2.4.

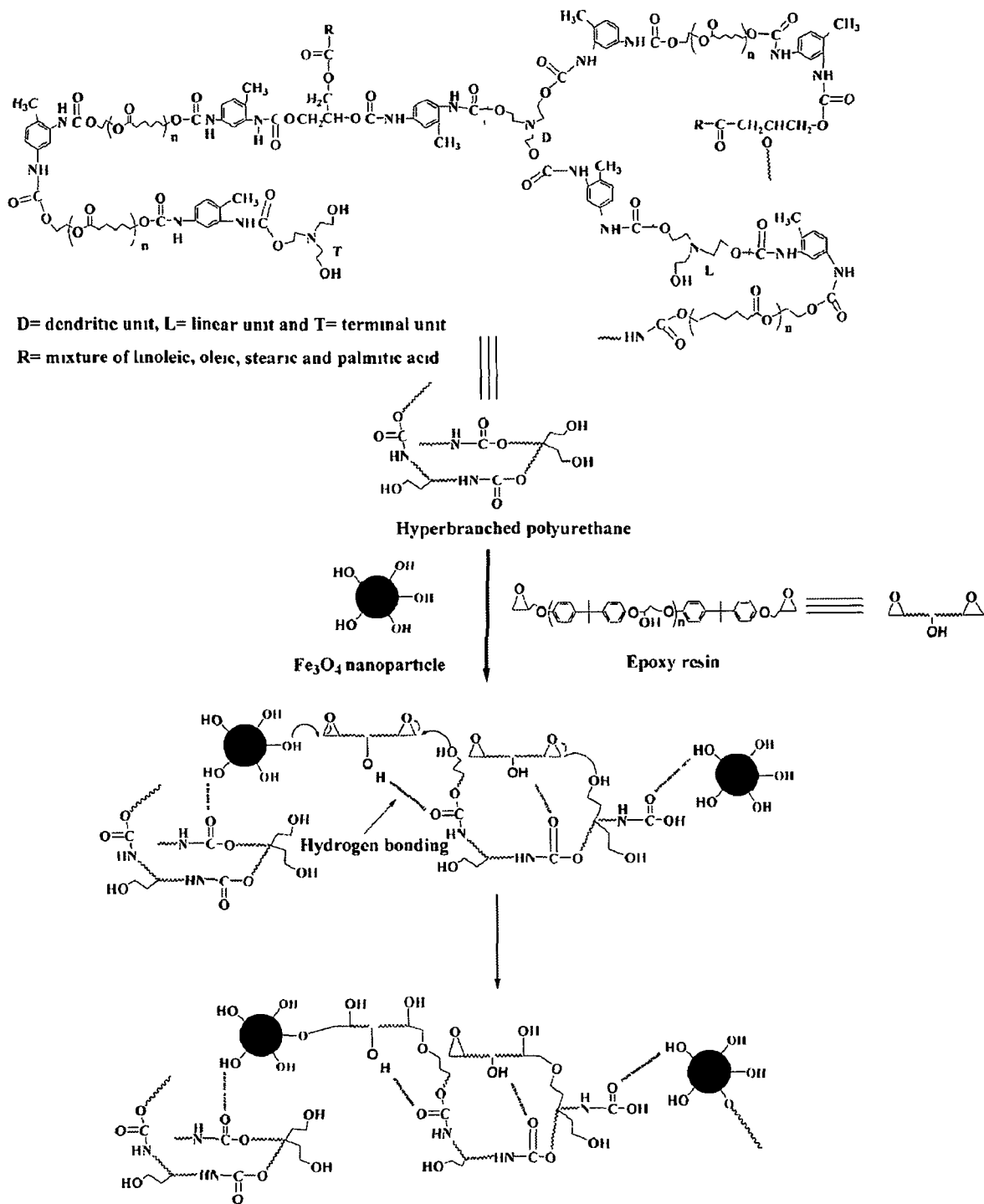
The shape memory behaviors of the thermosets were measured by the same method using microwave as a stimulus as described in subchapter 4A, section 4A.2.4.

### 4B.3. Results and discussion

#### 4B.3.1. Curing study

The curing reaction occurred due to the presence of functionalities such as hydroxyl, urethane and epoxy groups in the system. It is pertinent to mention here that no additional cross-linking agent is required to obtain the desired thermosets. The touch free time at room temperature and drying time at 120 °C were decreased with the increase of loading of Fe<sub>3</sub>O<sub>4</sub> in the nanocomposites (Table 4B.1). This is due to the increased cross-linking density as a result of various chemical reactions among the hydroxyl/urethane groups of polyurethane, epoxy resin and hydroxyl groups of Fe<sub>3</sub>O<sub>4</sub> nanomaterials (Scheme 4B.1). Further, the increased of interactions is due to the homogeneous dispersion of Fe<sub>3</sub>O<sub>4</sub> in the polymer matrix that causes the more restriction of polymer chains on the surface of the nanoparticles. Therefore the increased intercross-linking offers the compact three dimensional network structure formation. The absence of the epoxy band at 915 cm<sup>-1</sup> in the FTIR spectra and the increased of cross-linking density (supported by swelling study in DMF, Table 4B.1) confirmed the formation of thermoset.





Scheme 4B.1: Proposed crosslinking reactions

**Table 4B.1:** Composition and curing time of the nanocomposites at 120 °C

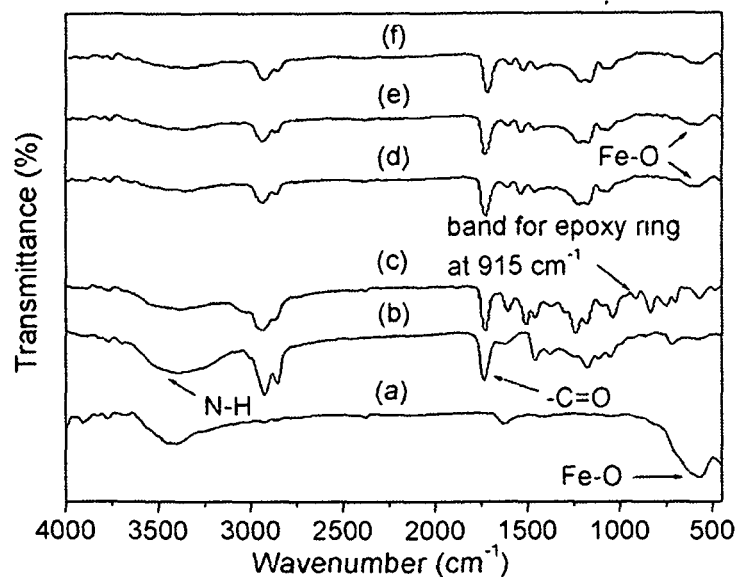
Code	MHBPU10 (wt%)	Epoxy (wt%)	Touch free time (min)	Drying time (min)	Swelling (%)
MHBPU10	100	-	-	-	-
EHPU2	100	10	55	59	30
EHPU5	100	10	44	51	23
EHPU10	100	10	36	42	16

#### 4B.3.2. FTIR study

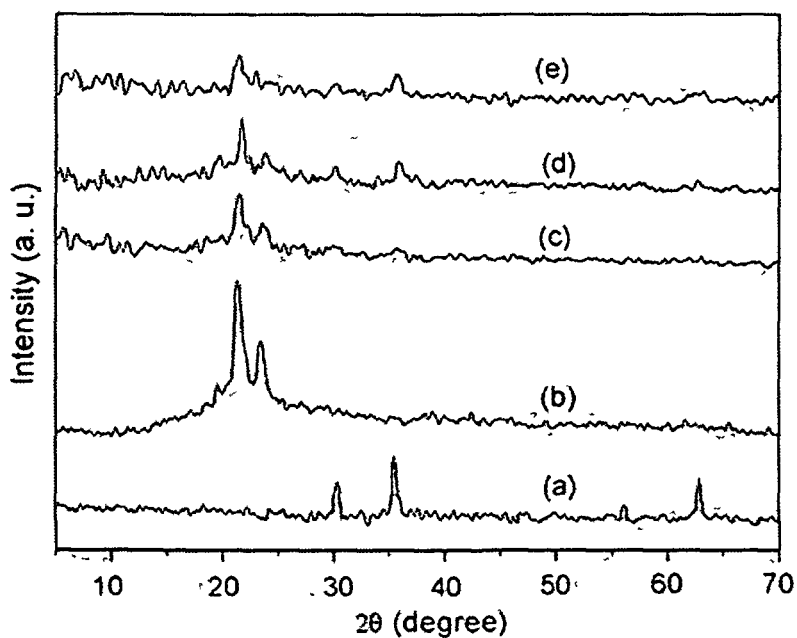
The FTIR spectra of Fe<sub>3</sub>O<sub>4</sub>, hyperbranched polyurethane and the thermosetting nanocomposites are shown in Fig. 4B.1. The bands at 3429 cm<sup>-1</sup> and 581 cm<sup>-1</sup> are due to the stretching vibration of Fe-OH groups present on the surface of Fe<sub>3</sub>O<sub>4</sub> nanoparticles and Fe-O stretching vibration, respectively. The band of urethane linkage at 3405-3431 cm<sup>-1</sup> (N-H stretching) was found to broaden after the nanocomposite formation. This implies the well dispersion of the nanoparticles and the presence of strong interaction of Fe<sub>3</sub>O<sub>4</sub> nanoparticles within the polyurethane matrix. Moreover, the band corresponding to Fe-O of Fe<sub>3</sub>O<sub>4</sub> nanoparticles was broadened in the nanocomposites. This ascribed that polymer chains are immobilized on the surface of Fe<sub>3</sub>O<sub>4</sub> nanoparticles. The results confirmed the presence of interactions among the nanoparticles, epoxy resin and the polyurethane chains.

#### 4B.3.3. X-ray diffraction study

The X-ray diffractograms of Fe<sub>3</sub>O<sub>4</sub>, hyperbranched polyurethane and the nanocomposites are shown in Fig. 4B.2. The peaks appear at 2θ=30.34°, 35.53°, 56.72° and 62.74°, which correspond to (220), (311), (511) and (440) planes of Fe<sub>3</sub>O<sub>4</sub>, respectively as already discussed in the earlier subchapter. The diffraction peaks at 2θ=21.81° and 2θ=23.72° are due to the (100) and (200) planes of PCL crystals of the hyperbranched polyurethane. The crystalline domain size of Fe<sub>3</sub>O<sub>4</sub> was found to 10 nm, which was determined by using the Scherrer equation.



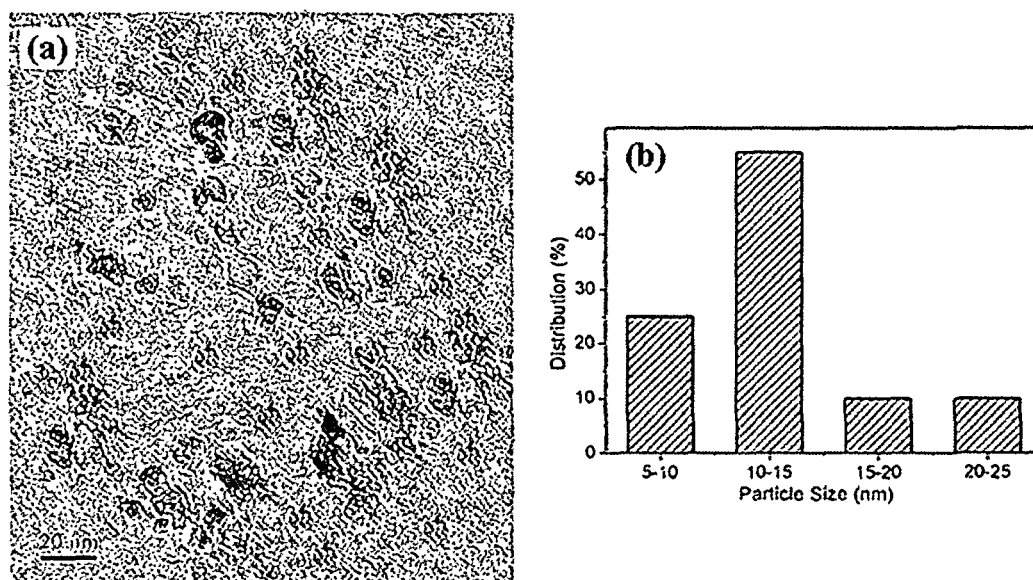
**Fig. 4B.1:** FTIR spectra of (a)  $\text{Fe}_3\text{O}_4$ , (b) MHBPU10, (c) EHPU2 before curing, (d) EHPU2, (e) EHPU5 and (f) EHPU10



**Fig. 4B.2:** XRD diffractograms of (a)  $\text{Fe}_3\text{O}_4$ , (b) MHBPU10, (c) EHPU2, (d) EHPU5 and (e) EHPU10

#### 4B.3.4. TEM study

A representative TEM micrograph and histogram of Fe<sub>3</sub>O<sub>4</sub> nanoparticles in the polymer nanocomposite are shown in Fig. 4B.3. The average diameter of the nanoparticles was found to be 12 nm, which is in good agreement with XRD result. Therefore the average surface area of Fe<sub>3</sub>O<sub>4</sub> nanoparticles in the nanocomposite was 452.16 nm<sup>2</sup>. The TEM image indicates the homogeneous distribution with almost no aggregation or agglomeration of Fe<sub>3</sub>O<sub>4</sub> nanoparticles in the polyurethane matrix. This is due to the good interfacial interaction between the nanoparticles and the polyurethane chains. The distribution of spherical Fe<sub>3</sub>O<sub>4</sub> nanoparticles in the nanocomposites clearly indicated that more than 50% of the nanoparticles are within the size range of 10-15 nm.



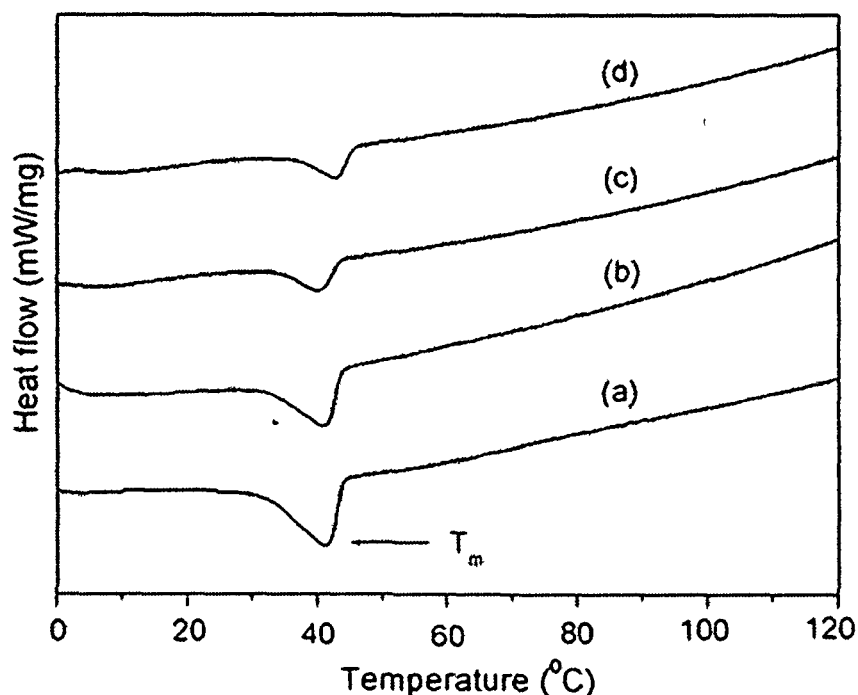
**Fig. 4B.3:** (a) TEM image and (b) distribution of nanoparticles for EHPU5

#### 4B.3.5. Thermal property

The DSC curves of hyperbranched polyurethane and the nanocomposites are shown in Fig. 4B.4. The melting temperature ( $T_m$ ) and melting enthalpy are given in Table 4B.2. From the table it is clear that the melting temperature increases with the increase of the loading of Fe<sub>3</sub>O<sub>4</sub> nanoparticles. This can be attributed to the increased restricted movement of the polymer chains due to the various physical and chemical cross-linking in the systems. The slight decrease in melting enthalpy value of the nanocomposites with loading of Fe<sub>3</sub>O<sub>4</sub> nanoparticles as compared

to hyperbranched polyurethane (Table 4B.2) indicated the decrease of crystallinity of the polymer matrix in the presence of nanoparticles. In other words  $\text{Fe}_3\text{O}_4$  nanoparticles have retarding effect on the crystallization process of hyperbranched polyurethane.

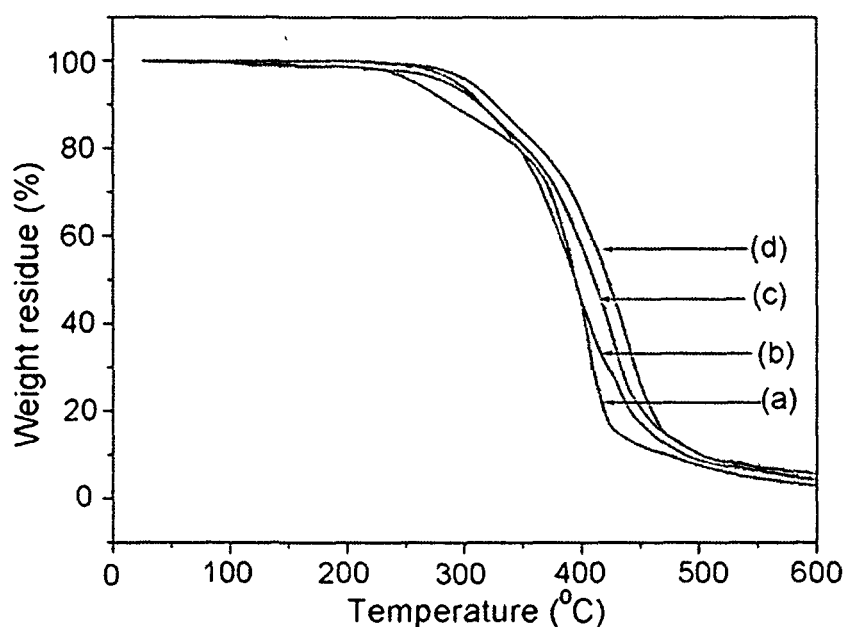
The thermo-gravimetric profiles of hyperbranched polyurethane and the thermosetting nanocomposites are shown in Fig. 4B.5. The thermal stability of the nanocomposites increased with the increase of content of  $\text{Fe}_3\text{O}_4$  nanoparticles. From the figure it is seen that the initial decomposition starts at 240 °C, 258 °C, 264 °C and 275 °C for the 0, 2, 5 and 10 wt% of  $\text{Fe}_3\text{O}_4$  loading, respectively. This beneficial effect can be attributed to the increased various physico-chemical interactions among the epoxy, polyurethane and  $\text{Fe}_3\text{O}_4$  nanomaterials.<sup>20</sup> Therefore the polymer chains configuration were changed as well as mobility restricted on the surface of nanoparticles, which conferred the rigidity and compactness of the nanocomposites. The improvement of thermal stability of the nanocomposites can also be attributed to the presence of  $\text{Fe}_3\text{O}_4$  nanoparticles, which acted as gas barriers to reduce the permeability of oxygen and volatile degradation products throughout the nanocomposite.



**Fig. 4B.4:** DSC curves of (a) MHBPU10, (b) EHPU2, (c) EHPU5 and (d) EHPU10

**Table 4B.2:** Melting temperature and melting enthalpy of the thermosetting nanocomposites

Code	Melting temperature ( $T_m$ °C)	Melting enthalpy ( $\Delta H_m$ J/g)
MHBPU10	40.3	42.8
EHPU2	40.9	41.6
EHPU5	41.4	39.8
EHPU10	42.5	39



**Fig. 4B.5:** TGA thermograms of (a) MHBPU10, (b) EHPU2, (c) EHPU5 and (d) EHPU10

#### 4B.3.6. Mechanical property

The effect of  $\text{Fe}_3\text{O}_4$  nanoparticles loading on the performance characteristics such as tensile strength, elongation at break, scratch hardness, impact resistance etc. of the thermosetting nanocomposites are shown in Table 4B.3. The tensile strength increases from 6.2 to 18 MPa with the increase of loading of  $\text{Fe}_3\text{O}_4$  from 2 to 10 wt%. This can be explained from the homogeneous dispersion of  $\text{Fe}_3\text{O}_4$  nanoparticles and the increased physico-chemical interactions among the epoxy resin, urethane linkages and hydroxyl groups of  $\text{Fe}_3\text{O}_4$  nanoparticles.<sup>20, 21</sup> Therefore stress in the nanocomposites is transferred easily to the rigid nanoparticles, as a result, the tensile

strength of the nanocomposites was enhanced. Furthermore the increased cross-linking density (supported by the swelling values, Table 4B.1) is also responsible for the improvement of the tensile strength. However, the elongation at break decreased with the increase of the loading of Fe<sub>3</sub>O<sub>4</sub> nanoparticles due to the molecular restriction of the polymer chains on the surface of the nanoparticles. The scratch resistance was found to be increased (Table 4B.3) with the increase of loading of Fe<sub>3</sub>O<sub>4</sub> nanoparticles as a result of the increase of stiffness and compactness of the material. This is due to the presence of various interactions as stated earlier. This combined effect produced the tough surface that becomes more difficult for penetration. All the nanocomposites showed good impact resistance (~1m) that is the ability of the material to absorb the applied energy. The flexibility of pristine polymer remains intact even after the formation of nanocomposites as indicated by the bending test results. The gloss of the nanocomposites increased as compared to the neat polymer with loading of the nanoparticles. This can be attributed to the compatibility among the components, higher cross-linking density, higher dimension stability and the smoothness of the surface compared to pristine hyperbranched polyurethane.

**Table 4B.3:** Mechanical properties of hyperbranched polyurethane and the thermosetting nanocomposites

Property	MHBPU10	EHPU2	EHPU5	EHPU10
Tensile strength (MPa)	6.2 ± 0.4	11 ± 0.2	14.3 ± 0.2	18 ± 0.2
Elongation at break (%)	595 ± 3.1	482 ± 1.4	432 ± 1.4	396 ± 1.1
Scratch resistance (kg)	3 ± 0.1	5.4 ± 0.1	6.2 ± 0.1	7 ± 0.15
Impact resistance* (m)	0.95 ± 0.05	0.95 ± 0.05	0.95 ± 0.05	0.95 ± 0.02
Bending (m)	<0.001	<0.001	<0.001	<0.001
Gloss (60°)	83 ± 2	87 ± 2	92 ± 2	95 ± 2

\* 1.0 m is the limit of the instrument

#### 4B.3.7. Magnetic property

The magnetic hysteresis loop of the nanocomposite (EHPU5) at room temperature is shown in Fig. 4B.6. The saturation magnetization value was found to be 0.22 emu/g. The low value of magnetization of the nanocomposite is due to the low content of the nanomaterials (2

wt%); smaller size and the surface coating of the  $\text{Fe}_3\text{O}_4$  nanoparticles by the polymer chains as described in subchapter 4A, section 4A.3.6.

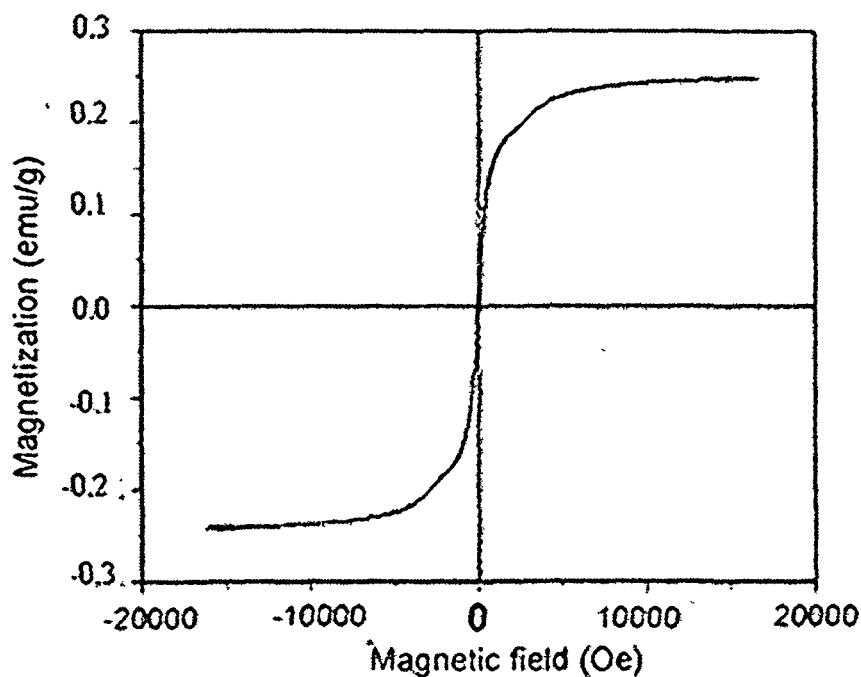


Fig. 4B.6: Magnetic hysteresis loop for EHPU5

#### 4B.3.8. Shape memory property

The shape memory behaviors of the hyperbranched polyurethane and the thermosetting nanocomposites are shown in Fig. 4B.7. The nanocomposites exhibited good shape fixity over the repeated cycles of test. The micro-Brownian movements of the polymer chains and the applied stress are frozen during the cooling process. This resulted good shape fixity of the nanocomposites (Table 4B.4). The fixed shape can be retained for a long time at the room temperature. The nanocomposites also showed good shape recovery under the application of microwave energy. When the microwave irradiated on the samples, the dipole moment oscillates due to the oscillation of electric field component of the microwave. Therefore heat is generated due to the molecular friction and collisions, and the shape recovery was observed when the induced heat is close to the  $T_{\text{trans}}$ . The shape recovery speed was found to increase with the increase of loading of  $\text{Fe}_3\text{O}_4$  nanoparticles (Table 4B.4). This can be attributed to the homogeneous distribution of the nanoparticles and increased various physico-chemical



interactions in the system. Furthermore this can be attributed to the increased of microwave absorption characteristic of the nanocomposites due to the increase of loading of  $\text{Fe}_3\text{O}_4$  nanoparticles as  $\text{Fe}_3\text{O}_4$  nanoparticles are microwave absorbing material.<sup>4, 5</sup> The nanocomposites showed good shape fixity and shape recovery over the repeated cycles of test and might be utilized as advanced shape memory materials in different potential fields.

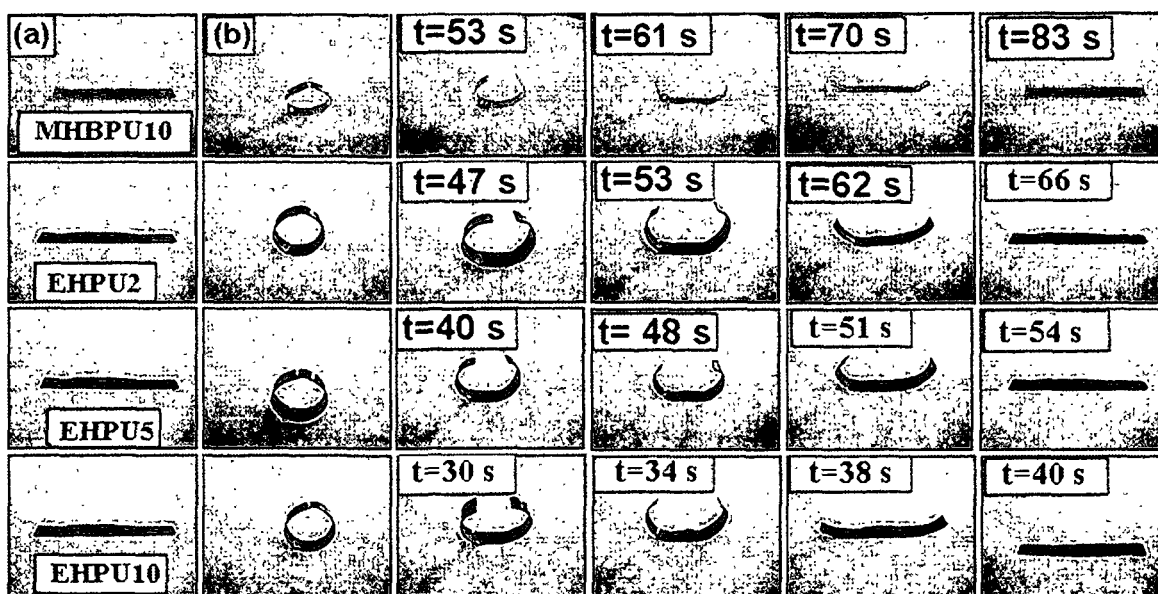


Fig. 4B.7: Shape memory behaviors of the hyperbranched polyurethane and the thermoset nanocomposites (a) original shape and (b) fixed shape

Table 4B.4: Shape memory behaviors of hyperbranched polyurethane and the nanocomposites

Code	Shape fixity (%)	Shape recovery (%)	Shape recovery time (s)
MHBPU10	$98.7 \pm 0.5$	$98.5 \pm 0.6$	$83 \pm 4$
EHPU2	$99.2 \pm 0.2$	$99.1 \pm 0.1$	$66 \pm 2$
EHPU5	$99.2 \pm 0.2$	$99.1 \pm 0.1$	$54 \pm 2$
EHPU10	$99.2 \pm 0.2$	$99.1 \pm 0.1$	$40 \pm 2$

#### **4B.4. Conclusion**

The *in-situ* polymerization of hyperbranched polyurethane in the presence of Fe<sub>3</sub>O<sub>4</sub> nanoparticles and subsequent modification with epoxy resulted mechanically strong thermosetting nanocomposites as microwave induced shape memory material. The incorporation of iron oxide nanoparticles in the epoxy modified hyperbranched polyurethane leads to significant improvement of tensile strength and thermal stability. In addition, the nanocomposites showed excellent shape fixity over the repeated cycle of test and exhibited almost full shape recovery under the application of microwave energy. Furthermore, the dose dependent shape recovery speed was observed, which is accelerated with the content of Fe<sub>3</sub>O<sub>4</sub> nanoparticles. Moreover the thermosetting nanocomposites exhibited the better performance including shape memory behaviors as compared to the thermoplastic nanocomposites. Thus the studied nanocomposites could be utilized as a microwave induced non-triggering shape memory materials.

## References

1. Ankamwar, B., et al. Biocompatibility of Fe<sub>3</sub>O<sub>4</sub> nanoparticles evaluated by in vitro cytotoxicity assays using normal, glia and breast cancer cells, *Nanotechnology* **21** (7), 75102-75111, 2010.
2. Sun, J., et al. Synthesis and characterization of biocompatible Fe<sub>3</sub>O<sub>4</sub> nanoparticles, *J. Biomed. Mater. Res. A* **80 A** (2), 333-341, 2007.
3. Weissleder, R., et al. Superparamagnetic iron oxide: pharmacokinetics and toxicity, *Am. J. Roentgenol.* **152** (1), 167-173, 1989.
4. Ni, S., et al. Hydrothermal synthesis and microwave absorption properties of Fe<sub>3</sub>O<sub>4</sub> nanocrystals, *J. Phys. D: Appl. Phys.* **42** (5), 055004-055009, 2009.
5. Ni, S., et al. Designed synthesis of wide range microwave absorption Fe<sub>3</sub>O<sub>4</sub>-carbon sphere composite, *J. Alloys Compd.* **489** (1), 252-256, 2010.
6. Lee, B.S., et al. Structure and thermomechanical properties of polyurethane block copolymers with shape memory effect, *Macromolecules* **34** (18), 6431-6437, 2001.
7. Ping, P., et al. Poly( $\epsilon$ -caprolactone) polyurethane and its shape-memory property, *Biomacromolecules* **6** (2), 587-592, 2005.
8. Jang, M.K., et al. Shape memory polyurethanes cross-linked by surface modified silica particles, *J. Mater. Chem.* **19** (8), 1166-1172, 2009.
9. Cai, Y., et al. Synthesis and properties of magnetic sensitive shape memory Fe<sub>3</sub>O<sub>4</sub>/poly( $\epsilon$ -caprolactone)-polyurethane nanocomposites, *J. Appl. Polym. Sci.* **127** (1), 49-56, 2013.
10. Xiao, Y., et al. Electro-active shape memory properties of poly( $\epsilon$ -caprolactone)/functionalized multiwalled carbon nanotube nanocomposite, *ACS Appl. Mater. Interfaces* **2** (12), 3506-3514, 2010.
11. Park, J.O. Silane treatment of Fe<sub>3</sub>O<sub>4</sub> and its effect on the magnetic and wear properties of Fe<sub>3</sub>O<sub>4</sub>/epoxy nanocomposites, *Appl. Surf. Sci.* **256** (23), 6945-6950, 2010.
12. Chattopadhyay, D.K., & Webster, D.C. Thermal stability and flame retardancy of polyurethanes, *Prog. Polym. Sci.* **34** (10), 1068-1133, 2009.
13. Deka, H., et al. Biocompatible hyperbranched polyurethane/multi-walled carbon nanotube composites as shape memory materials, *Carbon* **48** (7), 2013-2022, 2010.
14. Brydson, J.A. *Plastics Materials*, Butterworth scientific, London, 1982.

15. Barick, A.K., & Tripathy, D.K. Preparation and characterization of thermoplastic polyurethane/organoclay nanocomposites by melt intercalation technique: effect of nanoclay on morphology, mechanical, thermal, and rheological properties, *J. Appl. Polym. Sci.* **117** (2), 639-654, 2010.
16. Roy, N., & Bhowmick, A.K. Novel in situ carbon nanofiber/polydimethylsiloxane nanocomposites: synthesis, morphology, and physico-mechanical properties, *J. Appl. Polym. Sci.* **123** (6), 3675-3687, 2012.
17. Haghayegh, M., & Sadeghi, G.M.M. Synthesis of shape memory polyurethane/clay nanocomposites and analysis of shape memory, thermal, and mechanical properties, *Polym. Compos.* **33** (6), 843-849, 2012.
18. Gunes, I.S., et al. Evaluation of nanoparticulate fillers for development of shape memory polyurethane nanocomposites, *Polymer* **49** (9), 2223-2234, 2008.
19. Deka, H., & Karak, N. Shape-memory property and characterization of epoxy resin-modified *Mesua ferrea* L. seed oil-based hyperbranched polyurethane, *J. Appl. Polym. Sci.* **116** (1), 106-115, 2010.
20. Deka, H., & Karak, N. Vegetable oil-based hyperbranched thermosetting polyurethane/clay nanocomposites, *Nanoscale Res. Lett.* **4** (7), 758-765, 2009.
21. Wang, J.C., et al. Preparation of thermosetting polyurethane nanocomposites by montmorillonite modified with a novel intercalation agent, *J. Polym. Sci., Part B: Polym. Phys.* **45** (5), 519-531, 2007.

## ***Chapter 5***

# **Hyperbranched polyurethane/MWCNT nanocomposites**

### ***Highlights***

This chapter also consists of two subchapters, one on thermoplastic and other on thermosetting hyperbranched polyurethane/triethanolamine functionalized MWCNT nanocomposites. The covalently functionalized MWCNT were characterized by the Fourier transform infrared spectroscopic and Raman spectroscopic studies. The formation of nanocomposites was supported by the Fourier transform infrared spectroscopic and TEM studies. The mechanical, thermal and shape memory behaviors were studied for the prepared nanocomposites. Microwave energy was used to investigate the shape memory behavior. In the second subchapter hyperbranched polyurethane/multi-walled carbon nanotube thermosetting nanocomposites were prepared using glycidyl ether epoxy of bisphenol-A. The thermosetting nanocomposites exhibited better performance including shape memory behaviors as compared to the thermoplastic one.

---

*Parts of this work are published in*

1. Kalita, H., & Karak, N., *J. Nanosci. Nanotechno.* 2013.
2. Kalita, H., & Karak, N., *Polym. Int.* 2013.

## **5A. Hyperbranched thermoplastic polyurethane/triethanolamine functionalized MWCNT nanocomposites**

### **5A.1. Introduction**

The importance of hyperbranched polyurethane and its nanocomposites along with their shape memory behaviors were discussed in Chapter 1. Since their discovery in 1991 by Iijima, carbon nanotubes have opened the door to augment mechanical properties of polymer by incorporating small amount of them into the polymer matrix.<sup>1</sup> The efficient interfacial interactions between the carbon nanotubes and the polymer matrix are the most promising factors for significant improvement of the mechanical properties of the polymer which expand the applications of polymer materials in many fields.<sup>2-5</sup> The extent of interfacial adhesion between the carbon nanotubes and polymer matrix depends on various factors such as the types, purity, structure, dimension, loading, alignment, degree of functionalization and degree of dispersion of the nanotubes in the polymer matrix. However, the preparation of nanocomposites with homogeneous distribution of carbon nanotubes in the polymer matrix is very difficult, because they tend to agglomerate as they are thermodynamically stabilized by van der Waals forces and numerous  $\pi$ - $\pi$  interactions between the tubes as well as by high degree of entanglements.<sup>6, 7</sup> The agglomeration of nanotubes within a polymer matrix deteriorates the mechanical properties over the pristine polymer, due to easier crack initiation and propagation in the nanocomposites. Therefore, extensive investigations on chemical modification are undergoing where active organic groups are generated/grafted on the surface of carbon nanotubes.<sup>8-10</sup> These groups enhanced the dispersion of carbon nanotubes in the polymer matrix due to improved compatibility between carbon nanotubes and polymer matrix.<sup>2</sup> Therefore, by the modification of carbon nanotubes the interfacial adhesion between the carbon nanotubes and polymer matrix could be modified to enhance the load transfer capacity of the nanocomposites. In the current study esterification reaction was used for grafting triethanolamine to acyl chloride activated multi-walled carbon nanotubes (MWCNT).

In the current study, therefore, hyperbranched polyurethane/triethanolamine functionalized MWCNT nanocomposites were prepared to investigate the performance including shape memory behavior.

## 5A.2. Experimental

### 5A.2.1. Materials

The monoglyceride of the *Mesua ferrea* L. seed oil, TDI, PCL, 1,4-butanediol and triethanolamine (TEA) used for the preparation of hyperbranched polyurethane were same as described in Chapter 2, section 2A.2.1.

MWCNT with diameter and length of about 10–20 nm and 20  $\mu\text{m}$ , respectively, were purchased from Iiljin Nanotech, South Korea and used as received.

### 5A.2.2. Modification of MWCNT

MWCNT were treated by a mixture of concentrated  $\text{H}_2\text{SO}_4$  and  $\text{HNO}_3$  (3:1 v/v) at 80 °C for 3 h. After washing thoroughly with water, they were dried under vacuum at 80 °C for 24 h. Required amount of dried acid treated MWCNT were dispersed in DMF by ultrasonication followed by the addition of excess  $\text{SOCl}_2$ . Then the reaction mixture was stirred at 70 °C for 12 h to form acid chloride functionalized MWCNT (MWCNT-COCl). After washing several times with anhydrous THF, they were dried in a vacuum oven at 40 °C for 6 h. Finally, the MWCNT-COCl was reacted with TEA at 70 °C under magnetic stirring for 12 h followed by washing with THF. The obtained solid was dried at 40 °C for 3 h.

### 5A.2.3. Preparation of hyperbranched polyurethane/TEA-f-MWCNT nanocomposites

The details of the synthesis of hyperbranched polyurethane were described in Chapter 2, section 2A.2.3. For the preparation of nanocomposite, required amount of dispersed TEA-f-MWCNT was injected into the polymerization reaction before 1 h of completion and the reaction was continued. After completion of reaction the solution was cast over the inert substrates followed by vacuum degassing and drying at 60 °C for different testing. The nanocomposites were denoted as MHBPU10, HPUCNT0.2, HPUCNT1 and HPUCNT2 corresponding to the TEA-f-MWCNT content of 0, 0.2, 1 and 2 wt%, respectively.

#### 5A.2.4. Instrumentation

The hyperbranched polyurethane and its nanocomposites were characterized by different techniques such as FTIR, XRD and SEM as described in Chapter 2, section 2A.2.4.

The mechanical properties such as tensile strength, elongation at break, scratch resistance and impact resistance were measured by the same way as described in Chapter 2, section 2A.2.4. The thermal stability was studied by the same way as described in Chapter 2, section 2A.2.4.

The Raman spectra of MWCNT, a-MWCNT and TEA-f-MWCNT were recorded by Invia Renishaw Raman spectrometer, England (Argon ion laser 514.5 nm).

The shape memory behaviors of the samples were studied by the same way using microwave energy as described in Chapter 4, section 4A.2.4.

### 5A.3. Results and discussion

#### 5A.3.1. FTIR study

The FTIR spectra of pristine MWCNT, a-MWCNT and TEA-f-MWCNT are shown in Fig. 5A.1. The FTIR spectra of acid treated MWCNT showed the absorption at frequency  $1725\text{ cm}^{-1}$  ( $\text{-C=O}$ ). However, there was no such absorption band in this region for the pristine MWCNT. This confirmed the functionalization of  $\text{-COOH}$  group on the acid treated MWCNT. The FTIR spectra of TEA-f-MWCNT showed the absorption frequency at  $3145\text{ cm}^{-1}$  ( $\text{-OH}$  stretching),  $2930\text{ cm}^{-1}$  ( $\text{-CH}$  stretching),  $1732\text{ cm}^{-1}$  ( $\text{-C=O}$  of ester group),  $1460\text{ cm}^{-1}$  ( $\text{-CH}$  bending),  $1330\text{ cm}^{-1}$  ( $\text{C-N}$  stretching) and  $1190\text{ cm}^{-1}$  ( $\text{-C-O}$  of ester group) indicating the presences of TEA functionalized on the surface of MWCNT. FTIR spectra of hyperbranched polyurethane and all the prepared nanocomposites are shown in Fig. 5A.2. The characteristic bands of urethane group of pristine polymer appeared at  $3406\text{-}3430\text{ cm}^{-1}$  ( $\text{N-H}$  stretching) and  $1728\text{ cm}^{-1}$  ( $\text{-NHCOO-}$  stretching) as already stated in the earlier chapter. The band at  $3406\text{-}3430\text{ cm}^{-1}$  ( $\text{N-H}$  stretching) broaden after the nanocomposite formation. Further, the band at  $1728\text{ cm}^{-1}$  of  $\text{-NHCOO-}$  was shifted to lower wavenumber ( $1720\text{-}1715\text{ cm}^{-1}$ ) after the nanocomposites formation. All the above results confirmed the interactions of TEA-f-MWCNT with the polyurethane in the prepared nanocomposites.



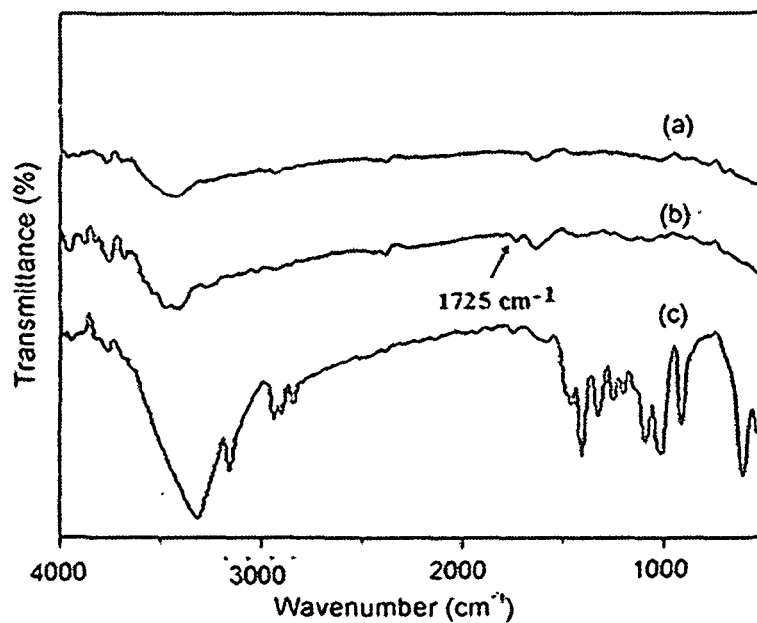


Fig. 5A.1: FTIR spectra for (a) pristine MWCNT, (b) acid treated MWCNT and (c) TEA -f- MWCNT

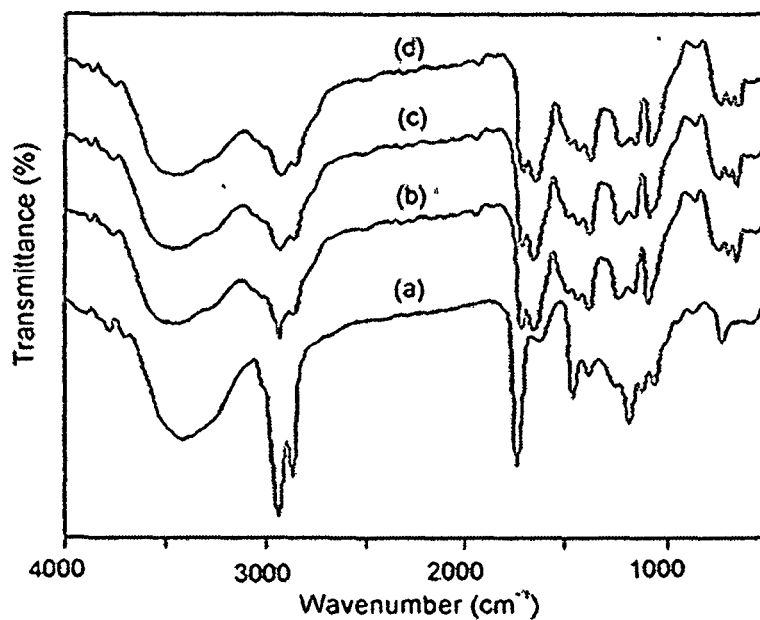
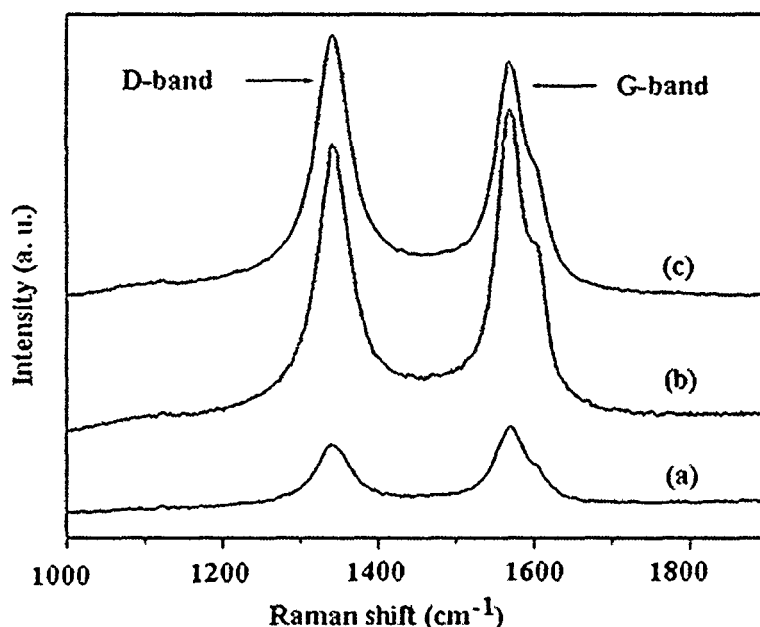


Fig. 5A.2: FTIR spectra for (a) MHBPU10, (b) HPUCNT0.2, (c) HPUCNT1 and (d) HPUCNT2

### 5A.3.2. Raman spectroscopic study

The functionalization of MWCNT was further characterized by the Raman spectroscopy. The Raman spectra of pristine MWCNT, a-MWCNT and TEA-f-MWCNT are shown in Fig. 5A.3. All the Raman spectra showed D band at  $1341\text{ cm}^{-1}$  and G band at  $1571\text{ cm}^{-1}$ . The intensity ratio between the D band and G band ( $I_D/I_G$ ) implies the degree of covalent functionalization of MWCNT. The value of intensity ratio was found to be 0.82, 0.91 and 1.10 for the pristine MWCNT, a-MWCNT and TEA-f-MWCNT, respectively. The increase in the value of intensity ratio indicated more defects are generated on MWCNT framework upon functionalization.

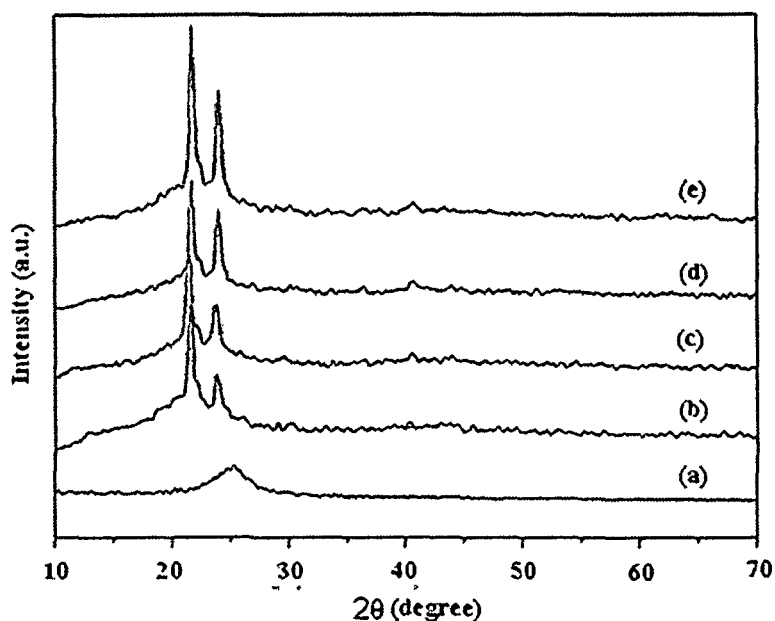


**Fig. 5A.3:** Raman spectra for (a) pristine MWCNT, (b) a-MWCNT and (c) TEA-f-MWCNT

### 5A.3.3. X-ray diffraction study

The XRD patterns of TEA-f-MWCNT, hyperbranched polyurethane and all the prepared nanocomposites are shown in Fig. 5A.4. The peak appears at  $2\theta=25.4^\circ$  corresponding to the (002) plane of carbon atoms of MWCNT.<sup>11</sup> There are two strong diffraction peaks at  $2\theta=21.90^\circ$  and  $2\theta=23.80^\circ$  due to the (100) and (200) planes of PCL crystals of the hyperbranched polyurethane. The peak intensity increased after the formation of nanocomposite. The results

showed that TEA-f-MWCNT serves as nucleating site to increase the crystallinity of hyperbranched polyurethane.



**Fig. 5A.4:** XRD diffractograms for (a) TEA-f-MWCNT, (b) MHBPU10, (c) HPUCNT0.2, (d) HPUCNT1 and (e) HPUCNT2

#### 5A.3.4. Morphology study

The morphology of the prepared nanocomposites was studied by using SEM. The fractured surface of the sample after tensile test was observed in SEM (Fig. 5A.5). The TEA-f-MWCNT appeared as bright lines in the micrographs of nanocomposites. TEM was used to examine the distribution of TEA-f-MWCNT in the polymer matrix. Fig. 5A.6 shows the TEM micrograph of nanocomposite (HPUCNT1). The micrograph depicts that TEA-f-MWCNT are well dispersed in the polymer matrix with average diameter 13 nm. Furthermore, TEA-f-MWCNT showed good dispersion in DMF and remained stable for 3 months. However, the pristine MWCNT in DMF settled down before 3 h from the date of sonication. The initial dispersion of MWCNT in the solvent has the great impact on the nanotubes dispersion in the polymer matrix.

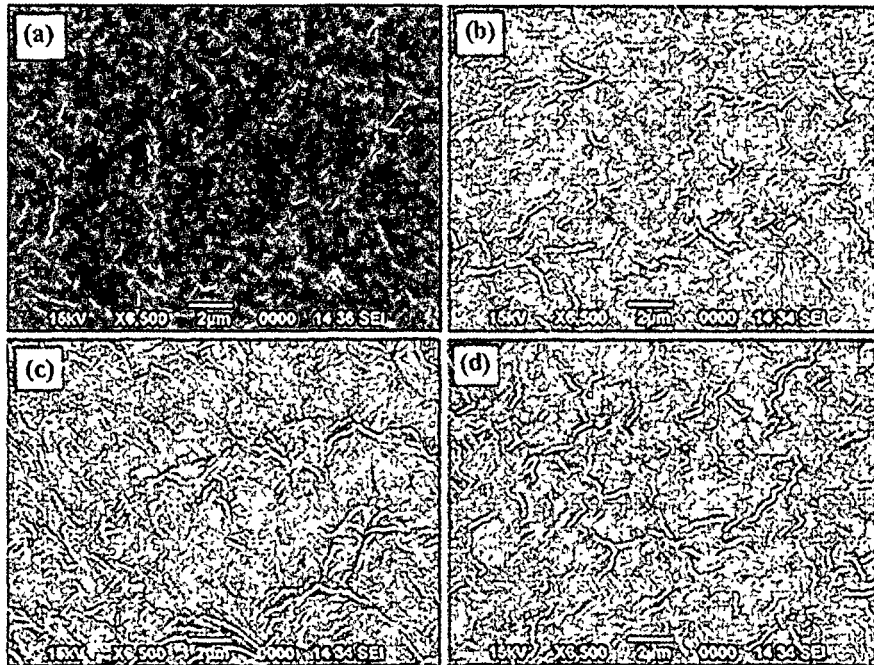


Fig. 5A.5: SEM micrographs for (a) MHBPU10, (b) HPUCNT0.2, (c) HPUCNT1 and (d) HPUCNT2

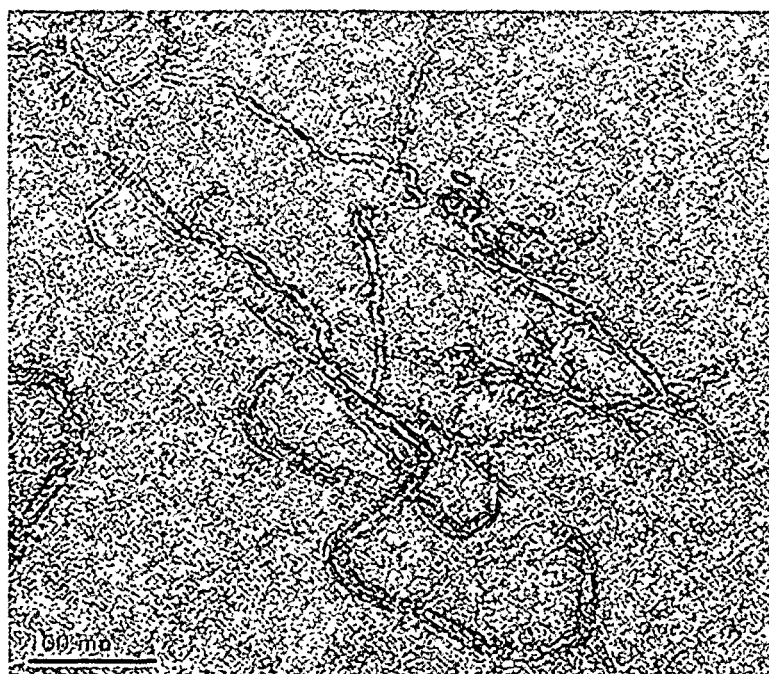


Fig. 5A.6: TEM image for HPUCNT1

#### 5A.3.5. Thermal property

The thermal stability of the prepared nanocomposites was studied by the TGA analysis and the thermograms are shown in Fig. 5A.7. The thermal decomposition of nanocomposites depends on the various factors such as size and nature of the nanomaterial, distribution of nanomaterial and interaction of nanomaterial in the polymer matrix.<sup>12</sup> Thermal stability of the nanocomposites increased with the increase of amount of TEA-f-MWCNT. This is due to the increased of various physical interactions such as H-bonding and polar-polar interactions along with the chemical bond formation in the nanocomposites. Therefore, the volatile products formed during the thermal decomposition process have to travel longer zigzag path to escape the matrix because the well dispersed nanotubes act as gas barrier as well as absorption of free radicals that were generated during the degradation of polymer.<sup>13</sup> Moreover, the molecular mobility of the chains decreases and confers the compactness in the structure of the nanocomposite. As a result, the bond breaking inside the bulk polymeric matrix needs more thermal energy. Incorporation of TEA-f-MWCNT in the polymer matrix enhances the thermal conductivity of the prepared nanocomposites that facilitates heat dissipation within the nanocomposites.

From Fig. 5A.8, it is seen that melting temperature ( $T_m$ ) (39.1 °C to 44.2 °C) of the nanocomposites increased with the increase of amount of TEA-f-MWCNT. This is due to uniform dispersion of this MWCNT that resulted the enhanced interactions as stated earlier. Thereby decreases the free volumes present in the nanocomposites and the thermal transition temperature raised. Furthermore the enhanced crystallinity is also responsible for the increase in  $T_m$  of the nanocomposites. This suggests that TEA-f-MWCNT act as a nucleating agent for the polyurethane.

#### 5A.3.6. Mechanical property

The mechanical properties of the hyperbranched polyurethane and its nanocomposites are given in Table 5A.1. Mechanical properties of the nanocomposites depend on the nanotube type, aspect ratio, surface functionality, dispersion in solvent and the type of polymer matrix as these factors control the dispersion, distribution, alignment and interfacial interaction in the nanocomposites.<sup>14-16</sup> From the result it is observed that tensile strength increased with the

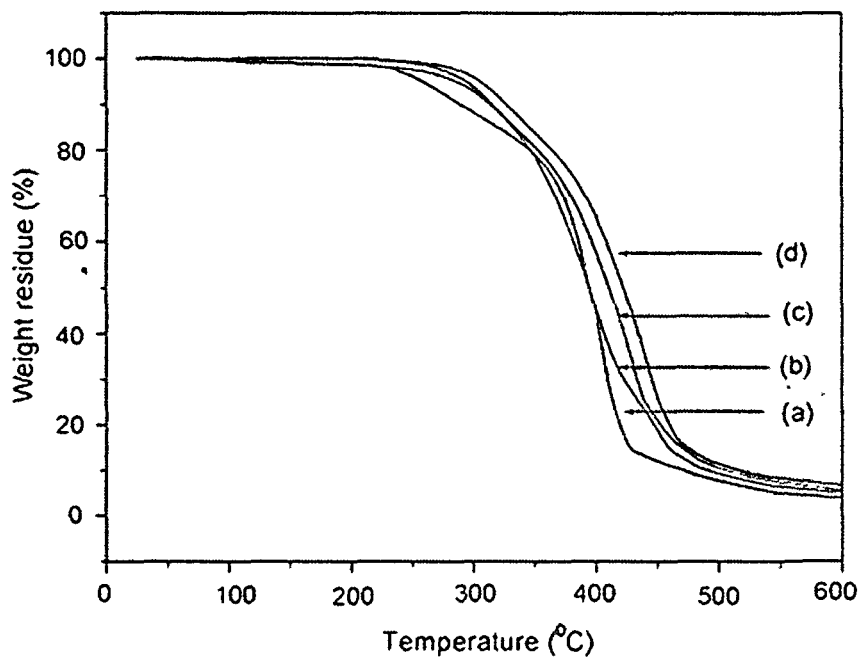


Fig. 5A.7: TGA thermograms for (a) MHBPU10, (b) HPUCNT0.2, (c) HPUCNT1 and (d) HPUCNT2

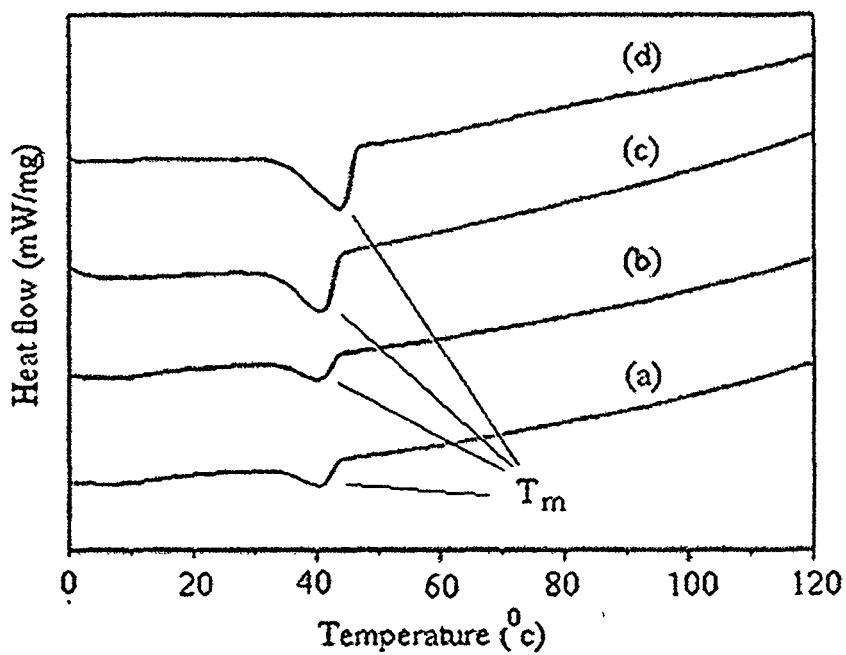


Fig. 5A.8: DSC curves for (a) MHBPU10, (b) HPUCNT0.2, (c) HPUCNT1 and (d) HPUCNT2

increase of the amount of TEA-f-MWCNT. This is attributed to the increased chemical cross-linking and physical interactions between the TEA-f-MWCNT and the polymer matrix. After the modification MWCNT become more compatible with the polymer matrix as well as they are well dispersed in the polymer matrix. The modification of acid treated MWCNT with TEA leads to the functionalization of MWCNT that resulted weakening of the interactions among the MWCNT. This facilitates the dispersion of MWCNT in the polymer matrix. The high degree of dispersion leads to the extensive chemical derivatization and provides the highest interfacial area for stress transfer to the polymer matrix. The interactions such as physical cross-linking of the free  $-COOH$  and  $-OH$  groups of the nanotubes with the urethane linkages and free  $-OH$  of the polyurethane are taken placed. Moreover, chemical cross-linking such as urethane linkage may form between the free  $-OH$  of TEA-f- MWCNT and the free  $-NCO$  of the polymer matrix. As a consequence they make the material stiffer and lead to the enhanced load transfer from the polymer matrix to the carbon nanotubes. Furthermore the increased degree of crystallinity with the increase of amount of TEA-f-MWCNT increased the mechanical properties of the nanocomposites. However, the elongation at break of the nanocomposites decreases with the increase of amount of TEA-f-MWCNT. This may be due to the increased molecular restriction of the polymer chains by physical as well as chemical interactions on the surface of the MWCNT, result in decrease of flexibility. The scratch resistance of the nanocomposites increased with the increase of the content of TEA-f-MWCNT in the nanocomposite. This may be due to the enhancement of overall toughness of the nanocomposites arises from various interactions as stated earlier. The prepared nanocomposites exhibited sufficient flexibility as the films could be bent onto a rod of 0.001m diameter without any crack in the bent films as indicated in the bending test. This indicates retention of flexibility in all the nanocomposites. This is mainly due to the high flexibility of the soft segment and the presence of long chain fatty acid moiety in the structure of the polyurethane.

**Table 5A.1:** Mechanical properties of hyperbranched polyurethane and its nanocomposites

Properties	MHBPU10	HPUCNT0.2	HPUCNT1	HPUCNT2
Tensile strength (MPa)	6.5 ± 0.4	13 ± 0.3	20.5 ± 0.3	28.5 ± 0.2
Elongation at break (%)	685 ± 3	480 ± 2	444 ± 2	405 ± 3
Scratch resistance (kg)	3.0 ± 0.1	4.2 ± 0.1	5.5 ± 0.1	7 ± 0.1
Bending (m)	<0.001	<0.001	<0.001	<0.001
Impact resistance* (m)	0.95 ± 0.05	0.95 ± 0.05	0.95 ± 0.05	0.95 ± 0.05

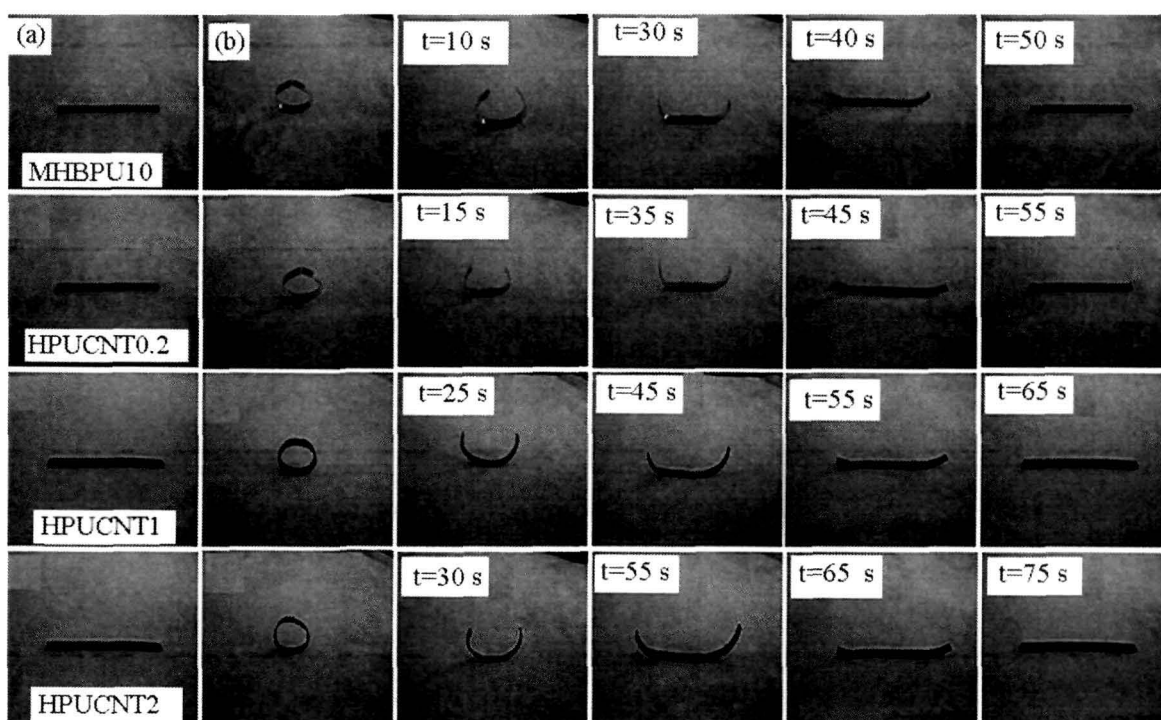
\* 1.0 m is the limit of the instrument

#### 5A.3.7. Shape memory property

The shape memory behaviors of hyperbranched polyurethane and its nanocomposites under microwave irradiation are shown in Fig. 5A.9. All the prepared nanocomposites exhibited good shape fixity and the fixed shape was retained for a very long time at room temperature. The micro-Brownian movements of the molecular chains are frozen at low temperature and the strain energy is stored in the form of internal stress in the fixed shape. The shape recovery was studied under four different microwave powers at 140, 210, 350 and 455 W. The shape recovery effect was not observed when the microwave irradiation output power was 140 W. This can be attributed to the slow reorientation of the dipoles due to the low value of output power. Therefore, induced heat was not sufficient to activate the polymer chains due to the low molecular friction and collisions. The shape recovery increased with the increase of the microwave output power. The shape recovery time decreased with the increase of microwave output power (Table 5A.2). When the microwave irradiated on the sample, the dipole moment moves to align with the external electric field. This dipole movement generates friction inside the dielectric as a result heating effect arises as already discussed in Chapter 4, section 4A.3.7. The polymer chains are activated when the heat is close to the transition temperature ( $T_{trans}$ ) and release the stored strain energy to recover the original shape. When the microwave output power increases, the temperature of the sample also increases due to the high molecular friction and collisions, which causes the high recovery speed. It can be noted that the shape recovery and shape recovery speed strongly dependent on the magnitude of the output microwave power. There are many reports available in the literature that the carbon nanotube has microwave



absorption capacity. However the nanocomposites showed higher recovery time as compared to the pristine polyurethane. This may be due to the increased  $T_{\text{trans}}$  ( $T_m$ ) (supported by the DSC) of the nanocomposites with increase in the loading of TEA-f-MWCNT, which required more heat energy to activate the polymer chains. This is due to the increased compactness as well as toughness of the nanocomposites. The prepared nanocomposites have shown good shape recovery and shape fixity. Thus the nanocomposites may be utilized as shape memory materials in sensors, actuators, self deployable sun sails in spacecraft, automobile, heat shrinkable tube and biomedical devices.



**Fig. 5A.9:** Shape memory behaviors of hyperbranched polyurethane and its nanocomposites at microwave output power 455 W (a) original shape and (b) fixed shape

**Table 5A.2:** Shape memory behaviors of hyperbranched polyurethane and its nanocomposite at different microwave output powers\*

Sample code	Shape recovery <sup>a</sup> (%)	Shape recovery time <sup>a</sup> (s)	Shape recovery <sup>b</sup> (%)	Shape recovery time <sup>b</sup> (s)	Shape recovery <sup>c</sup> (%)	Shape recovery time <sup>c</sup> (s)
MHBPU10	75 ± 1.2	150 ± 2	100	65 ± 2	100	50 ± 2
HPUCNT0.2	71 ± 1.2	170 ± 2	100	72 ± 2	100	55 ± 2
HPUCNT1	65 ± 1.1	185 ± 2	100	85 ± 2	100	65 ± 2
HPUCNT2	60 ± 1.0	194 ± 2	100	90 ± 2	100	75 ± 2

\*Microwave power output (W) <sup>a</sup>210, <sup>b</sup>350 and <sup>c</sup>455

#### 5A.4. Conclusion

The hyperbranched polyurethane/TEA-f-MWCNT nanocomposites were successfully prepared by 'in-situ' pre-polymerization technique. The nanocomposites exhibited good thermal and mechanical properties. The tensile strength and thermal stability was found to be increased with the increase of amount of TEA-f-MWCNT. Microwave was found to be an effective stimulus for the shape recovery of the hyperbranched polyurethane and its nanocomposites. The shape recovery rate as well as shape recovery time can be tuned by using the microwave output powers. All the prepared nanocomposites exhibited good shape fixity. Thus the prepared nanocomposites with tunable dose dependent performance may be utilized as microwave induced shape memory materials in different fields of application.

## **5B. Hyperbranched thermosetting polyurethane/triethanolamine functionalized MWCNT nanocomposites**

### **5B.1. Introduction**

From the above subchapter it has been found that the formation of hyperbranched polyurethane nanocomposites with covalent functionalized MWCNT by triethanolamine, enhanced the performance over the pristine polyurethane. Further, in Chapter 4, it is clearly demonstrated that the thermosetting nanocomposites of such hyperbranched polyurethane exhibited many superior properties including shape memory behavior compared to its thermoplastic counterpart. Thus the proposition for investigating the performance along with shape memory behaviors of such triethanolamine functionalized MWCNT/hyperbranched polyurethane thermosetting nanocomposites is worthy. Again, in Chapter 4, it is also found that glycidyl ether epoxy of bisphenol-A has good compatibility with such hyperbranched polyurethane, so attempt was made to form the thermosetting nanocomposites with this epoxy resin. The importance of glycidyl ether of bisphenol-A based epoxy was already discussed in Chapter 3, section 3.1. Further, the free hydroxyl groups present in the functionalized MWCNT as well as in the hyperbranched polyurethane would react with the oxirane rings of epoxy resin and thereby taking part in crosslinking reactions to form the dimensionally stable thermosets. In addition to that this phenomenon helps in uniform and stable dispersion of MWCNT into the polyurethane matrix and thus considerable and strong interfacial interactions would result, which in turn offer significant improvement in many desired properties including shape memory behaviors. The effect of crosslinking points or net points on the shape memory property of such polymeric materials is already described in subchapter 4B. A number of reports were found in literature on curing of MWCNT nanocomposites. Chapartegui et al. studied the curing behavior of epoxy/MWCNT nanocomposites.<sup>17</sup> Tseng et al. reported the diamine cured maleic anhydride grafted CNT/epoxy nanocomposites.<sup>18</sup>

In the present subchapter, therefore, hyperbranched thermosetting polyurethane/triethanolamine covalent functionalized MWCNT nanocomposites were fabricated to investigate the effect of epoxy resin along with the nanomaterial on the performance including shape memory behaviors of such nanocomposites.

## **5B.2. Experimental**

### **5B.2.1. Materials**

The monoglyceride of *Mesua ferrea* L. seed oil, TDI, PCL, 1,4-butanediol and triethanolamine used for the preparation of hyperbranched polyurethane were same as described in Chapter 2, section 2A.2.1.

The epoxy resin, a glycidyl bisphenol-A based epoxy used was same as described in Chapter 3, section 3.2.1.

MWCNT with diameter and length of about 10–20 nm and 20  $\mu\text{m}$ , respectively, used were same as mentioned in subchapter 5A, section 5A.2.1.

### **5B.2.2. Modification of MWCNT**

The covalent modification of MWCNT with triethanolamine was already described in subchapter 5A, section 5A.2.2.

### **5B.2.3. Preparation of hyperbranched thermosetting polyurethane/TEA-f-MWCNT nanocomposites**

The nanocomposites were prepared by the same way as described in subchapter 5A, section 5A.2.3. This nanocomposite was then homogenized with 10 wt% of the epoxy resin (100% solid content) to obtain the desired thermoset. The polymer solution was cast on the inert substrates followed by vacuum degassing and finally cured at 120 °C for specified time (Table 5B.1). The cured films were coded as EHPUCNT0.2, EHPUCNT1 and EHPUCNT2 corresponding to 0.2, 1 and 2 wt% of TEA-f-MWCNT, respectively. Before curing, one representative nanocomposite was coded as BEHPUCNT1 with 1 wt% TEA-f-MWCNT content.

### **5B.2.4. Instrumentation**

The hyperbranched polyurethane and its nanocomposites were characterized by different techniques such as FTIR, XRD and SEM as described in Chapter 2, section 2A.2.4.

The mechanical properties such as tensile strength, elongation at break, scratch resistance and impact resistance were measured by the same way as described in Chapter 2, section 2A.2.4.

The thermal stability was studied by the same instrument using same procedure as described in the Chapter 2, section 2A.2.4.

The shape memory behaviors of the samples were studied by the same way using microwave energy as described in Chapter 4, section 4A.2.4.

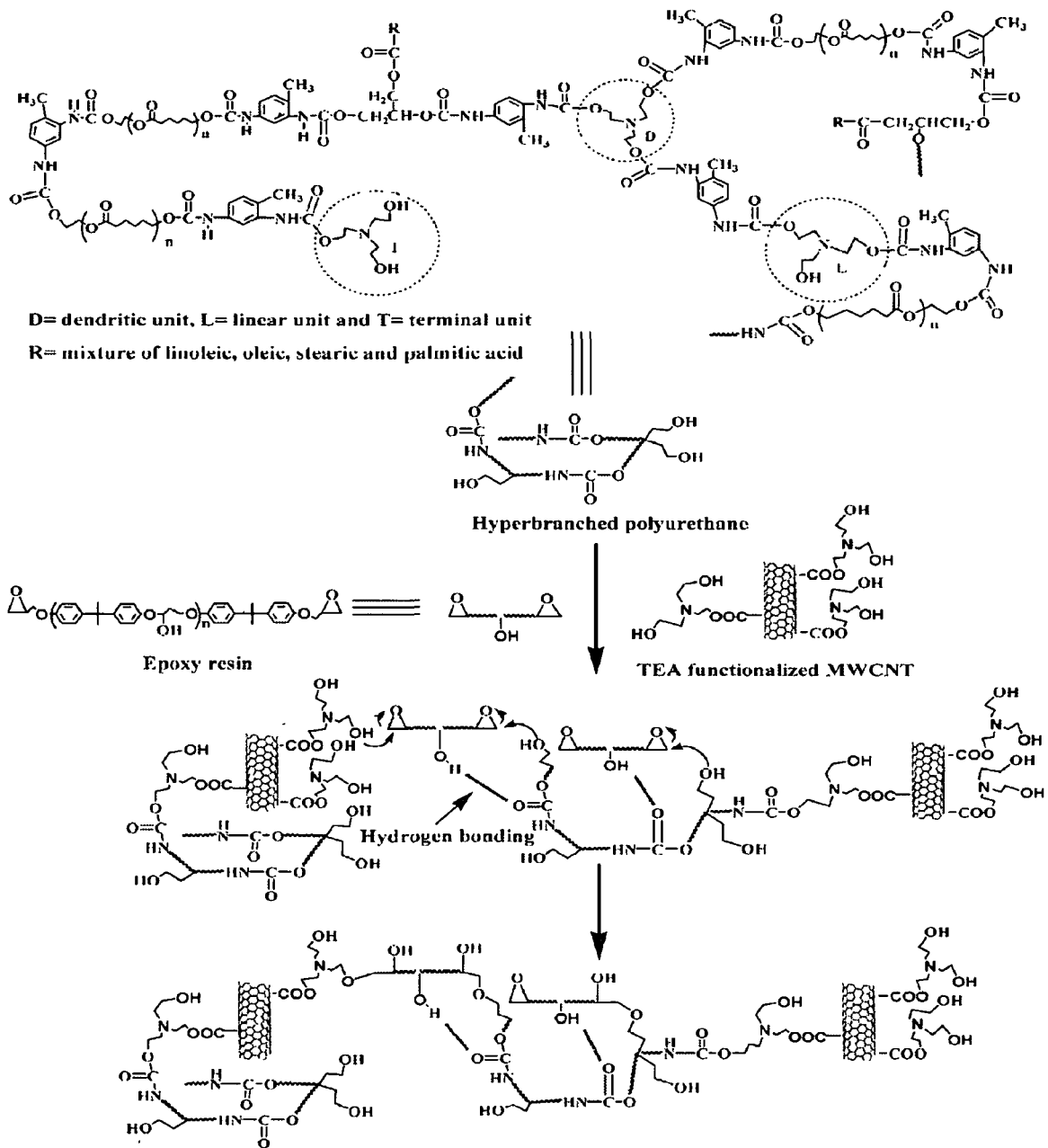
### **5B.3. Results and discussion**

#### **5B.3.1. Curing study**

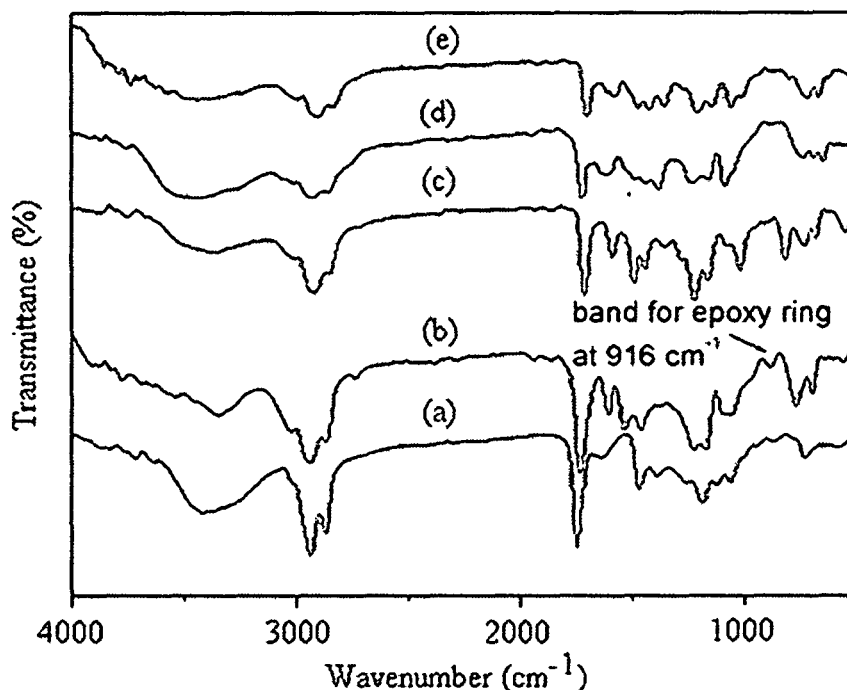
From the curing study it was found that the touch free time and the drying time decreased with the increase of the loading of TEA-f-MWCNT in the nanocomposites as cured at 120 °C (Table 5B.1). This is attributed to the increased degree of cross-linking reaction among the free –OH of TEA-f-MWCNT, epoxy/hydroxyl groups of the epoxy resin and free -OH groups of the hyperbranched polyurethane without using any additional external hardener (Scheme 5B.1). This is due to the fact that the number of free –OH and triethanolamine moiety increases with the increase of loading of TEA-f-MWCNT in the system. These intercross-linking network formations resulted three dimensional network structures. The absence of the epoxy band at 916  $\text{cm}^{-1}$  after curing in FTIR spectra confirmed the formation of the network structure. The increased cross-linking density of the nanocomposites was also confirmed by the swelling test in DMF (Table 5B.2).

#### **5B.3.2. FTIR study**

The FTIR spectra of pristine MWCNT, a-MWCNT and TEA-f-MWCNT are already given in subchapter 5A, section 5A.3.1. FTIR spectra of hyperbranched polyurethane and its thermosetting nanocomposites are shown in Fig. 5B.1. The band at 3406-3432  $\text{cm}^{-1}$  (N–H stretching) of nanocomposites was found to broaden as compared to the pristine polyurethane. Further, after the formation of nanocomposite the band of –C=O at 1728  $\text{cm}^{-1}$  was shifted to lower wavenumber, 1719-1715  $\text{cm}^{-1}$ . All the above observations confirmed the interactions of TEA-f-MWCNT with the polyurethane chains in the prepared thermosetting nanocomposites.



**Scheme 5B.1:** Proposed crosslinking reactions



**Fig. 5B.1:** FTIR spectra for (a) MHBPU10, (b) BEHPUCNT1, (c) EHPUCNT0.2, (d) EHPUCNT1 and (e) EHPUCNT2

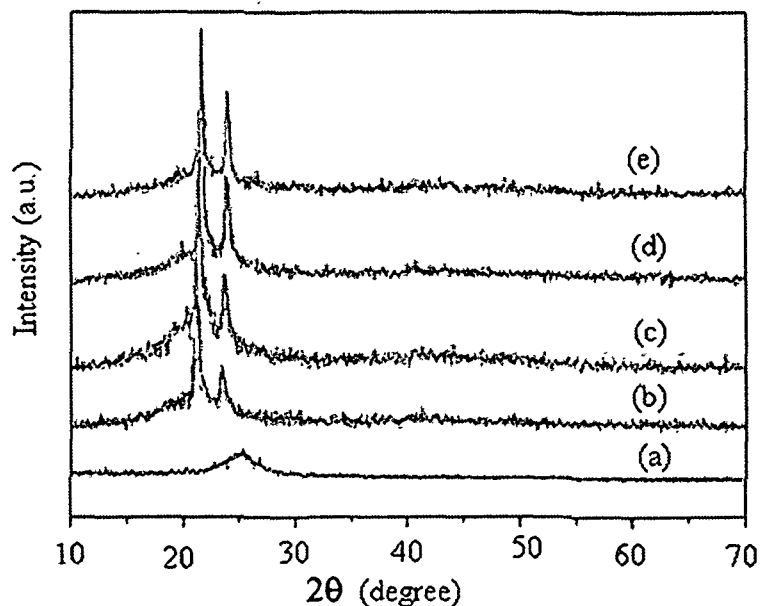
**Table 5B.1:** Composition and curing time of the nanocomposites at 120 °C

Code	MHBPU10 (wt%)	Epoxy (wt%)	Touch free time (min)	Drying time (min)
MHBPU10	100	-	-	-
EHPUCNT0.2	100	10	45	54
EHPUCNT1	100	10	34	47
EHPUCNT2	100	10	30	42

### 5B.3.3. XRD study

The XRD patterns of TEA-f-MWCNT, hyperbranched polyurethane and the thermosetting nanocomposites are shown in Fig. 5B.2. The peak at  $2\theta=25.4^\circ$  is due to the (002) plane of carbon atoms of MWCNT.<sup>11</sup> The two strong diffraction peaks at  $2\theta=21.9^\circ$  and  $2\theta=23.8^\circ$  were observed because of the (100) and (200) planes of PCL crystals present in the

hyperbranched polyurethane. The peak intensity was found to be increased after the nanocomposite formation. This may be due to the nucleating effect of the TEA-f-MWCNT.

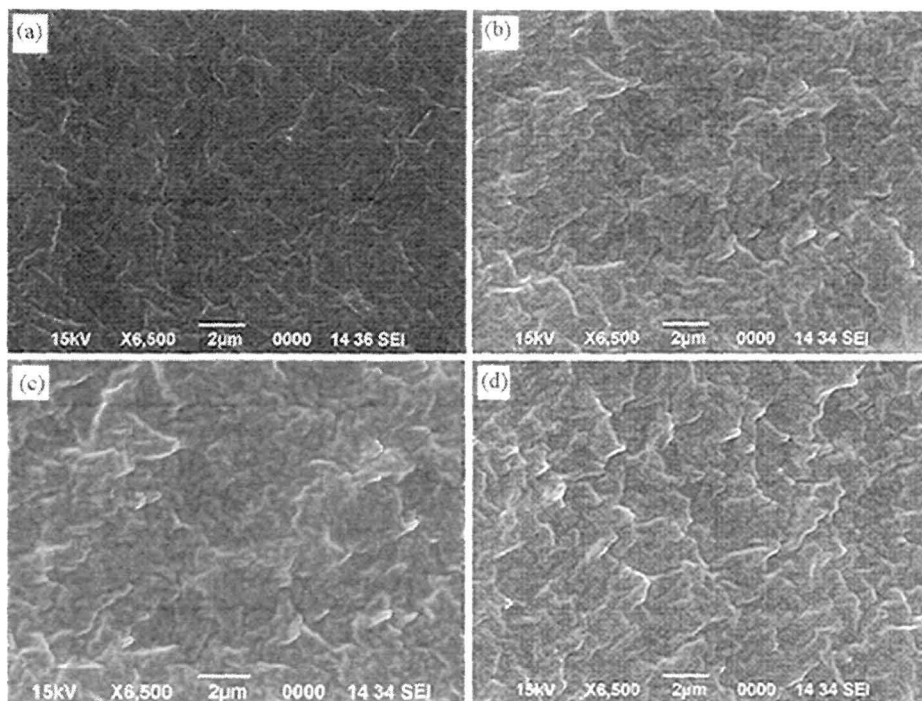


**Fig. 5B.2:** XRD diffractograms for (a) TEA-f-MWCNT, (b) MHBPU10, (c) EHPUCNT0.2, (d) EHPUCNT1 and (e) EHPUCNT2

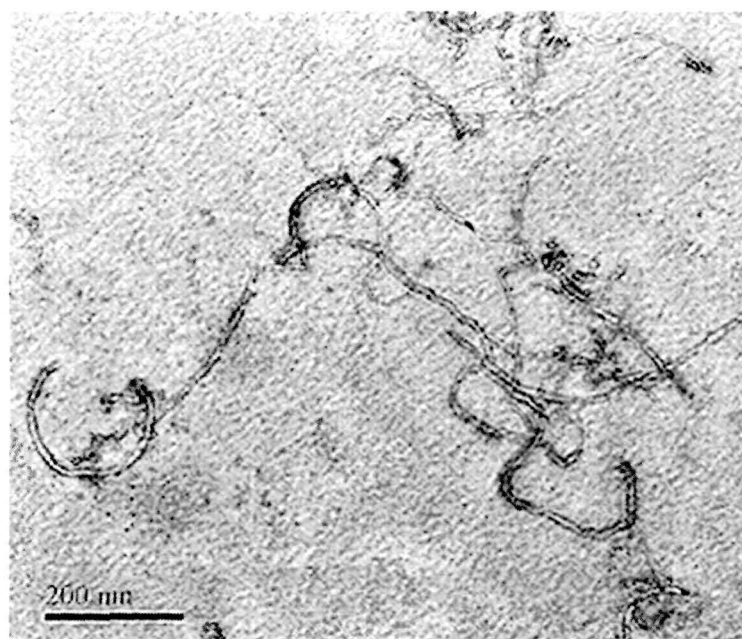
#### 5B.3.4. Morphology study

The morphology of the fractured surface of nanocomposites was observed by SEM (Fig. 5B.3). The TEA-f-MWCNT appeared as bright lines in the micrographs of nanocomposites. Furthermore functionalized MWCNT were broken rather than being pulled out on tensile fracture. This depicts a strong interfacial adhesion between the nanomaterial and the polyurethane matrix. TEM was used to observe the dispersion of TEA-f-MWCNT in the nanocomposite (Fig. 5B.4). From the micrograph it was observed that nanotubes were homogeneously distributed in the polymer matrix with an average diameter of 12 nm.





**Fig. 5B.3:** SEM micrographs for (a) MHBPU10, (b) EHPUCNT0.2, (c) EHPUCNT1 and (d) EHPUCNT2



**Fig. 5B.4:** TEM image of EHPUCNT1

### 5B.3.5. Thermal property

The TGA thermograms of pristine MWCNT, a-MWCNT and TEA-f-MWCNT are shown in Fig. 5B.5. The pristine MWCNT did not show weight loss below 550 °C. However, the a-MWCNT gradually lost their weight with the increase of temperature due to the decomposition of –COOH groups from the surface of the MWCNT. The TGA thermogram of TEA-f-MWCNT showed an initial weight loss from 190 to 250 °C. This can be attributed to the decomposition of triethanolamine present on the surface of MWCNT. The thermal stability of the polymer nanocomposite plays a vital role in determining their processing and service life. The TGA thermograms of the hyperbranched polyurethane and the thermosetting nanocomposites are shown in Fig. 5B.6. The thermal stability increased with the increase of content of TEA-f-MWCNT in the thermosetting nanocomposites. This is due to the increased compactness and rigidity of the nanocomposites as cross-linking density increases with the same and supported by the swelling results (Table 5B.2). This is also attributed to the homogeneous distribution of the TEA-f-MWCNT as well as increased of various interactions such as polar-polar interaction, H-bonding, van der Waals forces etc. All these cause molecular restriction of the polymer chains in the nanocomposites and thus the volatile products formed during the decomposition have to follow a longer diffusion path to escape from the matrix.

The DSC curves of hyperbranched polyurethane and its thermosetting nanocomposites are shown in Fig. 5B.7. The melting temperature ( $T_m$ ) was found to be increased (40 to 45 °C) with the increase of TEA-f-MWCNT content in the nanocomposites. This is attributed to the increased compactness of the structure due to the various interactions as stated in the earlier chapter.

### 5B.3.6. Mechanical property

The mechanical properties of the hyperbranched polyurethane and the thermosetting nanocomposites are shown in Table 5B.2. The tensile strength increases, whereas the elongation at break decreases with the increase of loading of TEA-f-MWCNT in the nanocomposites. This enhancement could be attributed to the well distribution of TEA-f-MWCNT that results efficient interfacial interactions between TEA-f-MWCNT and the polymer matrix. The presence of different physical interactions such as polar-polar, H-bonding etc. of free –OH of

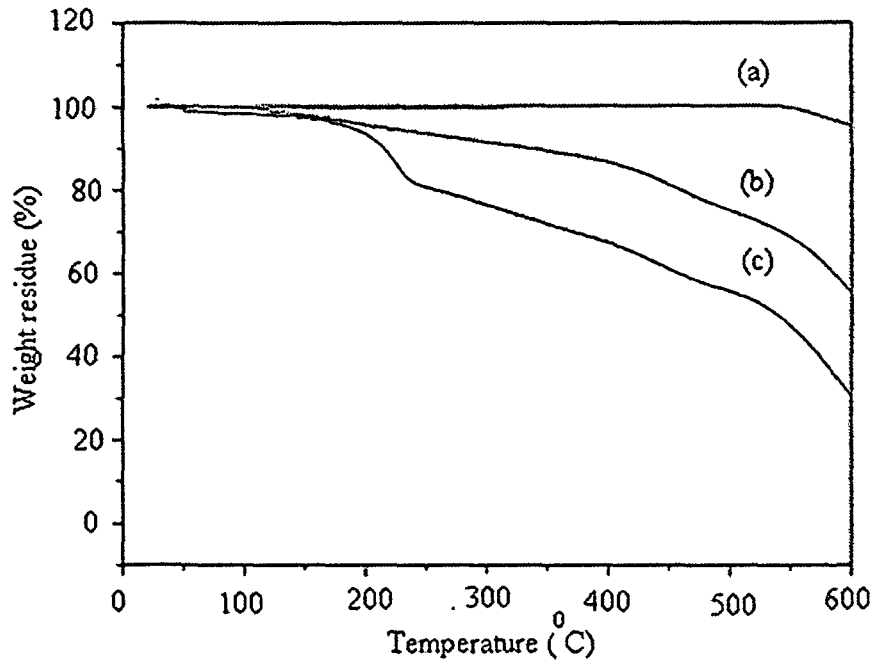


Fig. 5B.5: TGA thermographs for (a) MWCNT, (b) a-MWCNT and (c) TEA-f-MWCNT

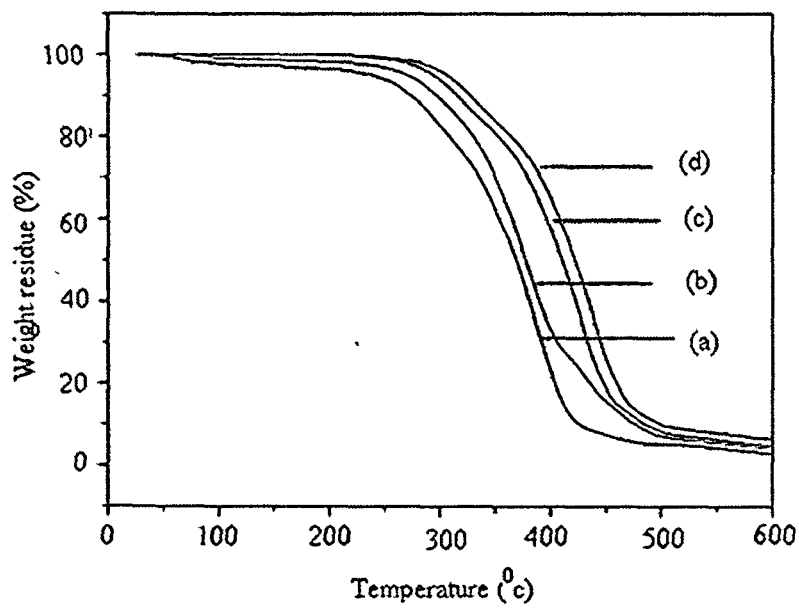
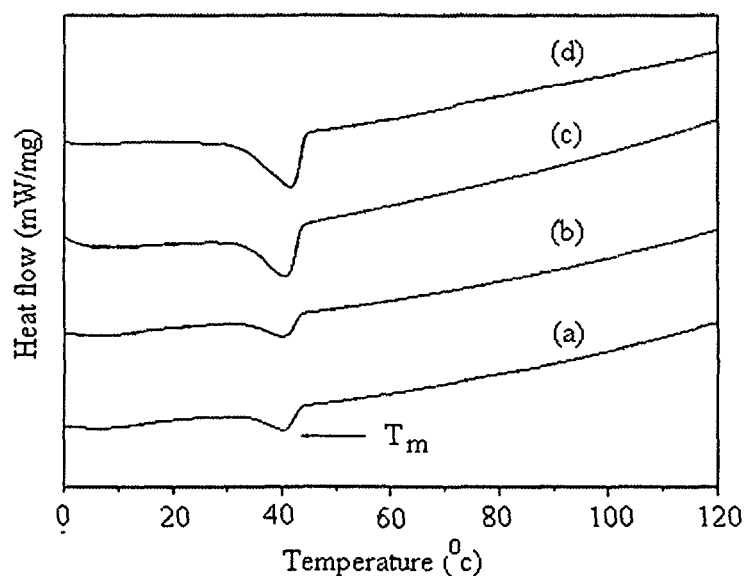


Fig. 5B.6: TGA thermographs for (a) MHBPU10, (b) EHPUCNT0.2, (c) EHPUCNT1 and (d) EHPUCNT2



**Fig. 5B.7:** DSC curves for (a) MHBPU10, (b) EHPUCNT0.2, (c) EHPUCNT1 and (d) EHPUCNT2

TEA-f-MWCNT with the urethane linkages of the hyperbranched polyurethane as well as increased cross-linking density as supported by swelling values (Table 5B.2) resulted enhancement of tensile strength. The scratch hardness which is the resistance of materials to the dynamic surface deformation increases with the increase of content of TEA-f-MWCNT. The significant improvement of the scratch hardness is due to the increased compactness and rigidity of the nanocomposites. All the prepared nanocomposites exhibited good impact resistance. The gloss of the nanocomposites increases with the increase of the loading of TEA-f-MWCNT in the nanocomposites. This is attributed to the compatibility among epoxy resin, TEA-f-MWCNT and hyperbranched polyurethane and increased dimension stability of the nanocomposites.

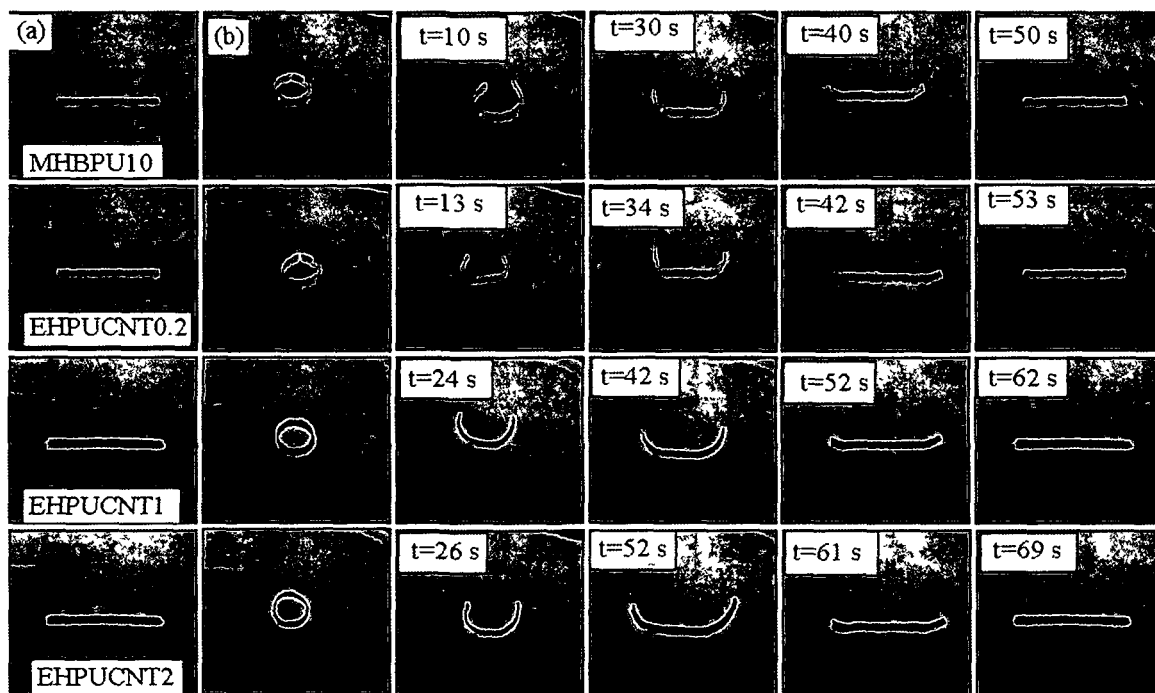
**Table 5B.2:** Mechanical properties of hyperbranched polyurethane and the nanocomposites

Properties	MHBPU10	EHPUCNT0.2	EHPUCNT1	EHPUCNT2
Tensile strength (MPa)	6.5 ± 0.4	16.5 ± 0.3	25 ± 0.3	34.5 ± 0.2
Elongation at break (%)	614 ± 3	389 ± 2	333 ± 2	305 ± 2
Scratch hardness (kg)	3.0 ± 0.1	5 ± 0.1	6.5 ± 0.1	8.5 ± 0.1
Bending (m)	<0.001	<0.001	<0.001	<0.001
Impact resistance* (m)	0.95 ± 0.05	0.95 ± 0.05	0.95 ± 0.05	0.95 ± 0.05
Swelling (%)	-	27 ± 1.2	20 ± 1.2	15 ± 1.1

\* 1.0 m is the limit of the instrument

### 5B.3.7. Shape memory property

The shape memory behaviors of the hyperbranched polyurethane and its thermosetting nanocomposites are shown in Fig. 5B.8. The thermal motion of the molecular chains was activated during heating the samples at 60 °C for 5 min and facilitated to form ring shape. However, the molecular chains are frozen on cooling at low temperature (0-5 °C) and help to fix the shape. The hyperbranched polyurethane and the nanocomposites exhibited excellent shape fixity. Further the fixed shape was retained for long time at room temperature. The micro-Brownian movements of the molecular chains are frozen at low temperature and thereby prevent its reorientation of molecular chains, showing the perfect shape fixity.<sup>19, 20</sup> The shape recovery test was studied under the microwave irradiation at 455 W. The hyperbranched polyurethane and the nanocomposites showed almost full shape recovery. No significant change of shape recovery of the nanocomposites was obtained over the ten cycles of test. The shape recovery time found to increase with the increase of loading of TEA-f-MWCNT in the thermosetting nanocomposites. This can be attributed to the increased transition temperature (supported by DSC) due to the increased physico-chemical interactions among the polymer chains, epoxy resin and TEA-f-MWCNT in the thermosetting nanocomposites.



**Fig. 5B.8:** Shape memory behaviors of hyperbranched polyurethane and its nanocomposites at microwave output power 455 W (a) original shape and (b) fixed shape

#### 5B.4. Conclusion

The hyperbranched polyurethane/TEA-f-MWCNT thermosetting nanocomposites were prepared successfully by an '*in situ*' polymerization technique. MWCNT were functionalized by TEA using a covalent approach. The mechanical and thermal properties of the thermosetting nanocomposites were significantly enhanced with the increase of content of TEA-f-MWCNT. The thermosetting nanocomposites exhibited the enhanced mechanical and thermal properties as compared to the thermoplastic one. All the prepared nanocomposites exhibited excellent shape fixity and shape recovery. The shape recovery time found to be lowered in the thermosetting nanocomposites as compared to the thermoplastic one. Thus the prepared nanocomposites could be utilized as advanced SMP in different suitable applications.

## References

1. Iijima, S. Helical microtubules of graphitic carbon, *Nature* **354**, 56–58, 1991.
2. Esawi, A.M.K., & Farag, M.M. Carbon nanotube reinforced composites: potential and current challenges, *Mater. Des.* **28** (9), 2394-2401, 2007.
3. Sahoo, N.G., et al. Polymer nanocomposites based on functionalized carbon nanotubes, *Prog. Polym. Sci.* **35** (7), 837-867, 2010.
4. Xia, H., & Song, M. Preparation and characterization of polyurethane-carbon nanotube composites, *Soft Matter* **1**(5), 386-394, 2005.
5. Montazeri, A., et al. The effect of functionalization on the viscoelastic behavior of multi-wall carbon nanotube/epoxy composites, *Mater. Des.* **45**, 510-517, 2013.
6. Wang, M., et al. Enhancement of the mechanical properties of poly(styrene-co-acrylonitrile) with poly(methyl methacrylate)-grafted multiwalled carbon nanotubes, *Polymer* **46** (25), 11510-11516, 2005.
7. Petrov, P.D., et al. Dispersion of multi-walled carbon nanotubes with pyrene-functionalized polymeric micelles in aqueous media, *Polymer* **53** (24), 5502-5506, 2012.
8. Wang, X., et al. Superamphiphobic coatings with coralline-like structure enabled by one-step spray of polyurethane/carbon nanotube composites, *J. Mater. Chem.* **22** (19), 9624-9631, 2012.
9. Wang, M., et al. Preparation and properties of polysiloxane grafting multi-walled carbon nanotubes/polycarbonate nanocomposites, *Polym. Adv. Technol.* **22** (12), 1738-1746, 2011.
10. Yoon, J.T., et al. Effects of grafted chain length on mechanical and electrical properties of nanocomposites containing polylactide-grafted carbon nanotubes, *Compos. Sci. Technol.* **70** (5), 776-782, 2010.
11. Zhang, Y., et al. Thermally conductive, insulated polyimide nanocomposites by AlO(OH)-coated MWCNTs, *J. Mater. Chem.* **21** (38), 14563-14568, 2011.
12. Chattopadhyay, D.K., & Webster, D.C. Thermal stability and flame retardancy of polyurethanes, *Prog. Polym. Sci.* **34** (10), 1068-1133, 2009.
13. Kim, J.Y., et al. Multiwall-carbon-nanotube-reinforced poly(ethylene terephthalate) nanocomposites by melt compounding, *J. Appl. Polym. Sci.* **103** (3), 1450-1457, 2007.
14. Moniruzzaman, M., & Winey, K.I. Polymer nanocomposites containing carbon nanotubes, *Macromolecules* **39** (16), 5194-5205, 2006.

15. Pandey, G., & Thostenson, E.T. Carbon nanotube-based multifunctional polymer nanocomposites, *Polym. Rev.* **52** (3), 355-416, 2012.
16. Ayatollahi, M.R., et al. Effect of multi-walled carbon nanotube aspect ratio on mechanical and electrical properties of epoxy-based nanocomposites, *Polym. Test.* **30** (5), 548-556, 2011.
17. Chapartegui, M., et al. Curing of epoxy/carbon nanotubes physical networks, *Polym. Eng. Sci.* **52** (3), 663-670, 2012.
18. Tseng, C.H., et al. Functionalizing carbon nanotubes by plasma modification for the preparation of covalent-integrated epoxy composites, *Chem. Mater.* **19** (2), 308-315, 2007.
19. Tobushi, H., et al. The influence of shape-holding conditions on shape recovery of polyurethane-shape memory polymer foams, *Smart. Mater. Struct.* **13** (4), 881-887, 2004.
20. Du, H., & Zhang, J. Shape memory polymer based on chemically cross-linked poly(vinyl alcohol) containing a small number of water molecules, *Colloid. Polym. Sci.* **288** (1), 15-24, 2010.



**Chapter 6**

**Fe<sub>3</sub>O<sub>4</sub> nanoparticles decorated  
MWCNT/hyperbranched polyurethane  
nanocomposites**

***Highlights***

This chapter consists of two subchapters, one is on thermoplastic and other is on thermosetting hyperbranched polyurethane/Fe<sub>3</sub>O<sub>4</sub> nanoparticle decorated MWCNT nanocomposites. The MWCNT were decorated with Fe<sub>3</sub>O<sub>4</sub> by a wet chemical technique. The decoration of Fe<sub>3</sub>O<sub>4</sub> on the surface of MWCNT was confirmed by the FTIR, XRD and TEM studies. The formation of nanocomposites was characterized by the FTIR, XRD, SEM and TEM studies. The mechanical and thermal properties were evaluated for the prepared thermoplastic nanocomposites. The shape memory behaviors were studied by the microwave irradiation. The second subchapter describes the preparation of hyperbranched polyurethane/Fe<sub>3</sub>O<sub>4</sub> nanoparticle decorated MWCNT thermosetting nanocomposites using glycidyl ether epoxy of bisphenol-A. The shape recovery time found to decrease in both the nanocomposites with the increase of the content of nanoparticles. The thermosetting nanocomposite exhibited better performance compared to the thermoplastic one.

---

*Parts of this work are published in*

1. Kalita, H., & Karak, N., *J. Nano. Eng. Manufac.* **3** (3), 194-201, 2013.
2. Kalita, H., & Karak, N., *J. Mater. Res.* **28** (16), 2132-2141, 2013.

## **6A. Fe<sub>3</sub>O<sub>4</sub> nanoparticles decorated MWCNT/hyperbranched polyurethane thermoplastic nanocomposites**

### **6A.1. Introduction**

The importance of hyperbranched polyurethane as well as nanocomposites with the MWCNT is already described in Chapter 5. The carbon nanotubes (CNT) with their various exceptional attributes such as outstanding mechanical, electrical and thermal properties resulted their wide applications in various fields, which encourage the scientists and the technologists to use them as nanomaterials for designing of composite to obtain high performance materials.<sup>1-5</sup> However the stable dispersion of CNT is very difficult due to the strong van der Waals forces and numerous  $\pi$ - $\pi$  interactions between the tubes as already discussed in Chapter 5. The modification of CNT is therefore, essential for their well dispersion in the polymer matrix. The decoration of other suitable nanomaterials on the surface of CNT may add new features into them. The advantages of Fe<sub>3</sub>O<sub>4</sub> nanoparticles were already described in Chapter 4, section 4A.1. In the recent year, extensive studies have been made to decorate CNT with magnetic nanomaterials due to their potential applications in magnetic recording media, electrical devices, color imaging, heterogeneous catalysis, magnetic force microscopy as nanoprobes, microwave absorption materials, smart materials, etc.<sup>6-8</sup> Zhang et al. reported the improved electrical conductivity of MWCNT/Fe<sub>3</sub>O<sub>4</sub> nanocomposite as compared to the pristine MWCNT.<sup>9</sup> The enhanced microwave absorption of nanocomposites of CNT and magnetic nanoparticles as compared with that of both pure CNT and magnetic nanoparticles was also observed by Che et al.<sup>10</sup> In this study, MWCNT were decorated with the Fe<sub>3</sub>O<sub>4</sub> nanoparticles to achieve synergistic effect of reinforcement as well as microwave absorption.

In the present investigation, therefore, Fe<sub>3</sub>O<sub>4</sub> nanoparticles decorated MWCNT (Fe<sub>3</sub>O<sub>4</sub>-MWCNT)/hyperbranched polyurethane nanocomposites were prepared to investigate the performance including shape memory behaviors.

### **6A.2. Experimental**

#### **6A.2.1. Materials**

The monoglyceride of the *Mesua ferrea* L. seed oil, toluene diisocyanate, poly( $\epsilon$ -caprolactone) diol, 1,4-butanediol and triethanolamine used for the preparation of hyperbranched polyurethane were same as described in Chapter 2, section 2A.2.1.

Iron (III) chloride hexahydrate and iron (II) chloride tetrahydrate purchased from Merck, India and Germany, respectively were same as described in Chapter 4, section 4A.2.1.

MWCNT purchased from Iiljin Nanotech, South Korea were same as mentioned in Chapter 5, section 5A.2.1.

#### 6A.2.2. Preparation of Fe<sub>3</sub>O<sub>4</sub> decorated MWCNT (Fe<sub>3</sub>O<sub>4</sub>-MWCNT)

At first, pristine MWCNT were treated with the mixture of concentrated H<sub>2</sub>SO<sub>4</sub> and HNO<sub>3</sub> (3:1 v/v) at 80 °C under constant stirring for 2 h. Then they were washed with distilled water, filtered until the pH value was reached to 7, followed by drying in a vacuum oven at 60 °C for 24 h. 0.04 g of acid treated MWCNT (a-MWCNT) were ultrasonically dispersed in 50 mL of distilled water for 30 min. Then, 0.1 g of FeCl<sub>3</sub>.6H<sub>2</sub>O and 0.06 g of FeCl<sub>2</sub>.4H<sub>2</sub>O were added to the above dispersed solution and stirred continuously under the N<sub>2</sub> atmosphere for 1 h. An aqueous ammonia solution (30%) was then added drop wise into the mixture until the pH was reached to 11-12. Then, the solution was heated at 80 °C for 1.5 h. The black products were separated by magnetic decantation and washed with distilled water until the pH was reached to 7. Finally, the washed Fe<sub>3</sub>O<sub>4</sub>-MWCNT was dried at 60 °C for 24 h under vacuum.

#### 6A.2.3. Preparation of Fe<sub>3</sub>O<sub>4</sub>-MWCNT/ hyperbranched polyurethane nanocomposites

The hyperbranched polyurethane was prepared by the same procedure as described in Chapter 2, section 2A.2.3. The monoglyceride of *Mesua ferrea* L. seed oil, PCL and TDI based pre-polymer was reacted with 1, 4-butanediol and TEA to obtain the desired hyperbranched polyurethane. For the preparation of nanocomposite, required amount of Fe<sub>3</sub>O<sub>4</sub>-MWCNT was dispersed in DMF by ultra-sonication for 15 min. Then the dispersed solution was injected into the polymerization reaction mixture before 1 h of completion and the reaction was continued. After completion of reaction, the solution was cast on the inert substrates followed by vacuum degassing and dried for 24 h at 60 °C for different testing. The nanocomposites were coded as

MHBPU10, HPUFCNT0.2, HPUFCNT1 and HPUFCNT2 corresponding to Fe<sub>3</sub>O<sub>4</sub>-MWCNT content of 0, 0.2, 1 and 2 wt%, respectively.

#### 6A.2.4. Instrumentation

The hyperbranched polyurethane and its nanocomposites were studied by different characterization techniques such as FTIR, XRD and SEM, and TEM as described in Chapter 2, section 2A.2.4 and in Chapter 4, section 4A.2.4, respectively.

The mechanical properties such as tensile strength, elongation at break, scratch resistance and impact resistance were measured by the same way as described in Chapter 2, section 2A.2.4. The thermal stability was studied by the same way as described in Chapter 2, section 2A.2.4.

The Raman spectra of MWCNT, a-MWCNT and Fe<sub>3</sub>O<sub>4</sub>-MWCNT were recorded by the same instrument as described in Chapter 5, section 5A.2.4.

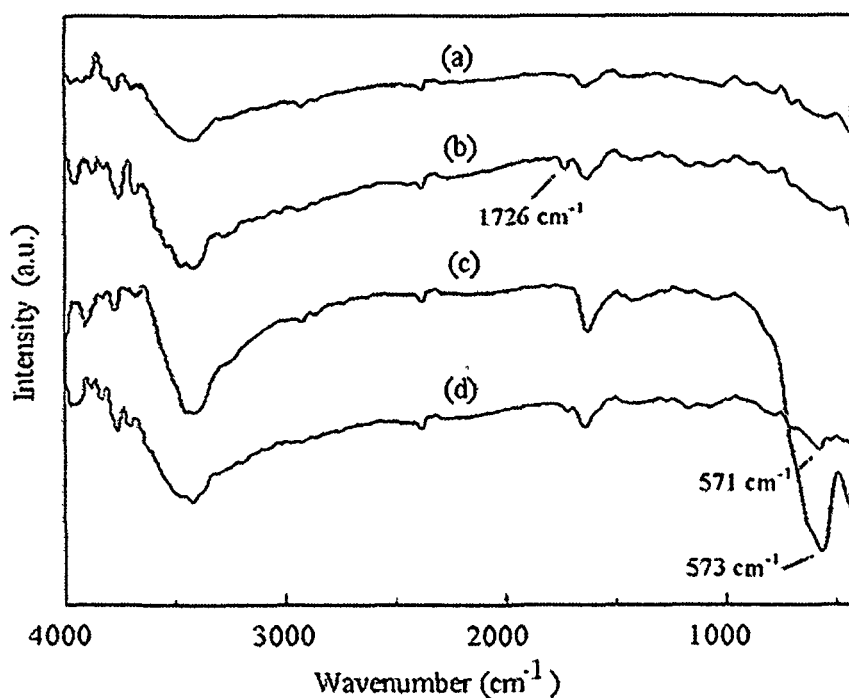
The shape memory behaviors of the nanocomposites were studied by the same way using the same instrument as described in Chapter 4, section 4A.2.4.

### 6A.3. Results and discussion

#### 6A.3.1. FTIR study

The FTIR spectra of pristine MWCNT, a-MWCNT, Fe<sub>3</sub>O<sub>4</sub> and Fe<sub>3</sub>O<sub>4</sub>-MWCNT are shown in Fig. 6A.1. The FTIR spectrum of a-MWCNT showed the absorption band at frequency 1726 cm<sup>-1</sup> (-C=O). However, there was an absence of such absorption band in this region for the pristine MWCNT. The characteristic absorption band at 573 cm<sup>-1</sup> in the spectrum of Fe<sub>3</sub>O<sub>4</sub> corresponds to Fe-O bending vibration of Fe<sub>3</sub>O<sub>4</sub>. The band at 3429 cm<sup>-1</sup> is assigned to the stretching vibration of FeO-H group of Fe<sub>3</sub>O<sub>4</sub> nanoparticles. The spectrum of Fe<sub>3</sub>O<sub>4</sub>-MWCNT showed the absorption band at 3426 cm<sup>-1</sup> and at 571 cm<sup>-1</sup> for the stretching vibration of FeO-H and bending vibration of the Fe-O bond, respectively.<sup>11</sup> The FTIR spectra of hyperbranched polyurethane and the nanocomposites are shown in Fig. 6A.2. The characteristic bands of urethane group of pristine polymer appeared at 3406-3430 cm<sup>-1</sup> (N-H stretching) and 1728 cm<sup>-1</sup> (-C=O stretching of urethane linkage) as already discussed in the earlier chapter. The band at 3406-3430 cm<sup>-1</sup> (N-H stretching) of nanocomposites was found to be broadened after the nanocomposite formation as compared to the pristine hyperbranched polyurethane. Further, the

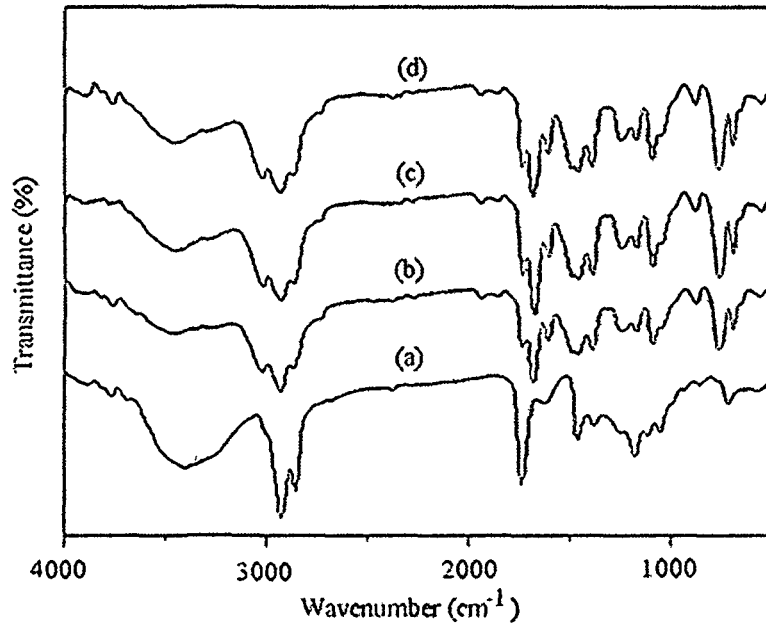
band of  $\text{-C=O}$  at  $1728\text{ cm}^{-1}$  was shifted to  $1721\text{-}1716\text{ cm}^{-1}$  after the nanocomposite formation. All the above results confirmed the presence of strong interactions of  $\text{Fe}_3\text{O}_4\text{-MWCNT}$  with the polyurethane chains in the prepared nanocomposites.



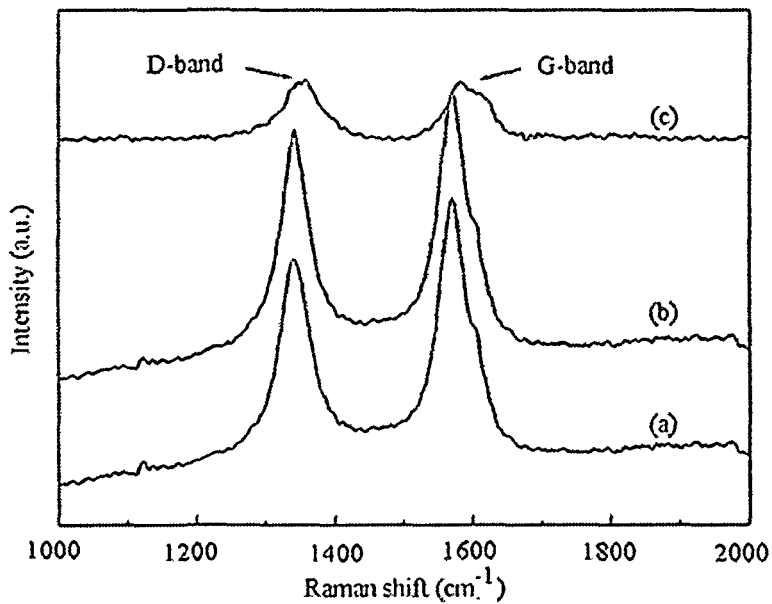
**Fig. 6A.1:** FTIR spectra for (a) pristine MWCNT, (b) a-MWCNT, (c)  $\text{Fe}_3\text{O}_4$  and (d)  $\text{Fe}_3\text{O}_4\text{-MWCNT}$

### 6A.3.2. Raman spectroscopic study

The Raman spectra of pristine MWCNT, a-MWCNT and  $\text{Fe}_3\text{O}_4\text{-MWCNT}$  are shown in Fig. 6A.3. The Raman spectrum of a-MWCNT showed the D and G bands at  $1341\text{ cm}^{-1}$  and  $1571\text{ cm}^{-1}$ , respectively, while the  $\text{Fe}_3\text{O}_4\text{-MWCNT}$  showed the D and G bands at  $1352\text{ cm}^{-1}$  and  $1583\text{ cm}^{-1}$ , respectively. The D band corresponds to the defect of the MWCNT, while the G band corresponds to the tangential mode of vibrations. The intensity ratio between the D band and the G band ( $I_D/I_G$ ) implies the degree of defect of MWCNT. The values of intensity ratio were found to be 0.82, 0.91 and 1.02 for the pristine MWCNT, a-MWCNT and  $\text{Fe}_3\text{O}_4\text{-MWCNT}$ , respectively. The increase in the value of intensity ratio indicated more defects are generated on the surface of MWCNT due to the functionalization.



**Fig. 6A.2:** FTIR spectra for (a) MHBPU10, (b) HPUFCNT0.2, (c) HPUFCNT1 and (d) HPUFCNT2



**Fig. 6A.3:** Raman spectra for (a) pristine MWCNT, (b) a-MWCNT and (c) Fe<sub>3</sub>O<sub>4</sub>-MWCNT

### 6A.3.3. X-ray diffraction study

The XRD patterns of a-MWCNT, Fe<sub>3</sub>O<sub>4</sub> and Fe<sub>3</sub>O<sub>4</sub>-MWCNT are shown in Fig. 6A.4. The XRD pattern of a-MWCNT exhibited a single peak at  $2\theta=25.40^\circ$  corresponds to the (002) plane of carbon atoms of MWCNT.<sup>9</sup> The XRD diffractogram of Fe<sub>3</sub>O<sub>4</sub> showed the peaks at  $2\theta=30.34^\circ$ ,  $35.41^\circ$ ,  $56.72^\circ$  and  $62.73^\circ$ , which correspond to (220), (311), (511) and (440) planes of Fe<sub>3</sub>O<sub>4</sub>, respectively.<sup>12</sup> The XRD pattern of Fe<sub>3</sub>O<sub>4</sub>-MWCNT exhibited peaks of Fe<sub>3</sub>O<sub>4</sub> along with the peak at  $25.40^\circ$  for MWCNT. From the results it is confirmed that Fe<sub>3</sub>O<sub>4</sub> nanoparticles are decorated on the surface of MWCNT. The XRD diffractograms of hyperbranched polyurethane and the nanocomposites are shown in Fig. 6A.5. Two strong diffraction peaks at  $2\theta=21.90^\circ$  and  $2\theta=23.80^\circ$  are due to the (100) and (200) planes of PCL crystals of the hyperbranched polyurethane. The peaks intensity was found to increase after the formation of nanocomposite. This can be attributed that Fe<sub>3</sub>O<sub>4</sub>-MWCNT act as nucleating site to increase the crystallinity of the hyperbranched polyurethane.

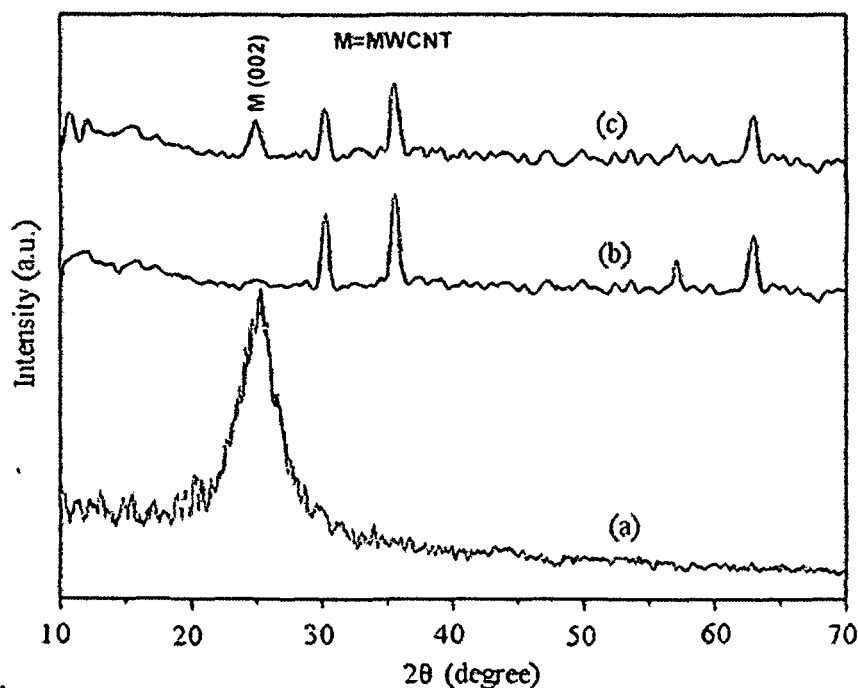
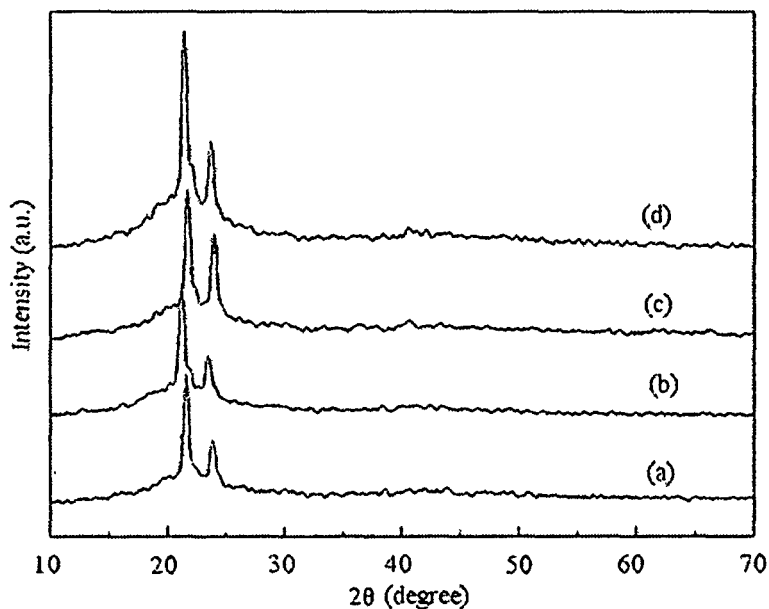


Fig. 6A.4: XRD diffractograms for (a) a-MWCNT, (b) Fe<sub>3</sub>O<sub>4</sub> and (c) Fe<sub>3</sub>O<sub>4</sub>-MWCNT

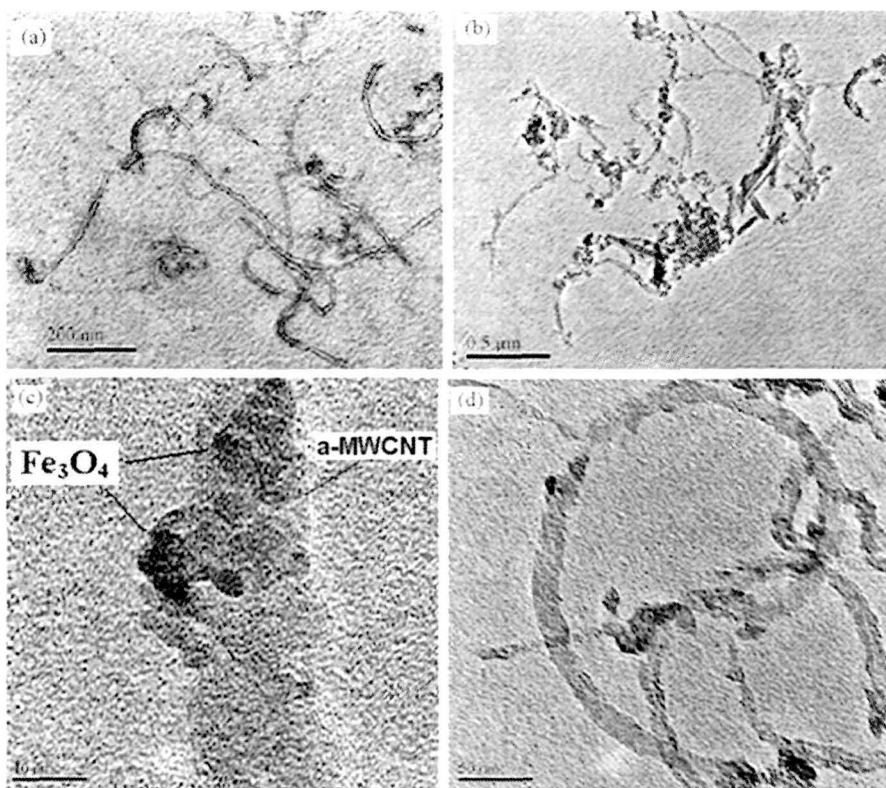


**Fig. 6A.5:** XRD diffractograms for (a) MHBPU10, (b) HPUFCNT0.2, (c) HPUFCNT1 and (d) HPUFCNT2

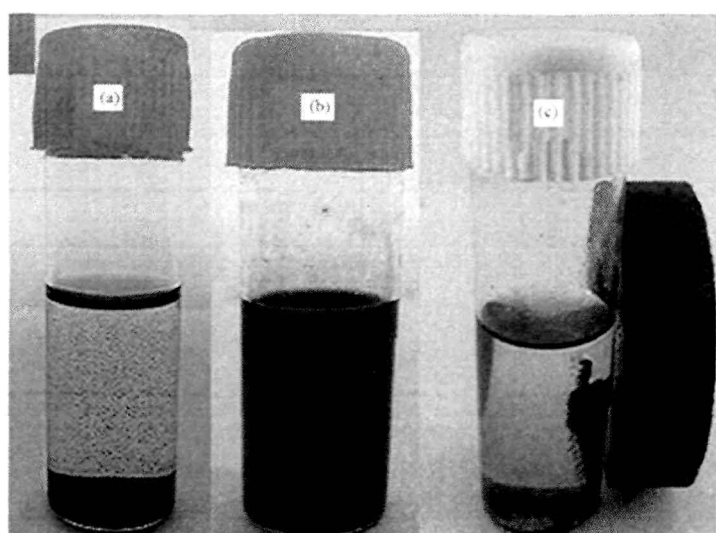
#### 6A.3.4. Morphology study

The morphologies of the a-MWCNT, Fe<sub>3</sub>O<sub>4</sub>-MWCNT and the nanocomposite (HPUFCNT1) are shown in Fig. 6A.6. The TEM image of a-MWCNT showed the smooth surface, whereas Fe<sub>3</sub>O<sub>4</sub>-MWCNT showed the rough surface. From the TEM micrograph it is observed that Fe<sub>3</sub>O<sub>4</sub> nanoparticles are decorated on the surface of the MWCNT. The TEM image of the nanocomposite (HPUFCNT1) showed the homogeneous distribution of Fe<sub>3</sub>O<sub>4</sub>-MWCNT in the polymer matrix (Fig.6A.6 (d)). This is attributed to the good interaction of Fe<sub>3</sub>O<sub>4</sub>-MWCNT with the polyurethane matrix. The Fe<sub>3</sub>O<sub>4</sub>-MWCNT showed good dispersion in DMF for long time, whereas pristine MWCNT showed very poor dispersion (Fig. 6A.7).





**Fig. 6A.6:** TEM image for (a) a-MWCNT, (b) and (c) Fe<sub>3</sub>O<sub>4</sub>-MWCNT and (d) HPUFCNT1

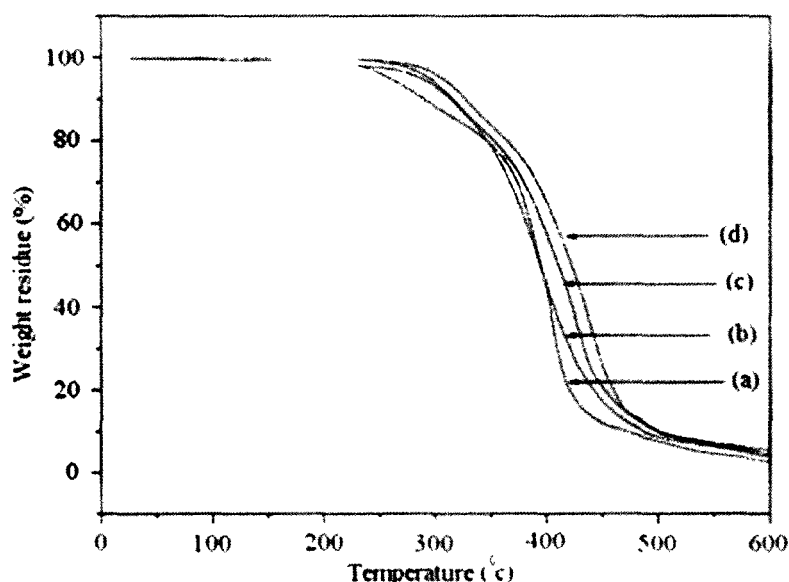


**Fig. 6A.7:** Dispersion stability in DMF for (a) pristine MWCNT, (b) Fe<sub>3</sub>O<sub>4</sub>-MWCNT and (c) response of Fe<sub>3</sub>O<sub>4</sub>-MWCNT to a magnet

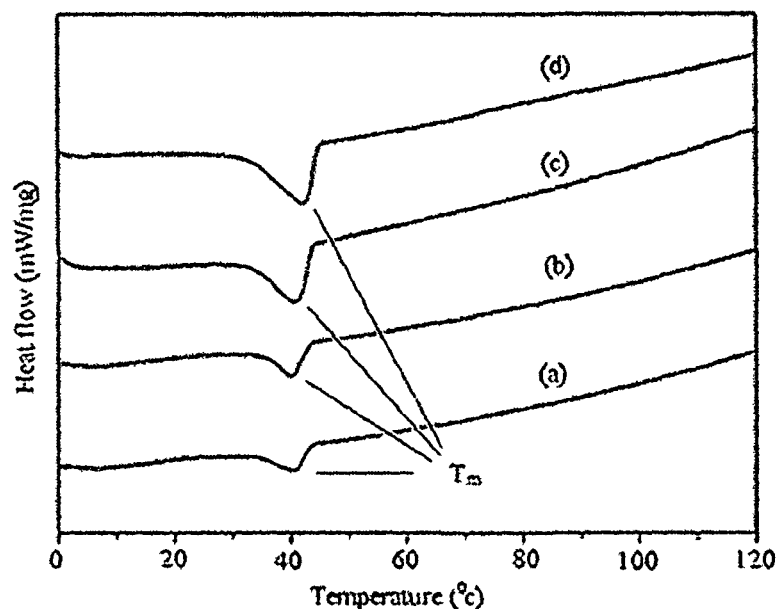
### 6A.3.5. Thermal property

The thermal degradation behavior of the prepared nanocomposites was studied by TGA analysis and thermograms are shown in Fig. 6A.8. From this Figure, it is clear that by increasing the weight percentage of Fe<sub>3</sub>O<sub>4</sub>-MWCNT increases the thermal stability of the nanocomposites. The onset of the thermal degradation was increased by about 9%, 13% and 18.3% for the nanocomposites with 0.2, 1 and 2 wt% of Fe<sub>3</sub>O<sub>4</sub>-MWCNT content, respectively. This is due to the decreased in thermal motion of the polymer chains in the nanocomposites due to various interactions such as H-bonding, polar-polar interaction between Fe<sub>3</sub>O<sub>4</sub>-MWCNT and polyurethane matrix. Furthermore, the increase in thermal stability of the nanocomposites is due to the homogeneous distribution of highly thermostable Fe<sub>3</sub>O<sub>4</sub>-MWCNT that resists the diffusion of volatile products generated during the decomposition process.<sup>13</sup>

The DSC curves of hyperbranched polyurethane and nanocomposites are shown in Fig. 6A.9. From the figure, it is observed that melting temperature ( $T_m$ ) (39.5 °C to 42.2 °C) of the nanocomposites increased with the increase of amount of Fe<sub>3</sub>O<sub>4</sub>-MWCNT. This is due to the increased rigidity of the nanocomposites due to various interactions between Fe<sub>3</sub>O<sub>4</sub>-MWCNT and polymer matrix.



**Fig. 6A.8:** TGA thermograms for (a) MHBPU10, (b) HPUFCNT0.2, (c) HPUFCNT1 and (d) HPUFCNT2



**Fig. 6A.9:** DSC curves for (a) MHBPU10, (b) HPUFCNT0.2, (c) HPUFCNT1 and (d) HPUFCNT2

#### 6A.3.6. Mechanical property

The mechanical properties of the hyperbranched polyurethane and the nanocomposites are given in Table 6A.1. The tensile strength was found to enhance from 6.5 MPa to 30.5 MPa with the increase of the content of Fe<sub>3</sub>O<sub>4</sub>-MWCNT from 0 to 2 wt%. This can be attributed to the good dispersion of Fe<sub>3</sub>O<sub>4</sub>-MWCNT in the polyurethane matrix. Better the dispersion of Fe<sub>3</sub>O<sub>4</sub>-MWCNT, greater is the surface area available for different interactions such as H-bonding, polar-polar interaction with the polymer matrix and causes the enhanced tensile strength.<sup>14</sup> However, elongation at break decreases with the increase of content of Fe<sub>3</sub>O<sub>4</sub>-MWCNT in the nanocomposites. This is due to the increased molecular restriction of the polymer chains on the surface of Fe<sub>3</sub>O<sub>4</sub>-MWCNT, as a result of the various interactions stated earlier. The scratch hardness of the nanocomposites increases with the increase of the amount of Fe<sub>3</sub>O<sub>4</sub>-MWCNT. This is due to the enhanced rigidity and toughness of the nanocomposites. The prepared nanocomposites exhibited adequate flexibility as indicated in the bending test. This is attributed to the high flexibility of the soft segment and the presence of long chain fatty acid moiety in the structure of the polyurethane.

**Table 6A.1:** Mechanical properties of hyperbranched polyurethane and its nanocomposites

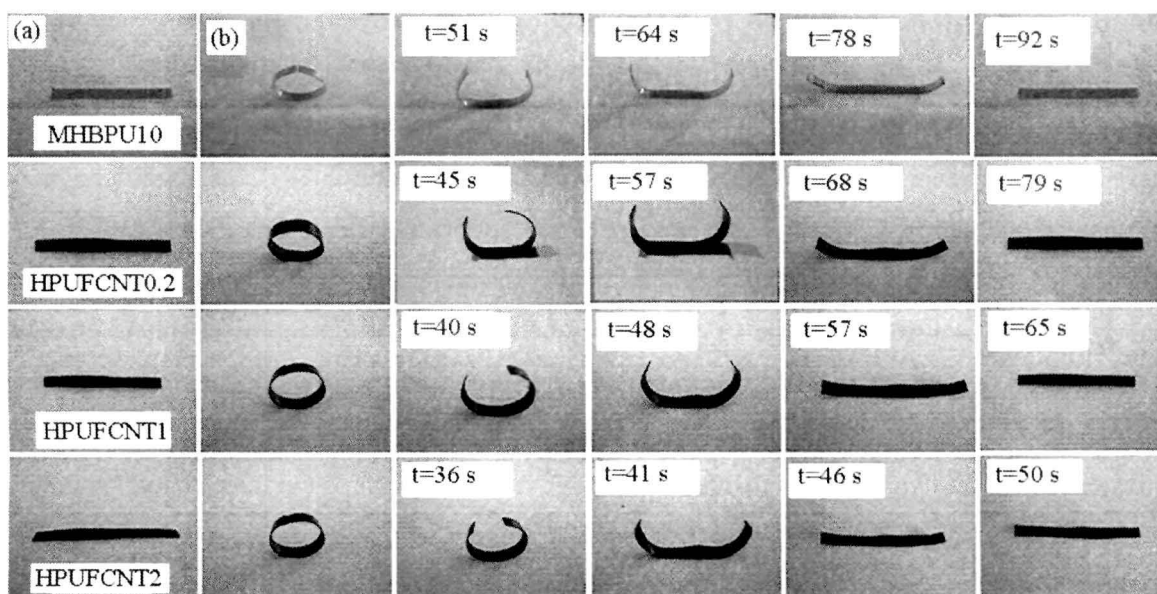
Property	MHBPU10	HPUFCNT0.2	HPUFCNT1	HPUFCNT2
Tensile strength (MPa)	6.5 ± 0.4	14 ± 0.3	21.5 ± 0.3	30.5 ± 0.2
Elongation at break (%)	610 ± 3	493 ± 2	443 ± 2	401 ± 3
Scratch hardness (kg)	3.0 ± 0.1	4.1 ± 0.1	5.5 ± 0.1	7.2 ± 0.1
Bending (m)	<0.001	<0.001	<0.001	<0.001
Impact resistance* (m)	0.95 ± 0.05	0.95 ± 0.05	0.95 ± 0.05	0.95 ± 0.05

\* 1.0 m is the limit of the instrument

#### 6A.3.7. Shape memory property

The shape memory behaviors of hyperbranched polyurethane and its nanocomposites under microwave irradiation are shown in Fig. 6A.10. The nanocomposites exhibited good shape fixity and this shape was retained for a long time at room temperature. The micro-Brownian movements of the molecular chains are frozen at low temperature and the applied stress is stored in the fixed shape. All the materials exhibited almost full shape recovery under the microwave stimulus. When the microwave irradiated on the sample, the dipole moment moves to align with the external electric field components. Due to the oscillations of the electric field components of the microwave, the dipole field of the molecules attempt to follow these oscillations, as a result heating effect arises as already discussed in Chapter 4, section 4A.3.7. The polymer chains are activated when the heat is close to the transition temperature ( $T_{trans}$ ) and release the stored energy to recover the original shape. No significant change of shape recovery of nanocomposites was observed over the five cycles of test. It was noticed that the shape recovery time decreased with the increase of concentration of  $Fe_3O_4$ -MWCNT in the nanocomposites. This can be attributed to the homogeneous distribution of  $Fe_3O_4$ -MWCNT and the increased various interactions with the polymer matrix. Thereby more energy is stored in the system and immediately released the stored energy when the induced heat activated the polymer chains. Moreover the increased shape recovery speed is due to the microwave absorption characteristic of MWCNT and  $Fe_3O_4$  nanoparticles.<sup>15, 16</sup> The molecular friction and collisions increase within the system with the increase of the content of  $Fe_3O_4$ -MWCNT in the nanocomposites due to the microwave absorption characteristic of these nanomaterials, as a result the polymer chains activation are

faster. Furthermore the increase in shape recovery speed is due to the increase of the thermal conductivity of nanocomposites due to the presence of  $\text{Fe}_3\text{O}_4$ -MWCNT. The prepared nanocomposites have shown good shape fixity and shape recovery. Thus the nanocomposites may be utilized as shape memory materials in sensors, actuators, automobile, heat shrinkable tube and biomedical devices.



**Fig. 6A.10:** Shape memory behaviors of hyperbranched polyurethane and the nanocomposites under microwave stimulus (a) original shape and (b) fixed shape

#### 6A.4. Conclusion

The  $\text{Fe}_3\text{O}_4$  nanoparticles were successfully decorated on the surface of a-MWCNT.  $\text{Fe}_3\text{O}_4$ -MWCNT/hyperbranched polyurethane nanocomposites were successfully prepared by the in situ solution polymerization technique. The mechanical property and thermal stability found to be enhanced with the increase of amount of  $\text{Fe}_3\text{O}_4$ -MWCNT in the nanocomposites. All the nanocomposites showed excellent shape fixity. The prepared nanocomposites exhibited almost full shape recovery under the microwave actuation. The shape recovery speed was found to be increased with the increase of the content of  $\text{Fe}_3\text{O}_4$ -MWCNT in the nanocomposites. Thus the prepared nanocomposites could be utilized as advanced SMP in suitable applications.

## **6B. Fe<sub>3</sub>O<sub>4</sub> nanoparticles decorated MWCNT/hyperbranched polyurethane thermosetting nanocomposites**

### **6B.1. Introduction**

The importance of thermosetting hyperbranched polyurethane and its nanocomposites are already discussed in the earlier chapters. The modification of polyurethanes with other compatible polymers dramatically improved their performance as well as shape memory behaviors. The CNT decorated with the inorganic nanomaterials such as ZnO, Fe<sub>3</sub>O<sub>4</sub>, Au, Cu etc. have taken increasing attention because of increasing dispersion as well as modification of intrinsic properties of CNT, and thus find potential applications in different fields.<sup>7, 17-20</sup> The importance of decoration of MWCNT with the magnetic nanoparticles are discussed in subchapter 6A, section 6A.1. The shape memory behaviors of commercially available glycidyl bisphenol-A based epoxy resin modified hyperbranched polyurethane thermosetting nanocomposites were studied by the noncontact way using the microwave irradiation. The advantages of glycidyl bisphenol-A based epoxy resin such as good mechanical, thermal, dielectric behavior, low shrinkage during cure, low creep etc. were discussed in Chapter 3, section 3.1. The presence of hydroxyl and carboxyl groups on the surface of Fe<sub>3</sub>O<sub>4</sub>-MWCNT as well as hydroxyl groups of the polyurethane interact with the oxirane ring of the epoxy resin and thereby making the crosslinked structure. Xin et al. reported the enhancement of mechanical properties and electrical conductivity of silver nanoparticles decorated CNT/polymer nanocomposites.<sup>21</sup> Rangari et al. studied the antimicrobial activity of the Ag/CNT nanohybrid based nylon-6 polymer nanocomposite.<sup>22</sup>

In the present study, therefore, Fe<sub>3</sub>O<sub>4</sub>-MWCNT/hyperbranched polyurethane thermosetting nanocomposites were prepared to investigate the performance including shape memory behaviors.

### **6B.2. Experimental**

#### **6B.2.1. Materials**

The reagents used for the preparation of hyperbranched polyurethane were monoglyceride of the *Mesua ferrea* L. seed oil, TDI, PCL, 1,4-butanediol and triethanolamine as same as described in Chapter 2, section 2A.2.1.

Epoxy resin purchased from the Ciba Geigy was same as described in Chapter 3, section 3.2.1.

MWCNT purchased from Iiljin Nanotech were same as described in Chapter 5, section 5A.2.1.

Iron (III) chloride hexahydrate and iron (II) chloride tetrahydrate were used same as described in Chapter 4, section 4A.2.1.

#### 6B.2.2. Preparation of Fe<sub>3</sub>O<sub>4</sub>-MWCNT nanohybrid

The preparation of Fe<sub>3</sub>O<sub>4</sub>-MWCNT nanohybrid was same as discussed in subchapter 6A, section 6A.2.2.

#### 6B.2.3. Preparation of thermosetting hyperbranched polyurethane/Fe<sub>3</sub>O<sub>4</sub>-MWCNT nanocomposites

The hyperbranched polyurethane and nanocomposites were prepared by the same way as described in the earlier chapter. In order to obtain the thermosetting polymer the above prepared nanocomposite was mixed with 10 wt% of glycidyl bisphenol-A based epoxy resin (100% solid content) by mechanical stirring followed by ultra-sonication for 10 min. The polymer solution was cast on the inert substrates followed by vacuum degassing and cured at 120 °C. The cured films were denoted as EHPUFCNT0.2, EHPUFCNT1 and EHPUFCNT2 corresponding to the Fe<sub>3</sub>O<sub>4</sub>-MWCNT content of 0.2, 1 and 2 wt%, respectively.

#### 6B.2.4. Instrumentation

The hyperbranched polyurethane and its thermosetting nanocomposites were characterized by the same characterization techniques as stated in subchapter 6A, section 6A.2.4. The magnetic behavior of the samples was studied by the same instrument as described in Chapter 4, section, 4A.2.4.

The mechanical properties such as tensile strength, elongation at break, scratch resistance and impact resistance were measured by the same procedure as described in Chapter 2, section 2A.2.4. The thermal stability was studied by the same method as described in Chapter 2, section 2A.2.4.

The shape memory behaviors of the nanocomposites were studied by the same approach using the same instrument as described in Chapter 4, section 4A.2.4.

### 6B.3. Results and discussion

#### 6B.3.1. Curing study

From the curing study it was noticed that the touch free time at room temperature and the drying time at 120 °C decreased with the increase of the loading of Fe<sub>3</sub>O<sub>4</sub>-MWCNT in the nanocomposites (Table 6B.1). This is due to the increased cross-linking reaction among the –OH/-C=O of Fe<sub>3</sub>O<sub>4</sub>-MWCNT, epoxy/hydroxyl groups of the epoxy resin and free -OH groups of the hyperbranched polyurethane (Scheme 6B.1). Due to the increase of the content of Fe<sub>3</sub>O<sub>4</sub>-MWCNT, the number of free –OH and -C=O groups increases in the system, as a result intercross-linking network formation increased and thereby confers the three dimensional network structures. The absence of the epoxy band at 916 cm<sup>-1</sup> after curing in FTIR spectra confirmed the formation of the network structure. The increased cross-linking density of the thermosetting nanocomposites was also confirmed by the swelling test in DMF as discussed later.

**Table 6B.1:** Compositions and curing time of the nanocomposites at 120 °C

Code	MHBPU10 (wt%)	Epoxy (wt%)	Touch free time (min)	Drying time (min)
MHBPU10	100	-	-	-
EHPUFCNT0.2	100	10	51	58
EHPUFCNT1	100	10	43	50
EHPUFCNT2	100	10	35	43



### 6B.3.2. FTIR study

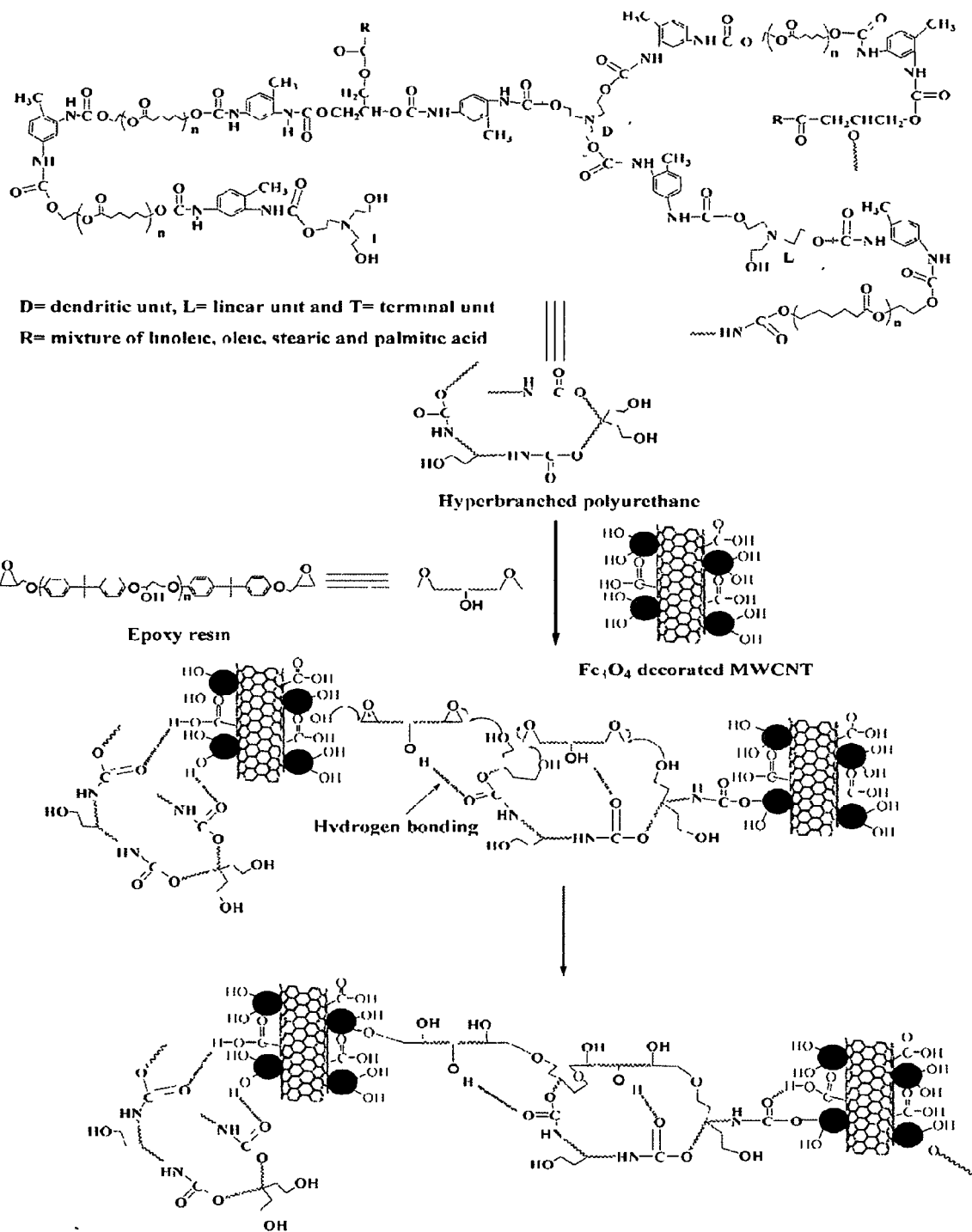
The FTIR study of pristine MWCNT, a-MWCNT, Fe<sub>3</sub>O<sub>4</sub> and Fe<sub>3</sub>O<sub>4</sub>-MWCNT are already discussed in subchapter 6A, section 6A.3.1. Fig. 6B.1 presents the FTIR spectra of hyperbranched polyurethane and thermosetting nanocomposites. The bands appeared at 3410-3433 cm<sup>-1</sup> (N-H stretching) and 1726 cm<sup>-1</sup> (-C=O stretching of urethane linkage) for the urethane groups of pristine polyurethane. The bands at 1726 cm<sup>-1</sup> (-C=O) and at 3410-3433 cm<sup>-1</sup> (N-H stretching) were found to be shifted to lower wavenumber (1719-1715 cm<sup>-1</sup>) and broadened after the formation of nanocomposite, respectively. The presence of strong interactions between the Fe<sub>3</sub>O<sub>4</sub>-MWCNT and the polyurethane chains in the nanocomposites are confirmed from the above results.

### 6B.3.3. X-ray diffraction study

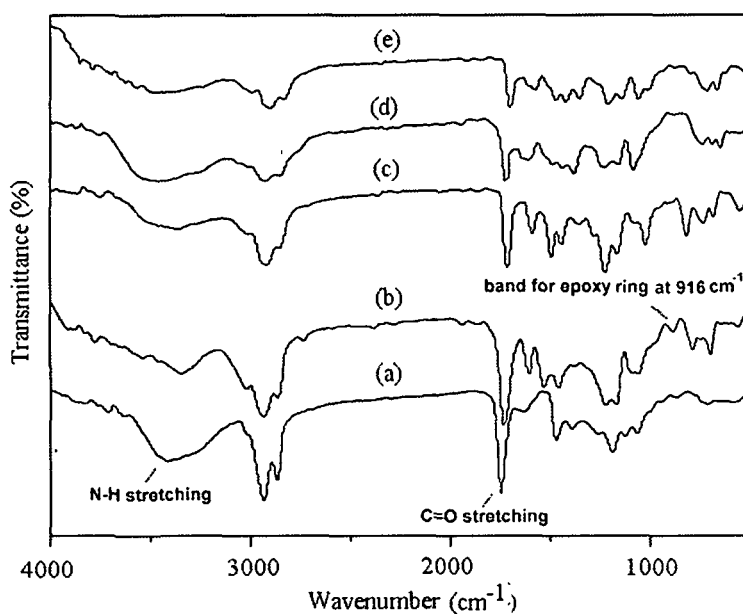
The XRD study of a-MWCNT, Fe<sub>3</sub>O<sub>4</sub> and Fe<sub>3</sub>O<sub>4</sub>-MWCNT are already discussed in subchapter 6A, section 6A.3.3. Fig. 6B.2 shows the crystalline structures of hyperbranched polyurethane and the thermosetting nanocomposites. The diffraction peaks at 2 $\theta$ =20.98° and 2 $\theta$ =23.82° are due to the (100) and (200) planes of PCL crystals of the hyperbranched polyurethane.<sup>13</sup> The peaks intensity was increased after the formation of nanocomposite. This can be attributed to the increased crystallinity for the nucleating effect of Fe<sub>3</sub>O<sub>4</sub>-MWCNT in the nanocomposites. The size of the Fe<sub>3</sub>O<sub>4</sub> nanoparticle using (220) crystal plane was found to be 9 nm as determined by the Scherrer formula.

### 6B.3.4. Magnetic property

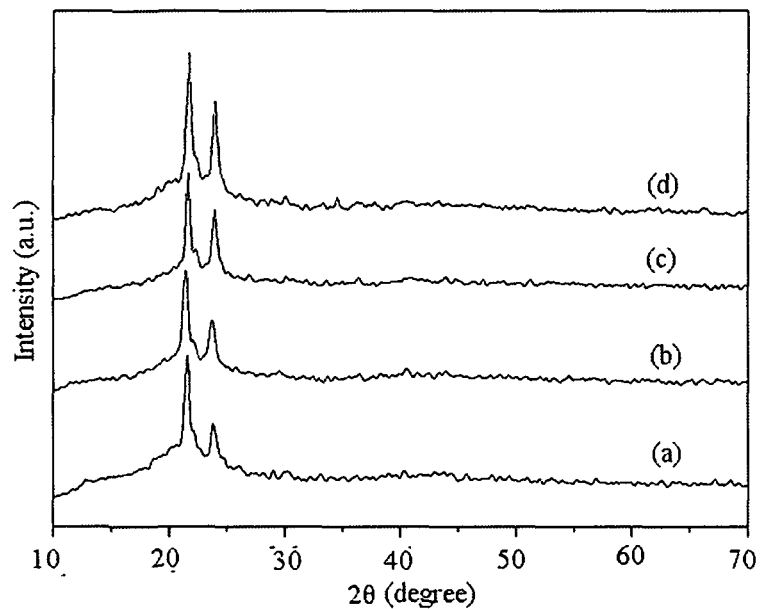
The magnetic property of Fe<sub>3</sub>O<sub>4</sub>-MWCNT and the nanocomposites were studied by the vibrating sample magnetometer at room temperature (Fig. 6B.3). The saturation magnetization values of Fe<sub>3</sub>O<sub>4</sub>-MWCNT and nanocomposite (EHPUFCNT0.2) were found to be 0.23 emu/g and 0.08 emu/g, respectively. The saturation magnetization value of nanocomposite was lower than Fe<sub>3</sub>O<sub>4</sub>-MWCNT nanohybrid. This is due to the low content of nanomaterials (0.2 wt%) and surface coating of Fe<sub>3</sub>O<sub>4</sub>-MWCNT by the polymer chains in the nanocomposite. The bare MWCNT do not show any magnetic behavior, which indicates that either the amount of remaining catalyst is extremely low or it does not have any magnetic property.



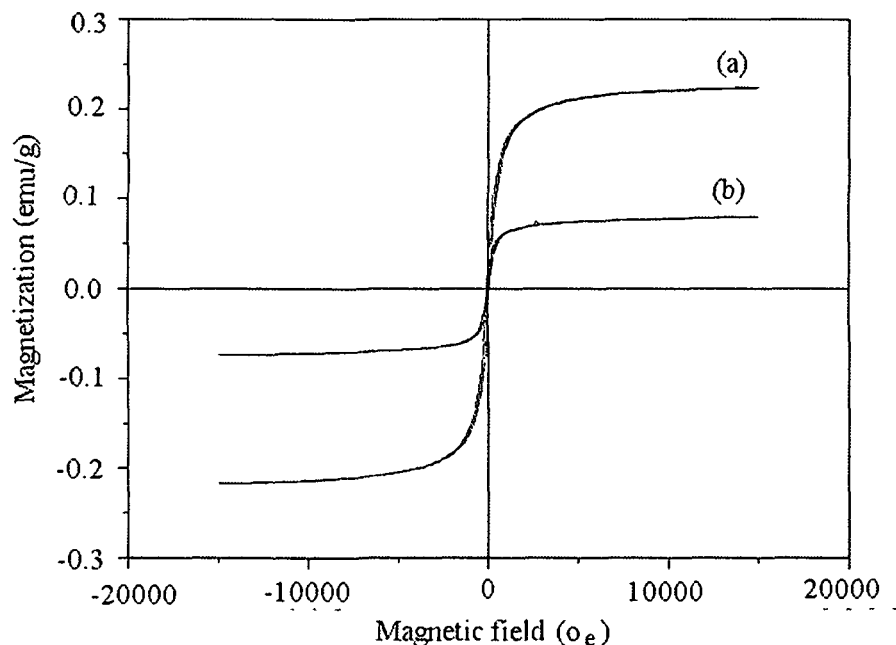
Scheme 6B.1: Proposed crosslinking reactions



**Fig. 6B.1:** FTIR spectra for (a) MHBPU10, (b) EHPUFCNT0.2 (before curing), (c) EHPUFCNT0.2, (d) EHPUFCNT1 and (e) EHPUFCNT2



**Fig. 6B.2:** XRD diffractograms for (a) MHBPU10, (b) EHPUFCNT0.2, (c) EHPUFCNT1 and (d) EHPUFCNT2



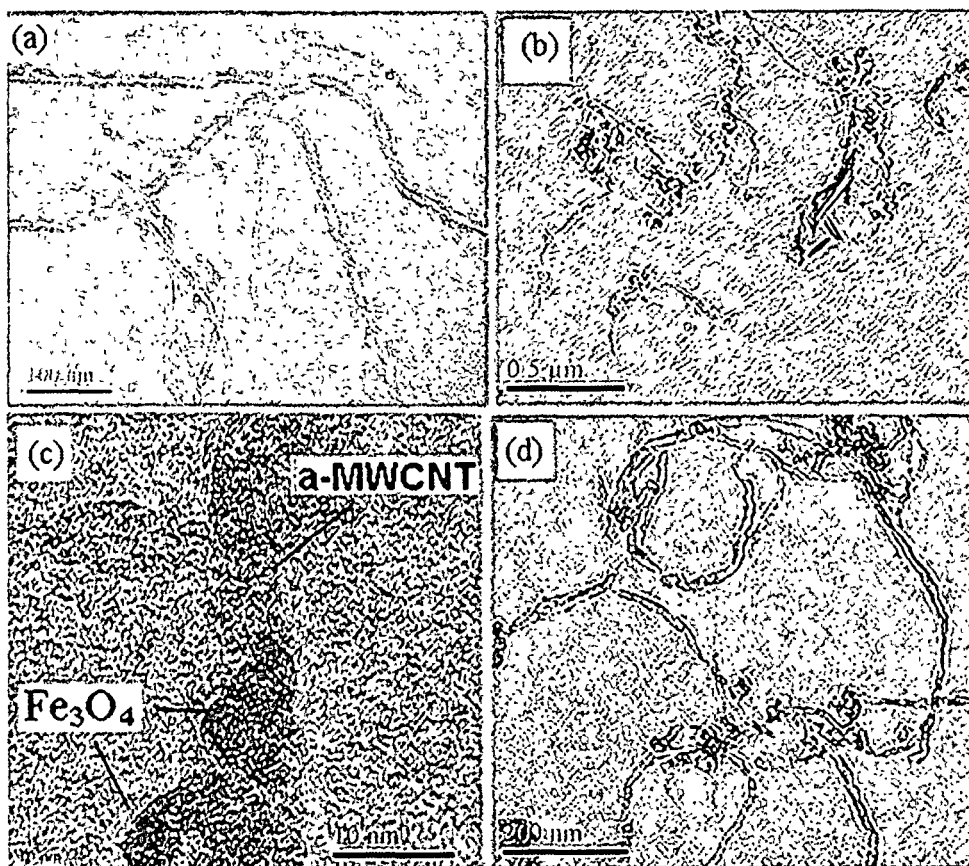
**Fig. 6B.3:** Magnetic hysteresis loops for (a) Fe<sub>3</sub>O<sub>4</sub>-MWCNT and (b) EHPUFCNT0.2

#### 6B.3.5. Morphology study

The morphologies of a-MWCNT, Fe<sub>3</sub>O<sub>4</sub>-MWCNT and the thermosetting nanocomposite are observed by TEM and shown in Fig. 6B.4. The morphology of a-MWCNT was observed as smooth surface, whereas Fe<sub>3</sub>O<sub>4</sub>-MWCNT was rough. From TEM images it is observed that Fe<sub>3</sub>O<sub>4</sub> nanoparticles are adhered on the surface of a-MWCNT. The TEM image of the nanocomposite (EHPUFCNT1) showed the homogeneous distribution of Fe<sub>3</sub>O<sub>4</sub>-MWCNT in the polyurethane matrix (Fig. 6B.4d). This is due to the good interaction of Fe<sub>3</sub>O<sub>4</sub>-MWCNT with the polyurethane matrix. The average size of Fe<sub>3</sub>O<sub>4</sub> nanoparticles was 11 nm.

#### 6B.3.6. Thermal property

The TGA and DTG thermograms of hyperbranched polyurethane and the thermosetting nanocomposites are shown in Fig. 6B.5 (I and II). The thermal stability was found to be enhanced with the increase of concentration of Fe<sub>3</sub>O<sub>4</sub>-MWCNT in the nanocomposites. This is due to the restricted movement of the polymer chains in the nanocomposites because of



**Fig. 6B.4:** TEM images for (a) a-MWCNT, (b) and (c) Fe<sub>3</sub>O<sub>4</sub>-MWCNT and (d) EHPUFCNT1

various interactions such as H-bonding, polar-polar interaction and chemical cross-linking among Fe<sub>3</sub>O<sub>4</sub>-MWCNT, glycidyl bisphenol-A based epoxy and polyurethane matrix. This can also be attributed to the increased rigidity and compactness of the system. Moreover the well dispersed highly thermostable Fe<sub>3</sub>O<sub>4</sub>-MWCNT act as gas barrier to the volatile products formed during the decomposition that decreased the permeability and enhanced the thermal stability.<sup>13, 23</sup>

Fig. 6B.6 shows the DSC curves of hyperbranched polyurethane and the thermosetting nanocomposites. The melting temperature ( $T_m$ ) and melting enthalpy ( $\Delta H_m$ ) were found to be increased with the increase of content of Fe<sub>3</sub>O<sub>4</sub>-MWCNT in the nanocomposites (Table 6B.2). This is due to the increased rigidity of the nanocomposites due to various interactions among Fe<sub>3</sub>O<sub>4</sub>-MWCNT, epoxy and polyurethane matrix. The degree of crystallinity values of all the

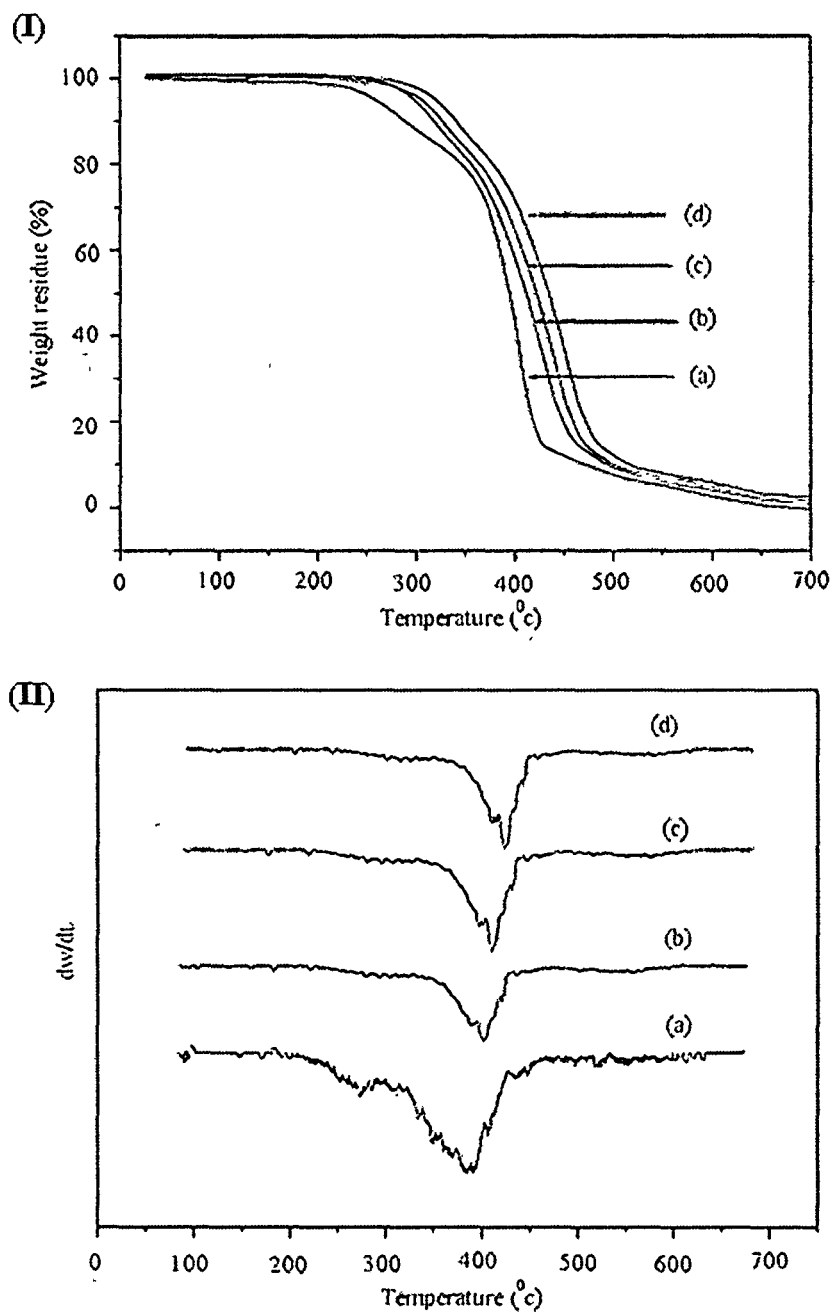
nanocomposites are given in Table 6B.2. This is determined by the measurement of  $\Delta H_m$  on cooling and with an enthalpy value of 136 J/g for 100% crystalline PCL.

**Table 6B.2:** Thermal behaviors of the hyperbranched polyurethane and its nanocomposites

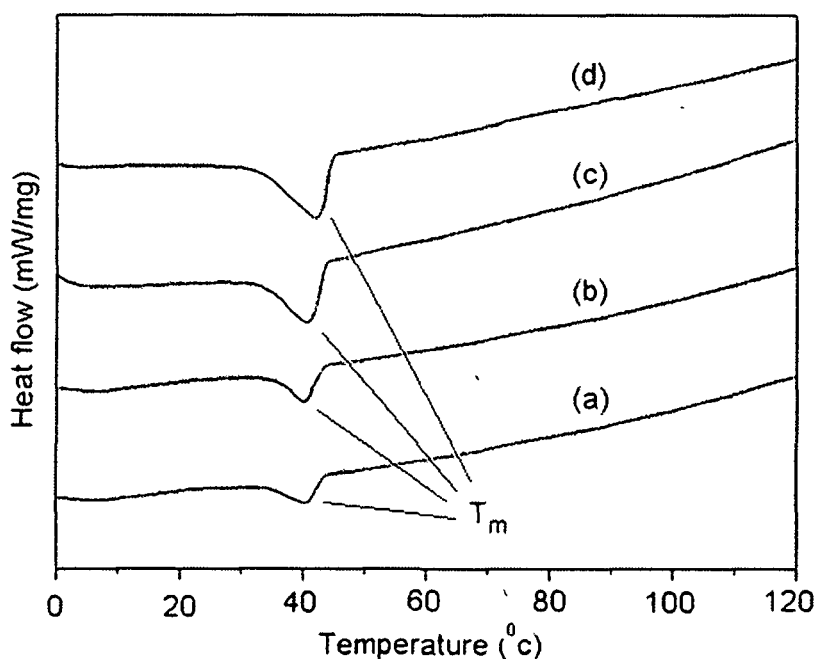
Code	Initial decomposition temperature (°C)	Melting temperature ( $T_m$ °C)	Melting enthalpy ( $\Delta H_m$ J/g)	Degree of crystallinity (%)
MHBPU10	241	39.5	41	30.14
EHPUFCNT0.2	260	40.6	43.1	31.69
EHPUFCNT1	274	42.1	44.2	32.5
EHPUFCNT2	291	43.2	45.4	33.38

#### 6B.3.7. Mechanical property

The data for mechanical properties of the hyperbranched polyurethane and its thermosetting nanocomposites are given in Table 6B.3. The tensile strength of the nanocomposites increased with the increase of the loading of  $Fe_3O_4$ -MWCNT. This is due to the well dispersion of  $Fe_3O_4$ -MWCNT and enhanced interactions among  $Fe_3O_4$ -MWCNT, epoxy and the polymer matrix.<sup>24-26</sup> As a result molecular chains are restricted on the surface of MWCNT and the chains slippage decreased during the application of loading. Moreover this can be attributed to the increased cross-linking density in the system due to the interaction among the epoxide groups, -OH and -COOH of functionalized MWCNT and free -OH groups of the hyperbranched polyurethane. However the elongation at break decreases with the increase of loading of  $Fe_3O_4$ -MWCNT in the nanocomposites. This is due to the restricted movement of molecular chains due to the presence of various physico-chemical interactions in the nanocomposites as stated above. The scratch hardness increased with the increase of the content of  $Fe_3O_4$ -MWCNT. The significant improvement of the scratch hardness is due to the increased compactness and rigidity of the nanocomposites. All the prepared nanocomposites exhibited good impact resistance. The gloss of the nanocomposites increased with the increase of loading of  $Fe_3O_4$ -MWCNT in the nanocomposites. This is attributed to the good compatibility of epoxy resin,  $Fe_3O_4$ -MWCNT and hyperbranched polyurethane and increased dimension stability of the thermosetting nanocomposites.



**Fig. 6B.5:** (I) TGA thermograms for (a) MHBPU10, (b) EHPUFCNT0.2, (c) EHPUFCNT1 and (d) EHPUFCNT2, and (II) DTG curves for (a) MHBPU10, (b) EHPUFCNT0.2, (c) EHPUFCNT1 and (d) EHPUFCNT2



**Fig. 6B.6:** DSC curves for (a) MHBPU10, (b) EHPUFCNT0.2, (c) EHPUFCNT1 and (d) EHPUFCNT2

**Table 6B.3:** Mechanical properties of hyperbranched polyurethane and its thermosetting nanocomposites

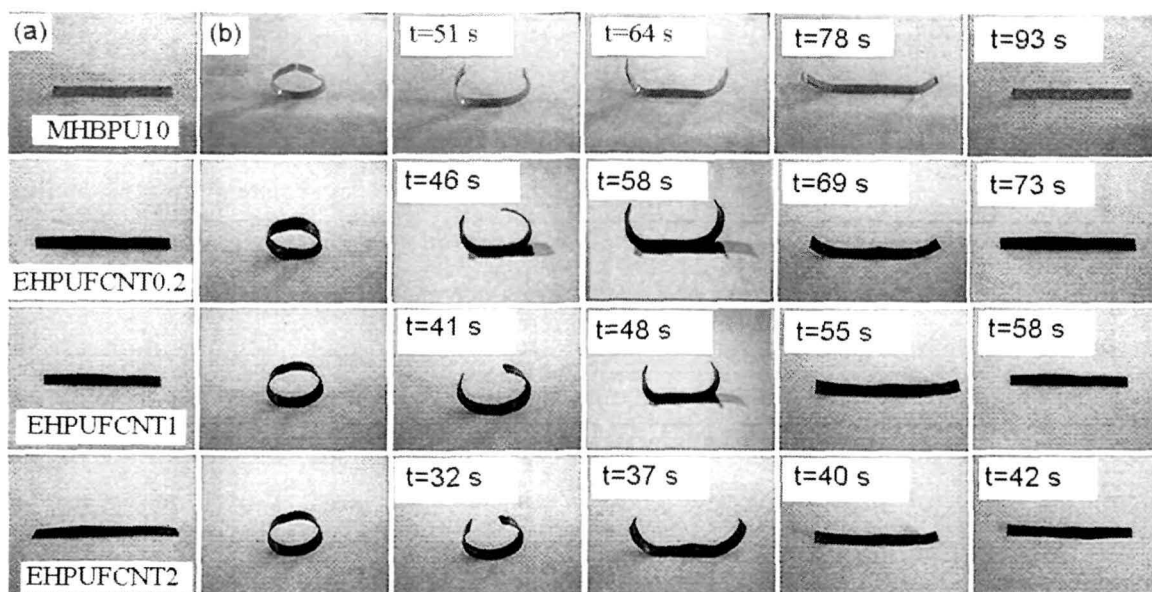
Property	MHBPU10	EHPUFCNT0.2	EHPUFCNT1	EHPUFCNT2
Tensile strength (Mpa)	$6.4 \pm 0.4$	$17 \pm 0.3$	$25.5 \pm 0.3$	$36.5 \pm 0.2$
Elongation at break (%)	$595 \pm 3$	$483 \pm 2$	$434 \pm 2$	$398 \pm 2$
Scratch hardness (kg)	$3.0 \pm 0.1$	$4.6 \pm 0.1$	$6.5 \pm 0.1$	$8.5 \pm 0.1$
Bending (m)	<0.001	<0.001	<0.001	<0.001
Impact resistance* (m)	$0.95 \pm 0.05$	$0.95 \pm 0.05$	$0.95 \pm 0.05$	$0.95 \pm 0.05$
Gloss (60°)	$84 \pm 2$	$87 \pm 2$	$91 \pm 2$	$95 \pm 2$
Swelling (%)	-	$29 \pm 1.2$	$22 \pm 1.2$	$16 \pm 1.1$

\*1.0 m is the limit of the instrument



#### 6B.3.8. Shape memory property

The shape memory behaviors of the hyperbranched polyurethane and the nanocomposites are shown in Fig. 6B.7. The nanocomposites exhibited good shape fixity. The micro-Brownian movements of the polymer chains are frozen and transformed to a rigid state during the cooling. When the polymers are deformed, the orientations of the polymer chains are changed. The free volume or the distance between the polymers chains decreases on stretching which enhances various interactions such as H-bonding and polar-polar interaction. Thereby it resists the recoiling of the polymer chains and gives the fixed shape. The hyperbranched polyurethane and the nanocomposites exhibited almost full shape recovery under the microwave stimulus. No significant change of shape recovery of the nanocomposites was observed over the repeated ten cycles of test. When the microwave irradiated on the sample, the dipole moment oscillates to align with the external electric field, as a result heat is generated as already discussed in Chapter 4, section 4A.3.7. The shape recovery effect was observed when the induced heat closes to the transition temperature ( $T_{trans}$ ). The microwave chamber temperature was found to be 45 °C. The shape recovery time decreased with the increase of the content of  $Fe_3O_4$ -MWCNT in the nanocomposites. This can be attributed to the increased stored energy in the nanocomposites due to the homogeneous distribution of  $Fe_3O_4$ -MWCNT and the increased physico-chemical cross-link in the systems. CNT favor to stabilize the crystalline domains of the polymer.<sup>27</sup> They are able to lock the mechanical constrains. Thus by increasing the toughness of the polymer, carbon nanotubes can allow more energy to be absorbed and restored. Therefore the strain energy released immediately, when the induced heat is close to the  $T_{trans}$ . Furthermore the increment of shape recovery speed may be due to the enhanced microwave absorption characteristic of the nanohybrid system as both  $Fe_3O_4$  and MWCNT are microwave absorbing materials.<sup>15, 16, 28</sup> The increased shape recovery speed may also be due to the enhanced thermal conductivity of the nanocomposites as  $Fe_3O_4$ -MWCNT is conducting material. The nanocomposites showed the almost full recovery in the time period of 42-93 s, so no effect was observed for longer time of microwave exposure. However as the exposure time was lesser the shape recovery was found to be lowered. The prepared nanocomposites showed good shape fixity and shape recovery. Hence the nanocomposites might be utilized as potential SMP in various fields of applications such as sensors and micro-actuators, automobile, biomedical devices and so on.



**Fig. 6B.7:** Shape memory behaviors of hyperbranched polyurethane and the thermosetting nanocomposites under microwave stimulus (a) original shape and (b) fixed shape

#### 6B.4. Conclusion

From this study it can be concluded that epoxy modified  $\text{Fe}_3\text{O}_4$ -MWCNT/hyperbranched polyurethane thermosetting nanocomposites exhibited excellent shape recovery under the application of microwave stimulus. The shape fixity over the repeated cycles of test was also very good. The dose dependent shape memory behavior offers tuning of such property as per the requirement. Significant improvements of tensile strength along with other desired properties including thermal stability were achieved by the formation of nanocomposite. The thermosetting one exhibited the overall good performance including shape memory behavior as compared to the thermoplastic one. Thus the studied nanocomposites have strong potential to be used as noncontact microwave induced shape memory materials.

## References

1. Iijima, S. Helical microtubules of graphitic carbon, *Nature* **354**, 56–58, 1991.
2. Collins, P.G., et al. Nanotube nanodevice, *Science* **278** (5335), 100-102, 1997.
3. Zhang, J., & Jiang, D. Interconnected multi-walled carbon nanotubes reinforced polymer-matrix composites, *Compos. Sci. Technol.* **71** (4), 466-470, 2011.
4. Spitalsky, Z., et al. Carbon nanotube-polymer composites: chemistry, processing, mechanical and electrical properties, *Prog. Polym. Sci.* **35** (3), 357-401, 2010.
5. Supova, M., et al. Effect of nanofillers dispersion in polymer matrices: a Review, *Sci. Adv. Mater.* **3** (1), 1-5, 2011.
6. Zhou, H., et al. Decoration of Fe<sub>3</sub>O<sub>4</sub> nanoparticles on the surface of poly(acrylic acid) functionalized multi-walled carbon nanotubes by covalent bonding, *Polym. Sci. Part A: Polym. Chem.* **48** (21), 4697-4703, 2010.
7. Kong, L., et al. Facile synthesis of multifunctional multiwalled carbon nanotubes/Fe<sub>3</sub>O<sub>4</sub> nanoparticles/polyaniline composite nanotubes, *J. Solid State Chem.* **181** (3), 628-636, 2008.
8. Wang, X., et al. Fabrication and characterization of magnetic Fe<sub>3</sub>O<sub>4</sub>-CNT composites, *J. Phys. Chem. Solids* **71** (4), 673-676, 2010.
9. Zhang, Q., et al. The formation of magnetite nanoparticles on the sidewalls of multi-walled carbon nanotubes, *Compos. Sci. Technol.* **69** (5), 633-638, 2009.
10. Che, R.C., et al. Fabrication and microwave absorption of carbon nanotubes/CoFe<sub>2</sub>O<sub>4</sub> spinel nanocomposite, *Appl. Phys. Lett.* **88** (3), 033105-033108, 2006.
11. Li, H.Y., et al. Poly(lactide)-functionalized and Fe<sub>3</sub>O<sub>4</sub> nanoparticle-decorated multiwalled carbon nanotubes for preparation of electrically-conductive and magnetic poly(lactide) films and electrospun nanofibers, *J. Mater. Chem.* **22** (11), 4855-4860, 2012.
12. Park, J.O., et al. Silane treatment of Fe<sub>3</sub>O<sub>4</sub> and its effect on the magnetic and wear properties of Fe<sub>3</sub>O<sub>4</sub>/epoxy nanocomposites, *Appl. Surf. Sci.* **256** (23), 6945-6950, 2010.
13. Deka, H., et al. Biocompatible hyperbranched polyurethane/multi-walled carbon nanotube composites as shape memory materials, *Carbon* **48** (7), 2013-2022, 2010.
14. Xie, X.L., et al. Dispersion and alignment of carbon nanotubes in polymer matrix: a review, *Mat. Sci. Eng. R* **49** (4), 89-112, 2005.

15. Zhan, Y., et al. A novel carbon nanotubes/Fe<sub>3</sub>O<sub>4</sub> inorganic hybrid material: synthesis, characterization and microwave electromagnetic properties, *J. Magn. Magn. Mater.* **323** (7), 1006-1010, 2011.
16. Ni, S., et al. Hydrothermal synthesis and microwave absorption properties of Fe<sub>3</sub>O<sub>4</sub> nanocrystals, *J. Phys. D: Appl. Phys.* **42** (5), 055004-055009, 2009.
17. Song, P., et al. Fabrication of fullerene -decorated carbon nanotubes and their application in flame-retarding polypropylene, *Nanoscale* **1** (1), 118-121, 2009.
18. Khanderi, J., et al. Synthesis and sensoric response of ZnO decorated carbon nanotubes, *J. Mater. Chem.* **19** (28), 5039-5046, 2009.
19. Zhang, R., & Wang, X. One step synthesis of multi-walled carbon nanotube/gold nanocomposites for enhancing electrochemical response, *Chem. Mater.* **19** (5), 976-978, 2007.
20. Jha, N., & Ramaprabhu, S. Synthesis and thermal conductivity of copper nanoparticle decorated multi-walled carbon nanotubes based nanofluids, *J. Phys. Chem. C* **112** (25), 9315-9319, 2008.
21. Xin, F., & Li, L. Decoration of carbon nanotubes with silver nanoparticles for advanced CNT/polymer nanocomposites, *Composites Part A* **42** (8), 961-967, 2011.
22. Rangari, V.K., et al. Synthesis of Ag/CNT hybrid nanoparticles and fabrication of their Nylon-6 polymer nanocomposite fibers for antimicrobial applications, *Nanotechnology* **21** (9), 095102-095113, 2010.
23. Konwar, U., et al. Vegetable oil based highly branched polyester/multi-walled carbon nanotubes nanocomposites as advanced materials, *Adv. Sci. Lett.* **16** (1), 265-273, 2012.
24. Rana, S., et al. Enhanced dispersion of carbon nanotubes in hyperbranched polyurethane and properties of nanocomposites, *Nanotechnology* **19** (49), 495707-495715, 2008.
25. Yadav, S.K., et al. Synthesis of mechanically robust antimicrobial nanocomposites by click coupling of hyperbranched polyurethane and carbon nanotubes, *Polymer* **53** (10), 2023-2031, 2012.
26. Mahapatra, S.S., et al. Highly branched polyurethane: synthesis, characterization and effects of branching on dispersion of carbon nanotubes, *Composites Part B* **45** (1), 165-171, 2013.
27. Viry, L., et al. Nanotube fibers for electromechanical and shape memory actuators, *J. Mater. Chem.* **20** (17), 3487-3495, 2010.

28. Zhou, W., et al. Synthesis and electromagnetic, microwave absorbing properties of core-shell  $\text{Fe}_3\text{O}_4$ -poly(3, 4-ethylenedioxythiophene) microspheres, *ACS Appl. Mater. Interfaces* **3** (10), 3839-3845, 2011.

## ***Chapter 7***

### **Conclusions and future directions**

#### ***Highlights***

In this chapter, an effort has been made to re-scrutinize and critically analyse the preparation and properties including shape memory behaviors of hyperbranched polyurethane and its nanocomposites, reported in the thesis. The major achievements and the future prospects of the reported work are highlighted.

## 7.1. Summary and conclusions

The thesis highlights the synthesis, characterization, properties evaluation including shape memory behaviors of *Mesua ferrea* L. seed oil based hyperbranched polyurethanes and their nanocomposites with different types of nanomaterials. The first chapter of this thesis describes a general introduction and brief review on the vegetable oil based shape memory polyurethane nanocomposites emphasizing the importance, general techniques of preparation, characterization, properties and applications. The scopes, objectives and plans of work for the present investigation are also focused here. The entire technical work of the present investigation is divided into ten subchapters in five consecutive chapters.

In the second chapter, the synthesis, characterization and properties evaluation including shape memory behaviors of vegetable oil based hyperbranched polyurethanes are described. The first subchapter of this technical part describes the hyperbranched polyurethanes with three different vegetable oils, whereas the second subchapter deals with the variation of the amount of monoglyceride of *Mesua ferrea* L. seed oil for the same polymer. However the third subchapter presented the hyperbranched polyurethane with varying amount of multifunctional moiety, triethanolamine. All the above hyperbranched polyurethanes were prepared by the pre-polymerization technique. The *Mesua ferrea* L. seed oil based hyperbranched polyurethane exhibited good thermal stability and shape memory behaviors among the other vegetable oils based polyurethane.

The third chapter deals with the study on modification, characterization, properties evaluation of monoglyceride (10 wt%) of *Mesua ferrea* L. seed oil based hyperbranched polyurethane. This polyurethane was modified with the commercially available glycidyl ether of bisphenol-A based epoxy resin in the presence of cycloaliphatic amine. The modified systems showed the enhanced performance including shape memory behaviors compared to the pristine system.

The fourth chapter consists of two subchapters. The study on Fe<sub>3</sub>O<sub>4</sub> based hyperbranched polyurethane thermoplastic nanocomposites is described in the first subchapter. The second subchapter deals with the thermosetting nanocomposites of the same. The prepared nanocomposites showed improved mechanical, thermal and microwave induced shape memory

behaviors compared to the pristine systems. The study showed the thermosetting nanocomposites exhibited better performance compared to the thermoplastic one.

The fifth chapter described MWCNT based hyperbranched polyurethane thermoplastic (first subchapter) and thermosetting (second subchapter) nanocomposites. The triethanolamine modified MWCNT plays an important role for enhancing the mechanical, thermal and shape memory behaviors of the pristine polyurethane. Moreover the thermosetting one exhibited enhanced performance as compared to the thermoplastic one.

Similarly the sixth chapter consists of two subchapters, where the first subchapter deals with preparation, characterization and properties evaluation including shape memory behaviors of hyperbranched polyurethane/Fe<sub>3</sub>O<sub>4</sub> decorated MWCNT thermoplastic nanocomposites. The second subchapter demonstrated on the same for the thermosetting nanocomposites. Fe<sub>3</sub>O<sub>4</sub> nanoparticles were successfully decorated on the surface of MWCNT by the wet chemical technique. The nanocomposites showed enhanced mechanical, thermal stability and shape memory behaviors as compared to pristine system for both the cases. The shape recovery time was found to be decreased in the nanocomposites under the microwave irradiation. However thermosetting one exhibited better mechanical, thermal and shape memory behaviors compared to thermoplastic one.

From the present investigation the following conclusions have been drawn.

- (i) The high potential non-edible *Mesua ferrea* L. seed oil, industrially important castor oil and dual purpose sunflower oil were successfully utilized for the preparation of shape memory hyperbranched polyurethanes. The monoglyceride of *Mesua ferrea* L. seed oil based shape memory hyperbranched polyurethane exhibited overall good performance as compared to the other. Thus structure and composition of oil can tune the ultimate properties of the polymer.
- (ii) The study showed that the amount of monoglyceride of oil as well as the multifunctional moiety has strong influence on the performance including shape memory behaviors of hyperbranched polyurethanes.
- (iii) The modified hyperbranched polyurethane with commercially available glycidyl ether of bisphenol-A based epoxy resin exhibited better mechanical, thermal and shape memory behaviors compared to the pristine polyurethane.



(iv) The  $\text{Fe}_3\text{O}_4$ /hyperbranched polyurethane thermoplastic and thermosetting nanocomposites were successfully prepared. The thermosetting one exhibited better performance as compared to the thermoplastic one. The shape recovery time was found to be decreased in the thermosetting nanocomposite as compared to the thermoplastic one under microwave irradiation.

(v) The mechanical, thermal stability and shape memory behaviors were strongly influenced by triethanolamine modified MWCNT in hyperbranched polyurethane thermoplastic and thermosetting nanocomposites. However, the thermosetting nanocomposites exhibited better performance including faster shape recovery compared to the thermoplastic one.

(vi) The  $\text{Fe}_3\text{O}_4$  nanoparticles were utilized to decorate the surface of MWCNT for improving compatibility and to achieve unique properties. The hyperbranched polyurethane/ $\text{Fe}_3\text{O}_4$  decorated MWCNT thermoplastic and thermosetting nanocomposites, thus showed better performance including microwave stimulated shape memory behavior compared to their respective pristine systems. The thermosetting nanocomposite exhibited better performance including faster shape recovery compared to the thermoplastic one.

## 7.2. Future directions

The thesis, even though presented a comprehensive and systematic study on vegetable oil based hyperbranched polyurethanes and their nanocomposites as advanced shape memory materials, still there are a few future scopes for further studies. Some of these are:

- (i) Vegetable oil based hyperbranched polyurethane with other nanomaterials such as graphene, carbon dot etc. can be studied as shape memory materials.
- (ii) The theoretical study of such nanocomposites can be conducted to understand the reinforcing mechanism as well as shape memory behavior.
- (iii) The shape memory behaviors of such nanocomposites can be conducted using other types of contact and noncontact stimuli.
- (iv) The biomedical applications of such bio-based hyperbranched polyurethane nanocomposites can be delved into.

## **List of Publications**

### **In Journals**

1. Kalita H., & Karak, N. Bio-based elastomeric hyperbranched polyurethanes for shape memory application, *Iran. Polym. J.* **21** (4), 263-271, 2012.
2. Kalita, H., & Karak, N. *Mesua-ferrea* L. seed oil based hyperbranched polyurethanes as shape memory materials: Effect of multifunctional component, *Polym. Eng. Sci.* **52** (11), 2454-2461, 2012.
3. Kalita, H., & Karak, N. Epoxy modified bio-based hyperbranched polyurethane thermosets, *Des. Monomers Polym.* **16** (5), 447-455, 2012.
4. Kalita, H., & Karak, N. Fe<sub>3</sub>O<sub>4</sub> nanoparticles decorated multi-walled carbon nanotube/hyperbranched polyurethane nanocomposites as shape memory materials, *J. Nanoeng. Nanomanuf.* **3** (3), 194-201, 2013.
5. Kalita, H., & Karak, N. Bio-based hyperbranched shape memory polyurethanes: Effect of different vegetable oils, *J. Appl. Polym. Sci.*, **131** (1), 39579-39586, 2014.
6. Kalita, H., & Karak, N. Bio-based hyperbranched polyurethane/Fe<sub>3</sub>O<sub>4</sub> nanocomposites as shape memory materials, *Polym. Adv. Technol.* **24** (9), 819-823, 2013.
7. Kalita, H., & Karak, N. Hyperbranched polyurethane/Fe<sub>3</sub>O<sub>4</sub> nanoparticles decorated multi-walled carbon nanotube thermosetting nanocomposites as microwave actuated shape memory materials, *J. Mater. Res.* **28** (16), 2132-2141, 2013.
8. Kalita, H., & Karak, N. Hyperbranched polyurethane/Fe<sub>3</sub>O<sub>4</sub> thermosetting nanocomposites as shape memory materials, *Polym. Bull.* **70** (11), 2953-2965, 2013.
9. Kalita, H., & Karak, N. Bio-based hyperbranched thermosetting polyurethane/triethanolamine functionalized multi-walled carbon nanotube nanocomposites as shape memory materials, *J. Nanosci. Nanotechnol.* doi:10.1166/jnn.2014.8749 (2013)
10. Kalita, H., et al. Biodegradable solvent induced shape memory hyperbranched polyurethane, *J. Polym. Res.* **19** (10), 9982-9990, 2012.
11. Kalita, H., & Karak, N. Bio-based hyperbranched polyurethane/multi-walled carbon nanotube nanocomposites as shape memory materials, *Polym. Compos.* doi: 10.1002/pc.22705.

12. Kalita, H., & Karak, N. Hyperbranched polyurethane/triethanolamine functionalized multi-walled carbon nanotube nanocomposites as remote induced smart materials, *Polym. Int.* (Accepted).

### **In conference/symposium**

1. Kalita, H., & Karak, N. *Mesua ferrea* L. seed oil modified hyperbranched polyurethane as shape memory materials, National conference on chemistry and chemical technology and society (NCCCTS-2011), Tezpur University, 11 November, 2011.
2. Kalita, H., & Karak, N. Bio-based hyperbranched polyurethane /Fe<sub>3</sub>O<sub>4</sub> nanocomposites as shape memory materials, National symposium on polymers and coatings (NSPC-2012), IICT Hyderabad, 7-8 September, 2012.
3. Kalita, H., & Karak, N. Bio-based hyperbranched polyurethane nanocomposites as microwave stimulated shape memory materials, APA international Conference on polymers: visions and innovation (APA-2014), (Accepted), IIT Delhi, 19-21 February, 2014.